NASA TECHNICAL MEMORANDUM

NASA TM X-3326

NASA TM X-3326

HIGH EFFICIENCY SILICON SOLAR CELL REVIEW

Lewis Research Center
Cleveland, Ohio 44135

NATIONAL AERONAUTICS AND SPACE ADMINISTRATION • WASHINGTON, D. C. • DECEMBER 1975

1. Report No. NASA TM X-3326	2. Government Accession No.	3. Recipient's Catalog No.
4. Title and Subtitle HIGH EFFICIENCY SILICON SOLAR CELL REVIEW		5. Report Date December 1975
		6. Performing Organization Code
7. Author(s)		8. Performing Organization Report No. E-8425
		10. Work Unit No.
9. Performing Organization Name and Address Lewis Research Center National Aeronautics and Space Administration Cleveland, Ohio 44135		11. Contract or Grant No.
		13. Type of Report and Period Covered Technical Memorandum
12. Sponsoring Agency Name and Address National Aeronautics and Space Administration Washington, D.C. 20546		14. Sponsoring Agency Code

15. Supplementary Notes

Meeting held at Lewis Research Center, Cleveland, Ohio, November 14-15, 1974. Edited by Michael P. Godlewski.

16. Abstract

In a 2-day meeting, sponsored by the NASA Lewis Research Center, representatives of 26 industrial, university, and government organizations presented an overview of the current research and development efforts to improve the performance of the silicon solar cell. The 24 papers presented reviewed the experimental and analytic modeling work that is being done, which emphasizes the improvement of conversion efficiency and the reduction of manufacturing costs. A summary is given of the round-table discussion, in which the near- and far-term directions of future efficiency improvements were discussed.

17. Key Words (Suggested by Author(s))	18. Distribution Statement
Silicon; Solar cells; Efficiency improvements; Electron damage; Meeting; Gallium arsenide	Unclassified - unlimited STAR category 33 (rev.)

19. Security Classif. (of this report)	20. Security Classif. (of this page)	21. No. of Pages	22. Price*
Unclassified	Unclassified	234	$7.50

* For sale by the National Technical Information Service, Springfield, Virginia 22161

PREFACE

Throughout the 1960's the air mass zero efficiency of the silicon solar cell stagnated somewhere around 10 percent. Yet it was accepted by most people that an efficiency greater than 20 percent was theoretically possible. There was, however, no good explanation for this gap. People were beginning to accept the possibility that it was a fact of nature that we would have about one-half of theoretical efficiency. Happily, a few years ago efforts were turned toward raising the efficiency, and they met with success. These efforts fell into two broad areas. The first I call product improvement, that is, an accumulation of information on obvious losses in the cell. This accumulation had led to substantial improvements in cell performance. The second area is research. The effort in this area revolves around several questions: Where do we want to be? Why haven't we been able to get there? What is it we don't understand about the cell?

We will cover both of these broad areas in this meeting. We want to focus specifically on where we are now, how far we have come, how far we can expect to go, and where we want to go. It is most important that we consider the goal or limit that we want to set for ourselves and then, of course, outline the best way to strive to reach that goal. NASA for the last few years has had a goal in its high efficiency solar cell program of 18 percent under space conditions, that is, under air mass zero conditions. The INTRODUCTION will explain how we set the 18-percent goal.

Daniel T. Bernatowicz,
NASA Lewis Research Center
Chairman

Preceding Page Blank

CONTENTS

Page

INTRODUCTION
Henry W. Brandhorst, Jr., NASA Lewis Research Center vii

RECENT EFFICIENCY IMPROVEMENTS
1. The COMSAT Non-Reflective Silicon Solar Cell: A Second Generation Improved Cell
J. Haynos, J. Allison, R. Arndt, and A. Meulenberg, COMSAT Laboratories 3
2. Higher Efficiency for Less Money
Joseph Lindmayer and Charles Wrigley, Solarex Corporation 13
3. Process Technology for High Efficiency Solar Cells
Peter A. Iles, Centralab Semiconductor. 19
4. Volume Production of Advanced Silicon Solar Cells
John A. Scott-Monck and Paul M. Stella, Spectrolab 23
5. Performance of Advanced Silicon Solar Cells in a Space Environment
Ronald W. Opjorden, Leland J. Goldhammer, and George S. Goodelle, Hughes Aircraft Company 31
6. Electron Damage in High Efficiency Solar Cells
W. Patrick Rahilly, Air Force Aero-Propulsion Laboratory 41
7. Electron and Proton Damage Coefficients in Low-Resistivity Bulk Silicon and Silicon Solar Cells
J. R. Srour, S. Othmer, K. Y. Chiu, and O. L. Curtis, Jr., Northrop Research and Technology Center 51

ALTERNATIVE STRUCTURES AND MATERIALS
8. Fabrication and Performance of Vertical Multijunction Solar Cells
R. K. Smeltzer, Texas Instruments Inc. 63
9. V-Grooved Silicon Solar Cells
Cosmo R. Baraona, NASA Lewis Research Center 71
10. A Summary of Investigations into the Performance of "Grating" Type Photovoltaic Devices
J. J. Loferski, L. Y. Chen, and E. E. Crisman, Brown University. 77
11. Gallium Arsenide Solar Cell Research at NASA Langley Research Center
Gilbert H. Walker, NASA Langley Research Center 97
12. High Efficiency Graded Band-Gap $Al_xGa_{1-x}As$-GaAs Solar Cell
James A. Hutchby, NASA Langley Research Center 103

Preceding Page Blank

EXPERIMENTAL RESULTS ON LOSS MECHANISMS

13. Application of the MOS C-V Technique to the Diffused Face of Silicon Solar Cells
Irving Weinberg, NASA Lewis Research Center. 113

14. Bulk Diffusion Lengths in Silicon Solar Cells Using the SEM
Victor G. Weizer, NASA Lewis Research Center 121

15. Correlation Between Mechanical Imperfections and Electrical Properties of Solar Cells
R. Kaul, B. Roessler, and J. J. Loferski, Brown University. . . . 129

16. Experimental Studies of Imperfection Centers in Low Resistivity Silicon p-n Junction Solar Cells
S. S. Li, F. A. Lindholm, and P. J. Chen, University of Florida; and C. T. Sah, University of Illinois 143

DEVICE ANALYSIS

17. Role of Recombination Current on Photovoltaic Parameters
Richard J. Stirn, Jet Propulsion Laboratory 157

18. A Semi-Empirical Analysis of Silicon Solar Cell Parameters as a Function of Solar Intensities
E. Y. Wang, Wayne State University 165

19. Some Computer Studies of Silicon Solar Cell Efficiency
J. R. Hauser and P. M. Dunbar, North Carolina State University. . 175

20. Comparison of Recent Solar Cell Performance Improvements
Martin Wolf, University of Pennsylvania 191

21. Studies of the BSF Cell
Joseph Mandelkorn, John H. Lamneck, and Larry R. Scudder, NASA Lewis Research Center 199

LIMITS TO PERFORMANCE

22. Low Resistivity Silicon Solar Cells - Promise and Problems
S. Soclof and P. Iles, Centralab Semiconductor. 209

23. Effects of High Doping Levels on Silicon Solar Cell Performance
Michael P. Godlewski and Henry W. Brandhorst, Jr., NASA Lewis Research Center 213

24. Studies of Some Fundamental Limitations of the Performance of pn Junction Silicon Solar Cells
F. A. Lindholm and S. S. Li, University of Florida; and C. T. Sah, University of Illinois. 223

SUMMARY OF ROUND TABLE DISCUSSION

Daniel T. Bernatowicz, NASA Lewis Research Center. 231

INTRODUCTION

Henry W. Brandhorst, Jr.
NASA Lewis Research Center
Cleveland, Ohio

About 4 years ago, the NASA Lewis Research Center began an examination of silicon solar cell efficiency in the hope of establishing a program leading to significant improvements in cell performance. This study followed that of Wolf (ref. 1), which indicated a maximum efficiency of 22 percent for 0.01-ohm-centimeter silicon material.

In setting the NASA Lewis goal, efficiency calculations were made by assuring a reduction of all losses to what was judged practical limits (ref. 2). These included technological areas for which little, if any, basic research was needed and research areas where further understanding was needed to approach the known fundamental limits. These areas were the following:

(1) Technological areas

- (a) Reduced grid coverage
- (b) Reduced series resistance
- (c) Reduced surface reflection

(2) Research Areas

- (a) Increased voltage
- (b) Increased lifetime
- (c) Reduced surface recombination velocity
- (d) Reduced excess junction current

The first technological improvement would be to reduce the then current 10-percent grid coverage to 5 percent. This could be accomplished either by use of a fine line grid pattern or by the use of conventional wraparound contacts. The second would be to reduce all series resistance by proper patterning of the grid. For these calculations a power loss of 3 percent due to series resistance was used. Finally, a reduction in reflection from 10 to 5 percent was assumed.

These technological factors increase cell output by only about 15 percent. In order to obtain a significant increase in cell efficiency, several basic research areas must be considered. The area for largest potential gain in output is the open circuit voltage. For these calculations, voltages were obtained by using simple diffusion theory and increases in base doping level. Lifetimes measured in ingots of appropriate resistivities were used as input to the calculations. The value of surface recombination velocity used was 10^2 centimeters per second, and an error function complement diffusion profile was assumed. No allowance was made for generation recombination currents, as these were

thought to be extrinsic and capable of being reduced to negligible values. Thus, only diffusion currents were assumed to flow in the cell.

Figure 1 shows the result of these calculations (ref. 2). Wolf's value of 22 percent for 0.01-ohm-centimeter material is indicated as the maximum possible, and the results of these calculations are shown as the curve labeled maximum practical. A broad peak in the vicinity of the 0.1-ohm-centimeter material was obtained. The maximum practical efficiency calculated was 18 percent. Also plotted in the figure are the efficiencies that had been measured about 5 years ago. Clearly, a wide gulf existed between practice and potential, especially with the more heavily doped material.

The NASA Lewis goal became to achieve an 18-percent-efficient silicon solar cell and thus reduce the spread between thought and practice. A research and development program was begun to explore the research areas listed previously. Three other major areas were studied: (1) lifetime and the effects of processing on lifetime, (2) surface states and surface recombination velocity, and (3) open circuit voltage and the role of excess junction current in cell behavior. A summary of the findings to date in each of these areas follows.

The first study focused on lifetime in silicon of different resistivities and attempted to understand why the lifetime in most solar cell devices was about 10 microseconds, whereas ingots had lifetimes of many hundreds of microseconds. This work was performed by Centralab and showed that the main reduction in measured lifetime occurred when the sample was sliced and not during subsequent processing steps. This reduction apparently resulted from a change in boundary conditions of the device and not from damage introduced in the slicing process.

Next, surface state and surface recombination velocity studies were initiated. The initial calculations (ref. 2) had shown that, by tailoring the diffusion profile, high blue outputs could be obtained even with S values as high as 10^5 centimeters per second. By elimination of the "dead layer" due to the constant phosphorus atom concentration in the first 0.03 to 0.04 micrometer of the diffused face, high responses at a 0.4-micrometer wavelength could be obtained. The measured values were consistent with theoretical predictions made by using erfc profiles. However, additional increases in output could be achieved with further reduction in S. Therefore, studies were initiated both in house and with Professor H. Gatos at MIT to delve more deeply into surface recombination velocity. It is hoped that these studies will lead to management and control of the surface properties of the cell and so achieve maximum cell blue response.

The final area of study, with the purpose of increasing the open circuit voltage and reducing the excess junction current, is critical to major improvements in cell efficiency. This problem is acute because the observed voltages of low resistivity cells are much lower than expected from simple theory. In the Centralab work on lifetime discussed earlier, in which cells were made from 0.01-to 10-ohm-centimeter material, open circuit voltages peaked just above 0.6 volt for about 0.1-ohm-centimeter cells.

For 0.01-ohm-centimeter material, even lower voltages (0.56 V) were obtained. Centralab was awarded a contract to investigate the cause of these less-than-expected voltages. They focused on the excess junction current because lifetimes in the material were sufficient to achieve voltages above 0.66 volt. The first area attacked was the elimination of surface leakage currents by oxide passivation. While passivation was successful, no increase in cell voltage was achieved. Therefore, the Centralab work went on to examine other areas that might account for the reduced voltages. Three mechanisms were uncovered that could account for the reduced voltages. These were recombination-generation currents, heavy doping effects, and lifetime gradients in the diffused layer.

As a result of the Centralab work, a grant was awarded to Professors F. Lindholm and S. Li of the University of Florida and to Professor C. T. Sah of the University of Illinois to study recombination centers and heavy doping effects in solar cells. Finally, a comprehensive computer program that could include all of our knowledge was needed. A grant was awarded to Professor J. R. Hauser of North Carolina State University to develop such a program and to test our theories against cell performance.

We are now in the midst of identifying the problems in the low resistivity cell. Progress has been made. We know a little more about open circuit voltages and lifetime and perhaps, also about excess junction currents, but there is much more to be learned. There are many paths to be pursued, and that is part of the purpose of this meeting. Our results will be presented as will be those of others across the country working toward the same goal. A consistent picture will appear as to where we now stand in the quest for a high efficiency cell, and the key outstanding problems will be defined.

REFERENCES

1. Wolf, M.: A New Look at Silicon Solar Cell Performance. Proceedings of the Eighth IEEE Photovoltaic Specialists Conference, Aug. 1970, p. 360.
2. Brandhorst, H. W., Jr.: Silicon Solar Cell Efficiency - Practice and Promise. Proceedings of the Ninth IEEE Photovoltaic Specialists Conference, May 1972, p. 37.

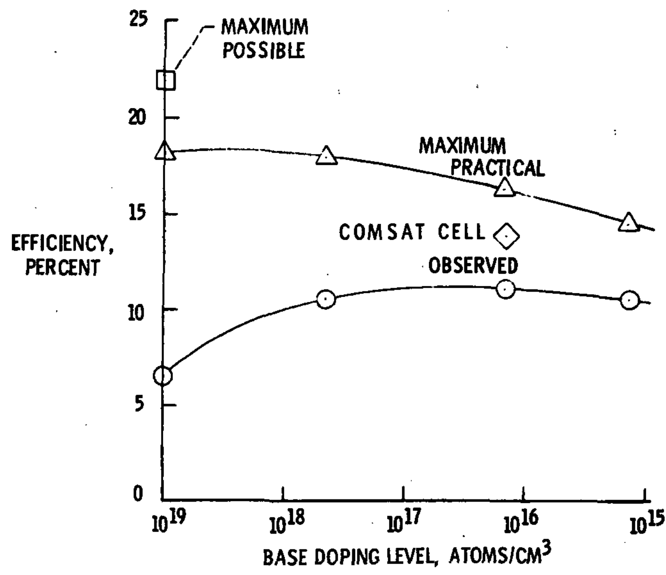

Figure 1. - Calculated efficiencies of silicon solar cells.

RECENT EFFICIENCY IMPROVEMENTS

Review of experimental evaluations of present day solar cells that incorporate design features to increase efficiency

1. THE COMSAT NON-REFLECTIVE SILICON SOLAR CELL:

A SECOND GENERATION IMPROVED CELL*

J. Haynos, J. Allison, R. Arndt, and A. Meulenberg
COMSAT Laboratories
Clarksburg, Maryland 20734

INTRODUCTION

Recently, a highly significant improvement in the efficiency of silicon solar cells has been achieved (1) at COMSAT Labs and the resulting product has been labeled the Violet Cell. The new cell makes use of newly developed (2) anti-reflection coatings of vitreous Ta_2O_5 or Nb_2O_5 which suppress reflection from the front surface as well as is possible for a single layer anti-reflection coating. However, since the coating can be tuned only for a single wavelength, an average residual reflection of 7 percent still persists over the spectral region in which a silicon cell is responsive.

Another approach to the problem of suppression of reflection losses was described (3) in the literature as early as 1960 and subsequently patented (4) by Rudenberg and Dale in 1964. This approach consisted of mechanically forming a large number of tetrahedra onto the surface of the solar cell prior to diffusion. It was claimed that multiple interactions between the surface and the light substantially increased the cell output current. Although some laboratory cells were fabricated to prove the physical principles, no further progress has been reported subsequently.

During the past year COMSAT Labs has independently developed a chemically selective etching process which produces microscopic tetrahedra uniformly over the entire surface of the cell. The process exhibits a high degree of reproducibility and has provided the take-off point for the development of a substantially improved second generation COMSAT solar cell known as the COMSAT Non-reflective (CNR) Cell. The surface geometry, an explanation of the reflection suppression, and the optical and electrical performance of the new cell under simulated space conditions are discussed below.

---

*This paper is based upon work performed in COMSAT Laboratories under the sponsorship of the Communications Satellite Corporation.

Preceding Page Blank

CNR CELL SURFACE GEOMETRY

The chemical etching process produces a surface with a high density of tetrahedra as shown in Figure 1. This is a SEM view normal to the cell surface. One can observe the regularity of the pyramid structure over the section shown and see the apex of the larger pyramids and the outline of the sloping sides and bases. The surface is covered with 10^8–10^9 tetrahedra per square centimeter and the average dimensions are 2 μm in height and 2 μm at the base. Figure 2 represents the same section displayed at an angle of 45° to the normal. Note the regularity and parallelism of the sloping sides.

INTERACTION OF LIGHT WITH SURFACE

An analysis of the enhanced surface absorption and its effect on the generation of carriers is outlined here for a CNR cell and for a conventional cell, both without anti-reflection coating and coverslide. With reference to Figure 3, which represents a schematic of a small portion of the CNR cell surface, light intensity I_o, incident normal to the plane of the solar cell, strikes the side of a pyramid at an angle of incidence of 57°. The reflection coefficient is about 0.33, and therefore $0.67I_o$ is refracted into the silicon at an angle of refraction of about 13° (dependent on wavelength) with respect to the face of the pyramid. The light from the first reflection strikes the face of another pyramid at an angle of incidence of 9°. At this second surface 67 percent of the intensity is refracted into the silicon at an angle of refraction of about 2.5° with respect to the face of the pyramid. The result of this double reflection is that an incoming beam of intensity I_o enters the solar cell in two parts: 1) a beam of intensity of $0.67I_o$ at an angle of about 44° from the normal to the cell, and 2) a beam intensity $0.22I_o$ at an angle of about 69.5° from the normal to the cell.

Light is attenuated in an absorber according to Beer's Law, which is

$$I = I' \ell^{-\alpha x}$$

where I is the intensity after light of intensity I' has traveled a distance x in a medium of absorption coefficient α. In the case of the first refracted beam, if the penetration depth of the light in the direction of refraction is x, then the penetration depth, d, in the normal direction is given by d = x cos 44°. Similarly, in the case of the second refraction, the distances x and d are related by d = x cos 59.5°.

Substituting for x in Beer's Law, we find, for the total intensity as a function of d after two refractions, the expression

$$I = 0.67I_o \ \ell^{-1.39\alpha d} + 0.22I_o{}^{-1.97\alpha d} \ .$$

The generation rate of carriers is proportional to the first derivative of the intensity with respect to d, or

$$g \sim -0.93\alpha I_o \ \ell^{-1.39\alpha d} - 0.43\alpha I_o \ \ell^{-1.97\alpha d} \ .$$

By way of contrast, for the case of light incident on a smooth surface, the carrier generation rate is given by

$$g \sim -0.67\alpha I_o \ \ell^{-\alpha d} \ .$$

The generation rates, in arbitrary units, are shown in the graph of Figure 4 for light of 1-μm wavelength for which α has the value of 64 cm^{-1}. Note the strikingly enhanced generation rate in the surface owing to the reduction of reflection loss and to the increased optical path length in the cell.

REFLECTANCE CHARACTERISTICS

Reflectance was measured on an apparatus consisting of a double beam, ratio recording, UV spectrophotometer equipped with an integrating sphere attachment. Figure 5 shows the highly significant reflection attenuation of the bare CNR surface compared to a polished silicon surface. The reflectance curves in Figure 6 were generated after these surfaces were coated with a one-quarter wavelength thickness of Ta_2O_5 and covered with 6-mil fused silica. They show the decided advantage of a CNR surface in that the reflectance is about 3 percent and quite independent of wavelength over the entire region of cell response. In contrast, the reflectance from the polished surface with a well-tuned single layer of AR coating is so high at the short and long wavelength ends of the spectrum as to represent an average reflection loss for sunlight of about 7 percent.

ELECTRICAL CHARACTERISTICS

In the present state of development the CNR cell exhibits current-voltage characteristics under simulated AM0 solar radiation as shown in Figure 7. The figure includes comparative plots for typical flight tested Violet and conventional (circa 1970) solar cells of the same size (2 x 2 cm). The increase in current and power output of the CNR cell with respect to the Violet Cell is attributable primarily to the increased light absorption. The maximum power output of the best cells to date is 86 mW, corresponding to an efficiency of 15.3 percent (Johnson spectrum, total area). It is of interest to note that, for terrestrial use, these cells exhibit an efficiency

of over 20 percent. Further improvement is anticipated with continued development.

RADIATION CHARACTERISTICS

Figure 8 represents a plot of maximum power output versus 1-MeV electron fluence for the same three classes of cell. Note that the relative power output advantage of the CNR cell relative to the Violet Cell and to the conventional cell persists over the entire range of fluences studied. The CNR cell power output after exposure to a fluence of $3 \times 10^{14}/cm^2$ (equivalent to a 7-year exposure at synchronous altitude) is equivalent to that of the Violet Cell at beginning of life.

SPECTRAL RESPONSE

Figure 9 is a plot of spectral response for the same three classes of cell before irradiation. It is interesting to note that the CNR cell response has been improved over the entire solar spectrum as would be expected. The spectral response of the same cells after exposure to a 1-MeV electron fluence of $2 \times 10^{15}/cm^2$ is shown in Figure 10. Note that the Violet Cell and conventional cell have degraded at this fluence to the same extent for wavelengths above 0.85 μm, whereas the CNR cell retains its advantage even over this spectral region. This effect is a result of the lengthened light paths in the CNR cell as compared to cells with a smooth surface.

CONCLUSIONS

A major change in the surface geometry of the silicon solar cell has improved the light absorption characteristics with consequent substantial improvement in the power output. The reflection characteristics are unaltered by ionizing radiation and the improvement in the red response resulting from the altered light paths is less susceptible to radiation damage than in the case of smooth surfaced cells. In view of the importance of the end-of-life performance, the CNR cell represents an advance over the Violet Cell comparable to that of the latter relative to the conventional cell.

ACKNOWLEDGMENTS

The authors wish to thank Dr. E. S. Rittner for his support and encouragement of this work, and J. Reynolds, A. Busch, D. Martin, F. Bland, and D. Perry for their assistance.

REFERENCES

1. J. Lindmayer and J. Allison, "The Violet Cell: An Improved Silicon Solar Cell," COMSAT Technical Review, Vol. 3, No. 1, Spring 1973, pp. 1–22.

2. A. Revesz, "Vitreous Oxide Antireflection Films on High Efficiency Solar Cells," 10th Photovoltaic Specialists Conference, November 1973.

3. B. Dale and H. Rudenberg, "High Efficiency Silicon Solar Cells," 14th Annual Proceedings—Power Sources Conference, May 17–19, 1960.

4. H. Rudenberg and B. Dale, U.S. Patent 3,150,999, September 29, 1964.

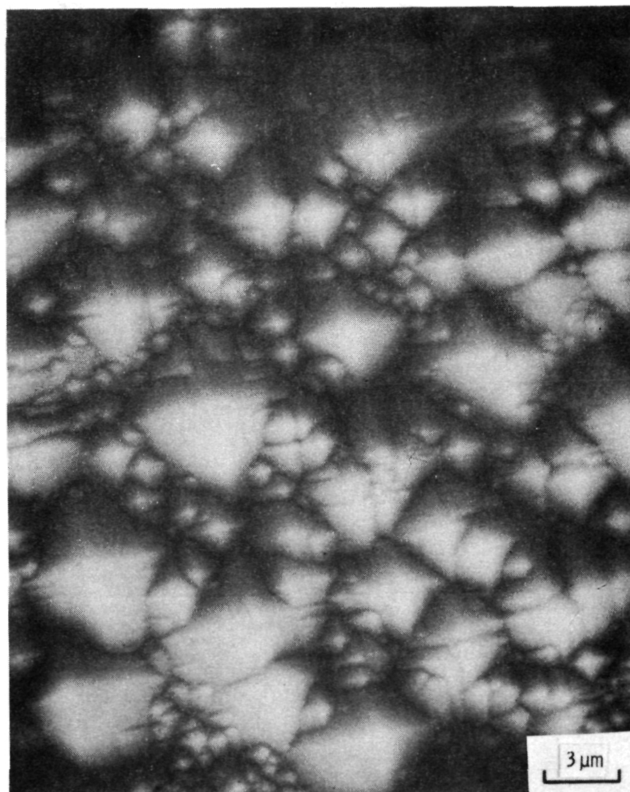

Figure 1. - SEM photomicrograph of normal to CNR surface.

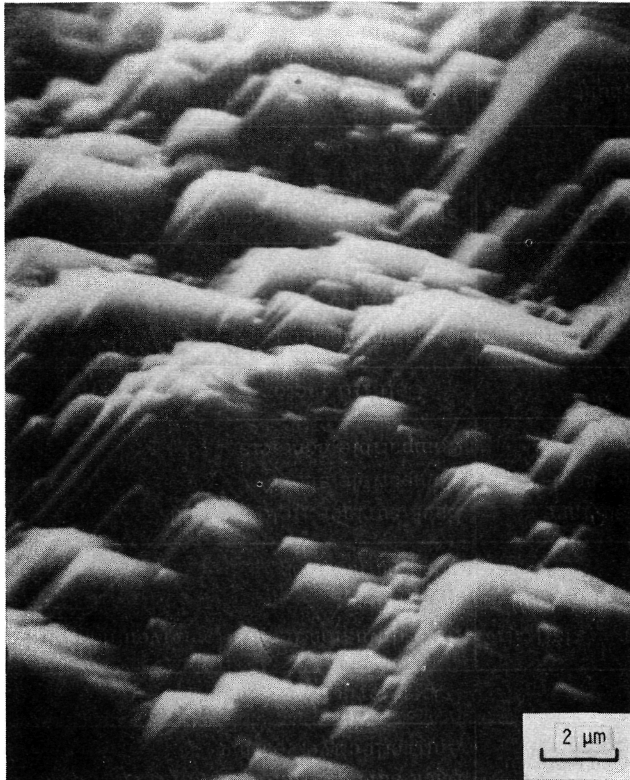

Figure 2. - SEM photomicrograph of CNR surface at 45° to normal.

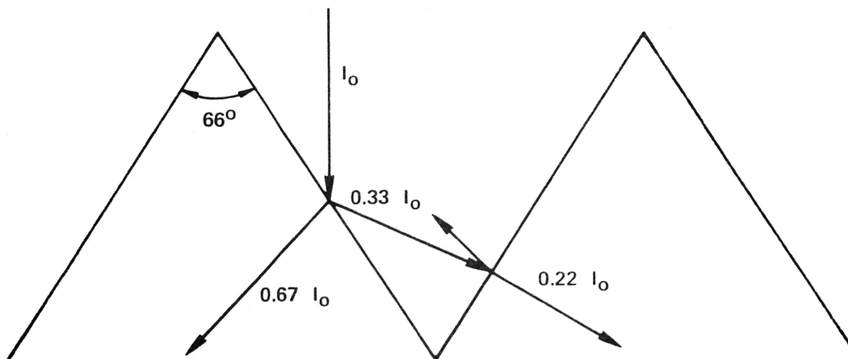

Figure 3. - Optical path schematic of CNR tetrahedral surface.

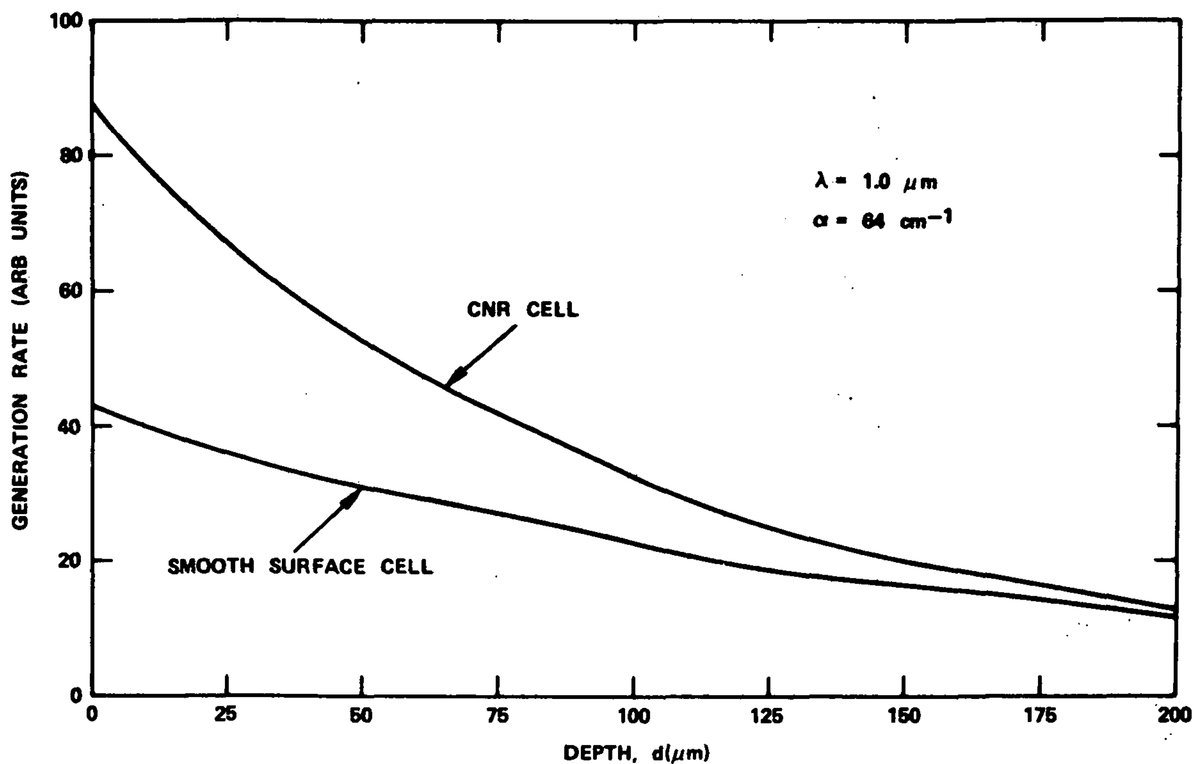

Figure 4. - Generation rate for 1.0-μm wavelength light as a function of light penetration depth.

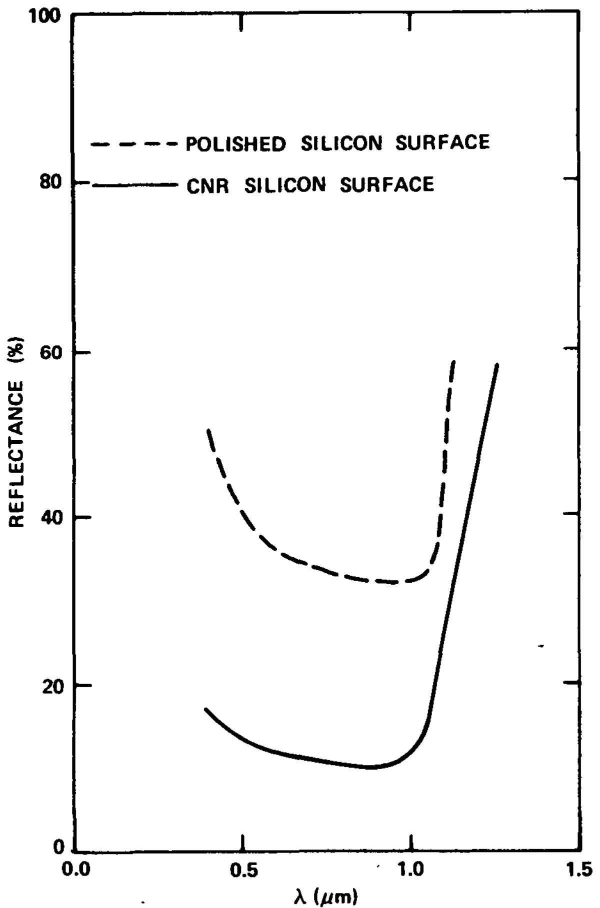

Figure 5. - Reflection as a function of incident light wavelength for polished and tetrahedral surface on bare silicon.

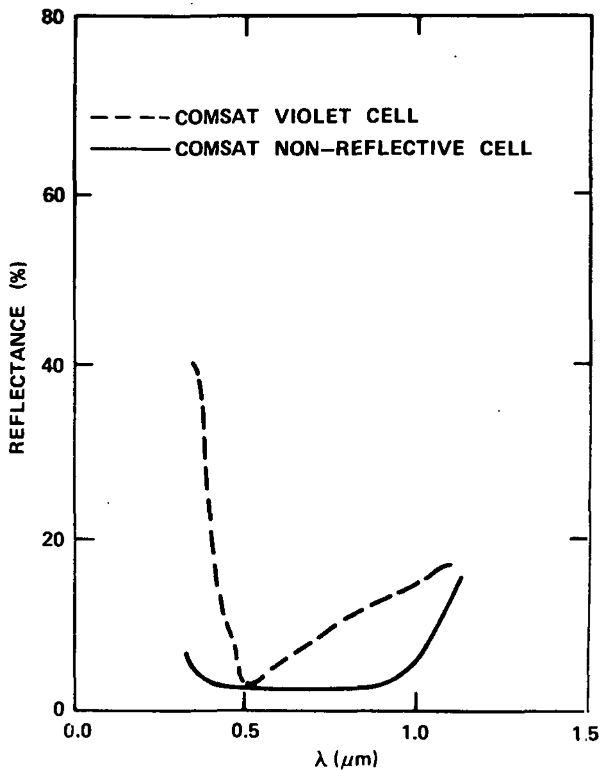

Figure 6. - Reflection as a function of incident light wavelength for covered violet cell and CNR cell.

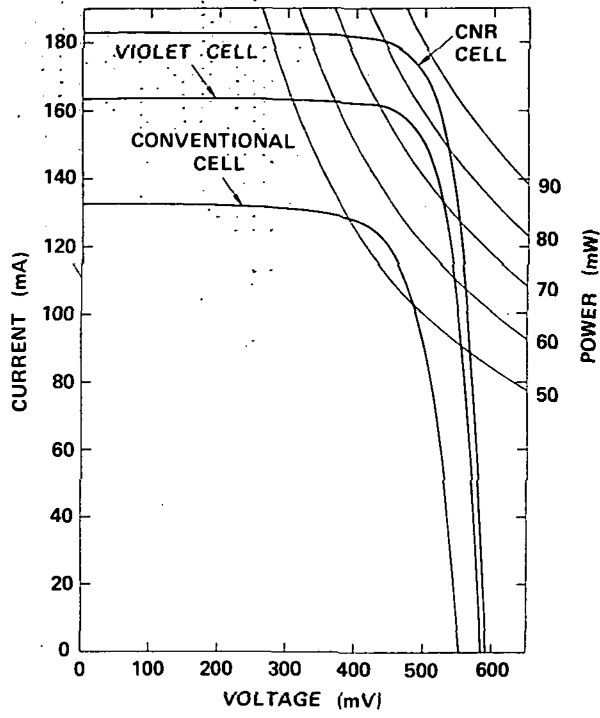

Figure 7. - Current-voltage characteristics of CNR, violet, and conventional cells under AMO illumination.

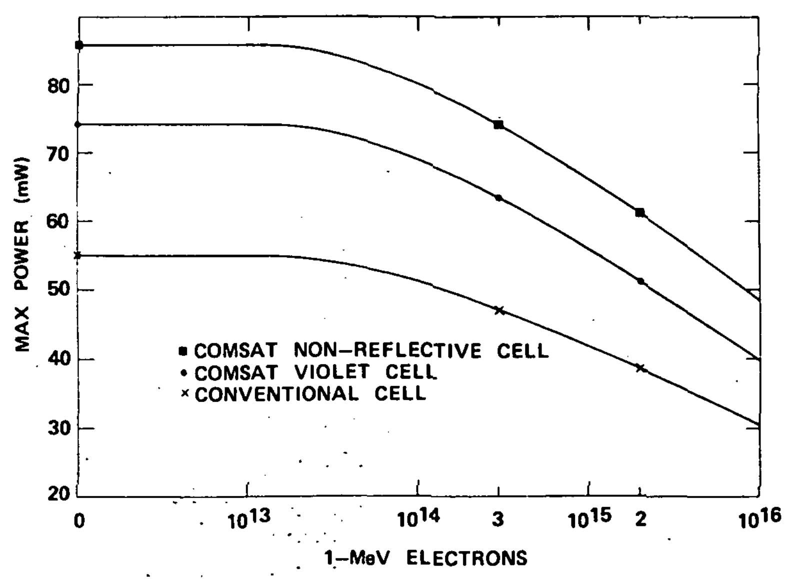

Figure 8. - Maximum power output as a function of 1-MeV electron irradiation fluence for CNR, violet, and conventional cells.

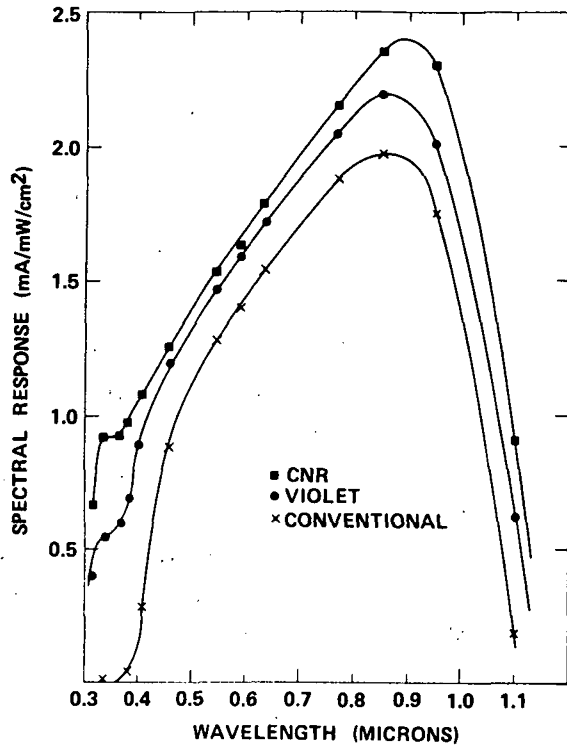

Figure 9. - Relative spectral response of CNR, violet, and conventional cells.

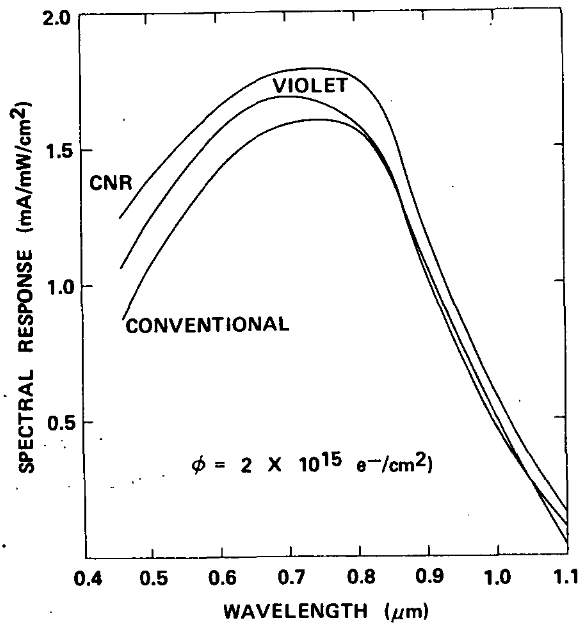

Figure 10. - Relative spectral response of CNR, violet, and conventional cells after a fluence of $2x10^{15}$ e/cm^2.

2. HIGHER EFFICIENCY FOR LESS MONEY

Joseph Lindmayer and Charles Wrigley
Solarex Corporation
Rockville, Maryland

Our aim at Solarex is to achieve the greater efficiency for the least cost. This requires a continual examination of approaches, especially in terms of reproducibility in yield in mass production. Efficiency is controlled to a large extent by defect states. Optical problems are not significant in efficiency since optical couplings can now be achieved quite well. For example, anti-reflection coating, graded index coating, surface texturing, etc. reduce reflection to an almost negligible value.

A large investment is not the main point for remaining changes in optical properties. A single coating alone produces an optical coupling of approximately 94%. Texturing of the front surface is useful if done in a cost effective manner. We are pursuing this approach and results are shown in our recent NSF quarterly report. Terrestrial cells do not require costly polishing techniques and the final surface texturing employed must be economical in achieving high efficiency. Efficiency areas limited by defect states are the following:

1. Damage to the front surface of a solar cell, which can be minimized by introducing less than 10^{15} impurities per square centimeter.

2. Defects throughout the bulk of silicon wafer, which control the lifetime of photogenerated carriers.

3. The back contact to the solar cell needs a high-low junction with a low defect state density to keep the surface recombination velocity low, that is, it should not introduce additional damage to the crystal while providing a retarding field.

4. Amorphous and polycrystalline forms of silicon are essentially manifestations of high densities of defect states. In the single crystal, the defect state density varies widely (Cz, float zone, etc.). Formation of junctions for the fronts and backs of solar cells can utilize any of a raft of possible

diffusion techniques, but the resulting defect state density can vary violently depending on technique. For example, it is extremely difficult to predict that a 830°C phosphorous diffusion will result in a particular number of states. Frequently, it is not the impurities per se which introduce the defects, as much as the control of the processing caution required; for example, in removing borosilicate glasses in microelectronic wafer processing before drive in. That alone is not sufficient, but helps to alleviate the problem.

5. It is not the purpose of this talk to relate magic formulas for cell processing. We are working on efficient terrestrial cells and also working under NSF grants to take a broad look at sources and mechanisms of efficiency degradation and attack each one in turn. We all need a much better depth and breadth of understanding. One, of course, prefers a set of processing procedures producing large areas with low defect densities and high reproducibility. We are presently working on a broad-range type of parameter tolerant process. It would also be desirable to avoid the use of batch type processing, such as in vacuum systems because of cost factors.

The output current of a solar cell is basically a measure of defect densities, ultimately approaching 55 mA/cm^2. The cell photovoltages also are of interest to us because they are much lower than they could be. We have formulated a general relationship and are studying the implications of such modeling. We have, as a start, the front and rear surface recombination velocities, bulk doping, and impurity profile. For light bulk doping, the cell benefits from the contribution by the low-high junction and the contribution from photogenerated carriers flooding above the doping level, which help to keep up the photovoltage at lighter doping levels.

At moderately heavy doping levels (.1 ohm cm p-type for example), the bulk lifetime decreases. The bulk contribution

to reverse diffusion current decreases but the front junction reverse current cannot then be ignored. The front is controlled by the lifetime of the diffused layer and the surface recombination velocity produced by introducing the impurity profile.

It appears that going toward intrinsic crystals rather obviously produces control of the photovoltage by carrier flooding and the high-low junction, with the net result of less than 600 mV. Going to heavier doping, the front takes over and it has the potential to control improvement. However, the particular impurity profile and the defect states introduced will control the photovoltage.

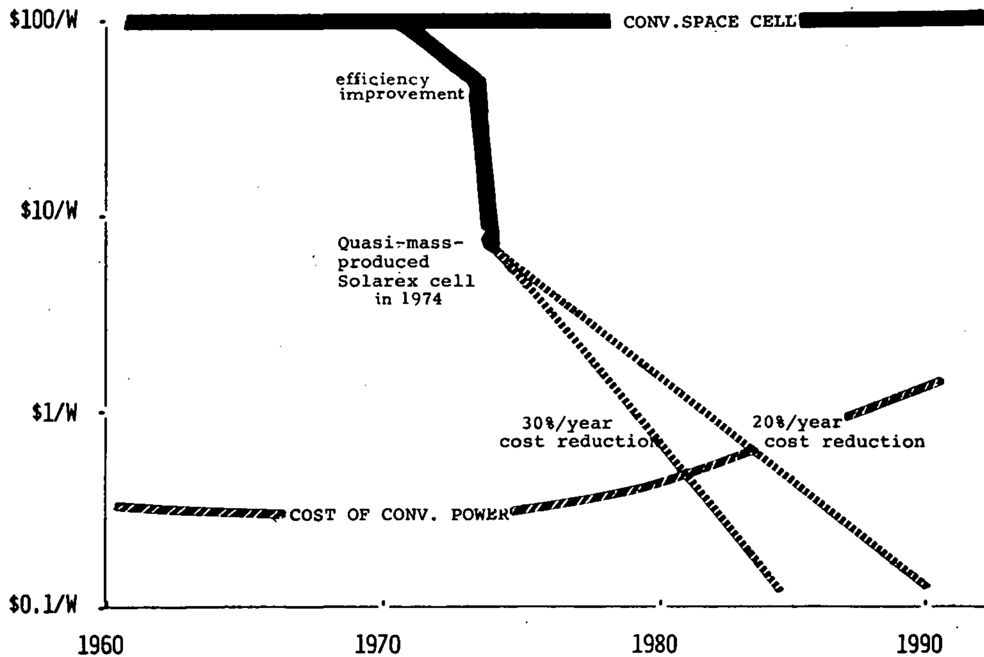

Figure 1. - Cost of solar cells as function of time at Solarex. Conventional space solar cells cost approximately $100/W. Solarex has reduced the cost to levels below $10/W in 1974. A continued cost reduction program is indicated by the 20% and 30%/year cost reduction lines. The cost of conventional power is intercepted between 1980 and 1990.

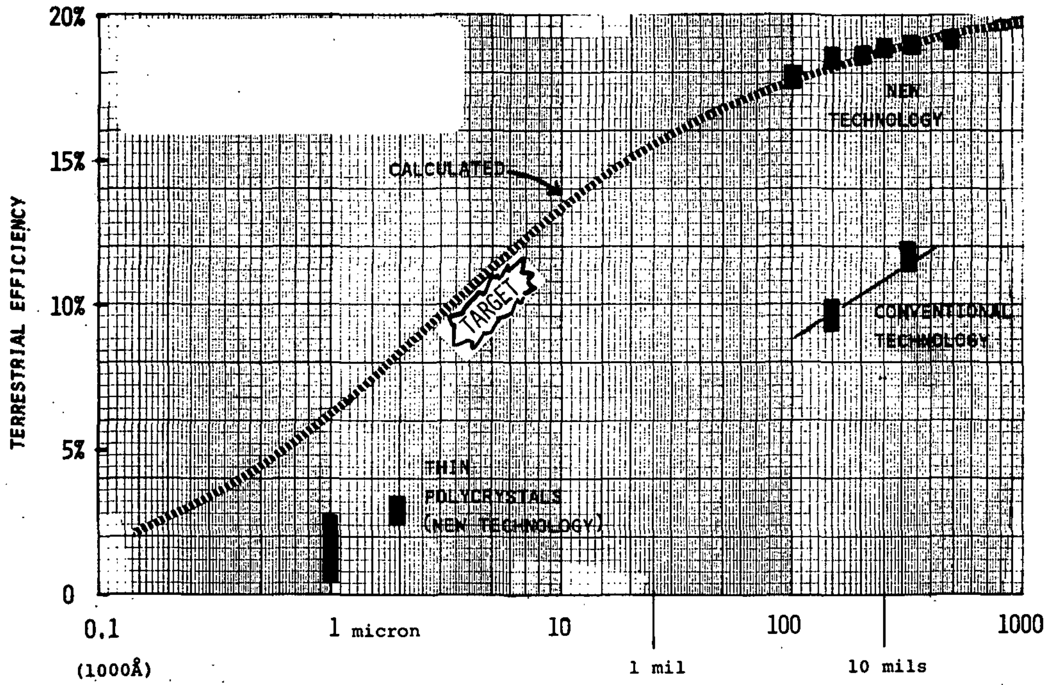

Figure 2. - Maximum efficiency as function of thickness.

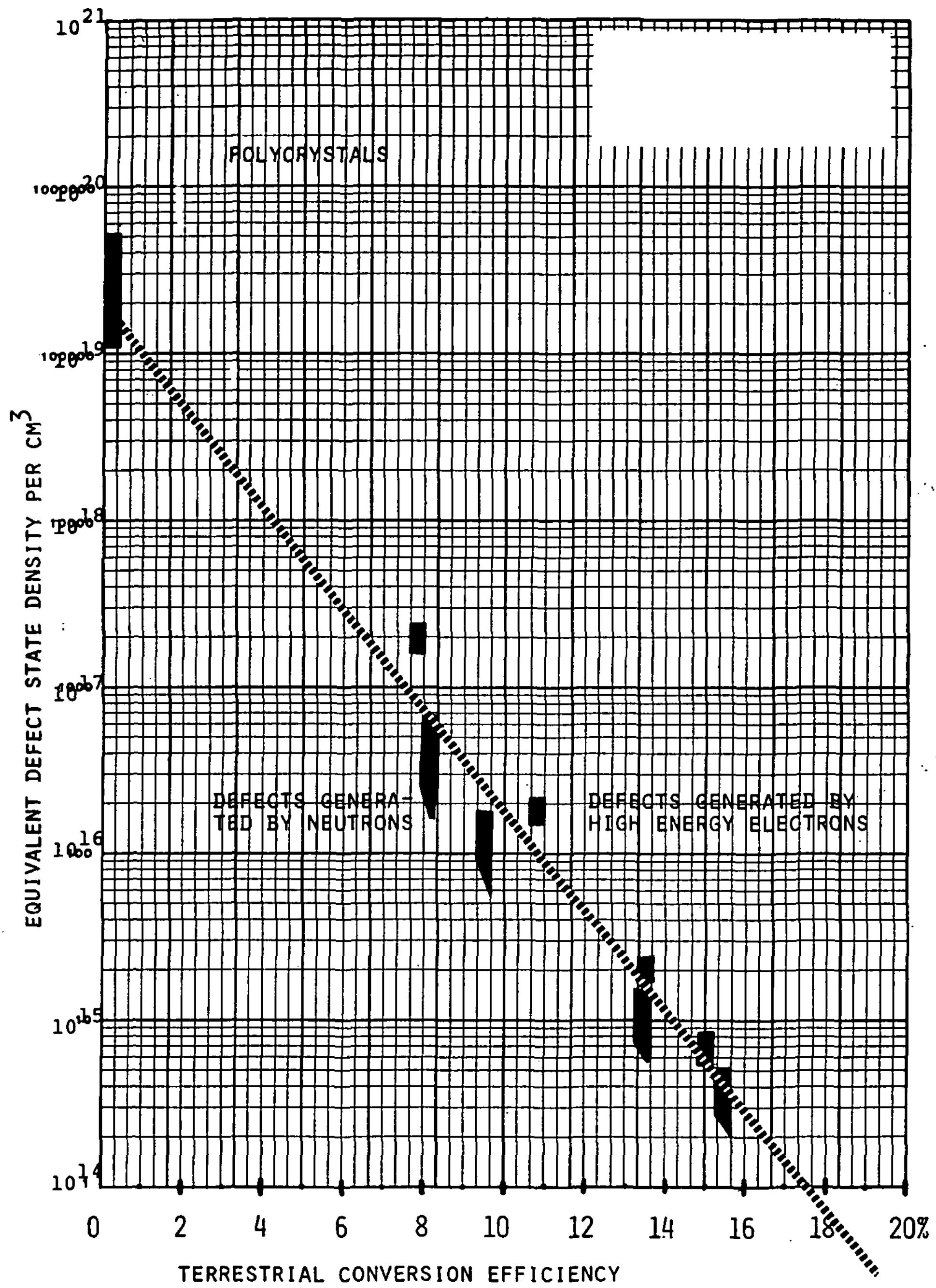

Figure 3. - Crystallographic order requirements for efficient conversion.

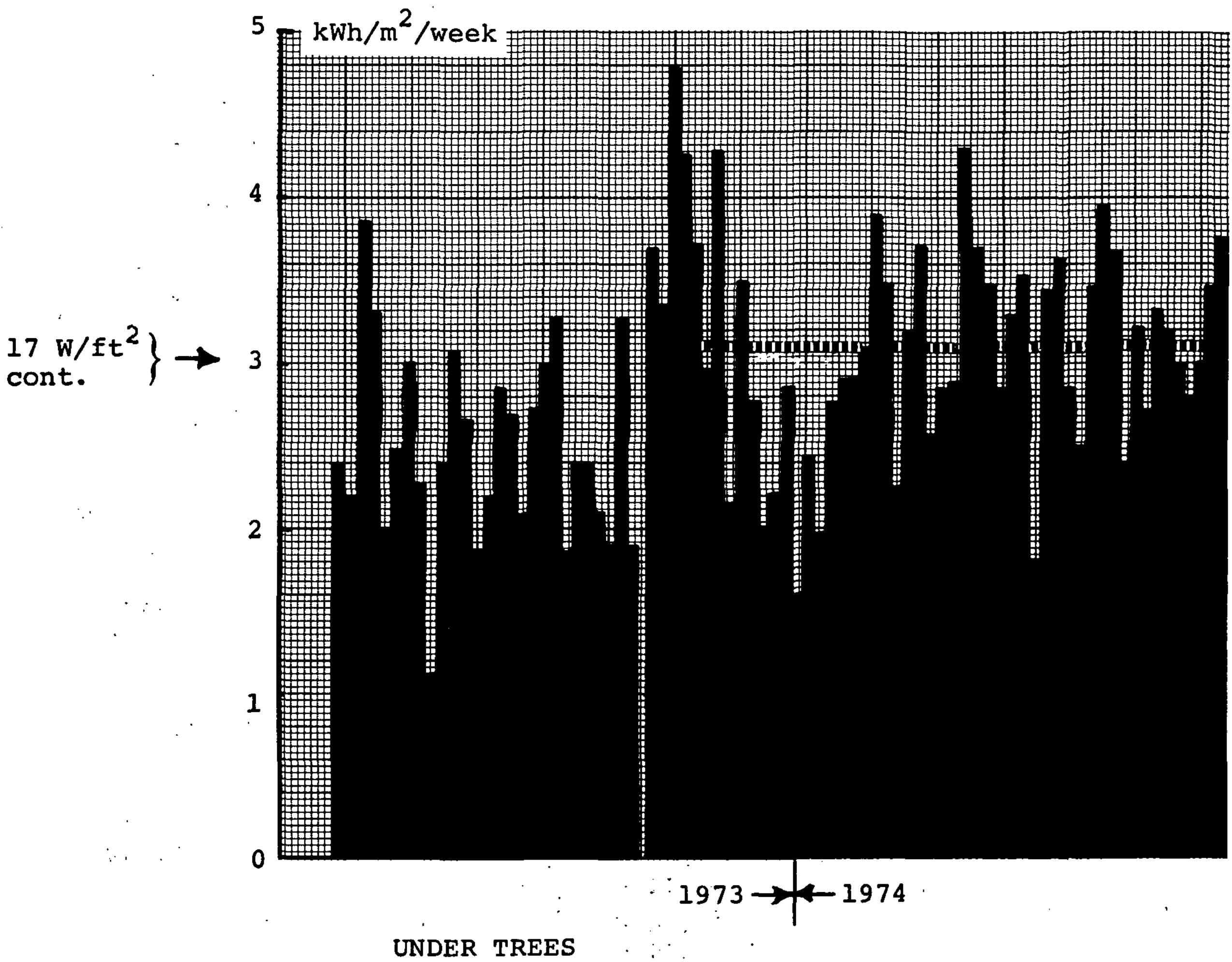

Figure 4. - Terrestrial insolation data for the Washington area. Weekly sums; 10% solar cells.

3. PROCESS TECHNOLOGY FOR HIGH EFFICIENCY SOLAR CELLS

Peter A. Iles
Centralab Semiconductor
El Monte, California

In the past few years, significant increases in silicon solar cell output have been achieved in laboratories. These increases included enhanced bulk (back surface field) cells, violet cells and the non-reflective modification of the violet cell. Work is also in progress to combine these techniques.

Because of the high interest of potential users, there are intense efforts to extend these research advances into large scale manufacturing methods.

On surveying the process technology, there are several requirements which are common to all the high output cells. These common requirements include:

a) growth of high quality large crystals with suitable slicing and surface finishing

b) formation of shallow PN junctions, with good silicon properties both in the diffused layer and in the bulk region

c) application of high conductivity contacts in a fine, multiline pattern, with good adhesion and no degradation of PN junction properties

d) application of an antireflective coating with good transmission over the whole wavelength range useable by silicon

In addition there are special requirements such as:

i) for enhanced bulk cells, a back surface field must be well established without affecting other cell properties

ii) violet cells require extremely shallow junctions with a correspondingly higher grid line density

iii) the non-reflective cells require special surface texturing and added care in contact application

On evaluating the increases in the main I-V parameters (Isc, Voc and CFF), all advanced cells have higher CFF, enhanced bulk cells gain in long wavelength response and Voc, violet cells gain mainly in the short wavelength Isc, while the non-reflective cells gain in Isc across the spectrum.

The production process sequence must achieve the required advantages of a particular cell design, and must also satisfy most of the user needs. Thus the process is chosen for best trade-off between output, environmental performance (including radiation) and detailed user needs, especially cost and delivery schedule. Careful cooperation between cell manufacturers and users, with feedback on test results, is helping to complete an iterative approach to the best blend of methods.

Turning to the future, it is possible that these advanced cells may converge to produce the highest Isc and CFF values. Thus it may be useful to work on optimum process methods which can adapt to a range of high output cells, e.g. work on improved methods to apply precise, fine line patterns with low cost.

Of the I-V parameters, Voc offers the most chance of additional increase but work is needed to increase Voc while maintaining other cell properties, such as short wavelength response and high radiation resistance.

The present period is full of promise and challenge for cell manufacturers.

TABLE I. - PHOTOVOLTAIC PARAMETERS FOR ADVANCED CELLS

[4-cm^2 cells; 28° C; AMO illumination.]

Cell type	ρ, Ω-cm	I_{SC}, mA	V_{OC}, mV	CFF	P_{max}, mW	η, percent
Conventional	10	144	550	0.73	58	10
	2	142	600	.75	63	11
Intermediate	10	154	550	0.76	64	12.5
Enhanced bulk	10	160	600	0.76	73	13
Violet	2	165	590	.78	76	13.5
Advanced violet	2	183	590	.79	85	15

TABLE II. - PROCESS NEEDS FOR PV PARAMETERS

Parameter	Process needs
Short circuit current	
Active area goal of 95 percent	Evaporation masks Photoresist Silk screens Preformed patterns
Increased short λ	Shallow diffusion Surface shaping Good antireflective coating (low α, n ~ 2.2) Multilayer antireflective coating
Increased long λ	High diffusion length for given dopant concentration (plus diffusion control) Back surface field cell (several methods) Antireflective coating
Open circuit voltage	
Lower resistivity (to ~1 ohm-cm)	High diffusion length for given dopant concentration Good pn junction
Back surface field technology	Back surface field methods Compatible short λ Compatible contacts
Cell fill factor	
Low saturation current	Good pn junction Good shallow layer Minimum stress
Low series resistance	Sheet resistance control Many grid lines of good conductivity
Low shunt leakage	Ingot surface control Compatible contacts and coating

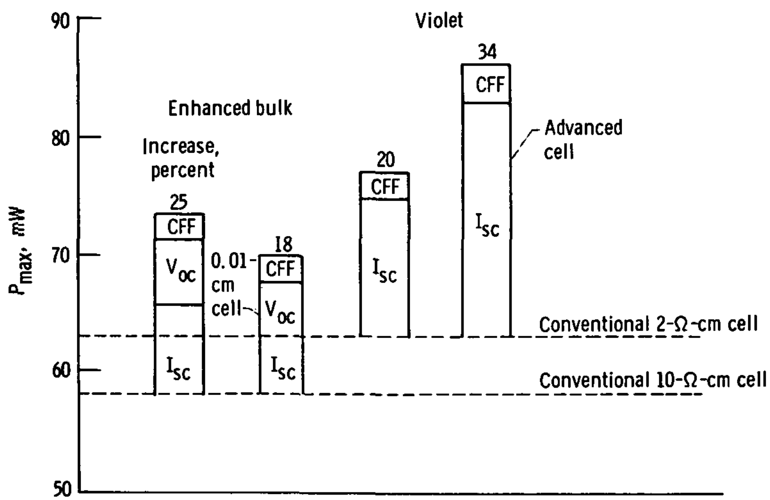

Figure 1. - Breakdown of P_{max} increases.

4. VOLUME PRODUCTION OF ADVANCED SILICON SOLAR CELLS

John A. Scott-Monck and Paul M. Stella
Spectrolab
Sylmar, California

Recent advancements in technology have generated pressure on the solar cell manufacturer to produce more efficient solar cells.[1,2] This paper describes the methodology used to transfer these improvements from the laboratory to the factory. It will also briefly describe some of our own advanced development aimed at producing a more useful cell for space applications.

During the past ten years the power output of the typical production cell has been relatively static, and most processes have remained constant. This stability has allowed a great deal of information to be accumulated on the cell's performance under a variety of mission environments. Thus a degree of confidence in its reliability has developed. The experience gained by the manufacturer has steadily reduced cost. Any "new" cell must show that it can meet previous reliability standards and be competitive in cost.

With these requirements as a baseline we undertook to understand and evaluate the changes necessary to produce advanced cells. A breakdown of those elements influencing short circuit current is contained in Figure 1. The standard cell is compared against two types of advanced cells, field and hybrid, now in production. The hybrid is an extension of basic technology while the field cell represents a more dramatic departure from cell fabrication methods. An estimate of future improvements in these cells is also included.

---

1. J. Lindmayer & J. Allison, Conf. Rec. Ninth Photovoltaic Specialists Conf., Silver Spring, Maryland (1972)

2. J. Mandelkorn & J. Lamneck, Jr., Conf. Rec. Ninth Photovoltaic Specialists Conf., Silver Spring, Maryland (1972)

The diffusion process is the key to the high efficiency space cell. Other process changes must be made in order to retain the increased short wavelength response and avoid compromising cell curve shape, both affected by the diffusion. Significant improvements were made by adjusting diffusion parameters, but not processes.

Reducing the junction depth by a factor of two required a sophisticated contact configuration to minimize series resistance effects. Although photoresist techniques can produce more refined contact patterns we chose to retain the conventional metal mask evaporation process on the basis of reliability and cost. This caused some reduction in the cell active area but still gave respectable curve shape.

There are high temperature (500-600°C) processes that the cell must experience after contact metallization. In the case of shallow junctions there is a high probability that contaminants contained in the titanium interface layer will migrate through the junction and reduce power output.[3] The laboratory approach eliminated titanium, but reliability considerations led us to change process sequences, even though this added cost, in order to retain the titanium-silver system.

Conservation of short wavelength response demanded an optical stack, AR coating and filter, that had optimized transmission characteristics. It was necessary to replace silicon monoxide with tantalum pentoxide (Ta_2O_5). The improved transmission in the region below 600 nM coupled with its higher refractive index made this an attractive choice. This was a major change in processing, requiring new equipment and a concentrated development effort to derive a reproducible process.

3. J. Lamneck, Jr. et. al. Conf Rec. Ninth Photovoltaic Specialists Conf., Silver Spring, Maryland (1972)

Once this was achieved the Ta_2O_5 coatings were rigorously tested to the same standards as silicon monoxide. Since a manufacturing facility does not have access to the more sophisticated analytical equipment possessed by other organizations, we provided samples, made under production conditions, for customer evaluation. At this time there is no evidence that Ta_2O_5 cannot perform as well or better than the conventional coating used previously.

A new cut-on filter was developed by the supplier for the advanced cells. The choice of the cut-on wavelength was conservative and based on reliability considerations. Since the Ta_2O_5 coating is a better optical match to coverglass, the completed assembly shows an improvement in output. Figure 2 shows a physical characterization of the new cell types compared to the conventional product.

The field cell was theoretically predicted a number of years ago[4], but it has only been recently reduced to practice[2]. The field is developed by creating a majority carrier gradient at the back surface of the cell which prevents recombination of light generated minority carriers at the back contact. This results in a significant increase in the long wavelength response (>700 nM) of the cell. Since the field tends to increase the effective minority carrier diffusion length it has a greater impact on thinner cells because the effective diffusion length can become much greater than the cell thickness. Although not completely understood, field cells also possess much higher open circuit voltages which are almost independent of the bulk resistivity.

Two techniques for creating the field have been demonstrated; diffusion from a source layer of evaporated aluminum and diffusion of boron using conventional methods. The former technique is much

4. M. Wolf, Proceedings IEEE, Vol. 51, No. 5, May (1963)

less complicated and can be done at relatively low temperatures (750-800°C) which aids in the preservation of the existing minority carrier lifetime. Since there is little difference in cell output using either process, we employ the aluminum diffusion technique.

Common facilities are used to manufacture both advanced cells. Although the field cell requires additional processing steps, their sequence has been arranged to fit the basic line flow. Presently all three cell types are being manufactured simultaneously with advanced cells making up over fifty percent of production. Advanced cells with average efficiencies in excess of 12.5 percent are now being produced in quantity.

We feel that the field cell holds the greatest potential for growth. Unlike the hybrid, the field cell can provide high initial power independent of both its thickness and base resistivity. Figure 3 shows a 0.1 mm (.004") thick field cell made from 100 ohm-cm material compared to a hybrid cell of the same thickness and resistivity. Efficiencies in excess of twelve percent have been achieved from 0.1 mm high resistivity field cells. There is some theoretical grounds for predicting that this cell might show superior behavior under radiation and we hope to test this in the near future.

ELEMENT	STANDARD	HYBRID		FIELD	
		1974	FUTURE	1974	FUTURE
DIFFUSION	102-105 mA	108-112	110-114	108-110	110-114
P+	-	-	-	4-6	6-8
CONTACT CONFIGURATION	-	1-2	2-3	1-2	2-3
AR COATING	40-42	42-44	44-46	44-46	46-49
COVER	(5)-(2)	2-3	3-5	2-3	3-5
TOTAL CURRENT (mA)	137-145	153-161	159-168	159-167	167-179

Figure 1. - Key cell parameters. 10 ohm-cm 2x2 cm N/P.

	STANDARD	HYBRID	FIELD
MATERIAL	C.G.	C.G.	C.G.
PREPARATION	CHEM ETCH	CHEM ETCH	CHEM ETCH
DIFFUSION DEPTH	3000-3500 Å	1200-1600 Å	1500-2000 Å
P+	NO	NO	YES
CONTACT MATERIAL	Ag-Ti-(Pd)	Ag-Ti-(Pd)	Ag-Ti-(Pd)
CONTACT CONFIGURATION	.040 ohmic 6 x .006 grids	.020 ohmic 18 x .002 grids	.020 ohmic 14 x .002 grids
AR COATING	SiO_x	Ta_2O_5	Ta_2O_5
ADHESIVE	R6-3489	DC93-500	DC93-500
COVERGLASS	7940 FUSED QUARTZ	7940 FUSED QUARTZ	7940 FUSED QUARTZ
U.V. FILTER	.41μ	.35μ	.35μ

Figure 2. - Cell physical characterization.

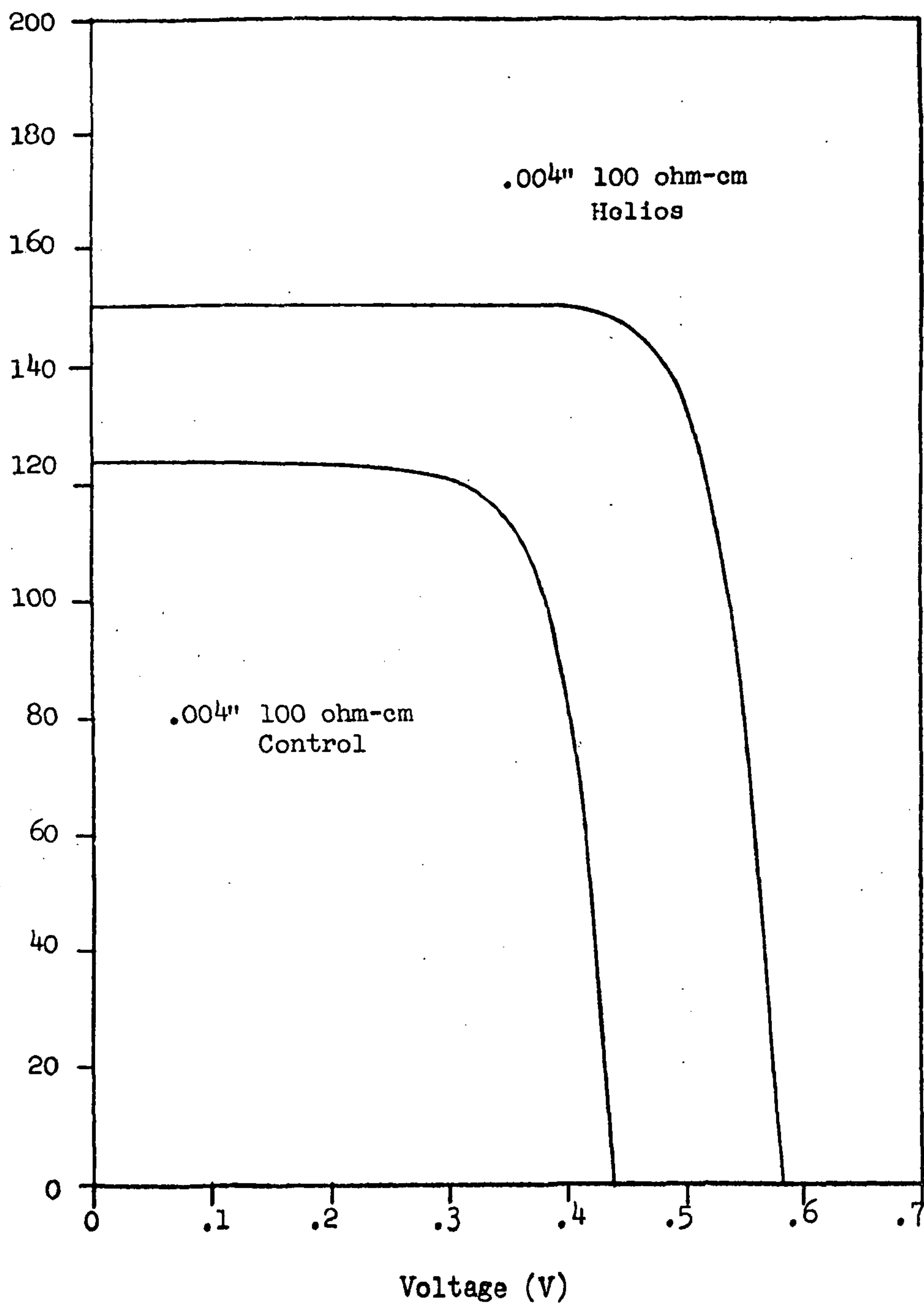

Figure 3. - Advanced development cell.

5. PERFORMANCE OF ADVANCED SILICON SOLAR CELLS IN A SPACE ENVIRONMENT†

Ronald W. Opjorden, Leland J. Goldhammer, and George S. Goodelle
Hughes Aircraft Company
El Segundo, California

INTRODUCTION

Significant improvements in cell efficiency have been obtained with laboratory or limited production quantity solar cells (for example, the Comsat Laboratories "violet" cell); the problem has been to mass-produce improved efficiency cells. In May 1973, therefore, a program was initiated and directed by Hughes Aircraft Company in cooperation with the Heliotek Division of Textron Electronics, Inc., and Optical Coating Laboratory, Inc. (OCLI), to develop and qualify a higher efficiency solar cell and cover(s) that would be available in production quantities in 15 months. The initial objective of this program was to produce a cell with 15 percent more power at beginning of life than the conventional cell.

Development of such a cell that could be manufactured in production quantities required the following:

1) An extensive test program
2) The use of proven, cost effective manufacturing processes
3) The incorporation of cell improvements that offered the greatest potential performance gains but were also based on existing technology.

The program was a success in demonstrating the performance of advanced cells in a space environment, and its end results were in effect two cell types, designated by Hughes as the intermediate and high efficiency solar cells; both included Heliotek and OCLI 0.35 μm covers. The intermediate cell has the same grid structure and cell blank as the conventional cell and incorporates only optical stack improvements. Flight production intermediate cells exhibit a performance gain of 10 percent over that of the standard cell. These cells have been received by Hughes from Heliotek in quantities of 6000 equivalent 2 x 2 cm cells per week beginning in August 1974.

The high efficiency cell, the end product of the full development program, uses a new optical stack, a shallow diffused junction, high base resistivity material, and back surface field technology; it has a 21 percent power gain,

---

†Presented by Edwin Stofel, Hughes Aircraft Company.

*All power numbers given in this paper relate to average production lot power at specification voltage for 2 x 2 and 2 x 6.2 cm solar cells; i.e., actual maximum power is higher.

Preceding Page Blank

beginning of life, compared with the state-of-the-art solar cell. It is being received in the same production quantities and rates as the intermediate cells.

Thus, in developing solar cells that demonstrably exceed present cell performance, are amenable to mass production processes, and are deliverable in production quantities, the program has exceeded its initial goals. This paper describes these cells and the test programs for their qualification.

CELL DESCRIPTION

Basically, the high efficiency cell (Figure 1) is a shallow diffused n/p cell with a p^+ back surface field and a 20Ω-cm base resistivity. The shallower n region results in an increase in the I_{sc} of the cell because of the increased spectral response in the blue wavelengths (0.35 to 0.5 μm). The cell has a narrower bar (0.064 cm) AgTiPd contact with solderless grids. The number of grid lines has been increased to compensate for the higher sheet resistivity of the shallower diffused layer (seven grid lines per centimeter versus three for the standard cell) so that the current output of the cell at the maximum power voltage is optimized. The grids are vapor deposited by means of mechanical shadow masking, as is the case with the conventional cell; shadow masking was used rather than a photoresist technique because it permitted the use of existing production technology, without necessitating a long period of process development.

To further increase output, both types of cells use an antireflective coating of Ta_2O_5 rather than SiO_x. Ta_2O_5 has an index of refraction better matched to that of the coverslide adhesive (Dow Corning 93-500), resulting in an increase in the I_{sc} of the solar cell after the cover has been applied, rather than the loss characteristic of the conventional cell. Furthermore, coverslides with a lower cutoff UV filter (0.35 versus 0.41 μm) are used, so that most of the increase in output due to the increased spectral response of the cell in the region below 0.41 μm can be utilized.

The high efficiency cell also has a back surface field, or p^+ region, located underneath the back contact of the cell. This p^+ layer is a highly doped region of the same conductivity type as the bulk material; the resulting gradient of the doping between this region and the bulk material region results in an additional increase in I_{sc} and V_{oc}.

The intermediate cell incorporates the 0.35 μm cover cutoff, Ta_2O_5 antireflective coating, and DC93-500 cover adhesive; in all other respects it is the same as the standard cell. Characteristics of the three cells are compared in Table 1; their structural differences can be see in Figure 2. Figure 3a presents "average" production lot I-V curves for a 2 x 6.2 cm conventional cell, a 2 x 6.2 cm intermediate cell, and a 2 x 6.2 cm high efficiency cell; Figure 3b shows the I-V curve for a high grade 2 x 6.2 high efficiency production cell and indicates what might be expected from the cell with further production experience. Data presented are based on X-25 test at 25°C and are traceable to new balloon flight primaries.

TEST PROGRAM

To qualify the cells for production, numerous tests were run, especially in the areas of particulate and UV radiation. Table 2 summarizes the scope of the test program; two of the tests — the UV and the electron irradiation tests — are discussed in more detail below.

UV Irradiation Tests

Extensive screening tests were performed on the coverglasses with the 0.35 μm UV filter and on the DC93-500 adhesive to determine the darkening factor due to UV irradiation. It was found that the 0.35 μm filters are at least equivalent to the 0.41 μm filters in their ability to prevent damaging UV irradiation from reaching the adhesive. Furthermore, the complete solar cell assembly was tested in a UV space environment so that the possibility of darkening caused by interaction between the antireflective coating, the silicon, the UV filter, and/or the DC93-500 adhesive could be evaluated. In this test, high efficiency solar cells and control cells were irradiated under a xenon light source equivalent to 1-1/2 suns of UV. The cells were mounted in a fixture under high vacuum to simulate the space environment; the plate on which the solar cell assemblies were mounted was water-cooled so that none of the components of the cell assemblies would be subjected to a temperature beyond the limits of its space environment.

The 1-1/2 sun UV irradiation was continued for more than 1500 equivalent sun hours. The short circuit currents and spectral responses of the solar cell assemblies were monitored at frequent intervals without interrupting the high vacuum. Cell temperature and light source intensity and spectrum were also monitored. A 0.3 to 2.7% loss in short circuit current was measured at the end of 1500 equivalent sun hours for the advanced solar cells. These cells had Ta_2O_5 antireflective coating and were covered with DC93-500 adhesive and 0.35 μm wavelength filtered quartz. Most of the loss occurred within the first 200 hours, indicating that the darkening effect saturates at longer times. The loss observed in conventional SiO_x coated cells, covered with R63489 adhesive and 0.41 μm wavelength filtered quartz, ranged from 2.2 to 4.2%. Thus, the new cells are equal to, or better than, the conventional cells that have been used in space for the past several years.

High Energy Electron Irradiation

To date, numerous particulate irradiation tests have been conducted, including high energy electrons, high energy protons, and low energy protons. Typical of these was the high energy electron test conducted at the Jet Propulsion Laboratory in Pasadena using their Dynamitron particle accelerator. This accelerator is capable of irradiating test speciments at energies of 200 keV to 2.5 MeV. The following energy levels and cumulative fluences were used:

Electron Energy, MeV	Electron Fluence, e/cm^2
0.75	5×10^{13}, 4×10^{14}, 1×10^{15}
1.0	1×10^{12} to 1×10^{16}
2.0	5×10^{13}, 4×10^{14}, 1×10^{15}

Figures 5a and 5b show the results of this test in terms of the normalized solar cell electrical parameters open circuit voltage, V_{OC}, short circuit current, I_{SC}, and maximum power, P_{max}, as a function of increasing 1 MeV electron fluence for the conventional and high efficiency solar cell assemblies, respectively. The figures show that the normalized P_{max} for the high efficiency cell design at 5×10^{14} e/cm^2 (a typical maximum mission environment for equivalent 1 MeV electrons) is on the order of 3 percent lower than that of the conventional design. However, because the combination of design parameters in the high efficiency cell yields an initial beginning-of-life output 21 percent higher than that of the standard cell of similar area and thickness, the net effect is a higher end-of-life output (i.e., at 5×10^{14} e/cm^2). A similar relationship has been obtained for high energy proton irradiation, i.e., a more rapid decay in voltage gain due to the back surface field than in current gain due to the p^+ at high equivalent 1 MeV fluence levels.

Balloon Flights

One area of uncertainty involved with the cell development was measurement of the air mass zero (AM0) output of the cell. Because the cell is "bluer" (that is, has a higher response in the lower wavelengths), if conventional solar cell standards were used to calibrate the light sources for measuring the higher efficiency cells it was possible that the cells would read higher or lower than their true AM0 values. In order to find out how much this difference was, and provide encapsulated standard cells that would accurately calibrate light sources, both advanced and standard cells were flown aboard four JPL balloon flights in the fall of 1973 and the spring of 1974. Table 3 is a matrix of the different design variables that were evaluated as part of this program.

Because most of the cells flown in the spring 1974 flights were prototype cells manufactured in the laboratory and included only the smaller 2 x 2 cm size, a further balloon flight program has been planned and is currently under way; this program will fly advanced cells taken from the production line.

CONCLUSION

Advanced intermediate and high efficiency solar cells have been developed and comprehensively tested in both ground simulated space environment and balloon flight tests. The tests have confirmed that the cells are ready for flight use.

TABLE 1. SOLAR CELL CHARACTERISTICS*

Characteristic	Standard Cell	Intermediate Cell	High Efficiency Cell
Power, mW	57.0	62.9	69.1
Size, cm	2 x 2	2 x 2 or 2 x 6.2	2 x 2 or 2 x 6.2
Diffusion depth, μm	0.3	0.3	0.2
Bar contact width, cm	0.089	0.064	0.064
Contact material	TiAg	TiPdAg	TiPdAg
Antireflective coating	SiO_x	Ta_2O_5	Ta_2O_5
UV filter, μm	0.41	0.35	0.35
Cover adhesive	R63489	DC93-500	DC93-500
Resistivity, Ωcm	10	10	20
Thickness, cm	0.030	0.030	0.028
Back surface field	No	No	Yes

*Based on 2 x 2 cm size and production lot power at specification voltage.

TABLE 2. ADVANCED SOLAR CELL QUALIFICATION TESTS

- Cover (0.35 μm Optical Coating Laboratory, Inc. and Heliotek)
  - Particulate irradiation, protons and electrons
  - UV
  - Transmission as function of angle of incidence and temperature (pre-, post-irradiation)
  - Mechanical (pre-, post-irradiation)
  - Elemental analysis of UV filter
  - UV leak scan to 0.12 μm
- Cover and adhesive
  - UV tests
    - Sandwich
    - Cover only
  - Particulate irradiation (adhesive)
    - Protons, neutrons, electrons
  - Outgassing
- Cell
  - Four electron screenings
  - Two "slow" electron screenings
  - High energy protons
  - Photon irradiation of electron irradiated cells
  - Interconnection
    - Seam welding
    - Soldering
  - Diffusion/blank characterization
  - Spectral characterization
  - 50°C anneal – post-irradiation
    - Electrons
    - Protons
  - Low energy protons
  - Transmission, absorptance, Ta_2O_5, TiO_x
  - UV irradiation, Ta_2O_5 TiO_x
- Assemblies
  - Electrical tests
  - Electrons, protons
  - UV tests
  - Balloon flights
  - Thermal characterizations
    - Absorptance and emittance (pre-, post-irradiation)
    - Temperature coefficients (pre-, post-irradiation)
  - Angle of incidence tests
  - Thermal, mechanical environments

TABLE 3. CELL TYPES USED IN BALLOON FLIGHTS

Cell Type	Junction Type	Back of Cell	Base Resistivity, Ωcm	Cell Thickness, cm	Contact	Cover	Cell Coating
I	0.30 μm n/p	Not P+	10	0.030	TiAg	0.41 μm	SiO_x
II	0.15 μm n/p	Not P+	10	0.030	TiPdAg	0.35 μm	Ta_2O_5
III	0.20 μm n/p	P+	10	0.020	TiPdAg	0.35 μm	Ta_2O_5
V	0.20 μm n/p	P+	1	0.020	TiPdAg	0.35 μm	Ta_2O_5
VI	0.15 μm n/p	Not P+	10	0.030	TiPdAg	Bare quartz	Ta_2O_5
VII	0.20 μm n/p	P+	10	0.030	TiPdAg	0.35 μm	Ta_2O_5
VIII	0.30 μm n/p	Not P+	10	0.030	TiAg	0.35 μm	Ta_2O_5
IX*	0.15 μm n/p	Not P+	10	0.030	TiAg	0.35 μm	Ta_2O_5
X*	0.15 μm n/p	Not P+	10	0.030	TiAg	Bare quartz	Ta_2O_5
XI	0.20 μm n/p	P+	20	0.030	TiPdAg	0.35 μm	Ta_2O_5

*Pre-irradiated to 1×10^{15} 1 MeV electrons.

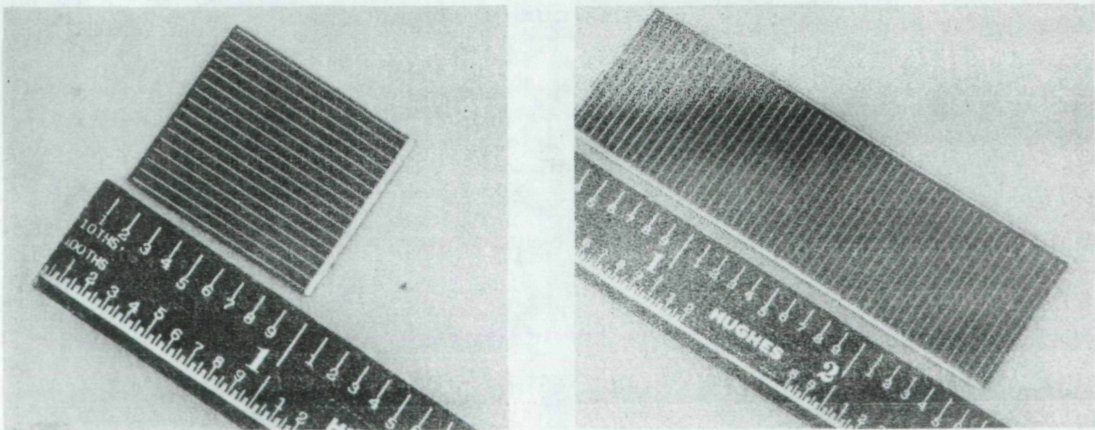

Figure 1. - High efficiency solar cells.

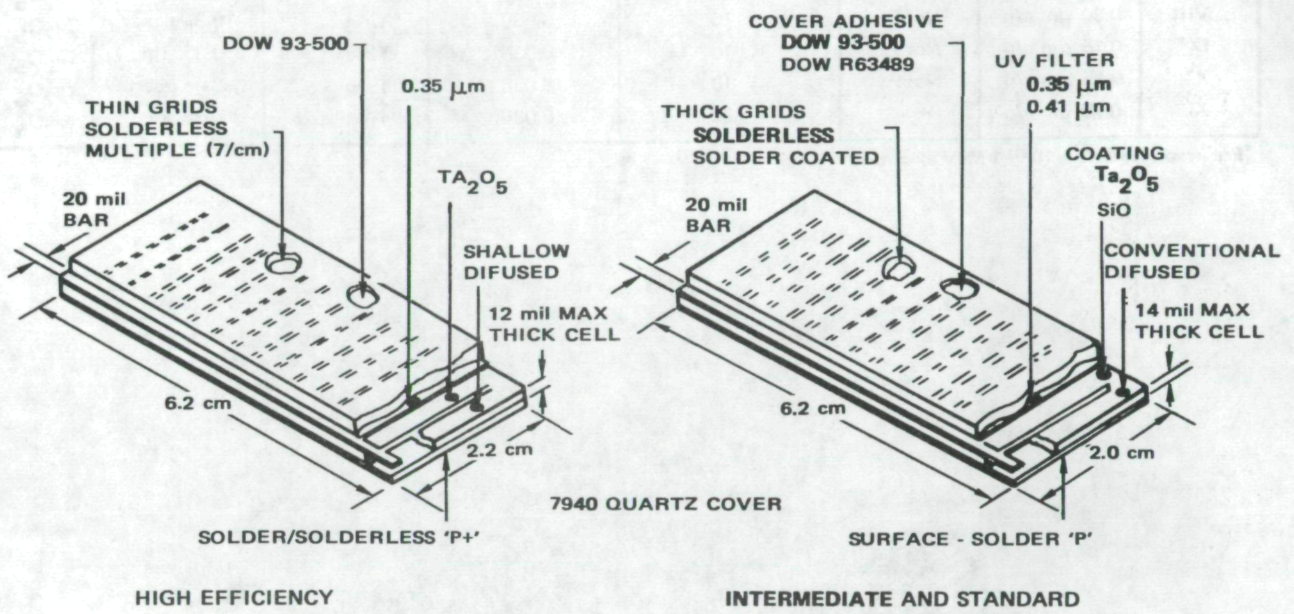

Figure 2. - Solar cell structure.

HIGH EFFICIENCY
INTERMEDIATE
CONVENTIONAL

CURRENT, MILLIAMPERES

VOLTAGE, VOLTS

a) 'AVERAGE' PRODUCTION LOT CELLS

b) HIGH GRADE HIGH EFFICIENCY PRODUCTION CELL

Figure 3. - Solar cell I-V curves.

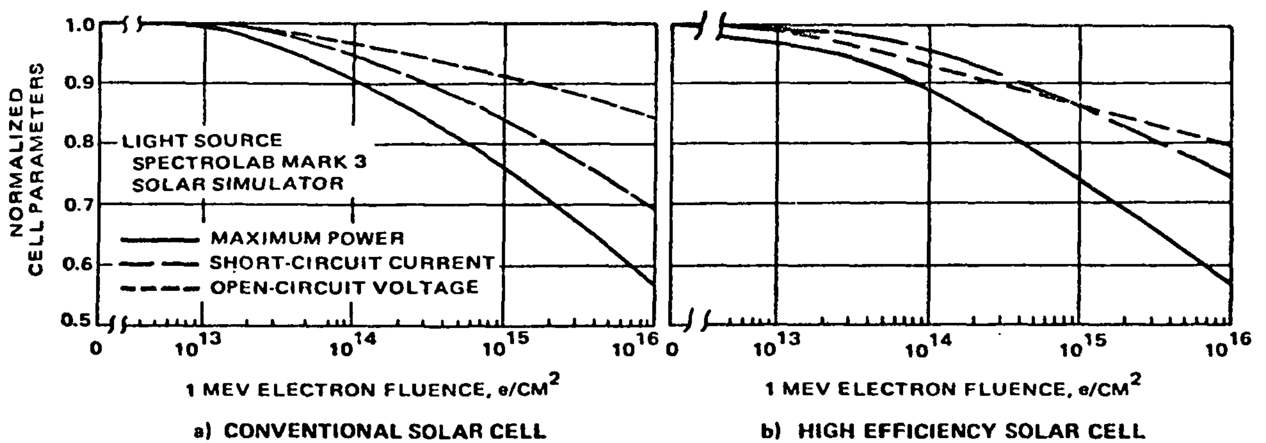

Figure 4. - High energy electron irradiation results.

6. ELECTRON DAMAGE IN HIGH EFFICIENCY SOLAR CELLS

W. Patrick Rahilly
Air Force Aero-Propulsion Laboratory
Wright-Patterson Air Force Base, Ohio 45433

INTRODUCTION - One Mev electron irradiations were performed on high efficiency and state-of-the-art conventional solar cells. The irradiations were performed at the Van de Graff facility at the Aerospace Research Laboratory, WPAFB. The cells were irradiated to four fluence levels. After each level was reached the cells were current-voltage tested at six temperatures. Spectral response data was taken at 28°C.

DESCRIPTION OF CELLS - Table I summarizes the gross physical, characteristics of the cells tested. Exact cell thicknesses and resistivities were not known; nominal values for these parameters are given. The cells were obtained from Centralab and Heliotek; the 50Ω cm Heliocells were provided to AFAPL for our evaluation and data exchange. The 2Ω cm and 10Ω cm Violet cells were provided by Centralab under Contract F33615-73-C-2073. The 10Ω cm Heliocells and conventional cells were obtained under purchase orders to the respective vendors.

TESTING PROCEDURE - Two cells from each category in Table I were evaluated at four fluence levels (10^{13}, 10^{14}, 10^{15}, and 10^{16} electrons/cm^2). The cells were pre-irradiation evaluated under the AFAPL Mark I Solar Simulator at six temperatures (45°F, 70°F, 95°F, 120°F, 145°F, 170°F). The cells were then irradiated to 10^{13} e's/cm^2 at room temperature and returned to the Mark I for evaluation at the aforementioned temperatures.

Preceding Page Blank

After evaluation, the cells were returned to the Van de Graff to accumulate fluence to the next level. This procedure was repeated until a fluence of 10^{16} electrons/cm^2 was reached. The electron fluxes were high; from 0 to 10^{13} e's/cm^2, $\dot{\Phi} = 7.81 \times 10^{10}$ e/cm^2/sec; 10^{13} to 10^{14}, $\dot{\Phi} = 7.81 \times 10^{11}$ e's/cm^2/sec; 10^{14} to 10^{15}, $\dot{\Phi} = 4.69 \times 10^{12}$ e/cm^2/sec; 10^{15} to 10^{16}, $\dot{\Phi} = 7.81 \times 10^{12}$e/cm^2/sec. It was assumed that these fluxes were not large enough to induce dose rate dependent effects. The I_{sc}, V_{oc}, P_{max} data obtained for each fluence level was least squares fit to a linear temperature dependence. The temperature coefficients obtained are summarized in Table II.

Spectral response data for each fluence level was taken on the AFAPL SCATS (Solar Cell Automatic Test System) at 28°C. The SCATS also provides AMO background illumination superimposed on the monochromatic light. A quick check revealed no injection level dependence of the spectral response.

RESULTS - Figure 1 illustrates the spectral content of the AFAPL Mark I solar simulator. It is quite clear that our Mark I is "blue deficient." Because of this, the shallow junction cells (Violet and Heliocells) did not show enhanced radiation resistance compared to the conventional solar cells. This is illustrated in Figure 2.

The 10Ω cm and 50Ω cm Heliocells displayed a marked annealing after 10^{16} e's/cm^2. Some anneal was expected but not to the extent shown in Figures 3 and 4. Because of the way the cells were tested, any annealing for the lower fluences was obscured. Figure 5 shows similar data for the 2Ω cm Violet cells; no annealing was apparent.

Figure 6 compares spectral responses for the 2Ω cm Violet cells and the 10Ω cm Heliocells. The Violet cells have a junction depth near .12μ; the Heliocells have junction depths slightly over .2μ. These depths are apparent from the response data. Also shown in Figure 6 is the relative radiation sensitivity of the three resistivities with 50Ω cm being the most resistant.

Figure 7 shows the absolute maximum power versus electron fluence at 70°F. The 2Ω cm Violet cells were higher in efficiency but as shown in Figure 2, none of the high efficiency cells tested demonstrated superior radiation resistance over the conventional cells.

DISCUSSION - The results are rather mundane except for the enhanced annealing of the Heliocells. The fact that the anneal occurs for the Heliocells is thought to be associated with the nature of the aluminum P^+ back surface region. A possible model for this anneal can be summarized as follows: After irradiation, vacancies and interstitial silicon atoms exist in large numbers. A large number of vacancy - interstitial silicon recombinations occur almost spontaneously - however, some vacancies and silicon interstitials remain along with the formation of vacancy-dopant impurity defects. It has been shown that substitutional aluminum atoms will interchange with silicon interstitials. This reaction results in aluminum atoms being ejected into interstial space within the lattice. The aluminum interstitial is stable at temperatures approaching 250°C. It is thought that the aluminum atom occupying on interstial position has three electronic levels within the band gap - a neutral atom level near the conduction

band, a singley ionized level somewhere near mid gap and a doubley ionized level near the valence band. If this set of levels exists, then the interstitial aluminum present would most likely be neutral and would act in competition with substitional dopants and remaining silicon interstitials as a sink for vacancies of any charge state moving about in the silicon. The interaction of the vacancies with the neutral aluminum atom would result in a substitutional aluminum which in turn will act as an acceptor. Thus immediately after exposure to the electron environment the built in electric field is weakened by the removal of acceptor aluminum thus causing a change in the effective boundary condition at the back contact. As the anneal progressed, the electric field builds until minority carrier loss in this region is significantly reduced.

The same arguments can be argued for the bulk region containing boron; however, the propensity for substituational boron - interstial silicon exchanges may be much lower than for aluminum. This would suggest that aluminum doped silicon might possibly be more radiation resistant than boron doped silicon (gallium may also be promising). Work by NASA Lewis in the mid 1960's did demonstrate that Al and Ga doped P type silicon was more radiation resistant than boron doped silicon.

CONCLUSION - These experiments resulted in the following conclusions:

(1) The spectral response data in conjunction with measured I_{SC} versus fluence demonstrates the need for good "blue content" simulators

TABLE I - CELL DESCRIPTION

CELL MFG.	GENERIC NAME	NOMINAL BASE	CONTACT METAL	COVERSLIDE	AR COATING	.35 μ CUT-OFF FILTER	NOMINAL THICKNESS	BACK SURFACE P +
CL	VIOLET	2 Ω CM	AG	NONE	TA_2O_5	NO	10 MIL	NO
CL	VIOLET(BF)	2 Ω CM	AG	CFQ, CEO_2	TA_2O	NO	10 MIL	NO
CL	VIOLET	10 Ω CM	AG	NONE	TA_2O_5	NO	10 MIL	NO
HLTK	HELIOCELL	10 Ω CM	AG	0211	TA_2O_5	YES	8 MIL	YES
HLTK	HELIOCELL	50 Ω CM	AG			YES	8 MIL	YES
CL	CONV.	10 Ω CM	AL	0211	SIO	NO	10 MIL	NO
CL	CONV.	10 Ω CM	AG	0211	SIO	NO	10 MIL	NO
HLTK	CONV.	10 Ω CM	AL	0211	TA_2O_5	NO	10 MIL	NO
HLTK	CONV.	10 Ω CM	AG	0211	TA_2O_5	NO	10 MIL	NO

TABLE II. - TEMPERATURE COEFFICIENTS

CELL MFG.	CELL TYPE	$\Delta I_{SC} / \Delta T$ (MA/°C)					$\Delta V_{OC} / \Delta T$ (MV/°C)					$\Delta P_M / \Delta T$ (MW/°C)				
		0	10^{13}	10^{14}	10^{15}	10^{16}	0	10^{13}	10^{14}	10^{15}	10^{16}	0	10^{13}	10^{14}	10^{15}	10^{16}
CL	2 Ω cm VIOLET	.0658	.0381	.1368	.1841	.2232	-2.180	-2.169	-2.066	-2.215	-2.218	-.3389	-.3433	-.2663	-.2212	-.1706
CL	2 Ω cm VIOLET (BF)	.0624	.0397	.1323	.1666	.2071	-2.091	-2.140	-2.066	-2.172	-2.264	-.3181	-.3239	-.2571	-.2106	-.1618
CL	10 Ω cm VIOLET	.0813	.0309	.1687	.2458	.2746	-2.306	-2.304	-2.114	-2.247	-2.292	-.3513	-.3676	-.2717	-.2300	-.1997
HLTK	10 Ω cm HELIOCELL	.0710	.0252	.1522	.1995	.2489	-2.156	-2.125	-1.906	-2.224	-2.303	-.2923	-.2960	-.2053	-.1938	-.1507
HLTK	50 Ω cm HELIOCELL	.0679	.0720	.1008	.2427	.3065	-2.094	-1.963	-1.958	-2.113	-2.273	-.2993	-.2952	-.2711	-.2323	-.1747
CL	10 Ω CONV (AL)	.0463	.0291	.1347	.2078	.2571	-2.295	-2.300	-2.108	-2.233	-2.319	-.2933	-.3021	-.2286	-.1920	-.1519
HLTK	10 Ω cm CONV (AL)	.0463	.0370	.1810	.2191	.2643	-2.218	-2.162	-1.984	-2.254	-2.272	-.3297	-.3148	-.2318	-.2112	-.1535
CL	10 Ω CONV (AG)	.0535	.0269	.1265	.2088	.2561	-2.259	-2.229	-2.112	-2.258	-2.330	-.2984	-.3004	-.2284	-.1900	-.1478
HLTK	10 Ω cm CONV (AG)	.0329	.0144	.1306	.1954	.2263	-1.916	-1.922	-1.922	-2.210	-2.280	-.2315	-.2303	-.1634	-.1476	-.1132

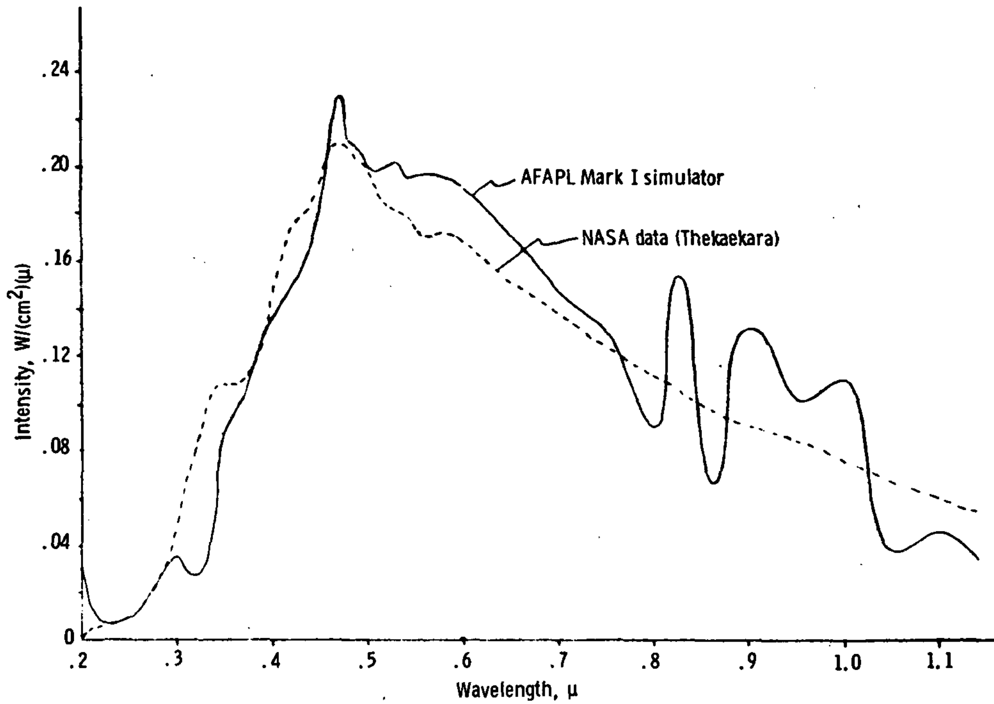

Figure 1. - Simulated and assumed AMO spectra.

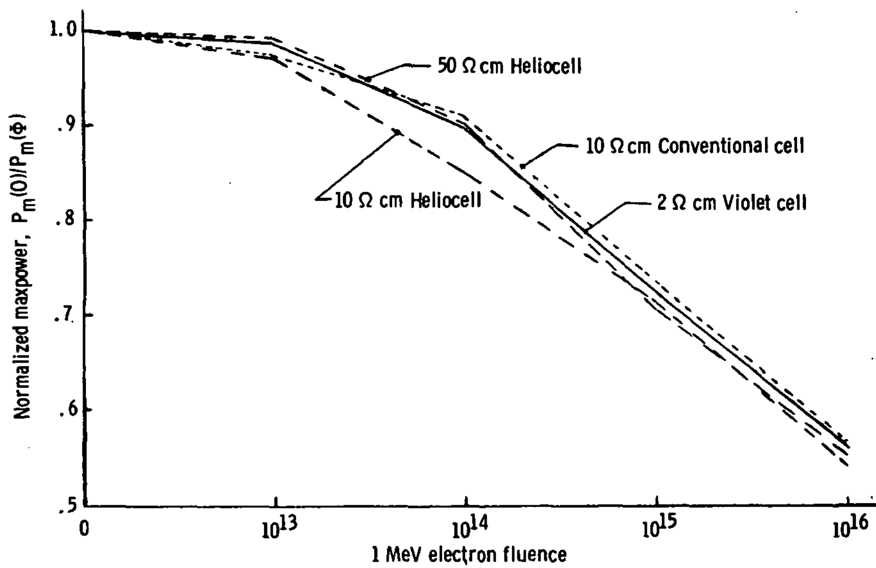

Figure 2. - Normalized maxpower as function of electron fluence at 70° F.

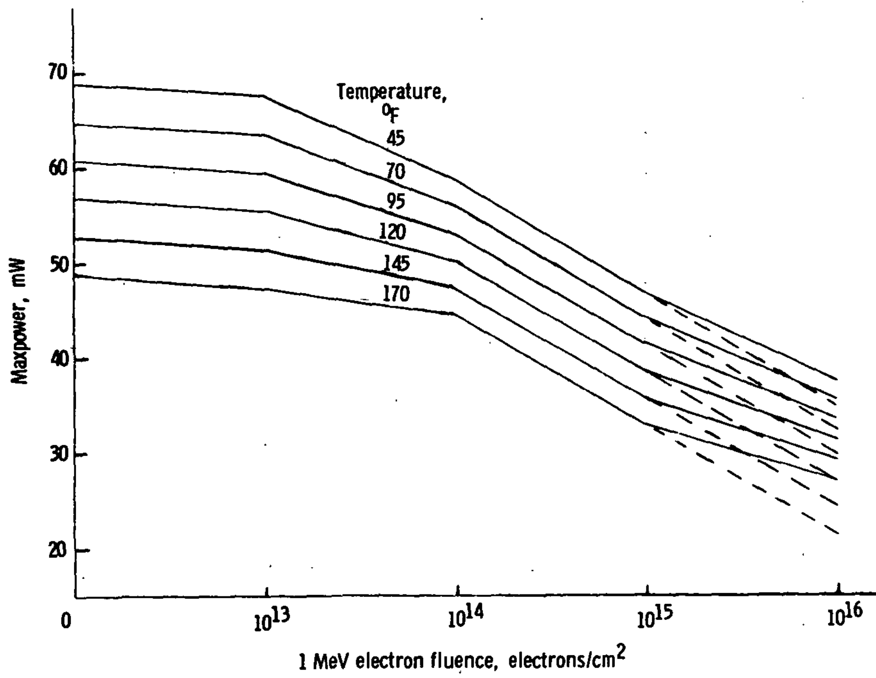

Figure 3. - 10 Ω cm Heliocell maxpower as function of electron fluence at various temperatures.

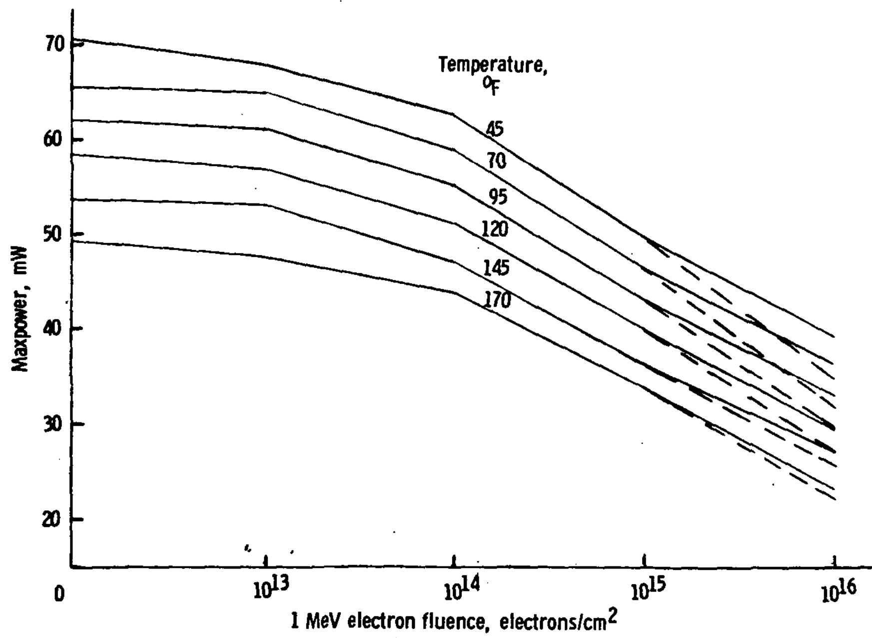

Figure 4. - 50 Ω cm Heliocell maxpower as function of electron fluence at various temperatures.

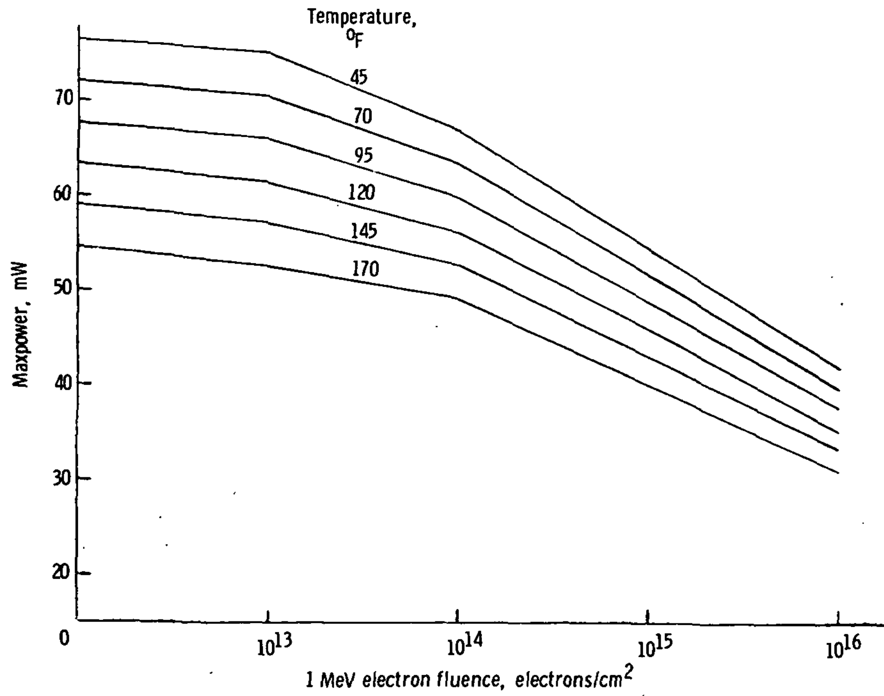

Figure 5. - 2 Ω cm Violet cell maxpower as function of electron fluence at various temperatures.

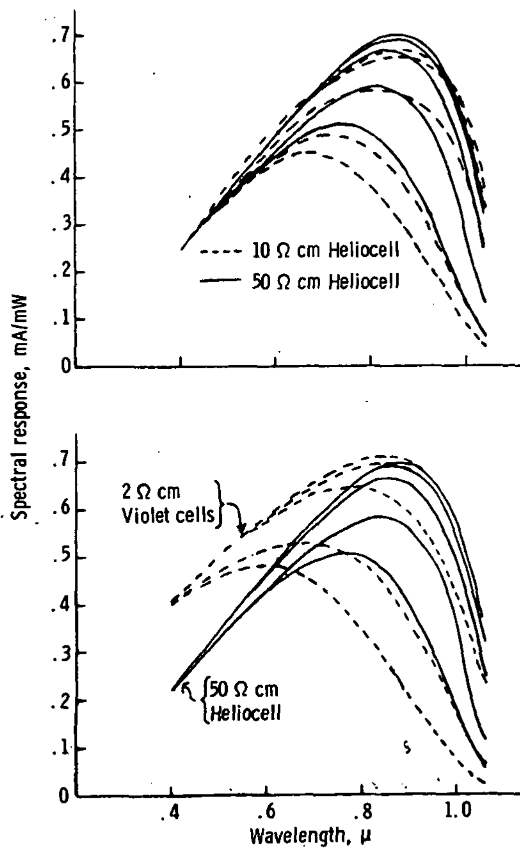

Figure 6. - Spectral response as function of wavelength.

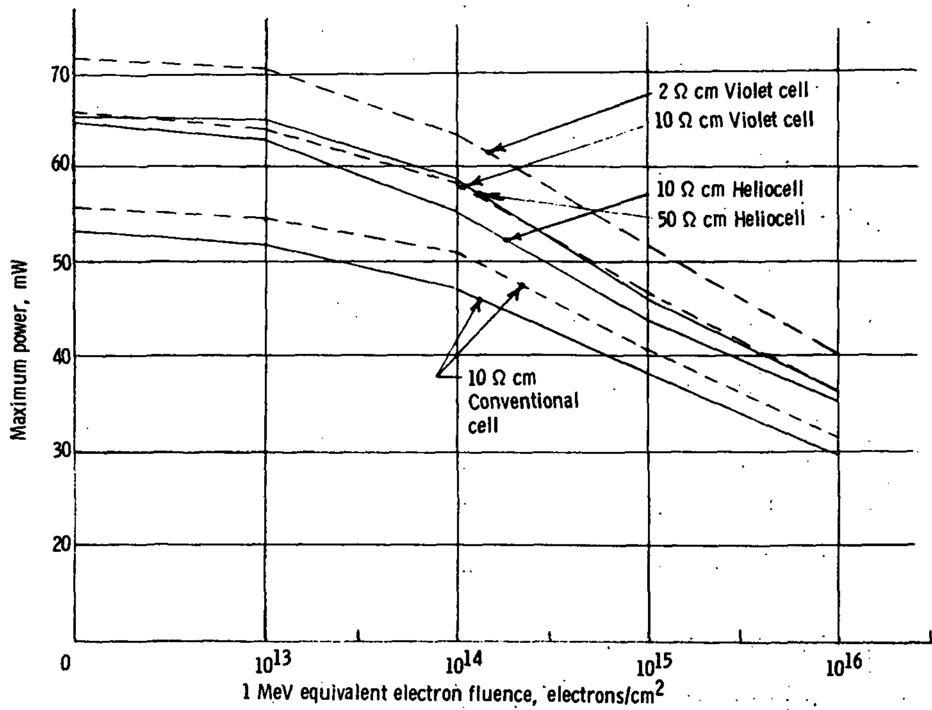

Figure 7. - Maxpower as function of electron fluence (at 70° F).

7. ELECTRON AND PROTON DAMAGE COEFFICIENTS IN LOW-RESISTIVITY BULK SILICON AND SILICON SOLAR CELLS

J. R. Srour, S. Othmer, K. Y. Chiu, and O. L. Curtis, Jr.
Northrop Research and Technology Center
Hawthorne, California 90250

Damage coefficients have been determined for low resistivity silicon based on minority-carrier lifetime measurements on bulk material and diffusion length measurements on solar cells. Irradiations were performed at three electron energies (0.5, 1.0, and 2.5 MeV) and one proton energy (10 MeV) on bulk samples and cells fabricated from four types of boron-doped 0.1 ohm-cm silicon ingots: 1) Czochralski (CZ), low dislocation density (LD); 2) CZ, high dislocation density (HD); 3) float-zone (FZ), LD; 4) FZ, HD. For comparison, measurements were also performed for higher resistivity specimens. All silicon employed in this investigation was obtained from Dow Corning and solar cells were fabricated by Centralab Semiconductor. The sample designation system employed gives the growth method, relative dislocation density, resistivity, and specimen number. Two illustrative examples are: a) FZLD 0.1/4--bulk specimen number four fabricated from float-zone, low-dislocation-density 0.1 ohm-cm material; b) CZHD 0.1/SC3--solar cell number three fabricated from Czochralski, high-dislocation-density 0.1 ohm-cm material. If no specimen number is given on a figure for a specific case, then the data points shown represent an average for several samples of the same type. Additionally, the designation HD or LD only appears if dislocation density was determined for a given ingot.

Figure 1 illustrates schematically the lifetime measurement technique employed for bulk specimens. A sample-under-test was connected in a constant-current circuit and the steady-state photoconductivity signal due to chopped-light illumination was then monitored using phase-sensitive detection. This signal yields excess carrier density. The measurement

system was carefully calibrated in terms of carrier generation rate. Lifetime was obtained by dividing measured excess density by the known generation rate. The background lamps shown in Figure 1 were employed to fill traps. Diffusion lengths were determined for solar cells by measuring short-circuit current during exposure to a Co-60 gamma source (known generation rate).

Values for damage coefficient (K_L) were determined using the relationship

$$L^{-2} - L_o^{-2} = K_L \phi , \tag{1}$$

where L_o and L are pre- and post-irradiation diffusion length, respectively, and ϕ is the fluence of the irradiating particle. Figure 2 presents the quantity ($L^{-2} - L_o^{-2}$) vs 0.5-MeV electron fluence for various specimens. The dashed lines have unity slope and thus yield values for K_L. The deviation from unity slope at high fluences noted in some cases is generally attributed to radiation-induced trapping effects and was also observed at other particle energies. Damage coefficients were generally obtained from lower fluence data where trapping effects were judged to be unimportant. Figure 3 presents K_L vs resistivity for the 0.5-MeV electron data of Figure 2. It is seen that K_L increases as resistivity decreases and that damage coefficients for low-resistivity CZ specimens are about a factor of three larger than their FZ counterparts. Additionally, no dependence of K_L on dislocation density is apparent.

Data for 1.0- and 2.5-MeV electron-irradiated specimens are shown in Figures 4 and 5, respectively. In Figure 4, K_L values for bulk CZ samples are seen to be a factor of ~2 larger than for FZ specimens. Additionally, solar cell damage coefficients are about a factor of two larger than corresponding bulk material values. Figures 4 and 5 further demonstrate the dependence of K_L on resistivity. In Figure 6, data for 10-MeV proton-irradiated specimens are presented and findings are qualitatively similar

to those for electron-irradiated samples. Figure 7 presents results obtained for 1.0-MeV electron-irradiated solar cells using a solar similator (at Centralab) under AMO conditions at an intensity of 140 mW/cm^2. The ratio of post- to pre-irradiation maximum power output is plotted versus electron fluence, and it is seen that the performance of irradiated 0.1 ohm-cm cells is considerably worse than their higher-resistivity counterparts. This finding is consistent with damage coefficient results obtained on bulk samples in that more damage is expected in lower resistivity cells.

For all three electron energies examined, empirical fits to the data yield the following approximate relation:

$$K_L \propto \rho^{-2/3} . \tag{2}$$

Hole density p_o was determined for p-type material over the resistivity range from 0.1 to 10 ohm-cm. Additionally, damage coefficient is proportional to $(L^{-2} - L_o^{-2})$, which can be interpreted as the reciprocal of radiation-induced carrier lifetime τ. Thus, $K_L \propto 1/\tau$. Equation 2 was then employed to obtain a plot of τ vs p_o, which is shown as the solid curve in Figure 8. This curve is thus representative of the experimental data obtained here for three electron energies.

We next attempted to fit the solid curve using the Hall-Shockley-Read (HSR) model. The HSR lifetime expression for a single recombination level in p-type material at low injection levels is

$$\tau = \frac{p_o + p_1}{c_n N p_o} + \frac{n_o + n_1}{c_p N p_o} , \tag{3}$$

where all terms have their usual meaning. As p_o increases, lifetime decreases due to the increased recombination rate. For ease of analysis and for purposes of illustration, a recombination level in the lower half of the bandgap was assumed. For any reasonable capture-probability-ratio assumed, Equation 3 then simplifies to

$$\tau = \frac{1}{c_n N}\left(1 + \frac{p_1}{p_o}\right) . \quad (4)$$

We attempted to fit Equation 4 to the solid curve in Figure 8 by treating the multiplicative term $1/c_n N$ as an adjustable scale factor. A reasonable fit was obtained for a level at $E_r - E_v \cong 0.12$ eV. However, an exact fit can be obtained by using a two-level HSR model, as shown in the figure. By assuming that each level can be expressed in the form of Equation 4 and by adding the contributions of each level reciprocally to obtain τ, the solid curve representing the experimental data can be fit exactly. As shown in Figure 8, the level more effective for higher resistivities is at $E_r - E_v \cong 0.18$ eV, whereas the level more effective at lower resistivities is at $E_r - E_v \cong 0.08$ eV. The ratio of the multiplicative scale factors for these two levels is ~22, with $c_n N$ for the 0.18 eV level being larger.

No physical significance should be attached to the above recombination parameters. Our purpose here was only to illustrate that a two-level HSR model describes the present data quite well. In order to obtain meaningful parameters from such a model, the temperature and injection-level dependences of radiation-induced lifetime are required. In terms of gaining increased understanding of the dependence of K_L on resistivity, it would be useful to measure the temperature dependence of damage coefficient for samples of several resistivities and then attempt to fit the data with two (or more) HSR levels.

Several of the major observations made and conclusions reached in this investigation are the following:

1. Low-resistivity boron-doped silicon may be an undesirable material for fabricating solar cells to be employed in a space radiation environment because damage coefficients increase with decreasing resistivity.

2. For 0.5-, 1.0-, and 2.5-MeV electron bombardment, empirical fits to experimental data can be approximately expressed as $K_L \propto \rho^{-2/3}$ for $0.1 \leq \rho \leq 20$. For 10-MeV proton bombardment, an empirical fit of the form $K_L \propto \rho^{-0.44}$ was found to describe the data reasonably well.

3. The dependence of damage coefficient on resistivity can be qualitatively accounted for quite well using a two-level Hall-Shockley-Read model.

4. Damage coefficients for solar cells were observed to be larger than their bulk-material counterparts.

5. Bulk samples and solar cells prepared from float-zone material were generally observed to be more radiation tolerant than their Czochralski counterparts at all resistivities examined.

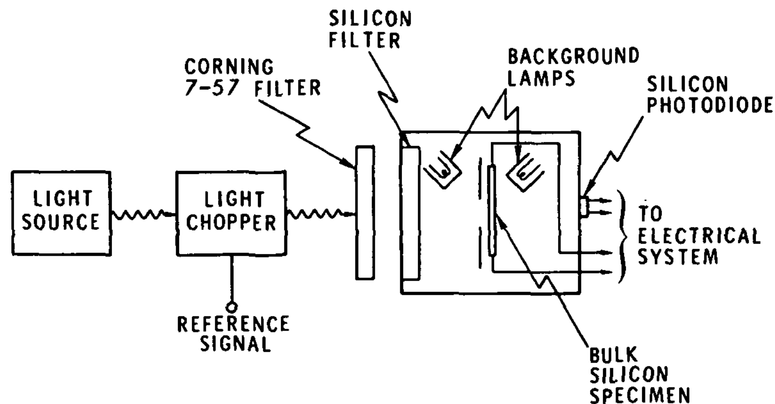

Figure 1. - Schematic representation of the steady-state photoconductivity (SSPC) apparatus employed to measure minority-carrier lifetime in bulk silicon specimens.

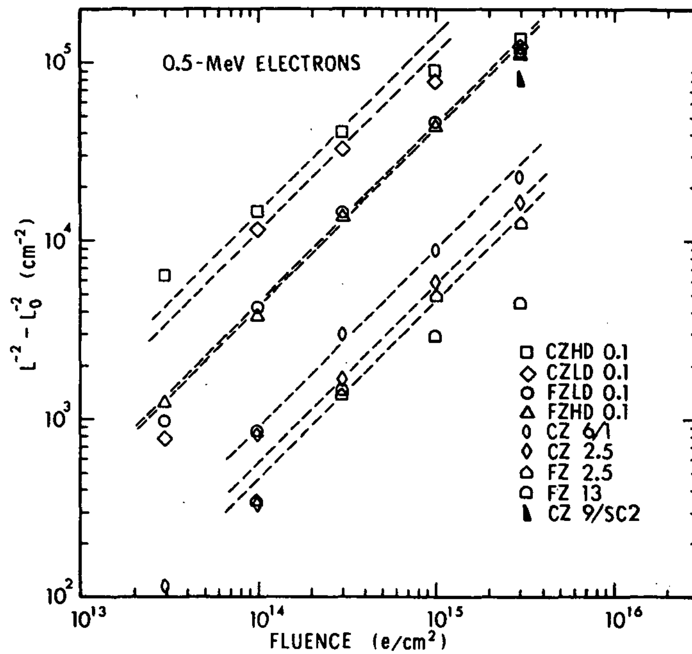

Figure 2. - The quantity $(L^{-2} - L_0^{-2})$ vs. fluence for 0.5-MeV electron-irradiated bulk silicon specimens. A data point obtained from an irradiated solar cell is also shown.

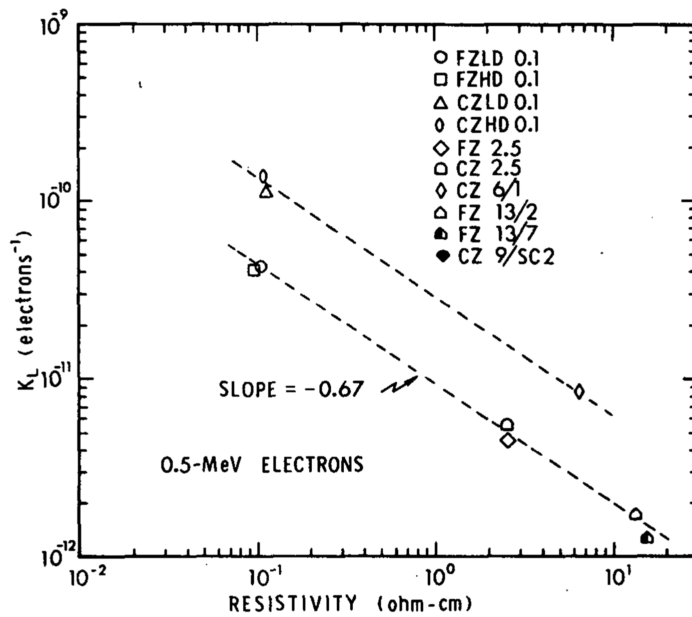

Figure 3. - Damage coefficient vs. resistivity for 0.5-MeV electron-irradiated specimens.

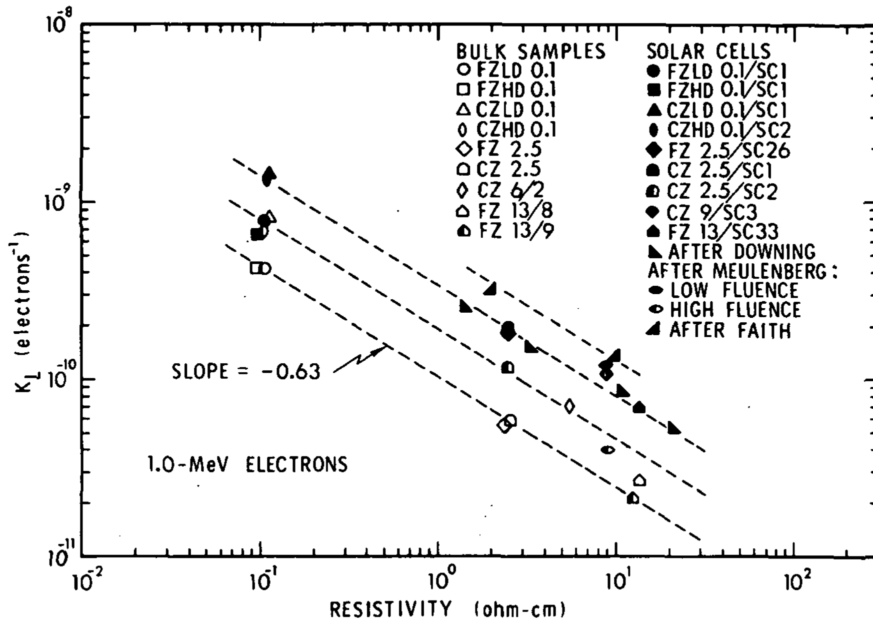

Figure 4. - Damage coefficient vs. resistivity for 1.0-MeV electron-irradiated bulk silicon specimens and silicon solar cells.

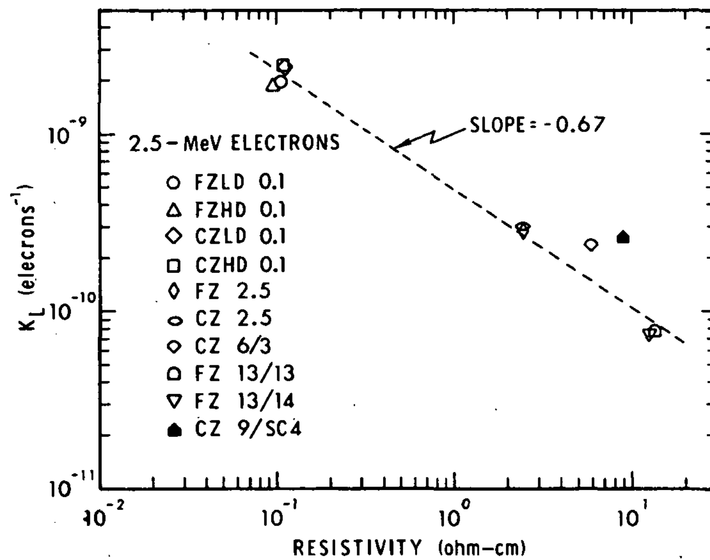

Figure 5. - Damage coefficient vs. resistivity for 2.5-MeV electron-irradiated specimens.

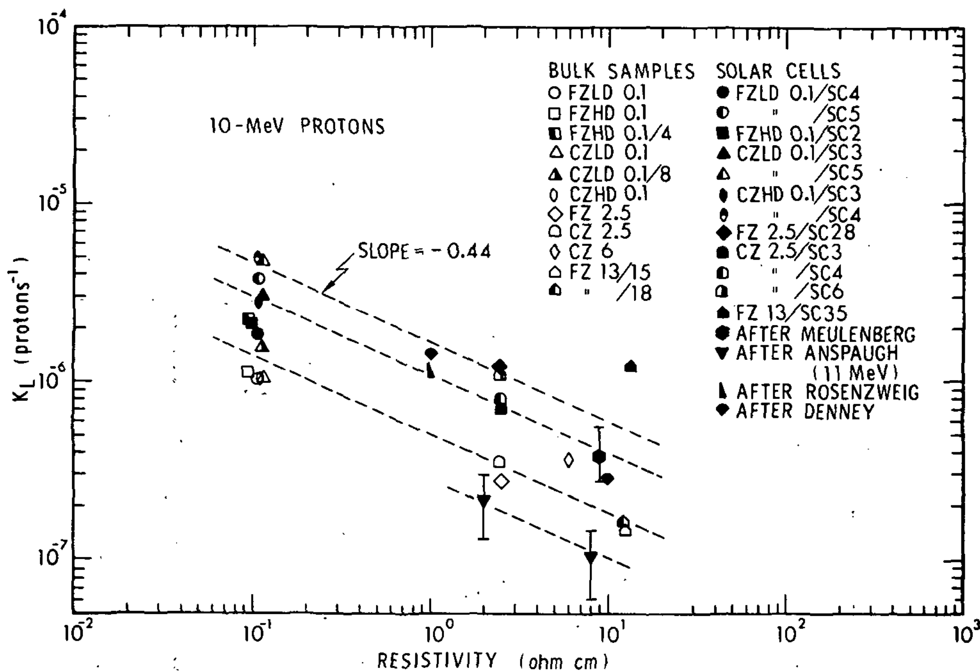

Figure 6. - Damage coefficient vs. resistivity for 10-MeV proton-irradiated bulk silicon specimens and silicon solar cells.

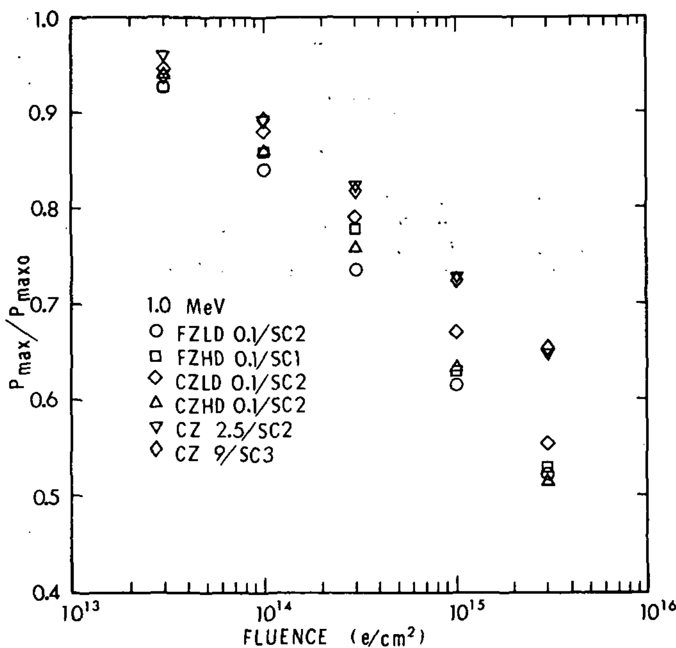

Figure 7. - The quantity P_{max}/P_{maxo} vs. fluence for 1.0-MeV electron-irradiated silicon solar cells.

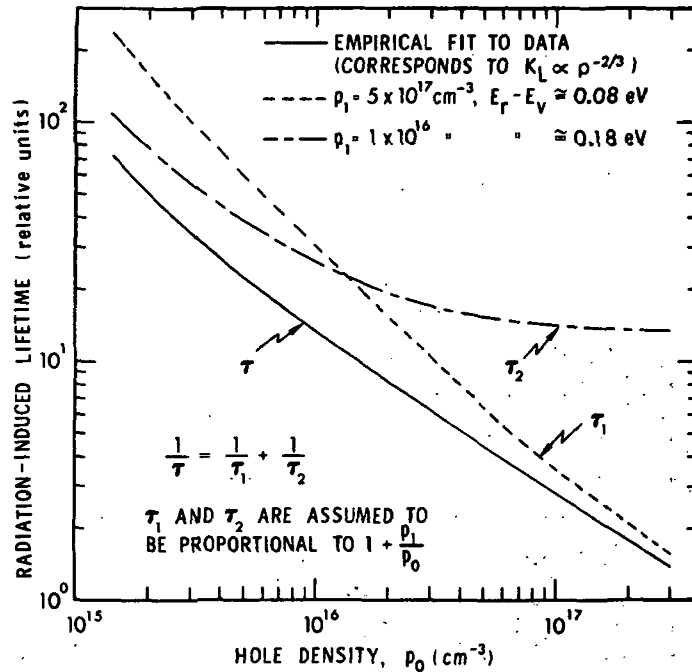

Figure 8. - Radiation-induced lifetime vs. hole density. It is demonstrated that recombination through two Hall-Shockley-Read levels can be employed to qualitatively explain the observed dependence of damage coefficient on resistivity for electron-irradiated boron-doped silicon.

ALTERNATIVE STRUCTURES AND MATERIALS

A review of some work on nonconventional solar cells (vertical multijunction, grating, grooved, and gallium arsenide cells)

Preceding Page Blank

8. FABRICATION AND PERFORMANCE OF VERTICAL MULTIJUNCTION SOLAR CELLS*

R. K. Smeltzer
Texas Instruments Inc.
Dallas, Texas

Introduction

The vertical multijunction (VMJ) structure, as conceived by J. F. Wise[1] and analyzed by W. P. Rahilly[2], is predicted to have the advantages of improved efficiency and improved radiation tolerance. (Fig. 1). It is only recently that the technology for fabricating the close-spaced vertical junctions became available.[3]

This paper discusses the fabrication technology for VMJ cells and gives the results of some preliminary characterization.

Fabrication of Type I, VMJ Cells

Although all three of the structures shown in Fig. 2 have been examined, only the fabrication of Type I cells will be described.

With reference to Fig. 3, a thermal oxide is grown on a (110) P-type silicon substrate and windows are opened in the oxide by standard photolithographic techniques. The windows are an array of parallel slots on 20 μm centers with each slot 8 μm wide.

Grooves are etched into the silicon using an orientation dependent etch (O.D.E.) of KOH in water, which etches 400 times faster in the (110) direction than in the (111) direction (4). Key to the process is the alignment of the oxide windows such that the groove walls are within 0.1° of (111) planes.

* Presented by William W. Lloyd; this work is supported by the United States Air Force, Aero Propulsion Laboratory, under Contract No. F33615-73-C-2019.

Preceding Page Blank

Fig. 4 is a microphotograph of 100 μm deep slots produced in this manner; the apparent V-shape is due to the method of sample preparation.

Antimony is then diffused into walls of the grooves and, as indicated in Fig. 5, the junction depth is quite uniform.

A short O.D.E etch is used to remove the junction from the bottom of the grooves prior to epitaxial refill.

Fig. 6 shows a cell after epitaxial refill. Alternate dopant-types have been used to delineate the shape of the growing surface at different times during the deposition cycle. The increase of depositionrate with groove depth, which is obtained by controlling the gas flow patterns and the temperature gradients, is a necessary condition for the prevention of void formation. It has been found that both silicon tetrachloride and trichlorosilane are unsatisfactory as silicon sources; silicon tetrachloride because of the high operating temperature, and trichlorosilane because of the precise temperature control need to obtain the correct balance between etching and void formation. Dichlorosilane is satisfactory providing the ratio of silicon to chlorine atoms in the incoming gases is controlled; for a given deposition temperature this ratio must be increased above the thermodynamic equilibrium value by a fixed and known amount.

Following the epitaxial refill, an N^+ junction is diffused across the top surface, linking together all the vertical junctions.

Thus, sufficient progress has been made in the advanced processes shown in Fig. 7 to permit the fabrication of VMJ cells.

Performance of VMJ Cells

The spectral response data of Fig. 8 is for some Type III cells and for some

conventional cells processed simultaneously. As can be seen, the response at 1 μm for the type III is the predicted 30% higher than that for the conventional cells. The poor blue response for both types of cell is believed due to an unnecessarily deep top junction.

The voltage-current characteristics for the same cells are shown in Fig. 9. As expected, the light currents for the VMJ cells are superior to those for the conventional cells while the open circuit voltages are lower. The lower voltages for the VMJ cells are presumably due to the increased junction area. Because of the long collection path inherent in the Type III structure, the series resistance of these cells is quite high.

Acknowledgments:

Acknowledgments are due to M. R. Peter Isles of Centralb, Inc. for both the antireflection coatings and the spectral response measurements.

References:

(1) J. F. Wise, "Vertical Junction Hardened Solar Cell", U. S. Patent 3,690,953

(2) W. P. Rahilly, "Vertical Multijunction Solar Cells", Conf. Record of the Ninth I.E.E.E. Photovoltaic Specialist Conf., May, 1972, p. 44.

(3) R. K. Smeltzer, D. L. Kendall and G. L. Varnell, "Vertical Multijunction Solar Cell Fabrication" Conf. Record of the Tenth I.E.E.E. Photovoltaic Specialist Conf., Nov. 1973, p. 194.

(4) D. L. Kendall, "On Etching Very Narrow Grooves in Silicon", Applied Physics Letters, Feb. 15th, 1975.

DEFINITION

- COMBINED PLANAR AND DEEP VERTICAL P-N JUNCTIONS
- VERTICAL JUNCTION PACKING DENSITY $\geq$ 1000 JUNCTIONS/CM

CHARACTERISTICS

- ALL GENERATED CARRIERS ARE NEAR THE JUNCTION
- ENHANCED RESPONSE AT LONG WAVELENGTHS

PREDICTED ADVANTAGES

- HIGHER EFFICIENCY
- RADIATION HARDENED

Figure 1. - Vertical multijunction solar cells.

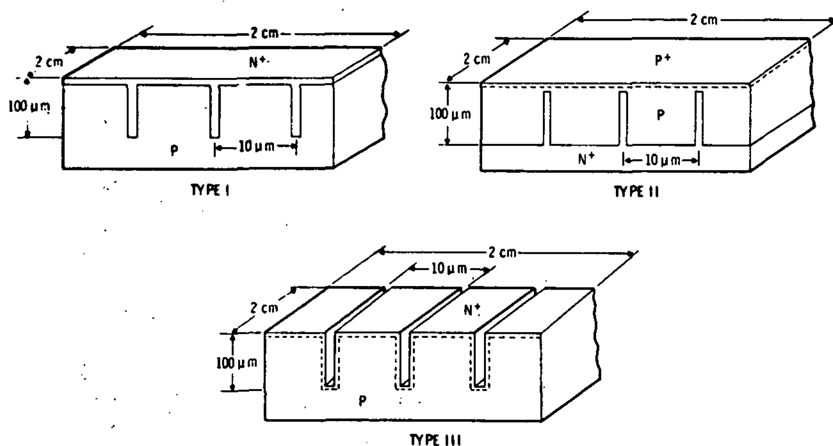

Figure 2. - Three designs for VMJ solar cells.

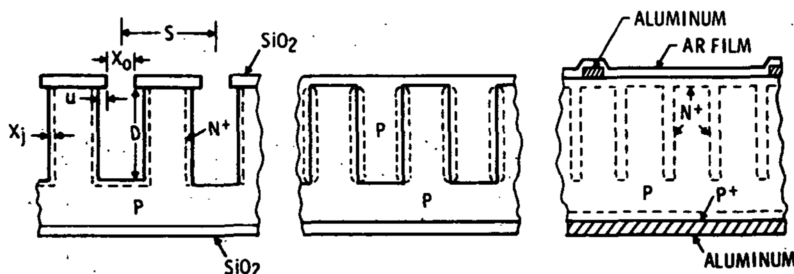

Figure 3. - Fabrication of Type I VMJ solar cells.
$S = 20 \mu m$, $X_0 + 2u = 10 \mu m$, $D = 100 \mu m$

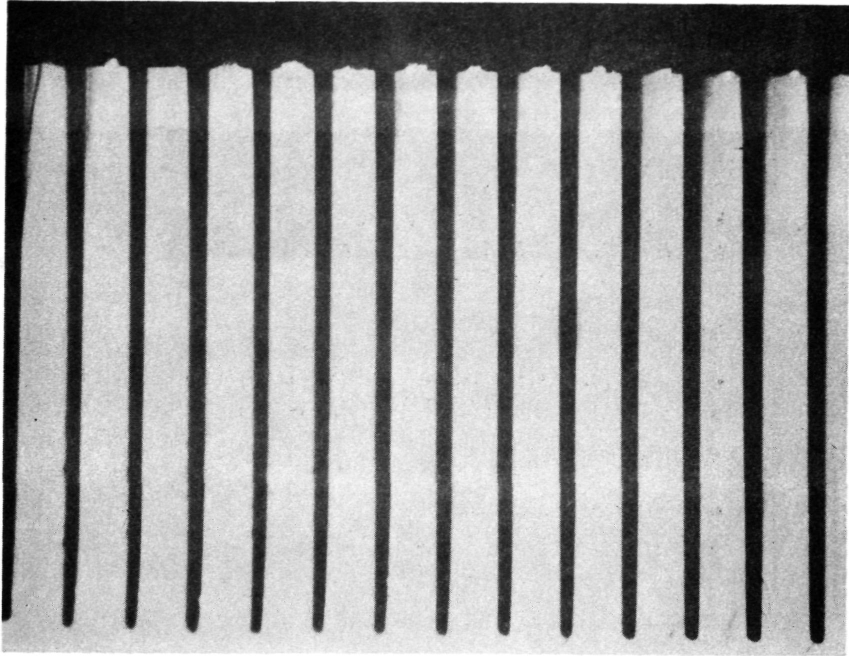

Figure 4. - Photomicrograph of 100-μm-deep etched grooves.

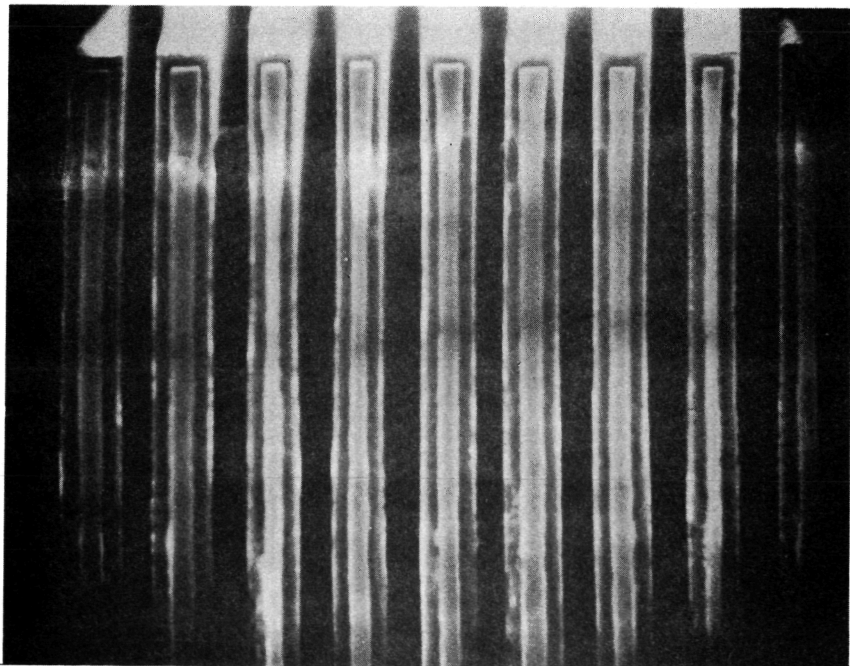

Figure 5. - Photomicrograph of grooved cell after antimony diffusion.

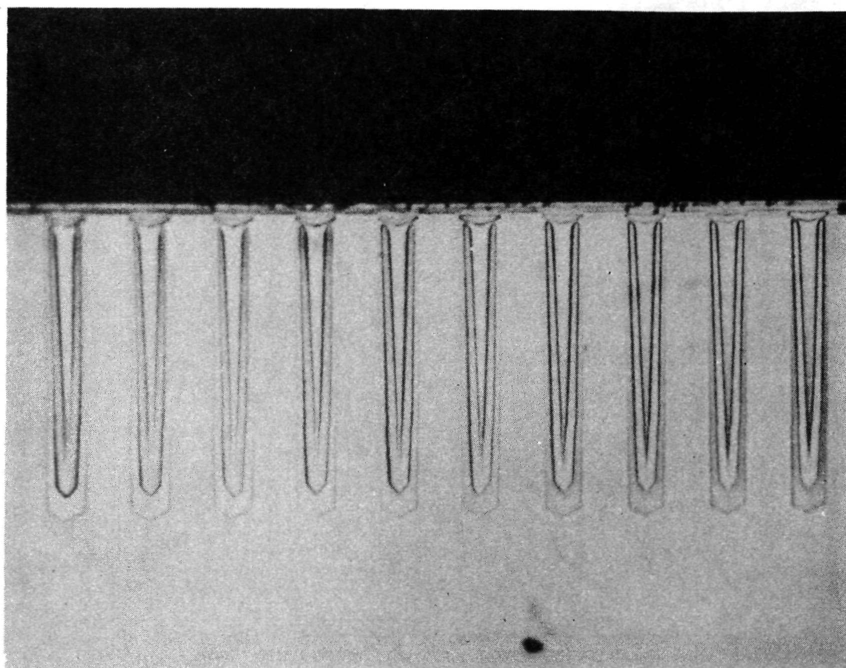

Figure 6. - Photomicrograph of grooved cell after epitaxial refill.

- Orientation Dependent Etching
- Epitaxial Refill of Deep Grooves
- Electron Beam Pattern Generation over Large Areas
- Deep Groove Diffusion

Figure 7. - Vertical multijunction solar cell technology development.

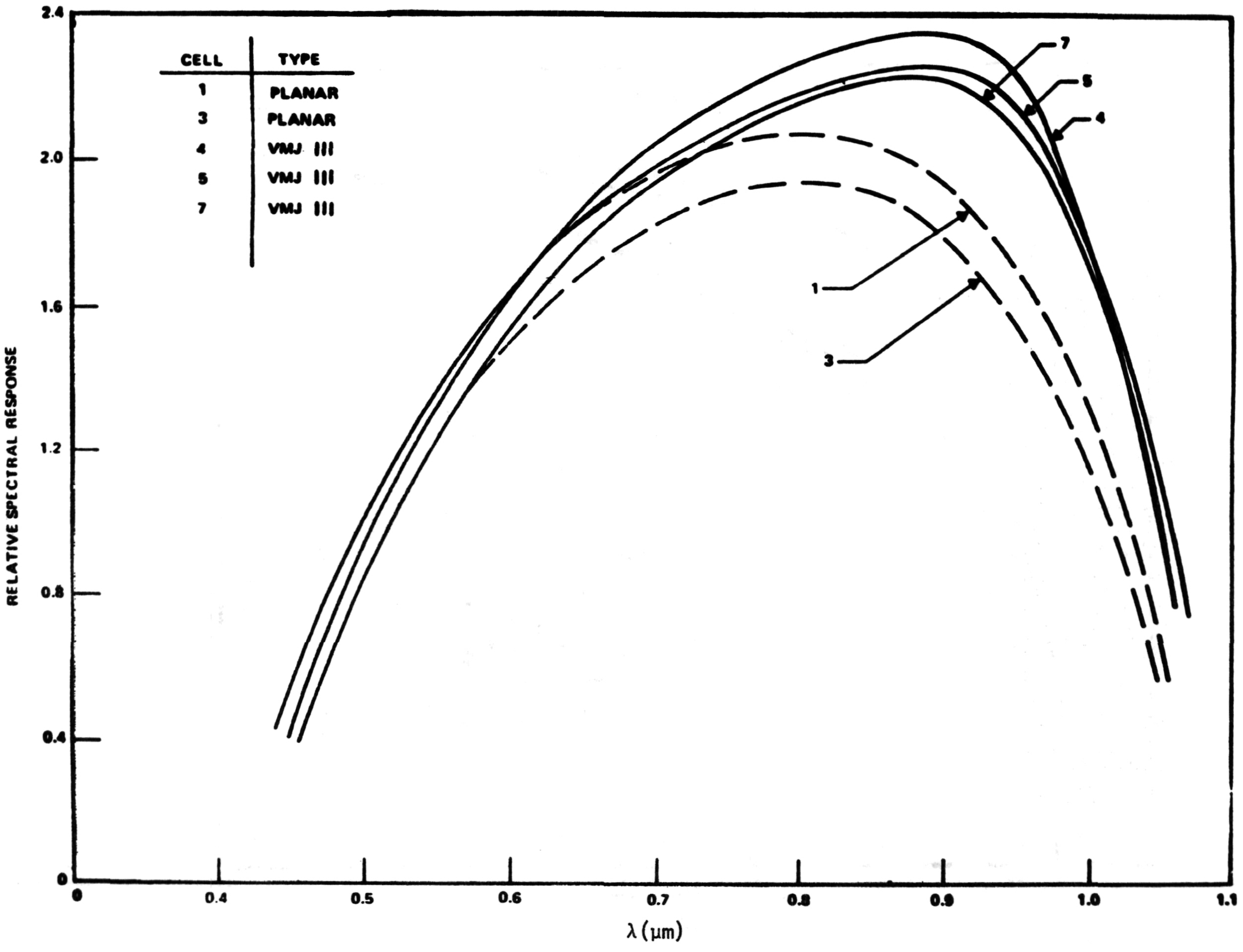

Figure 8. - Spectral response for Type III and conventional cells processed simultaneously.

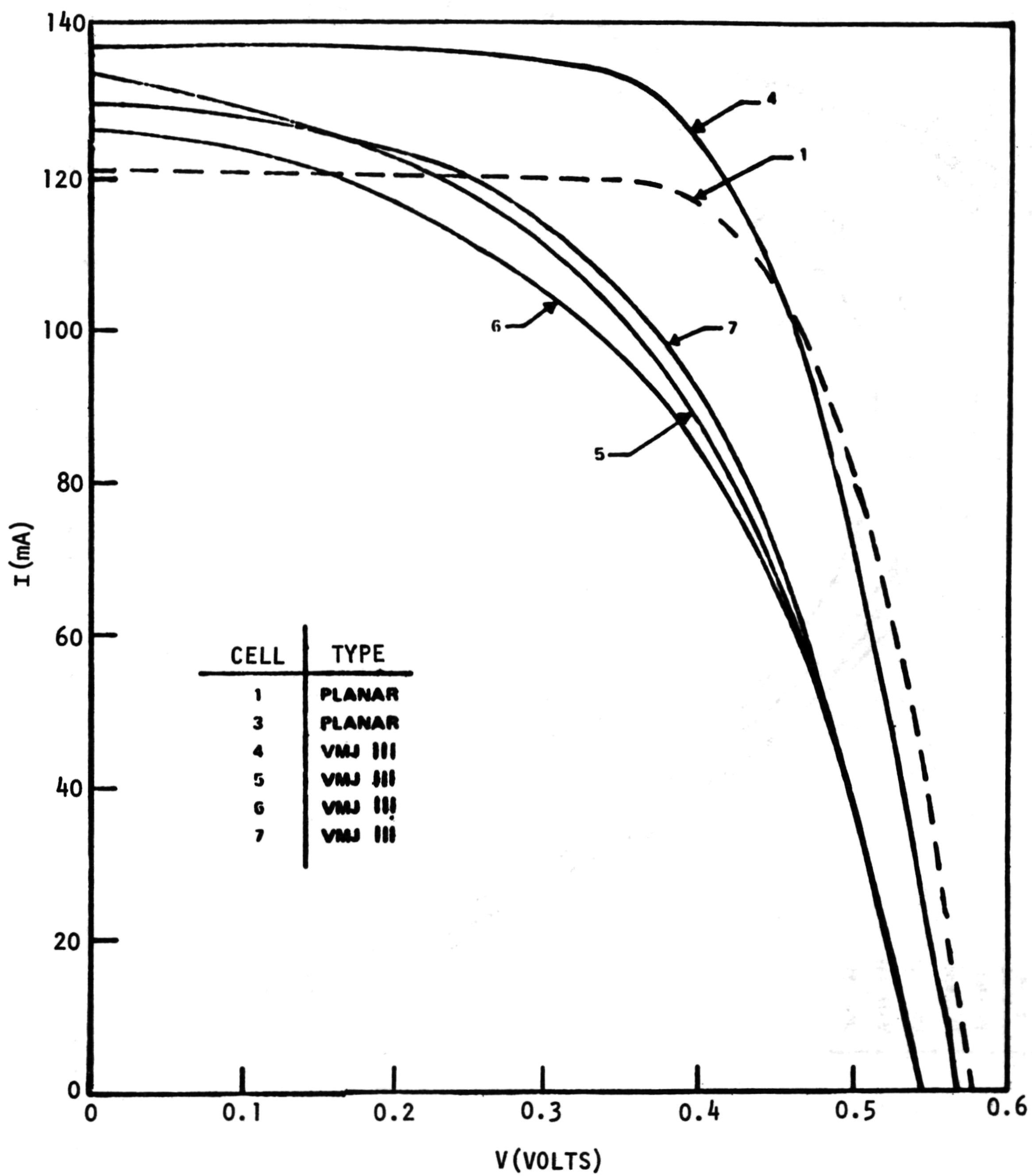

Figure 9. - Current-voltage characteristics of Type III and conventional cells.

9. V-GROOVED SILICON SOLAR CELLS

Cosmo R. Baraona
NASA Lewis Research Center
Cleveland, Ohio

The objective of making V-grooved silicon solar cells is to reduce the reflection loss and thus improve the efficiency of a silicon solar cell. Figure 1 shows what the simplest type of grooved cell looks like. Its front illuminated surface consists of a series of parallel grooves which are V-shaped in cross section. The mechanism by which reflection is reduced by such a structure is as follows. Light which is perpendicularly incident on a surface (such as the flat spots between the grooves in fig. 1) is perpendicularly reflected and lost after only one reflection. However, light incident on a groove wall will be reflected onto the adjacent groove wall, where it has a second chance to be absorbed. Thus, if at a given wavelength there is a 0.30 reflection loss on a flat surface, a grooved surface will have an effective reflectivity of 0.30×0.30 or 0.09. Note that this reflection loss mechanism is independent of the wavelength of the incident light.

A second mechanism operating on macroscopically grooved surfaces may result in improved carrier collection, because of the generation of carriers closer to the collecting junction. Light striking a groove wall enters the silicon and is refracted toward the perpendicular to the wall, that is, laterally in the cell. The lateral direction results in absorption and carrier generation closer to the front surface than in a cell with a smooth surface. Carriers generated closer to the junction have a higher probability of being collected, which results in improved collection efficiency. The amount of refraction depends on the wavelength of the light because of the varying index of refraction of silicon. The blue light, which is strongly absorbed, is also strongly refracted and therefore is absorbed not much closer to the local surface than in a smooth cell.

There are three methods of arranging the grooves on a surface: (1) parallel grooves, where the groove spacing (the width of flat spots between the grooves) can be varied; the lowest reflection would occur for a 100-percent-grooved surface, that is, a saw-tooth-cross-section surface with no flat spots; (2) a grid-type pattern with perpendicularly intersecting V channels resulting in regularly spaced, four-sided pyramids with either pointed or truncated tops; and (3) randomly spaced and randomly sized pointy pyramids or a textured surface.

There are at least two methods of making grooved or textured surfaces. The first we tried was a preferential caustic etch on <100> silicon, as reported by Stoller in the 1970 RCA Review. This method requires oxide masking and photoresist technology, which are not desirable for inexpensive cell production. A second preferential etch we tried was reported by Lee in the 1969 Journal of Applied Physics. On unmasked <100>

silicon this etch results in samples with black velvetlike surfaces. Views of this velvet surface are shown in figures 2 and 3. Figure 2 is a scanning electron micrograph taken at a 45° angle to the sample. Figure 3 is another portion of the surface viewed perpendicularly. The velvet surface consists of randomly spaced, four-sided, pointed tetrahedra with a maximum size and height of about 10 to 12 micrometers. Other textured surfaces with different tetrahedra sizes have also been made. These textured surfaces are desirable for reducing reflection losses.

Figure 4 shows the measured total reflectivity plotted against wavelength of the incident light for several kinds of samples. The top curve is for a mirrorlike mechanically polished silicon surface. The next two are for parallel-grooved samples, each with a different amount of surface area covered with grooves. This was accomplished by varying the groove spacing W_T, so that the measured groove ratios expressed in percent were 16 and 36 (see bottom of fig. 1). The total reflectivity of these surfaces is the flat ratio times the reflectivity of the flats R_F plus the groove ratio times the reflectivity of the flat raised to the 2.1 power $R_F^{2.1}$. The exponent is based on an estimate that most photons incident on a groove undergo two reflections, but a few undergo three, so that overall about 2.1 reflections are achieved. Thus, the equation in figure 1, when used to calculate the reflectivities of the 16- and 36-percent-grooved samples in figure 4, results in good agreement with the measured values. The velvet surface in figure 4 corresponds to a near-100-percent-grooved surface. The bottom curve is for a velvet texturized surface with an antireflection coating and encapsulated in Teflon FEP film. The reflectivity is very low (4 to 5 percent) and relatively independent of wavelength. Samples with 100-percent-grooved or textured surfaces have a very matte or velvet black appearance. This confirms the low reflection capability of modifying the surface structure.

The enhancement of collective efficiency has been seen by us in radiation damaged cells. A solar cell with 65 percent grooving was irradiated with 1-MeV electrons. Figure 5 shows the decrease in effective diffusion length (a measure of collective efficiency rather than true diffusion length) with electron fluence for the grooved cell and a conventional smooth cell.

Presumably the true diffusion length in both cells changed the same with irradiation, but the collection of carriers was not impaired as quickly in the grooved cell. The grooved cell therefore exhibits a lower damage coefficient. The grid-type pattern and the random or textured pattern are expected to exhibit the same effect. In summary, several methods of making different types of grooved silicon surfaces were demonstrated. Optical reflection was reduced and can be approximately predicted by using a simple formula. A texturized surface consisting of numerous random pyramids was created by using a hydrazine etch. This velvet surface, when covered with an antireflection coating, had a reflectivity of only 4 percent, which was relatively independent of wavelength. Radiation damage results suggest that collection efficiency declines with electron irradiation more slowly when solar cells are made with grooved surfaces.

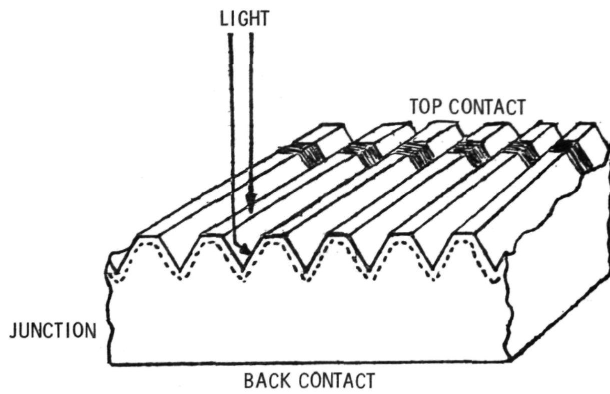

GROOVE SPACING = W_T

GROOVE RATIO = W_G / W_T

FLAT RATIO = $1 - W_G / W_T = W_F / W_T$

$$R_T = \frac{W_F}{W_T} R_F + \frac{W_G}{W_T} R_F^2 \quad 1$$

Figure 1. - Low reflection grooved surface solar cell.

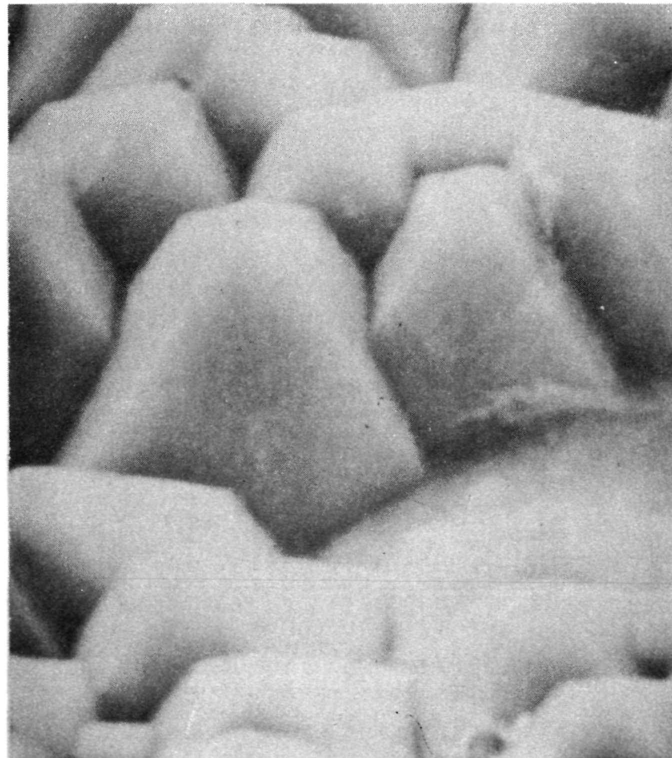

Figure 2. - Lewis velvet surface - 45^0 view.

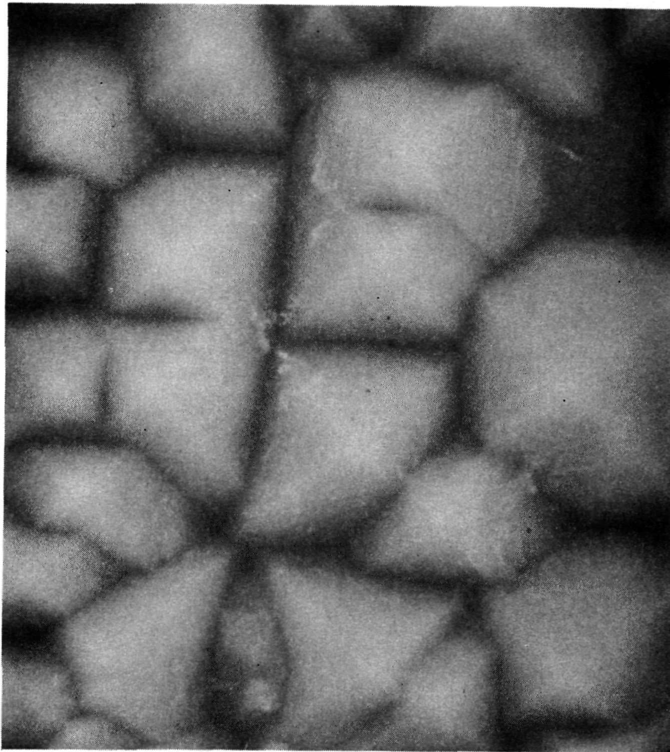

Figure 3. - Lewis velvet surface - normal view.

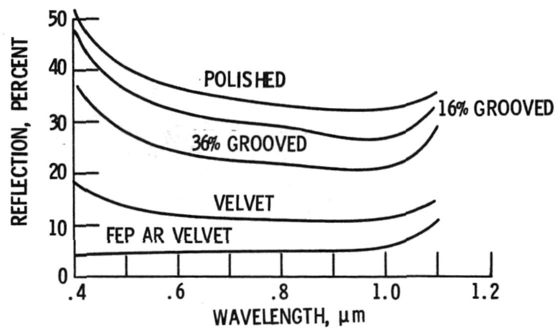

Figure 4. - Total reflection for various types of silicon surfaces.

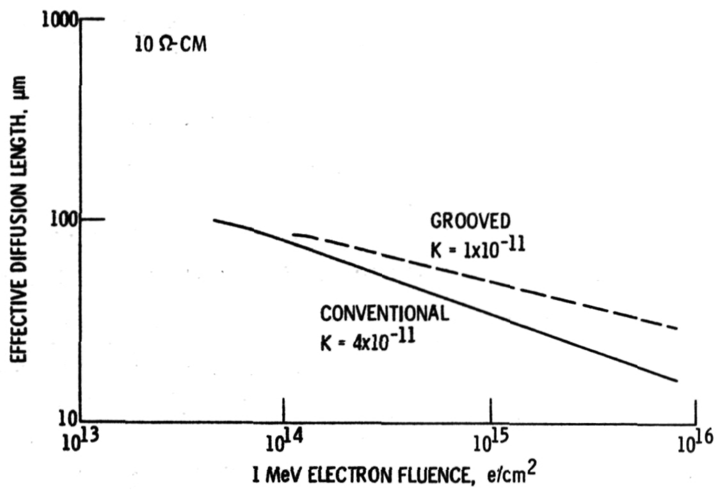

Figure 5. - Radiation damage of grooved solar cell.

10. A SUMMARY OF INVESTIGATIONS INTO THE PERFORMANCE OF "GRATING" TYPE PHOTOVOLTAIC DEVICES*

J. J. Loferski, L. Y. Chen, and E. E. Crisman
Brown University
Providence, Rhode Island 02912

For high photovoltaic conversion efficiency, a solar cell requires: (1) a minority carrier diffusion length, in the base material, which is comparable to the adsorption depth ($1/\alpha$) of, say, 95% of the photons having energies in excess of the band gap; (2) low surface recombination losses on the light receiving surface; and (3) a large potential barrier between the n and p regions of the cell. In the case of silicon these requirements translate to base materials with diffusion length of one hundred microns or greater; surface recombination velocities in the few hundred cm/sec range and; less than 1 Ω-cm resistivity. Such parameters must be maintained through the various processing steps and be realized in the finished cell. The planar diffusion technique commonly used in the commercial production of solar cells results in a highly disordered light receiving layer in which the lifetime of minority carriers is reduced by orders of magnitude from that of the starting crystal. A corresponding reduction in cell response is observed for the short wavelength ("blue") photons which are primarily absorbed in this diffused layer.

A possible way of realizing the performance criteria, enumerated above, is to redesign the cell geometry so that most of the light receiving surface is the base material maintained in the original chemo-mechanically polished condition, i.e., not subjected to diffusion or any other process which might introduce impurities or surface contamination or damage.

The approach described herein (referred to as the "grating" cell design) employs narrow strips, or fingers, of junction separated by wider regions of exposed base material. The fingers need not necessarily be made by diffusion. Indeed, the most recent work, reported here, has concentrated on the formation of an alloy junction of aluminum and n-type silicon. By such an approach both p/n junction and front surface contact are simultaneously formed

* This work has been supported primarily by NASA Grant 40-002-093 and in part by Micro Components Corporation of Cranston, Rhode Island.

Preceding Page Blank

in a single thermal cycle. Titanium-silver back surface contact can also be sintered during the same heat treatment. By heating below the Al-Si eutectic temperature ($\sim$576°C) aluminum/silicon Schottky barrier cells have also been produced in the grating format.

This paper summarizes the work which has been performed to date on the grating type silicon solar cell using the various junctions formation approaches, i.e., diffused, alloyed, and Schottky barrier.

PREVIOUS INVESTIGATIONS

1. Waffled Cells

The earliest attempt to produce blue shifted cells consisted of etching a grid pattern through the diffused layer of commercially produced solar cells. Both p/n and n/p cells were used. Details of the procedure employed can be found in references 1 and 2. The resulting pattern, consisting of 50 × 50 μ recesses spaced on 100 μ centers is shown in figure 2. The etching depth was approximately 1.5 μ. The normalized (to maximum value) short circuit current spectral response of such a "waffled" area is shown in figure 3 compared to the normalized response of the same portion of the cell before etching in the pattern. While there is apparent improvement in response at say 4000Å illumination by a factor of two for the etched compared to the pre-etched condition, the absolute response of etched areas was always lower than that of the untouched portion. Analysis of the i-V characteristics showed that the change in absolute short circuit current can be traced primarily to an increase, by a factor of about five, of the series resistance of the cell after waffling.

2. Small Area Cells

In an attempt to produce devices with series resistances comparable to those of commercial cells, four small area (1 × 1 mm) designs were produced on

single chips (2 × 2 mm)[*] which were subsequently bonded to standard TO-5 headers. About 400 such chips could be produced on a single wafer of silicon thereby reducing variations related to changes in individual wafer characteristics. Referring to figure 4, the four configurations consisted of: (a) an area diffused cell included for comparison purposes; (b,c) two "finger" diffused cells of different finger spacings; and (d) a (undiffused) metal-semiconductor, Schottky barrier cell. A comparison of the response of the four types of cells is shown in the illuminated i-V characteristics for the most efficient of each type (figure 5). As can be seen, the Schottky barrier cell was the least efficient owing primarily to the reduced open circuit voltage. Since aluminum was the metal used to form the barrier, it is to be expected that V_{oc} would be reduced for this type of cell. The short circuit current for the metal-semiconductor configuration is, however, comparable to that of the other three configurations. The estimated maximum efficiencies, at AM1, of the best cell of each design were:

Area Diffused	12.9%
Narrow Spaced Finger Diffused	11.9%
Wide Spaced Finger Diffused	12.2%
Metal-Semiconductor (Undiffused)	3.7%

A more important result of this phase of the investigation can be seen by examining figures 6 through 9, which give the normalized short circuit current response of the four cell types as a function of the wave length of illumination. The feature most evident is that all three types of grating cells have enhanced blue response compared to the area diffused cell. The relative response per photon

---

[*] These cells were prepared by Micro-Components Corp., of Cranston, R. I.

of the area diffused cell was typical of the commercial cells available at that time. At 4000Å the response was about 14% of peak output. The three grating designs all show significantly enhanced blue responses which vary between 60% and 84% of the peak output depending on design. Because the illumination source used for the i-V measurements was deficient in short wave length photons, it is likely that the use of a source with greater blue output (i.e., the sun) would result in an improvement of the efficiencies of the grating cell designs relative to the area diffused type.

A method for analyzing the response of the cell response as a function of position was developed during this phase of the investigation. In brief, it consists of locally exciting carriers using the electron beam of a microprobe and then displaying the resulting signal, proportional to i_{sc}, on an oscilloscope for photographic recording. The display can take the form of either an intensity enhancement (by putting the i_{sc} signal into the z-axis of the scope) or a 3-dimensional appearing perspective display by adding i_{sc} output to the y-deflection signal. Examples of the types of displays available from the electron microprobe are shown in figures 10 and 11 for the finger diffused cells and figures 12 and 13 for the metal-semiconductor cells. Note certain areas of reduced and enhanced response that are evident in the i_{sc} mappings which have no counterpart in the corresponding secondary emission surveys of the same areas. Also, by expanding the scale in the deflection enhanced mode, diffusion lengths in the various regions of the cells can be directly estimated. Such techniques have proved valuable in relating localized response changes to crystallographic imperfection as discussed elsewhere in this conference record.*

---

* R. Kaul, B. Roessler and J. J. Loferski, "Correlation Between Mechanical Imperfections and Electrical Properties of Solar Cells."

Descriptions of the fabrication techniques and testing procedures of the small area devices are given in references 3 and 4.

ALLOY GRATING CELLS.

After demonstrating that grating structure approach could produce the desired blue shifted device in either diffused junction or Schottky barrier junction form, efforts were directed to geometrically similar devices with the junction produced by alloying fingers of a dopant metal into polished base wafers. Aluminum was chosen as the alloying agent primarily for the following reasons: (1) The small but finite solid solubility of aluminum in silicon ($\sim 7 \times 10^{18}$ atoms/cc) should result in a transition to p-type material in the regrowth region for n-type base wafers with dopant concentrations in the range 10^{14} to 10^{18} atoms/cc commonly used for solar cells (i.e., 100 Ω-cm to 0.01 Ω-cm resistivities). (2) Aluminum is an inexpensive metal which would, therefore, lend itself to large-scale production of cells for terrestial applications. (3) The relative low eutectic temperature of Al-Si alloys ($\sim$ 576°C) permits investigation at temperatures significantly lower than normal diffusion temperatures for silicon. Such low temperatures should also help reduce costs of mass produced devices.

The alloying of aluminum with silicon was extensively investigated during the early days of the semiconductor industry. Extended analysis of the interaction can be found in references 5 through 8. Briefly, as the system is heated above the eutectic, the percentage of aluminum in the liquid phase increases (see figure 1). Lowering the system temperature through the eutectic points results in excess silicon in the liquid phase being rejected and a regrowth region forming at the liquid-silicon interface. It is believed that the silicon base wafer acts as a seed for recrystallization of the liquid, and that the regrown crystal is single crystal in form with the same orientation as the base

wafer. If the solid solubility of the aluminum is sufficient to overcome the n-type dopant of the base material an abrupt p/n junction is formed at the regrown region/base material interface.

Extensive theoretical and experimental investigations were undertaken to determine the effects of varying the finger/spacing ratio and the temperature profile of the alloying cycle. A summary of much of the early part of this work is given in references 4 and 9. At that time it was concluded that small area cells could be produced by the alloy-grating technique with short circuit densities equal to or greater than those of conventional planar diffused cells. Such devices, also, displayed strongly blue shifted collection efficiencies: essentially flat in response to photon wave length in the region from 8500Å to 4000Å. The main disadvantage of such cells was the reduced open circuit voltage which at best was only 0.440 Volts compared to a nominal 0.550 Volts for commercial cells. It was also observed during this earlier investigation of the alloy-grating cell that starting with a <100> oriented base wafer gave cells with a V_{oc} about 18% greater than <111> oriented wafers. No satisfactory explanation has thus far been offered to explain this difference. However, orientation dependent alloying has been observed by others (reference 10) and techniques have been presented in the literature to stabilize the junction formation during alloying.

To investigate effect of the alloying temperature cycle per se, a number of samples have been alloyed at successively high maximum temperatures with all other parameters being held constant. The result is shown in figure 14, which shows that the curve of open circuit voltage versus maximum temperature reaches a broad maximum of $V_{oc} \sim 0.500$ volts for alloying temperatures between 650°C and 750°C. While this represents an improvement over the 0.440 Volts maximum reported earlier it is still some 10% below the nominal 0.550 Volts of commercial cells.

An important conclusion can be made as a result of these experiments: the low V_{oc}'s reported earlier cannot be caused merely by the presence of the grating pattern. Since the samples used for the V_{oc} vs temperature measurement were 2 × 2 mm squares completely alloyed with about 7000Å of aluminum their exposed junction length was only the periphery of the squares or about 7000μ. The 2 × 2 mm alloyed-grating cells reported in reference 9 had effective exposed junction edges of 40000μ to 80000μ--about ten times as great. However, the open circuit voltages for alloying at 600°C were essentially the same for both cases.

This conclusion is further verified by the results of measurements made on large area (1 cm^2) cells which have been constructed by the alloy-grating technique. The configuration used for these cells is shown diagrammatically in figure 15. Figure 16 is the I-V characteristic of one such cell which was fabricated on the (100) plane of a 2-3.5 Ω-cm silicon wafer. The characteristic was measured using a Spectrolab artificial sun located at NASA Lewis Space Flight Center.* The I-V characteristic of this cell and a 2 cm^2 commercial silicon cell (without antireflection coating) were made with the source illumination set at 136 mw/cm^2. The commercial cell information has been displayed on a per square cm basis to facilitate the comparison.

Note that the grating cell produces a short circuit current comparable to, and indeed a little greater than, that produced by the commercial cell. However, the open circuit voltage (∿ 0.470 Volts) is about 14% lower. The efficiency at the maximum power point is consequently about 7.9% as compared to 11% for the commercial cell. The spectral response of the two cells is given in figure 17. Note here that the grating cell shows definitely higher output at the

---

* We wish to thank Dr. Henry Brandhorst of NASA Lewis who made arrangement for these measurements and helped to perform them.

shorter wave length end of the curve. Since the Spectrolab simulator is deficient in the blue region compared to true solar AMO conditions, the I_{sc} of the grating cell (in figure 16) should be even larger than the commercial cell for a true AMO illumination.

CONCLUSION

1. Large area cells have been constructed using the alloy-grating structure which have essentially the same characteristics as the small area ($< 4\ mm^2$) cells heretofore constructed.

2. The best large area cell fabricated to date has AMO efficiency of 8% without antireflection coating.

3. Large area cells made by the allow-grating technique are considerably blue shifted and have I_{sc} equal to or greater than commercial cells of the same area.

4. The reduced open circuit voltage of such cells is not primarily the result of the increase in exposed junction edge effected by the grating structure.

5. The lower process temperature and reduced number of fabrication steps suggest that real financial saving can be realized by employing the alloy-grating construction. If the mechanisms causing the reduced V_{oc} can be overcome, cells of this type should perform in a space environment at least as efficiently as conventional planar diffused cells.

6. At present the reduced V_{oc} of this design is not understood. Preliminary investigations seem to indicate that excess exposed junction edge is not the cause. It is also unlikely that the alloying process forms inherently poorer junctions than the diffusion process does. This contention is supported by the fact that no diffused grating cells have been fabricated with V_{oc}'s

significantly greater than those of the alloyed type (see figure 2). Theoretical predictions, which agree well with experimental data in other aspects of performance, suggest that surface recombination velocities as high as 1000 cm/sec should not significantly affect response. Such values should be readily obtainable with standard processing techniques.

REFERENCES

1. J. J. Loferski, N. Ranganathan, E. E. Crisman, and L. Y. Chen, "Methods of Improving the Efficiency of Photovoltaic Cells," Fourth Semiannual Report on NASA Grant 40-002-093, September 1, 1971, thru February 28, 1972.

2. N. Ranganathan, E. E. Crisman, and J. J. Loferski, "An Investigation of Silicon Photovoltaic Cells Aimed at Increasing Their Solar Energy Conversion Efficiency," Summary Report Number 1 on NASA Grant NGR 40-002-093.

3. W. F. Armitage, E. E. Crisman, J. J. Loferski, and L. Y. Chen, "Research and Development of Photosensitive Monolithic Integrated Circuit," Third Quarterly Progress Report to Micro Components Corporation, Cranston, R. I., June 1973.

4. J. J. Loferski, E. E. Crisman, L. Y. Chen, and W. Armitage, "Methods of Improving the Efficiency of Photovoltaic Cells," Sixth Semiannual Report on NASA Grant NGR 40-002-093, September 1, 1972, thru February 28, 1973.

5. F. J. Biondi (Editor), Transistor Technology, Vol. III, D. Van Nostrand Co., Inc., Princeton, N. J., 1958, pp. 3-16, 175-244.

6. J. J. Pankove, "Transistor Fabrication by the Melt-Quench Process," Proc. IRS, 44, 1956, p. 185.

7. G. L. Pearson and B. Sawyer, "Silicon p-n Junction Alloy Diodes," Proc. IRE, 40, 1952, p. 1348.

8. G. L. Pearson and P. W. Foy, "p-n Silicon Junction Diode Formation by the Alloying Process," Phys Rev., 87, p. 190, (1952).

9. J. J. Loferski, E. E. Crisman, L. Y. Chen, and W. Armitage, "Method of Improving the Efficiency of Photovoltaic Cells," Seventh Semiannual Report on NASA Grant NGR 40-002-093, March 1, 1973, thru August 31, 1973.

10. O. S. Herman, "Al-Si and Al-Cu Metalization Techniques for Silicon LSI IC's," IEEE Conference Record of the 1973 Conference on Electron Device Technology, pp. 92-97.

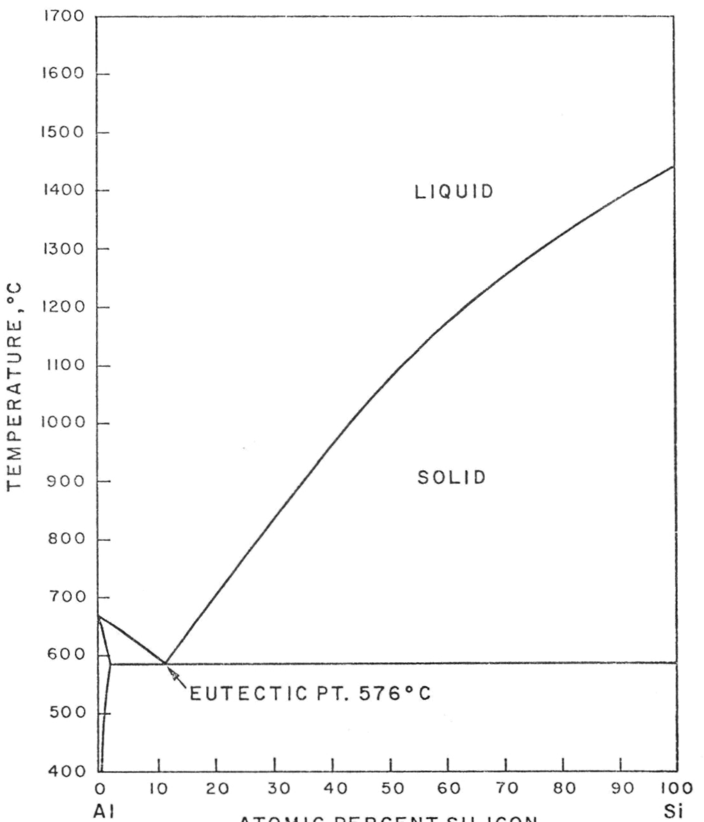

Figure 1. - Aluminum-silicon phase diagram.

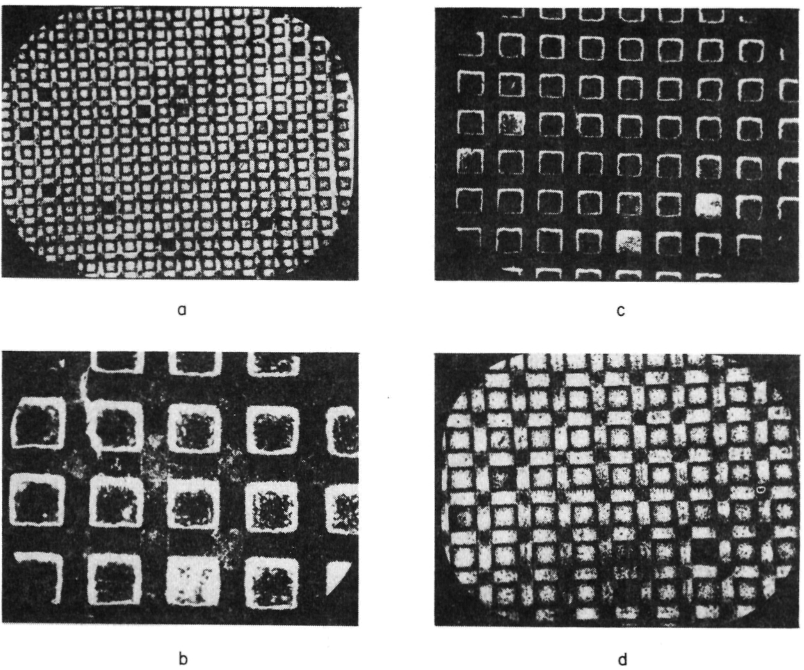

Figure 2. - Photomicrograph of n/p cell D113 after waffling using Ronchi grating mask. The depth of etching was about 1.5 microns, grid spacing 100 microns. Magnification: (a) 50x (light field); (b) 200x (dark field); (c) 100x (dark field); (d) 100x (light field).

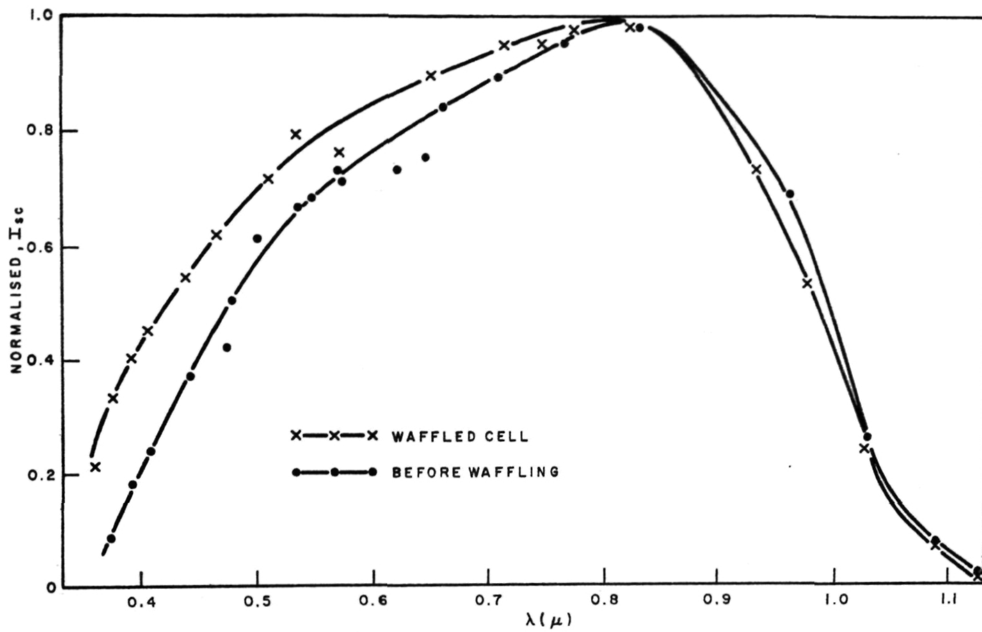

Figure 3. - Comparison of normalized spectral response of same area of n/p 10 Ω-cm cell (no. D118) before and after etching of waffle pattern.

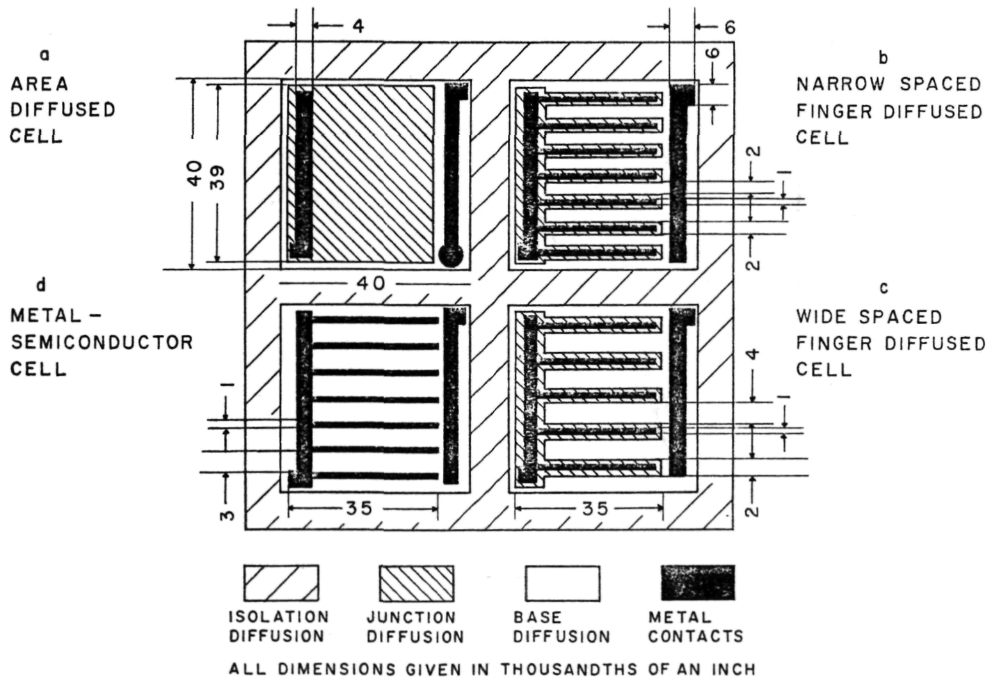

Figure 4. - Schematic of four (0.040 by 0.040 in. each) cell chips showing representative dimensions.

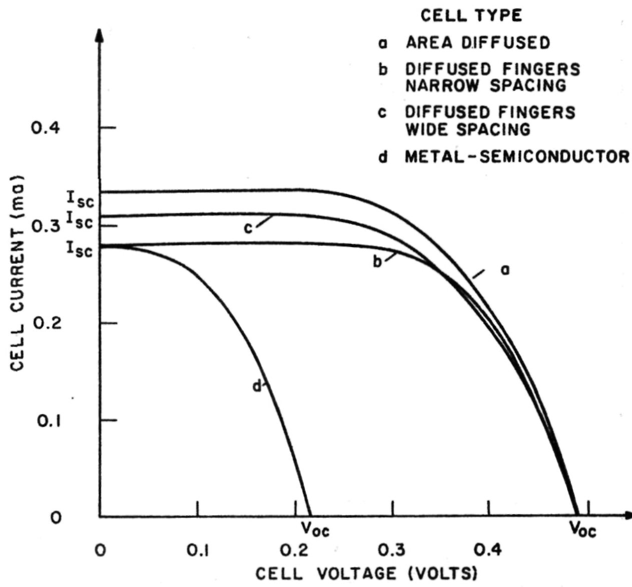

Figure 5. - Illuminated I-V characteristics of the most efficient cell of each design.

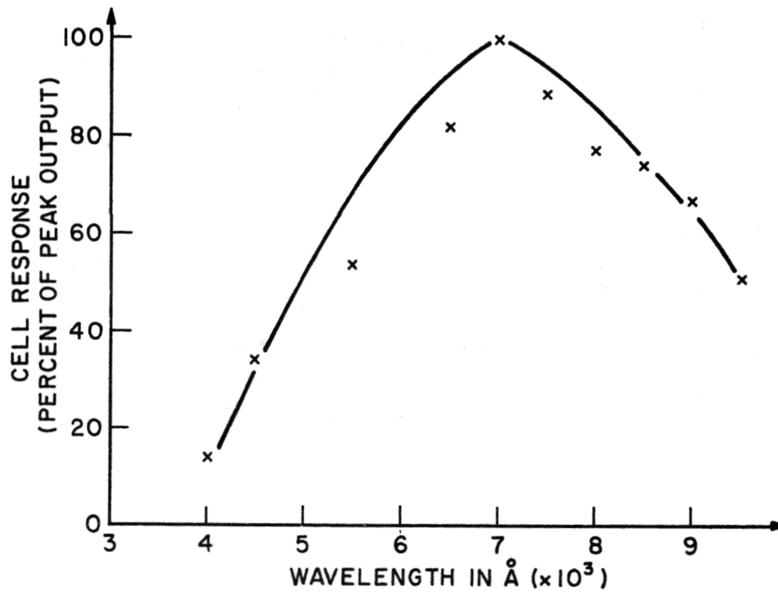

Figure 6. - Spectral response in area diffused cell.

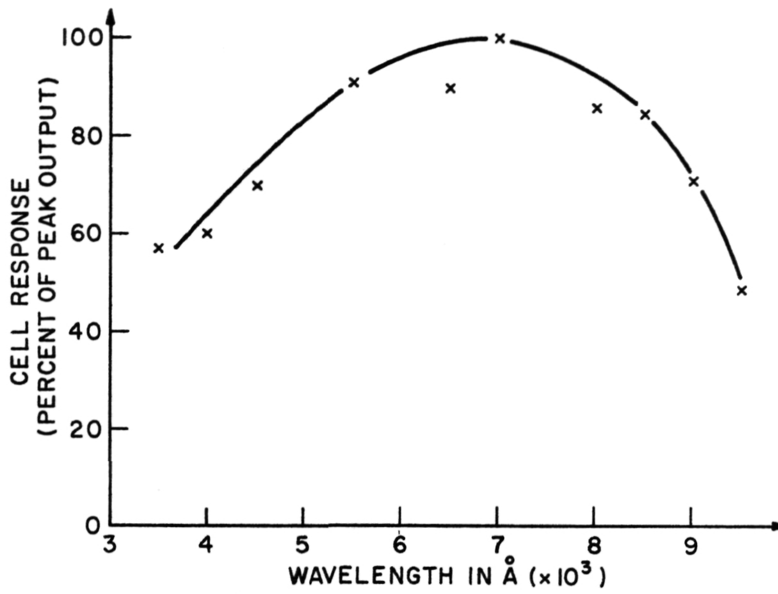

Figure 7. - Spectral response in finger diffused cell with narrow spacing.

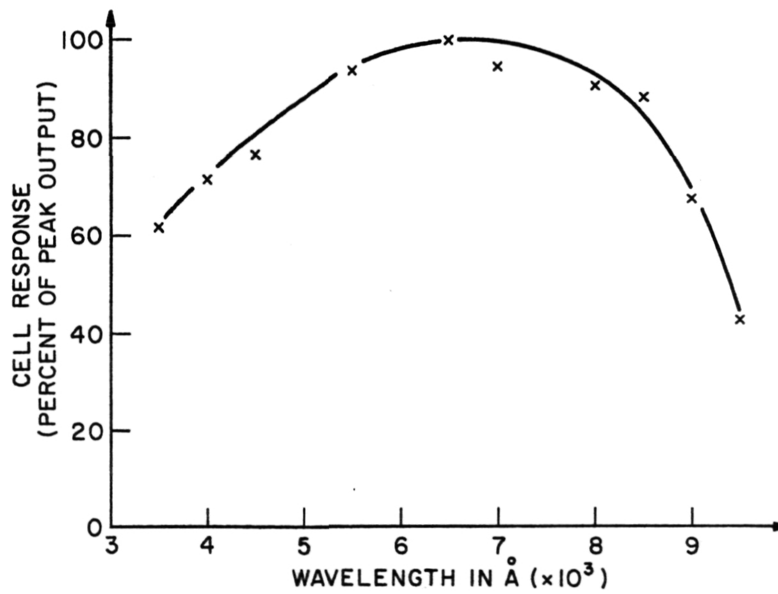

Figure 8. - Spectral response in finger diffused cell with wide spacing.

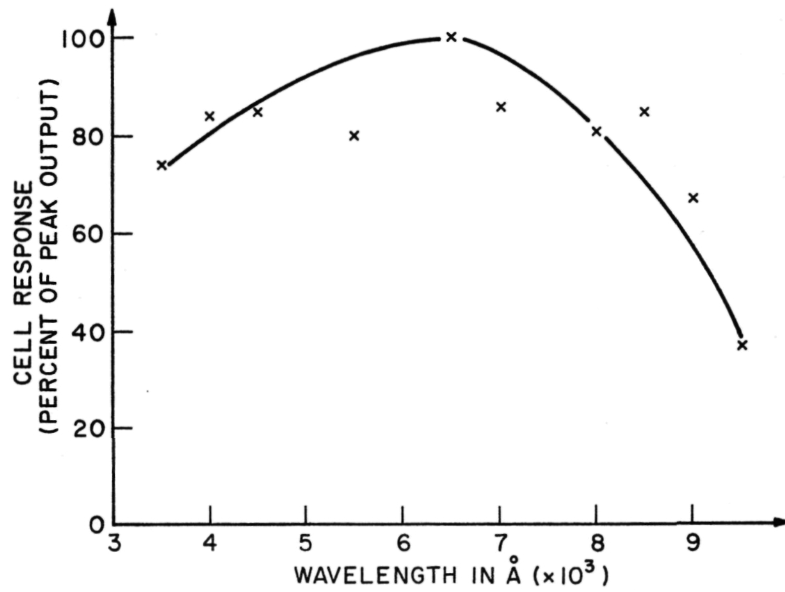

Figure 9. - Spectral response in metal/semiconductor cell.

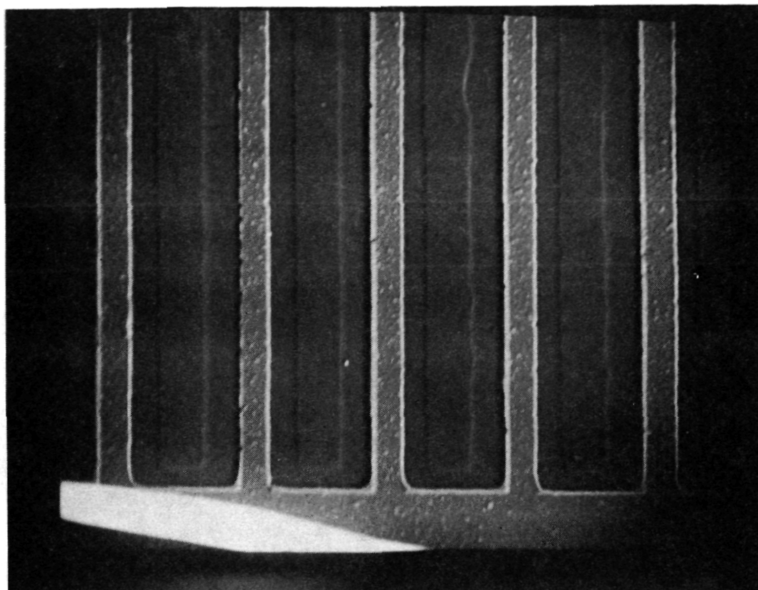

SECONDARY EMISSION RESPONSE

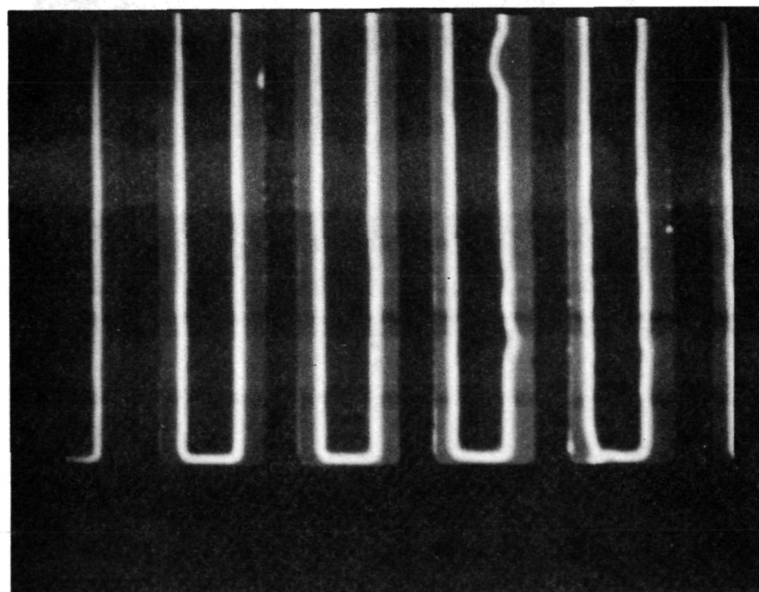

CELL CURRENT RESPONSE
(intensity enhanced)

Figure 10. - Narrow spaced diffused cell.

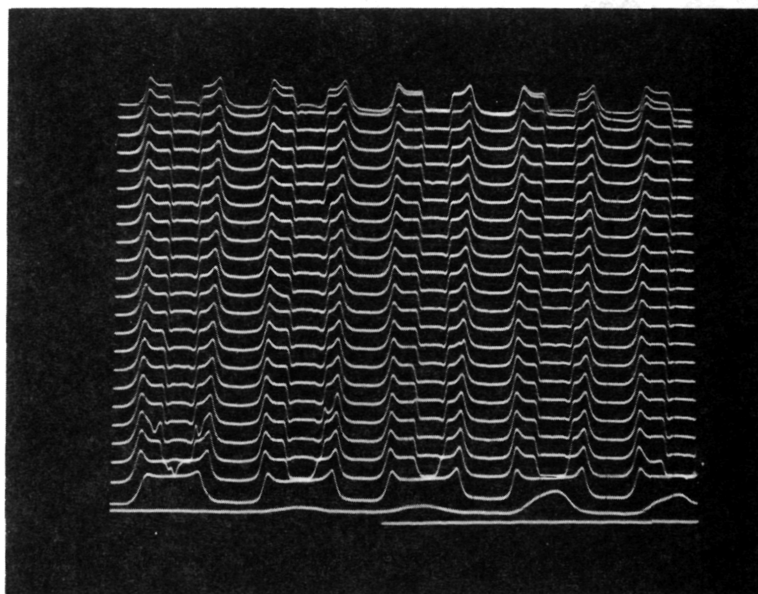

40μ

CELL CURRENT RESPONSE
(deflection enhanced)

Figure 11. - Narrow spaced diffused cell.

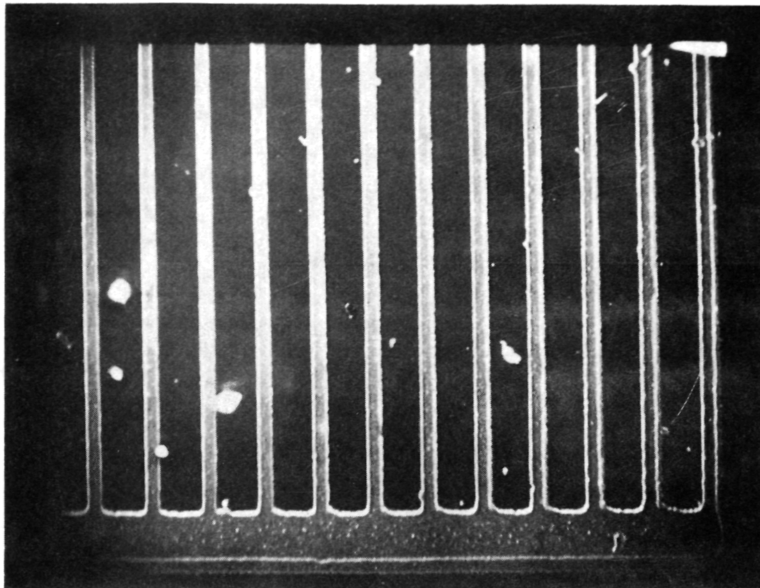

SECONDARY EMISSION RESPONSE

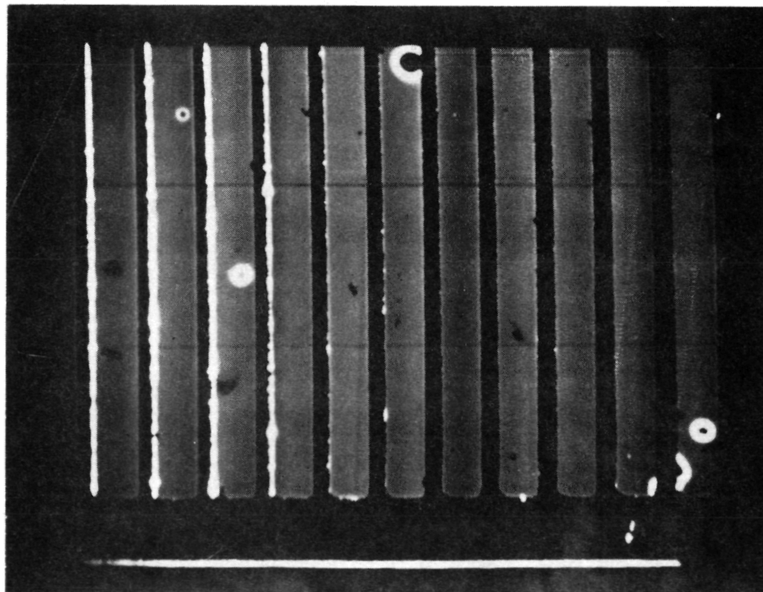

CELL CURRENT RESPONSE
(intensity enhanced)

Figure 12. - Metal/semiconductor cell.

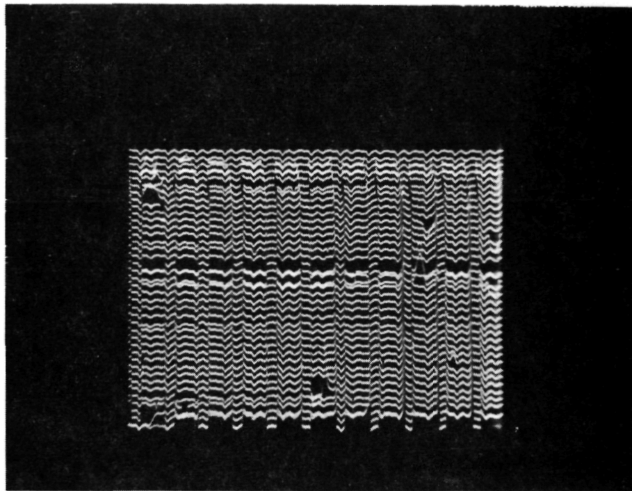

200μ

CELL CURRENT RESPONSE
(deflection enhanced)

Figure 13. - Metal/semiconductor cell.

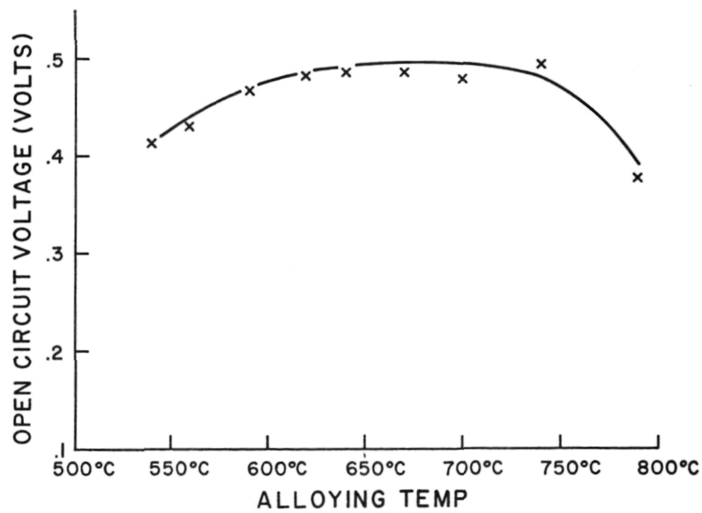

Figure 14. - Open circuit voltage versus alloying temperature.

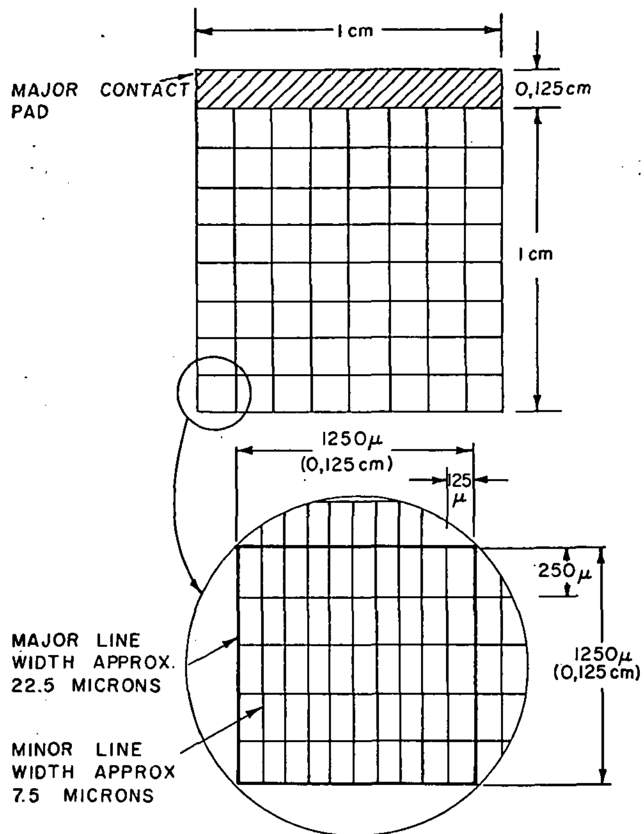

Figure 15. - Grating pattern used for alloyed and diffused cells.

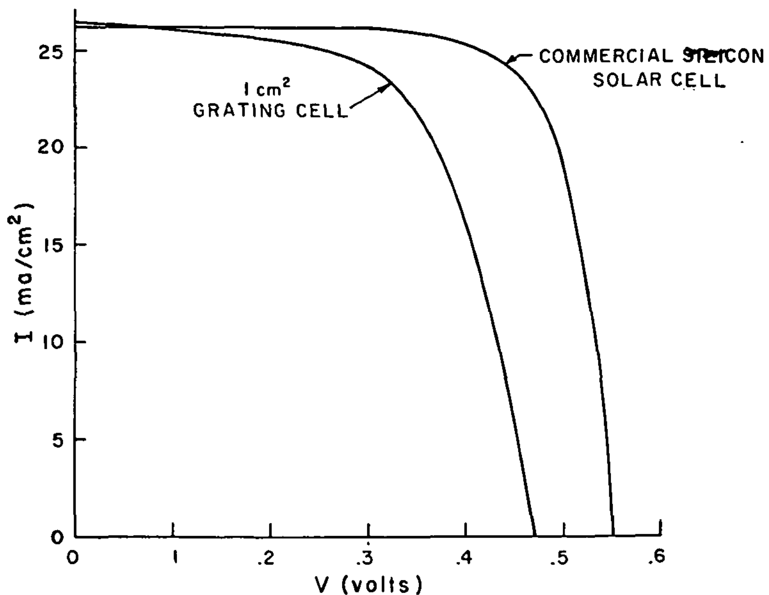

Figure 16. - Characteristic under simulated AMO illumination.

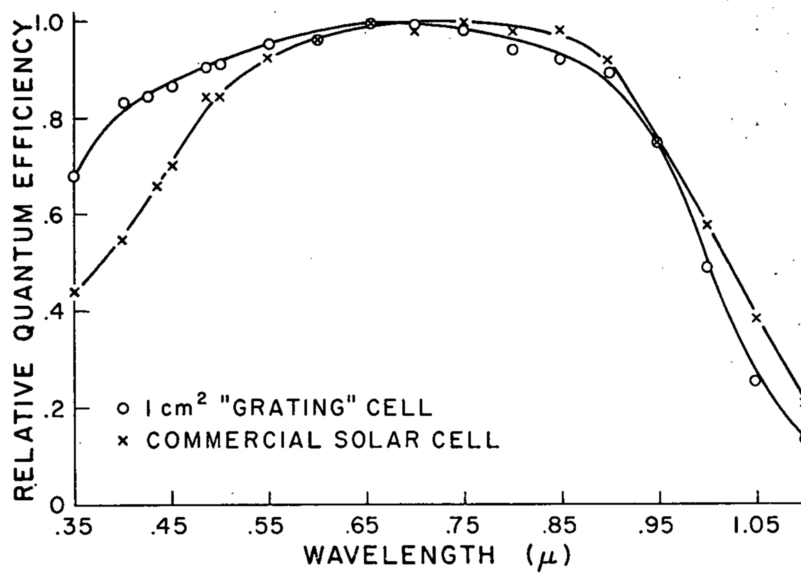

Figure 17. - Relative spectral response.

11. GALLIUM ARSENIDE SOLAR CELL RESEARCH AT NASA LANGLEY RESEARCH CENTER

Gilbert H. Walker
NASA Langley Research Center
Hampton, Virginia 23665

Gallium arsenide solar cells have a theoretical efficiency of about 26%.[1] GaAs has good high temperature properties such that operation at 300°C is possible. In addition to these two properties GaAs solar cells have good radiation resistance. This paper describes the gallium arsenide solar cell research program being conducted at NASA Langley Research Center. The goals of this program are to obtain GaAs solar cells with 20% efficiency at Air Mass Zero (AMO) and to obtain 5% efficient cells which will operate stably at 300°C.

The absorption coefficient of GaAs is such that the incoming photons are absorbed within a few microns of the front surface; therefore the surface properties are very important. Figure 1 is a theoretical plot by Ellis and Moss[2] of the log of the surface recombination velocity vs efficiency for a GaAs solar cell with a 0.25 micron p-n junction. For a surface recombination velocity of 10^7 cm/sec, the GaAs solar cell efficiency is limited to about 12%; however, if this recombination velocity can be reduced to 10^4 cm/sec, an efficiency of 24% is possible. Measurements of the surface recombination velocity of GaAs at Langley indicate that the value is between 10^7 cm/sec and 10^6 cm/sec. One method by which the surface recombination velocity can be reduced is by growing a heteroface

layer on the GaAs surface such that the number of interface states is reduced. Such a technique has been developed by Woodall and Hovel.[3] This structure consists of a p-GaAs n-GaAs solar cell with a layer of p-$Ga_{1-x}A\ell_xAs$ epitaxially grown on the p-GaAs surface. The value of x in the $Ga_{1-x}A\ell_xAs$ layer is chosen such that the layer is transparent to the incoming photons. The improved high energy responses of such solar cells indicate that the surface recombination velocity has been reduced to 10^4 cm/sec.

Another problem area in obtaining high efficiency GaAs solar cells is the low minority carrier diffusion length of the base n-type GaAs material. Figure 2 is a theoretical plot of current collected from the base region of a GaAs solar cell as a function of minority carrier diffusion length for a junction depth of 0.25 micrometers.[4] The base current contribution is 7 ma/cm^2 for a diffusion length of 0.5 micrometers. This current can be increased to 14 ma/cm by increasing the diffusion length to 3 micrometers. In an effort to determine if commercially available GaAs had the required 3-micrometer diffusion lengths, Carnegie-Mellon University (under an NASA Langley grant) undertook a survey of commercially available GaAs. The results of this survey are shown in the lower part of Figure 2. 57% of the material surveyed had diffusion lengths of 0.3 to 1.0 micrometers; 30% had diffusion lengths of 1.0-2.0 micrometers; 9% fell in the 2.0-3.0 micrometer range; while only 4% had the required diffusion length of greater than 3.0 micrometers. Because of epitaxial growth problem no complete cells were produced from the 6 samples of GaAs with diffusion length greater than 2 micrometers. A program is underway with the goal of obtaining GaAs with the required diffusion length.

The most efficient cell produced to date has an AMO efficiency of 13.5%. This cell is a p-$Ga_{1-x}A\ell_xAs$-p-GaAs-n-GaAs cell with an area

of 0.25 cm^2. The increase in the diffusion length of the base material should increase the efficiency of this structure to about 17%.

The results of high temperature studies of a p-$Ga_{1-x}A\ell_xAs$-p-GaAs-n-GaAs are shown in Figure 3.[5] The efficiency of the cell is 8% at 245°C. Optimization of this structure is continuing.

The continuing Langley program is outlined in Figure 4. The program consists of four subelements: materials improvement, surface improvement, cell development, and cell characterization. Research is being conducted in these areas through combined in-house, grant, and contract research efforts. The materials improvement part of the program is directed toward obtaining n-type GaAs with 3-micrometer diffusion lengths for use as substrates for epitaxial growth of cells. Both epitaxial growth techniques and bulk growth techniques are being used to obtain these substrates. At Brown University research is underway to determine the effect of crystal dislocations on diffusion length. In the surface improvement part of the program, fundamental studies of surface states and their relationship to recombination velocity will be conducted.

Development of the p-$Ga_{1-x}A\ell_xAs$-p-GaAs-n-GaAs heteroface solar cell is continuing. This cell will be optimized for maximum efficiency at air mass zero using the improved diffusion length base material. This cell is also being optimized for stable operation at 300°C. In addition to this heteroface cell, a heterojunction cell is being developed for operation at high temperatures. This cell consists of a layer of p-$Ga_{1-x}A\ell_xAs$ on n-$Ga_{1-y}A\ell_yAs$. This aluminum content of the p layer is chosen such that the p-$Ga_{1-x}A\ell_xAs$ has an indirect band gap and hence is transparent to the incoming solar radiation. The aluminum content of the n-$Ga_{1-x}A\ell_xAs$ is

chosen such that the n-type material has a larger band gap and hence has less degradation of efficienty with temperature.

The silicon grating cell was developed at Brown University under an NASA grant.[6] Techniques used to fabricate this cell will be applied to GaAs as a means of lowering processing costs.

In summary, the goal of this program is to obtain GaAs solar cells with efficiencies of 20% and to obtain GaAs solar cells that will operate at 300°C. Presently the AMO efficiency of GaAs solar cells is 13.5% at 20°C and 8% at 245°C.

References

1. Rappaport, P.; and Wypocki, J. J.: The Photovoltaic Effect in GaAs, CdS, and Compound Semiconductor. Acta Electronica, Vol. 5, 1961, pp. 364-375.
2. Ellis, B.; and Moss, T. S.: Calculated Efficiencies of Practical GaAs and S: Solar Cells Including The Effect of Built-In Electric Fields. Solid State Electronics, Vol. 13, 1970, pp. 1-24.
3. Woodall, J. M.; and Hovel, H. J.: High Efficiency $Ga_{1-x}Al_xAs$-GaAs Solar Cells. Applied Physics Letters, Vol. 21, No. 8, October 1972, pp. 379-381.
4. Milnes, A. G.; and Feucht, D. L.: Studies of Heteroface Solar Cell Performance. Semi-annual Status Report, Oct. 1972-April 1973. NASA Grant NGR 39-087-021.
5. Hovel, H.; and Woodall, J. M.: Optimization of Solar Cells for Air Mass Zero Operation and a Study of Solar Cells at High Tempera-

tures. Quarterly Progress Report, June 1974-October 1974, NASA Contract NAS1-12812.

6. Loferski, J. J.; Crisman, E. E.; Armitage, W.; and Chin, L. Y.: Theoretical and experimental Investigation of Grating Type Photovoltaic Cells. Proceedings of the Tenth IEEE Photovoltaic Specialists Conference, November 13-15, 1973, Palo Alto, California, pp. 58-63

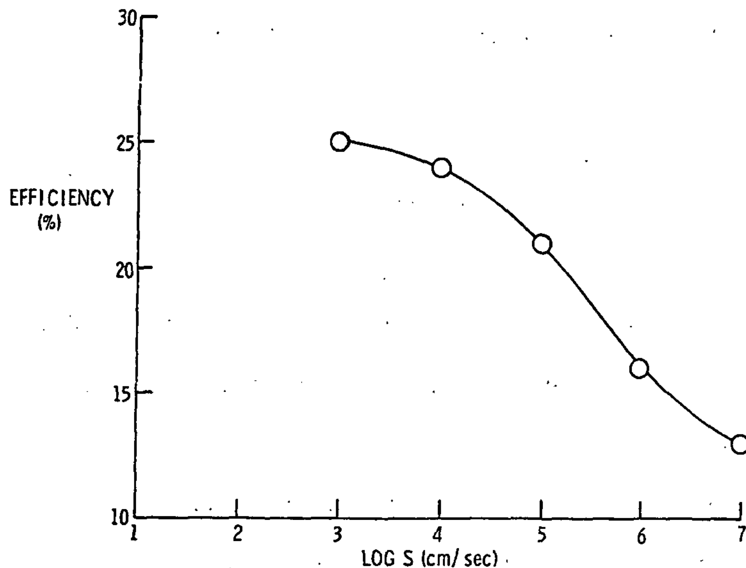

Figure 1. - Effect of surface recombination velocity on solar cell efficiency for a 0.25 μ p-n junction depth.

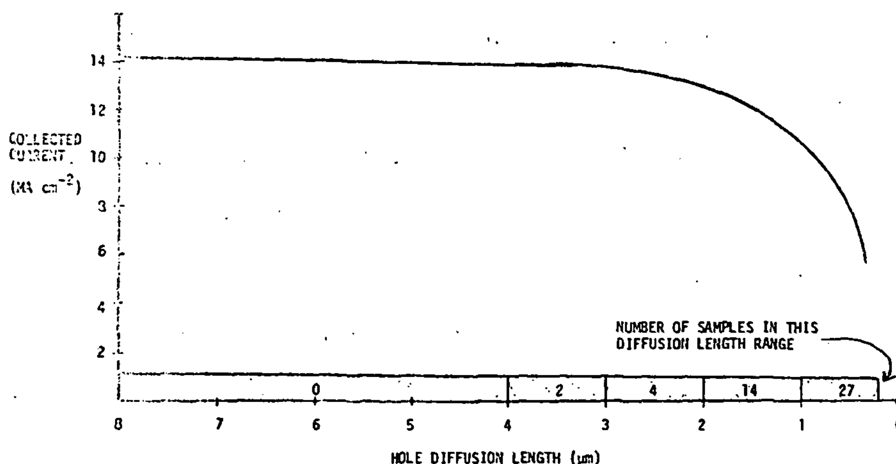

Figure 2. - GaAs base layer current collection vs. hole diffusion length.

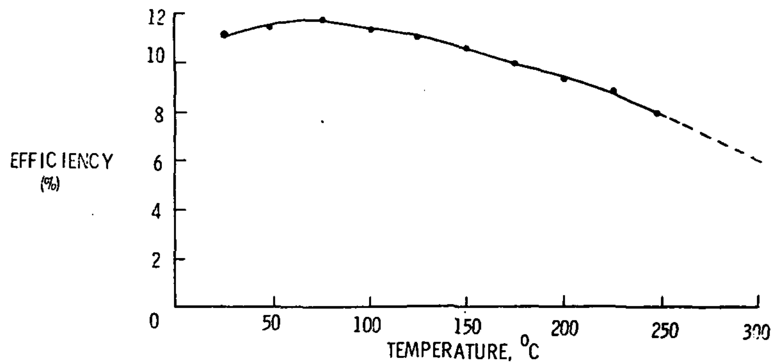

Figure 3. - High temperature efficiency of a GaAs solar cell.

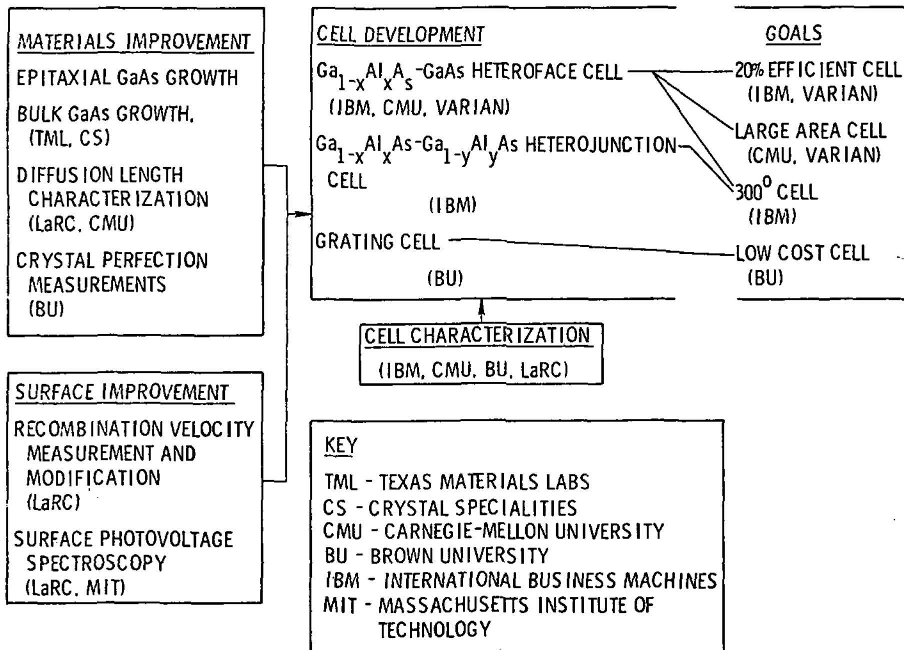

Figure 4. - GaAs solar cell program.

12. HIGH EFFICIENCY GRADED BAND-GAP $Al_xGa_{1-x}As$-GaAs SOLAR CELL

James A. Hutchby
NASA Langley Research Center
Hampton, Virginia 23665

It is well known, from the standpoint of optical band-gap energy, that GaAs is a near optimum material for solar cell fabrication, and is predicted to have a maximum theoretical air mass zero (AMO) power conversion efficiency of 23% compared to 20% for Si.[1] However, in early work with GaAs p on n diffused cells, maximum AMO efficiencies of only 9.3% were achieved.[2] A major difficulty in achieving higher efficiencies is the significant loss through surface recombination of photogenerated minority carriers, which are created near the surface (within approximately 1 μm) due to the direct nature of optical absorption in GaAs. The highest experimental AMO efficiencies of 11.0% - 12.1% (not corrected for contact area) for GaAs cells were reported by Hovel and Woodall[3] for the $Al_xGa_{1-x}As$-GaAs heteroface cell. In their device the surface $Al_xGa_{1-x}As$ layer was typically many diffusion lengths thick (4-20 μm) and the p-n junction was located approximately 1 μm below the intermetallic junction in the GaAs substrate. Thus, the main function of the surface layer was to reduce the surface recombination velocity (S) of the GaAs surface and to reduce the series resistance of the cell; i.e., photons absorbed in the epitaxial layer did not contribute significantly to the short-circuit current.

Another method proposed to reduce surface recombination loss is that of a built-in electric field in the surface layer to accelerate excess minority carriers toward the p-n junction and reduce the time required for their

collection.[4,5,6] Such a field can be accomplished by varying either the doping concentration or the energy band-gap in the surface layer. Theoretical analyses[2] and tentative experimental results[7] show that exponential doping profiles yield a significant improvement in efficiency of GaAs cells.

Also, an idealistic analysis[8] of a $Zn_xHg_{1-x}Te$ graded band-gap cell indicated improvements in efficiency particularly for very low doping concentration in the surface layer. In this letter initial results of a detailed analysis of an n on p graded band-gap $Al_xGa_{1-x}As$-GaAs cell are presented.

An energy band diagram of the cell structure, as shown in Fig. 1, depicts a surface $Al_xGa_{1-x}As$ layer divided into a region of indirect material for $y < y_c$ ($x \geq 0.29$) and a region of direct material for $y_c \leq y \leq y_j$. The electric field for holes in the indirect material, being proportional to the slope of the valence band, is lower than that in the direct material. Consequently for a fixed junction depth (y_j) the surface electric field for holes should increase with surface mole fraction of AlAs (X_{ALO}) until the surface material approaches the direct-indirect transition. Further increases in X_{ALO} yield a decreasing surface field until most of the free electrons reside in the indirect conduction band.

The analysis was performed using the standard continuity and current density expressions[9] for the bulk material assuming $S = 1 \times 10^5 - 1 \times 10^6$ cm/sec at $y = 0$ and $S \rightarrow \infty$ at $y = 125$ µm. The injected excess carrier concentrations at the p-n junction were assumed to be given by the standard Boltzman boundary condition.[10] In the graded $Al_xGa_{1-x}As$ layer the hole transport parameters were assumed to be constant, but the position dependence of the absorption coefficient required a numerical solution. An analytical solution was used for the GaAs region. The hole diffusion length (ℓ_{po}) in the $Al_xGa_{1-x}As$ layer and the

electron diffusion length (ℓ_{no}) in the GaAs substrate were assumed to have an empirical dependence on impurity concentrations as compiled and given by Ellis and Moss[6] for GaAs. Furthermore, junction recombination current density,[11] series resistance of the cell,[12] and surface reflection losses were considered.[13] The analysis was performed for AMO insolation given by Johnson.[14]

Optimum values of impurity concentrations and junction depth were first determined to yield maximum conversion efficiency. Donor concentrations below the optimum value of $N_d = 4 \times 10^{17}$ cm^{-3} significantly reduce cell voltage produced at the maximum power point through an excessively large series resistance. Larger donor concentrations reduce the cell current delivered at maximum power due to reduction of hole diffusion length and thereby hole collection efficiency in the $Al_xGa_{1-x}As$ region. An optimum acceptor concentration of $N_a = 2 \times 10^{17}$ cm^{-3} was used, although cell efficiency is rather insensitive to this parameter below $N_a = 1 \times 10^{18}$ cm^{-3}. Larger values of N_a reduce electron diffusion length and thereby electron collection efficiency in the GaAs region. A junction depth of $\ell_j = 1$ μm was determined as optimum. Smaller values of ℓ_j excessively increase the series resistance, and larger values reduce the hole collection efficiency in the $Al_xGa_{1-x}As$ layer.

Figure 2 shows the dependence of efficiency (not corrected for contact area) upon X_{ALO} for two values of S and for both assumed and degraded values for ℓ_{po}. In each case, X_{ALO} has a profound effect upon efficiency up to the direct-indirect transition, above which a decrease in surface field causes a slight drop in efficiency. Although the presence of an electric field decreases the sensitivity of efficiency to S and ℓ_{po}, these parameters (particularly the latter) are still important to achieving high efficiencies. As can be seen, an optimized cell having $\ell_{no} = 7.6$ μm, $\ell_{po} = 2.1$ μm, and

$S = 1 \times 10^5$ cm/sec is predicted to have an efficiency of 17%. The same cell with $S = 1 \times 10^6$ cm/sec has a predicted efficiency of 16%.

The primary effect of the built-in field is to improve the collection efficiency of photogenerated holes in the $Al_xGa_{1-x}As$ layer. These holes recombine with free electrons either at the surface or in the bulk or they are collected at the p-n junction. Plots of the areal densities of holes participating in these processes normalized to the total areal density of holes photogenerated in the undepleted n region are shown as functions of X_{ALO} in Fig. 3. The effect of the electric field for $X_{ALO} = 0.25$ compared to the zero field case is seen to be a 114% increase of the hole collection efficiency caused primarily by a 95% decrease in the dominant surface recombination loss and, to a lesser extent, by a 77% decrease in the bulk recombination loss. This illustrates the reduced sensitivity of the graded band-gap cell to high surface recombination velocity or reduced hole diffusion length.

These results lead to the conclusion that a graded band-gap $Al_xGa_{1-x}As$-GaAs cell with $X_{ALO} = 0.25$ should have a power conversion efficiency of 17% for reasonable values of surface recombination velocity and minority carrier diffusion lengths.

We acknowledge Mr. Richard L. Fudurich of Computer Science Corporation for his enthusiastic support and cooperation in programing this analysis.

REFERENCES

1. J. J. Loferski, J. Appl. Phys. 27, 777 (1956). The AMO condition is identical to the condition of m = 0 and w = 0 given in this reference.
2. S. C. Tsaur, A. G. Milnes, R. Sahai, and D. L. Feucht, in Proceedings of

the Fourth International Symposium on GaAs and Related Compounds, Conference Series Number 17 (The Institute of Physics, 47 Belgrave Square, London, England, 1973), pp. 156-167.

3. H. J. Hovel and J. M. Woodall, J. Electrochem. Soc. 120, 1246 (1973).
4. M. Wolf, Proc. I.R.E. 48, 1246 (1960).
5. M. Wolf, Proc. IEEE 51, 674 (1963).
6. B. Ellis and T. S. Moss, Solid St. Electron. 13, 1 (1970).
7. K. V. Vaidyanathan and G. H. Walker, Proc. 10th IEEE Photovoltaic Specialists Conference, IEEE Catalog Number 73 CHO 801-ED, p. 31 (1974).
8. Y. Marfaing, in Proc. of the International Colloquium on Solar Cells (Gordon and Breach Science Publishers, New York, 1970), p. 67.
9. S. M. Sze, Physics of Semiconductor Devices (John Wiley and Sons, New York, 1969), pp. 66-67.
10. S. M. Sze, Physics of Semiconductor Devices (John Wiley and Sons, New York, 1969), pp. 96-97.
11. S. C. Choo, Solid St. Electron. 11, 1069 (1968).
12. R. J. Handy, Solid St. Electron. 10, 765 (1967).
13. A. Vasicek, Optics on Thin Films (North-Holland Publishing Co., New York, 1960), p. 139.
14. F. S. Johnson, J. Meteorol. 11, 431 (1954).

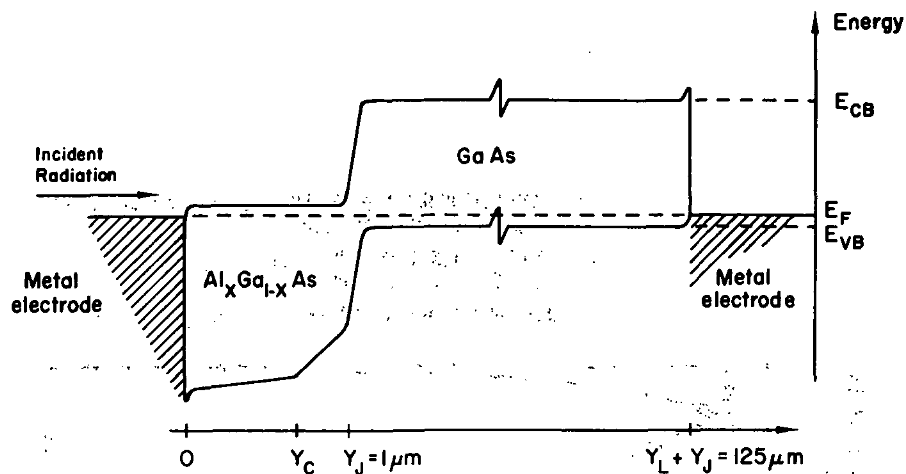

Figure 1. - Energy band diagram for $Al_xGa_{1-x}As$-GaAs graded band-gap solar cell.

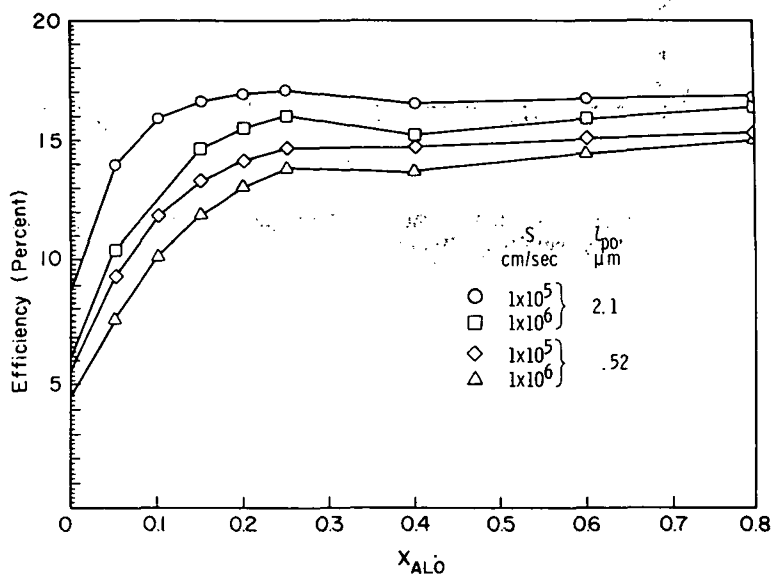

Figure 2. - Dependence of power conversion efficiency on X_{ALO}.

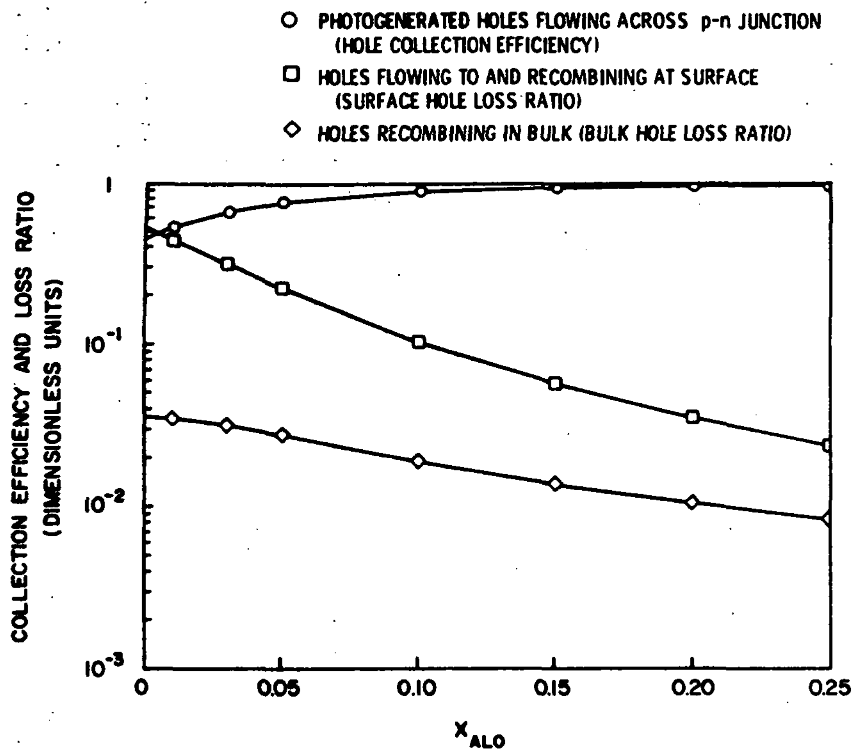

Figure 3. - Ratios of hole particle current density to photon flux density absorbed in undepleted $Al_xGa_{1-x}As$ layer for $S = 1x10^5$ cm/sec.

EXPERIMENTAL RESULTS ON LOSS MECHANISMS

A focus on the measurement and identification of surface and bulk parameters that can influence solar cell efficiency

Preceding Page Blank

13. APPLICATION OF THE MOS C-V TECHNIQUE TO THE DIFFUSED FACE OF SILICON SOLAR CELLS

Irving Weinberg
NASA Lewis Research Center
Cleveland, Ohio

The diffused face is perhaps the least understood portion of the silicon solar cell. In an attempt to remedy this deficiency, we have initiated an experimental program aimed at obtaining information concerning the states which contribute to recombination on the highly doped, diffused solar cell surface. The MOS, capacitance-voltage technique is the experimental method chosen for this investigation.[1] This technique has predominantly been used, in the past, to investigate the nature of the Si-SiO_2 interface and oxide states. The current investigation is concerned, however, with silicon coated with Ta_2O_5, an oxide used as a coating on advanced solar cells.[2] Although the diffused surfaces of solar cells are our primary interest, it is easier to understand the much simpler combination of Ta_2O_5 on moderately doped silicon. This latter research is concurrent with our experimental work on the solar cell diffused face. Hence, a summary is first given of initial results on the simpler system. Following this, a description is given of our initial solar cell results.

Our initial experiments on moderately doped single crystal Si-Ta_2O_5 are concerned with the effects of heat treatment after oxide deposition. Figure 1 shows the 1 MHz data for 3 ohm-cm n-type Si-Ta_2O_5. Postdeposition heat treatment details are shown in the figure. Oxide thicknesses were 595×10^{-10} and 625×10^{-10} m (595 and 625 Å) for the heat treated and as-deposited oxide, respectively. After oxide deposition and heat treatment, the MOS capacitor was completed by vacuum deposition of circular gold dots, 0.0254 cm in diameter, on the free oxide surface. The hysteresis observed in both cases is attributed predominantly to the presence of oxide traps.[3] In addition, the effects of mobile oxide ions are also observed.[4] The theoretical curve, calculated for the absence of surface states,[1] combined with additional frequency dependent data, indicates that a reasonable approximation to the high-frequency limit has been attained. Although instability is noted in both sets of data, C_{FB}, the flat band capacitance can be calculated by standard techniques.[1] Hence, for the as-deposited sample, C_{FB} = 39.7 pF, while for the heated sample C_{FB} = 44.4 pF. Additional information is obtained from the conductance-voltage data shown in figure 2. Curves similar to that shown in figure 2 were obtained over a frequency range extending from 10 kHz to 1 MHz and used to compute τ, the time constant for interface states.[5] Calculations for the flat-band point are summarized in figure 3. The density of fixed surface charge N_S includes oxide charge as well as charge in surface states. The density of states N_{SS} is obtained

Preceding Page Blank

from the slope of the C-V curve at the flat-band point. Implicit in this procedure is neglect of the effects of possible inhomogenities in the oxide charge distribution on the MOS C-V characteristics.[6] The as-deposited sample yielded no peak in the conductance data; hence, no values of τ are obtainable for this case.[5] Summarizing, postdeposition annealing reduces the charge density N_S, although the density of states N_{SS} remains approximately the same. These results indicate that additional postdeposition heat treatment is required in order to minimize the effects of oxide trapping and ion motion in the oxide.

The configuration used in obtaining the solar cell C-V data is shown in figure 4. Oxide thickness was 575×10^{-10} m (575 Å) and the gold dot is again 0.0254 cm in diameter. This configuration is used in order to avoid complications due to the p-n junction. The capacitance-voltage data shown in figure 5 are expanded to yield the enlarged curve shown in figure 6. The latter curve clearly shows the presence of a minimum and approaches a limiting maximum value. Excursions outside the voltage range shown are limited by dielectric breakdown. However, since a minimum is observed, the bulk impurity concentration close to the surface is obtainable from a plot of $1/C^2$ against applied voltage (fig. 7).[7] The data for the diffused face of the silicon solar cell are summarized in figure 8. The depletion width W was obtained after taking into account band gap narrowing due to heavy doping effects.[8] The impurity concentration N is the value at a depth W, 15×10^{-10} m (15 Å), from the diffused surface and is, in effect, a surface parameter. Furthermore, the value found for N is in reasonable agreement with the solid solubility limit for phosphorus in silicon at 850° C.[9] The surface fixed charge concentration N_S is obtained from the data at the flat-band point (220 pF). As before, N_S includes the effects of oxide charge as well as surface states. In obtaining N_S, correction was made for bulk resistance due to the configuration used. In addition, the oxide dielectric constant was obtained from an independent experiment on a similar oxide.

The solar cell C-V data are the first such data obtained for the heavily doped, diffused face. Furthermore, the MOS C-V technique can yield information regarding surface parameters for the highly doped, diffused face of the silicon solar cell.

REFERENCES

1. A. Goetzberger and S. M. Sze, "Metal-Insulator - Semiconductor Physics," Applied Solid State Science, vol. 1, p. 153, 1969.
2. J. Lindmayer and J. F. Allison, "The Violet Cell: An Improved Solar Cell," Comsat Tech, Review, vol. 3, p. 1, 1973.

3. F. P. Heiman and G. Warfield, "The Effects of Traps on the MOS Capacitance," IEEE Trans. Electronic Devices, vol. ED-12, p. 167, 1965.

4. E. H. Snow, A. S. Grove, B. E. Deal and C. T. Sah, "Ion Transport Phenomena in Insulating Films," Journ. Appl. Physics, vol. 36, p. 1664, 1965.

5. H. Dueling, E. Klausmann and A. Goetzberger, "Interface States in Si-SiO_2 Interfaces," vol. 15, p. 559, 1972.

6. M. J. McNutt and C. T. Sah, "Effects of Spatially Inhomogeneous Oxide Charge Distribution on the MOS Capacitance-Voltage Characteristic," Journ. Appl. Physics, vol. 45, p. 3916, 1974.

7. W. van Gelder and E. H. Nicollian, "Silicon Impurity Distribution as Revealed by Pulsed MOS C-V Measurements," Journal of the Electrochemical Society, vol. 118, p. 138, 1971.

8. R. J. Van Overstraeten, H. J. Deman and R. P. Mertens, Transport Equations in Heavily Doped Silicon," IEEE Trans. on Electron Devices, vol. ED-20, p. 290, 1973.

9. F. A. Trumbore, "Solid Solubilities of Impurity Elements in Germanium and Silicon," Bell Syst. Tech. Journ., vol. 39, p. 205, 1960.

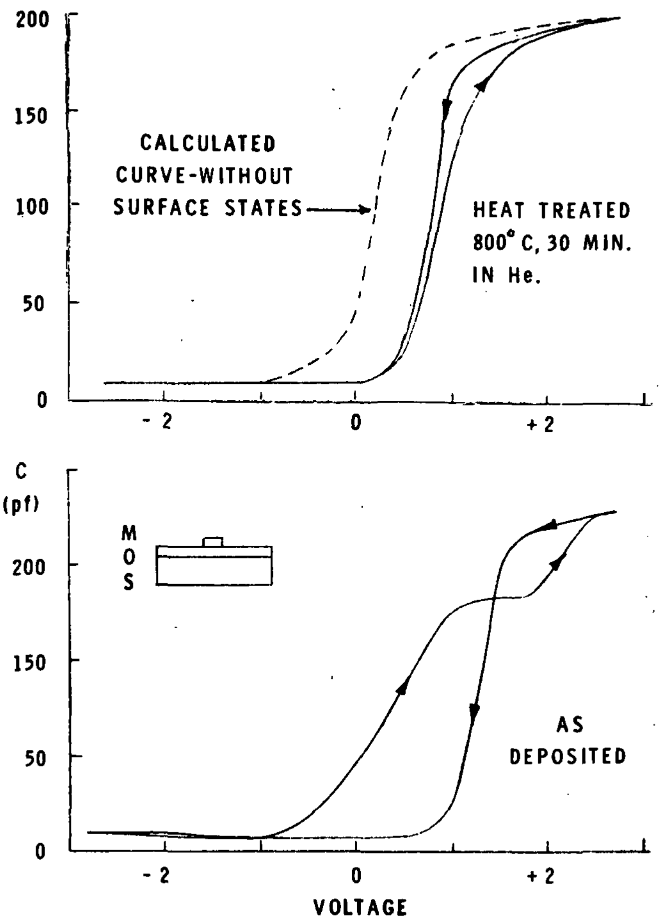

Figure 1. - C-V data for n-Si-Ta_2O_5 showing effects of heat treatment after oxide deposition.

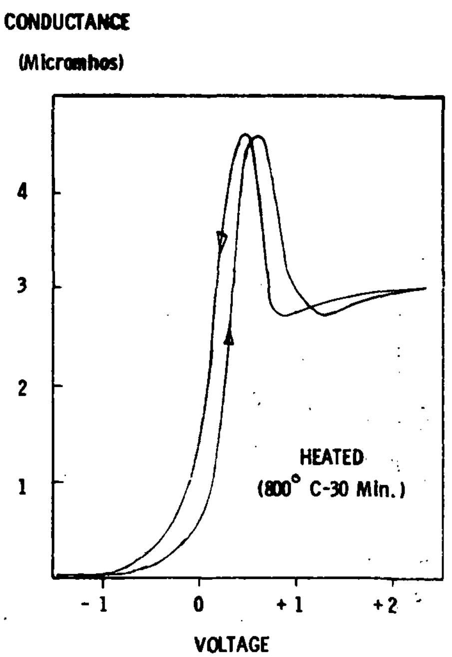

Figure 2. - Conductance-voltage data for heat treated sample.

	HEATED	UNHEATED
N_s (Cm^{-2})	$2x10^{11}$	$1.2x10^{12}$
N_{ss} ($Cm^{-2}ev^{-1}$)	$2.5x10^{12}$	$2.2x10^{12}$
τ (Sec)	$3.9x10^{-6}$	- -

$E_c - E_t = 0.25\ e_V$

Figure 3. - Summary of data, n-Si-Ta_2O_5.

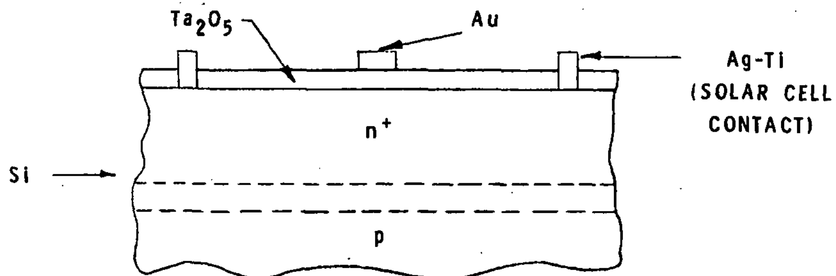

Figure 4. - Configuration used for MOS C-V experiment on solar cell diffused face.

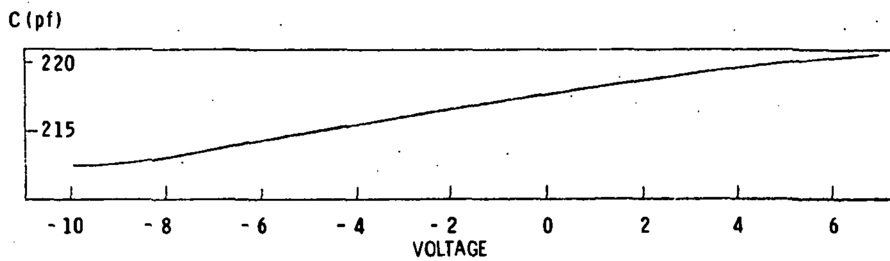

Figure 5. - C-V data for diffused face of silicon solar cell.

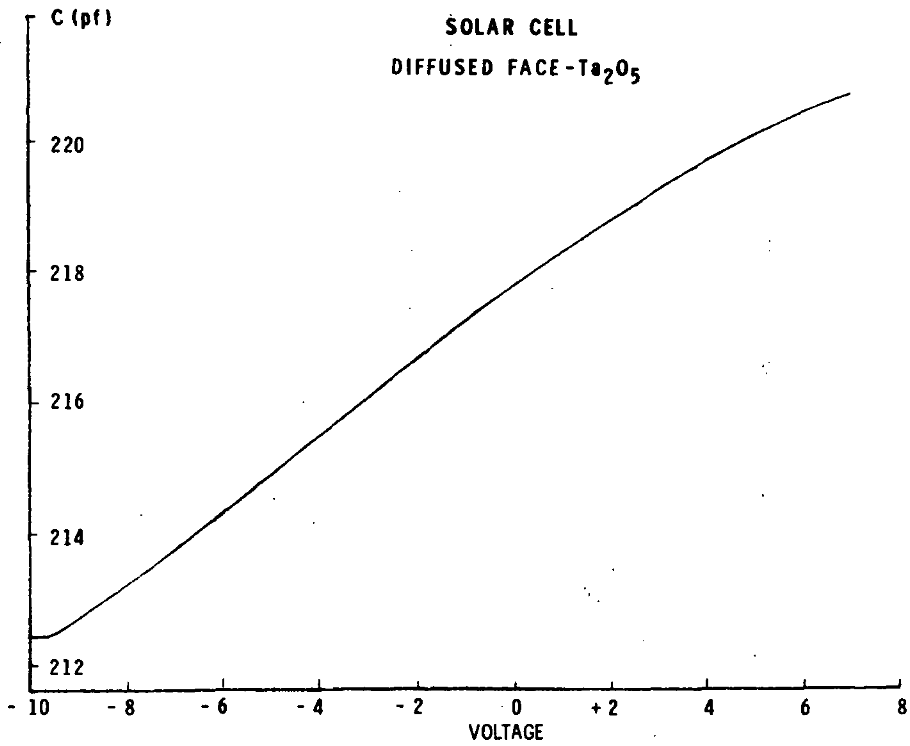

Figure 6. - Expanded C-V data plot.

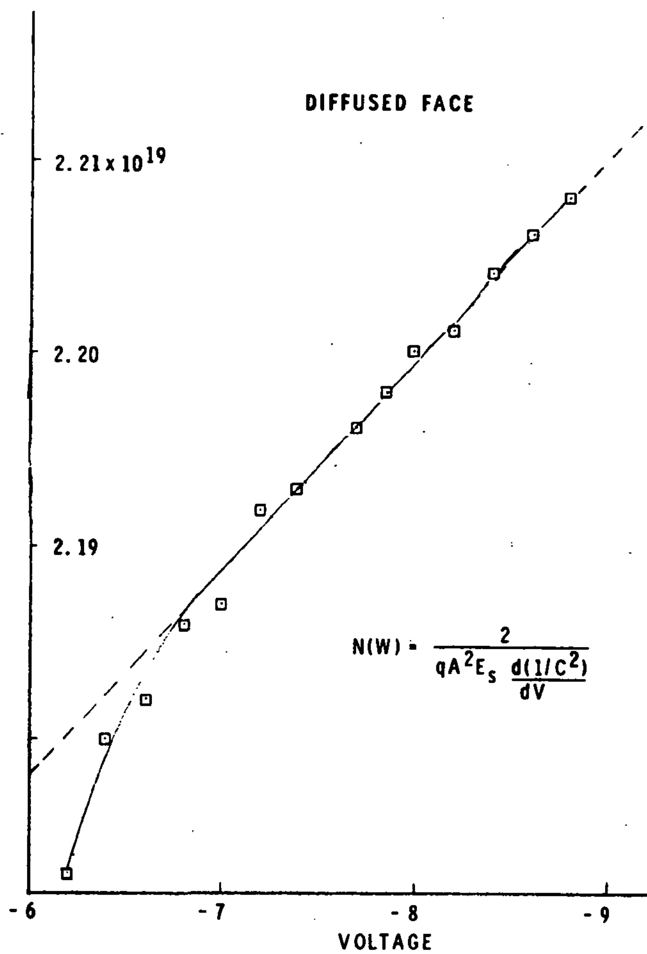

Figure 7. - Plot of $1/C^2$ against V.

DIFFUSED FACE - Ta_2O_5

$N (CM^{-3})$	W (CM)	$N_s (CM^{-2})$
4.3×10^{20}	15×10^{-8}	1.4×10^{13}

Figure 8. - Data summary for diffused face of silicon solar cell.

14. BULK DIFFUSION LENGTHS IN SILICON SOLAR CELLS USING THE SEM

Victor G. Weizer
NASA Lewis Research Center
Cleveland, Ohio

A diffusion length measurement technique is described, the main advantage of which is that bulk effects are isolated from surface effects. This method is ideally suited for measurements on silicon solar cells because of the geometry involved and the large magnitudes of diffusion length usually found therein. The results of measurements on a number of silicon cells are presented and compared with those obtained using a penetrating radiation (X-ray) technique. The values of diffusion length obtained are found to be significantly larger than, but proportional to, those obtained using penetrating radiation.

The method is a variation of the technique in which the highly focused electron beam in the scanning electron microscope (SEM) is used to generate carriers in a sample containing a collecting junction.[1] The relation between the measured short circuit current and the location of carrier injection is used to determine the diffusion length. The main difference in the present technique is that, by the employment of a highly doped field layer at the electron beam entry surface, carrier recombination there is reduced to negligible values. The actual recombination velocity at the beam entry surface is determined by measurements made on cells of special geometry.

The continuity equation describing point injection of carriers in a planar solar cell of thickness d at a distance x_i from the collecting junction is

$$\nabla^2 n(x) - \frac{n(x)}{L_2} = 0 \tag{1}$$

where L is the bulk diffusion length. A diagram of the geometry involved is given in figure 1(a). The solution of equation (1) under the boundary conditions

(1) At the junction, $x = 0$, $n = 0$

(2) At the rear surface, $x = d$, $D \frac{dn}{dx} = - S'n$

yields an expression for the short-circuit current

$$I = I_{max} \frac{1 + \frac{1 - S}{1 + S} \exp(-2y_1)}{\exp(-y_2) + \frac{1 - S}{1 + S} \exp(y_2)\exp(-2y_1)} \tag{2}$$

Preceding Page Blank

In equation (2) $y_1 = (d - X_i)/L$, $y_2 = -X_i/L$, I_{max} is the carrier injection rate, and S is the rear surface recombination velocity normalized to D/L, where D is the minority carrier diffusion coefficient.

Let us consider, now, generation of carriers by the SEM beam at a point just inside the rear surface of the cell. By setting $x_i = d$ in equation (2), we obtain the family of curves shown in figure 2. Here, I_{sc}/I_{max}, the fraction of the injected carrier flux which is collected by the junction, is plotted as a function of d/L for several values of S. From this plot one can determine L from the measured value of I_{sc}, if S and I_{max} are known.

The values of I_{max} can be determined theoretically from the known pair production energy (3.5 eV for silicon),[2] the incident beam energy (40 keV), the electron backscattering coefficient (0.16 for 40-keV electrons on silicon),[3] and the incident beam current I_B. Using these values we obtain the relation

$$I_{max} = 9.6\times10^3 \, I_B$$

The calculated value was verified experimentally from I_{sc} measurements when the carriers were injected in close proximity to the junction, where the collection efficiency is expected to approach 100 percent. Agreement was found to within 0.5 percent.

In order to reduce the effective rear surface S to as low a value as possible, a highly doped field (p^+) layer was employed (fig. 1(a)). In an attempt to obtain a quantitative estimate of the degree of reduction in S effected by the P^+ layer, several cells of the geometry described in figure 1(b) were fabricated. These cells contain crescent shaped slots, about 1 mm wide and 1 cm long, cut in their rear faces with a circular diamond saw. The slots were cut so that the cell thickness at the bottom of the slot is of the order of 25 μm. This geometry permits measurement of the variation of I_{sc} with cell thickness without the interference of edge effects which could be present if, for instance, an angle lapped geometry were used.

After slotting, the p^+ layers were incorporated by evaporating aluminum on the rear surface and diffusing for 60 minutes at a temperature of 875° C. Subsequent to the diffusion step, the remaining aluminum was removed from the slot and a small adjacent flat area.

Results of measurements of I_{sc} as a function of the location of carrier injection along the slot in a typical cell are shown in figure 3. As can be seen, I_{sc} drops sharply as the injecting beam begins to impinge on the slotted area, indicating a higher value of S in the slot than on the unslotted regions. The increase in S is very likely due to residual lattice damage from the grinding procedure. Although a short range variation in S across the surface cannot be ruled out, it is believed that the scatter in the data of figure 3 is due to the presence of tenacious aluminum-silicon alloy particles remaining on the surface which reduce the effective beam current that enters the underlying silicon.

Thus the true response of the uncovered silicon is best described by the upper envelope of the data.

The best fit of equation (2) to the data along the slotted region is indicated by the solid curve in figure 2. The theoretical fit requires a value of 0.315 for S and a value of 262 μm for L. This value of the diffusion length can then be used with equation (2) to determine S on the flat area. The results of such a calculation indicate that on the flat $S = 0.012$, a value several orders of magnitude less than the minority carrier diffusion velocity D/L. We can therefore assume that, for all practical purposes, the p^+ field layer, as described here, constitutes a perfectly reflecting barrier to minority carrier transport, effectively preventing recombination at the rear surface of the cell.

There are two points that were of some concern in the interpretation of the point injection data: (1) the possibility of the presence of high injection level effects and (2) the possibility of contributions to the measured I_{sc} from the low-high junction formed by the application of the highly doped field layer.[4]

In a search for high injection level effects, measurements of the current gain, i.e., the ratio of collected current to input beam current, were made for beam currents from a few picoamperes to over a nanoampere for a wide range of defocousing conditions. No variation in the gain was seen, indicating that the measurements are free of high injection effects.

Evidence of current contributions from the p-p^+ junction was sought in two ways.

(1) The p-n junctions were removed from a number of 10-ohm-cm n^+-p-p^+ BSF cells, isolating the p-p^+ junctions. Measurements of V_{oc} on the isolated junctions under roughly simulated AMO conditions show that there is no significant collection when this material is used, i.e., $V_{oc} \approx 0.005$ V. Similarly treated 100-ohm-cm cells, however, yielded open-circuit voltages of 0.050 to 0.100 V.

(2) The rear faces of a number of 10- and 100-ohm-cm n^+-p-p^+ BSF cells were divided into two regions by etching grooves across the rear of the cells. The I_{sc} was then measured (in the SEM) from one of the rear areas while carriers were injected first into one of the areas and then into the other (see fig. 1(c)). A significant increase in I_{sc} when injection takes place on the metered side would be an indication of majority carrier collection at the p-p^+ junction. In agreement with the first experiment no increase was found for the 10-ohm-cm cells, whereas the 100-ohm-cm cells showed a significant ($\sim$8 percent) increase in response.

We can conclude, therefore, that for the 10-ohm-cm cells of interest here, p-p^+ collection does not seem to be a concern. If higher base resistivities are used, however, current generation by the rear junction must be accounted for.

It is interesting to compare the results of the SEM measurements on a number of 10-ohm-cm BSF silicon solar cells with the values of L determined by an independent technique, in this case a penetrating radiation technique employing X-rays as carrier generators. The X-ray technique, which is described elsewhere,[5] has been extended

Page Intentionally Left Blank

4. Lade, R. W.; and Jordan, A. G.: J. Electronics Control, 13, 23 (1962).

5. Lamneck, J. H.: NASA TM X-1894 (1969).

TABLE I. - COMPARISON OF OBSERVED AND CALCULATED I_{sc}

Cell field layer	Cell type	Observed I_{sc}, μA	Original calibration		New calibration	
			L, μA	I_{sc}, μA	L, μm	I_{sc}, μA
362-5 (boron)	BSF	27	80	27	152	27
	Non-BSF	21.5	80	26.5	152	20.7
HAL-25 (aluminum)	BSF	55.7	215	55.7	410	55.7
	Non-BSF	29.9	215	33.5	410	28.1

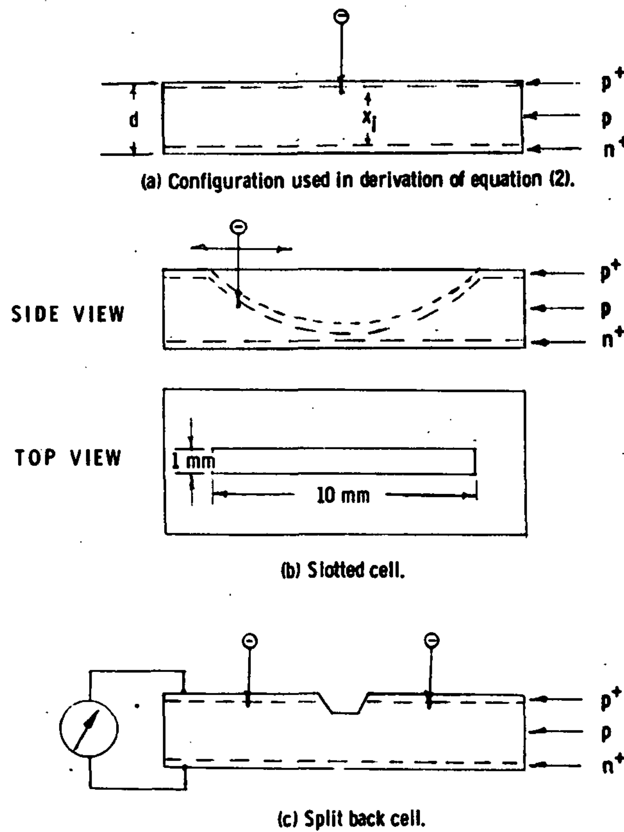

(a) Configuration used in derivation of equation (2).

(b) Slotted cell.

(c) Split back cell.

Figure 1. - Schematic diagrams of solar cell configurations.

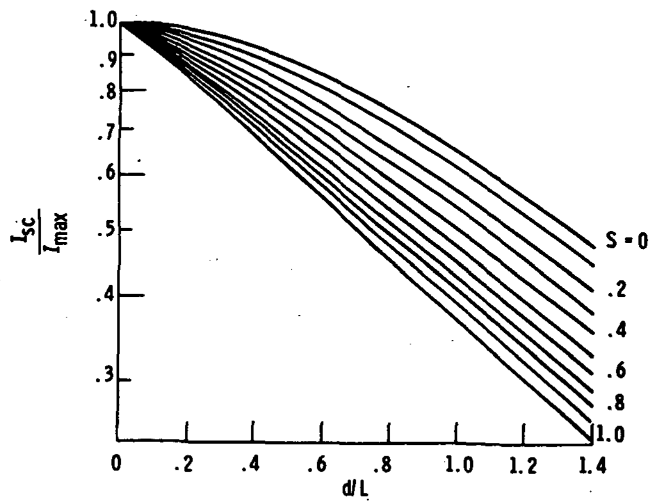

Figure 2. - A plot of the collected fraction of injected carriers as a function of the ratio d/L.

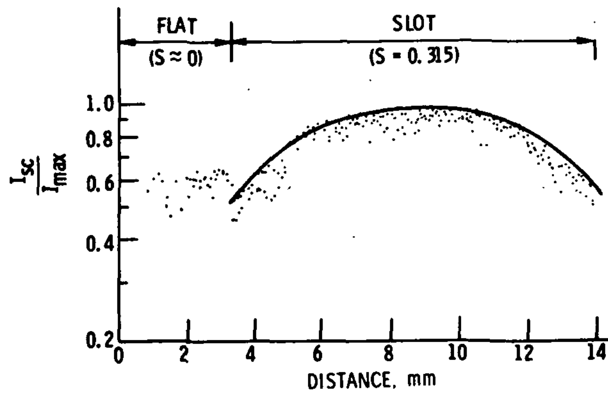

Figure 3. - A plot of the collected fraction of injected carriers as a function of distance across back of cell.

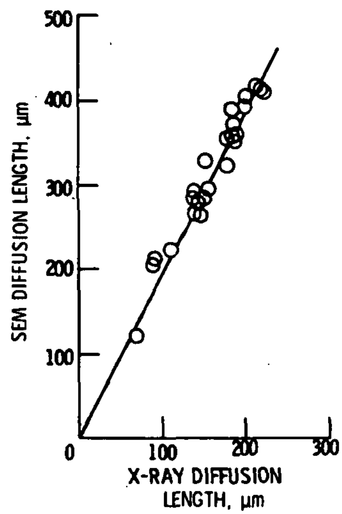

Figure 4. - A comparison of diffusion lengths measured in the SEM with those measured with penetrating radiation.

15. CORRELATION BETWEEN MECHANICAL IMPERFECTIONS AND ELECTRICAL PROPERTIES OF SOLAR CELLS

R. Kaul,* B. Roessler, and J. J. Loferski
Brown University
Providence, Rhode Island 02912

I. INTRODUCTION

This research has been supported on a grant entitled "Methods of Improving the Efficiency of Solar Cells" from NASA-Langley and by the Brown University-NSF-Materials Research Laboratory institutional grant-GH- 3631. This report describes a new part of our research activity which focuses on the localized characterization of solar cell materials by several different but complementary techniques. The initial, as-grown, condition, as well as the effects of processing steps during device manufacture, are of equal concern. The work is based upon the idea that imperfections in the crystal lattice can detract from ultimate device performance either directly through interactions with charge carriers or indirectly by influencing the distribution of dopants and impurities. The term imperfections is meant to include dislocations, precipitates of second phase, non-uniform impurity and dopant distributions, small angle grain boundaries, surface damage, and similar defects. Imperfections of these kinds are sometimes present initially or can be introduced during device fabrication. In GaAs, for example, such imperfections are often introduced during crystal growth.[1,2] An assessment of the importance of various imperfections is not straightforward. For example, in GaAs crystals of high perfection the minority carrier diffusion length is sometimes limited to the distance between dislocations[3]. A low dislocation density, on the other hand, does not--apparently--guarantee a long minority carrier diffusion length in GaAs[4]. Although an inverse relation between dislocation density and minority carrier lifetime has been reported by several workers for silicon of both high and low resistivity[5-10], this dependence is not always found[11].

*Present address: School of Business Administration, University of Chicago, Chicago, Illinois.

Preceding Page Blank

The minority carrier lifetime apparently can be affected in exactly the opposite fashion if a dislocation inhibits the capture of majority carriers[11]. Although dislocation free silicon is now readily available as starting material, this high perfection is not always found in finished commercially available cells[12]. The presence of dislocations may, in fact, be advantageous for certain applications[13]. For both direct (electronic) as well as indirect effects, the character of the dislocations, i.e. the relation between their Burgers and their tangent vectors, has had little experimental attention.

A surface of high perfection--free of damage from prior processing operations also seems desirable if high efficiencies are to be attained.

In this research we will focus our attention upon characterizing our specimens--as regards crystalline perfection--and then correlating <u>these</u> measurements with measures of device performance <u>localized</u> to regions in which we know the state of crystalline perfection. We have set up and begun to use a variety of characterization techniques including x-ray topography, scanning electron microscopy and differential interference microscopy. Device performance is indicated by measurements of localized spectral response at selected wavelengths and by electron voltaic response generated by electron beam excitation in the scanning electron microscope. Much of the impetus for this work came from an earlier observation in the scanning electron microscope[14] of the existence within the illuminated region of silicon solar cells of "dead areas" i.e. areas of reduced response.

II. DESCRIPTION OF THE TECHNIQUES

A.) X-Ray Topography

The experimental arrangement for the Lang x-ray topographic technique which we have used is shown in Fig. 1. An x-ray beam falls upon a crystal

arranged to diffract from a selected set of lattice planes. The diffracted beam is recorded on a fine grained film as the crystal and film are translated through the beam. The presence of any source of strain or strain gradient alters the diffraction conditions in the vicinity of the imperfection and gives rise to an image of the defect. As an example--an x-ray topograph from a specimen of silicon is shown in Fig. 2. It shows this as-received crystal to be of relatively low dislocation density. Fig. 3 shows this same specimen following a high temperature diffusion treatment in phosphorous oxychloride. Extensive slip has occurred starting from surface sources at the edges of the disc. An array of slip dislocations is seen at SL and circular defects are also seen at C and R. The dislocation density at the edges of the slab becomes extremely high.

X-ray topography, then provides a non-destructive method for specifying the state of crystalline perfection throughout the process of device fabrication. In addition to displaying the distribution and character of the dislocations in the specimen, other defects such as second phase particles, strains due to surface damage, and non-uniform oxide layers are also revealed.

B.) The Localized Electron Voltaic Response

In this technique, the short circuit current is displayed on the screen of a scanning electron microscope (SEM) as the electron beam is scanned over a selected region of the solar cell. Figs. 4-7 show such a display as the accelerating voltage of the SEM is increased from 10 to 25 kilovolts. The "dead areas" (the dark circular disks) are similar to those previously described[14]; they change in appearance as the accelerating voltage is increased because the penetration depth of the electrons increases for higher accelerating voltages.

C.) The Localized Spectral Response

The localized spectral response measurements consist of recording the short circuit current from a cell illuminated in an optical microscope by a

small collimated beam of selected wavelength. In our original equipment the beam was localized to a 200 micron diameter. Typical results are shown in Fig. 8. We now feel that the beam diameter must be reduced to about 10 to 20 microns so that the localization of the response more nearly matches the capabilities and resolving power of the x-ray methods as well as the scanning electron microscope. The wavelengths are selected to sample the photovoltaic effect to different depths. In Fig. 8 the wavelengths are a green for which the ($^1/e$) absorption depth is 1.2 microns, and an infrared for which the absorption depth is 8.3 microns.

D.) Localized Correlations of Imperfections and Electrical Response

When the photovoltaic response is sufficiently localized, we intend to correlate these measurements with the x-ray topographic display of crystalline perfection and surface condition in a finished cell. For this purpose an x-ray topographic stereo pair is recorded to give a three dimensional display of the state of perfection of the cell. An example is shown in Fig. 9. This stereo pair of a finished cell, together with additional topographs which reveal imperfections which are out of contrast in Fig. 9, are then used as a guide in selecting regions for measuring the electron voltaic and localized photovoltaic response.

Our initial attempts to correlate the results of the various techniques in silicon cells suggest that the regions of reduced electron voltaic response occur in regions where either dislocations pierce through the p-n junction to the surface or where nodes in the dislocation network occur. These results, however, are preliminary since we have not yet completed the kind of localized correlation that is needed; that will require some further improvements in both equipment and technique.

When the SEM is operated in the beam deflection mode a localized measure of the minority carrier lifetime is obtained.[15] Evaluation and

control of this important parameter and, in particular, an understanding of the reasons for its decrease to undesirably low values, is essential if maximum efficiency solar cells are to be attained.

REFERENCES

1.) J.J. Loferski, B. Roessler, E.E. Crisman, L.Y. Chen and R. Kaul, Eighth Semiannual Report, Sept. 1, 1973-February 28, 1974, Brown University NASA Grant NGR-40-002-093,"Methods of Improving the Efficiency of Photovoltaic Cells."

2.) J.J. Loferski, B. Roessler, E.E. Crisman, L.Y. Chen, R. Kaul, and J. Walker, Ninth Semiannual Report, March 1, 1974-August 31, 1974, Brown University, NASA Grant NGR-40-002-093, "Methods of Improving the Efficiency of Solar Cells."

3.) M. Ettenberg, "Effects of Dislocation Density on the Properties of Liquid Phase Epitaxial GaAs"., J. Appl. Phys. 45, No. 2, Feb. 1974, p. 901.

4.) G. Walker, private communication, Also see elsewhere in this NASA-Lewis report on High Efficiency Silicon Solar Cell Meeting, November 14-15, 1974.

5.) J. Okada, J. Phys. Soc. Japan 12, 1338 (1957).

6.) A.D. Kurtz, S.A. Kulin and B.L. Averbach, Phys. Rev. 101, 1285 (1956).

7.) A.D. Kurtz, S.A. Kulin and B.L. Averbach, J. Appl. Phys. 27, 1287 (1956).

8.) J.P. McKelvey, Phys. Rev. 106, 910 (1957).

9.) G.K. Wertheim and G.L. Pearson, Phys. Rev. 107, 694 (1957).

10.) H. Lemke, phys. status solidi, 12, 125 (1965).

11.) R.H. Glaenzer and A.G. Jordan, "The Electrical Properties of Dislocations in Silicon-I", Solid-State Electronics, vol. 2, p. 247-258, (1969).

12.) R. Kaul, M.S. Thesis, Brown University, 1974

13.) M.L. Joshi, and J.K. Howard, "Defects Induced in Silicon Through Device Processing", in Silicon Device Processing, N.B.S. Publication 337, p. 318, (1970).

14.) J.J. Loferski, N. Ranganathan, E. Crisman, and L.Y. Chen, Fifth Semiannual Report, March, 1972-August 31, 1972, Brown University

NASA-Grant NGR-40-002-093, "Methods of Improving the Efficiency of Photovoltaic Cells".

15.) J.J. Loferski, E.E. Crisman, L.Y. Chen and W. Armitage, Brown University, NASA-Grant NGR-40-002-093, "Methods of Improving the Efficiency of Photovoltaic Cells."

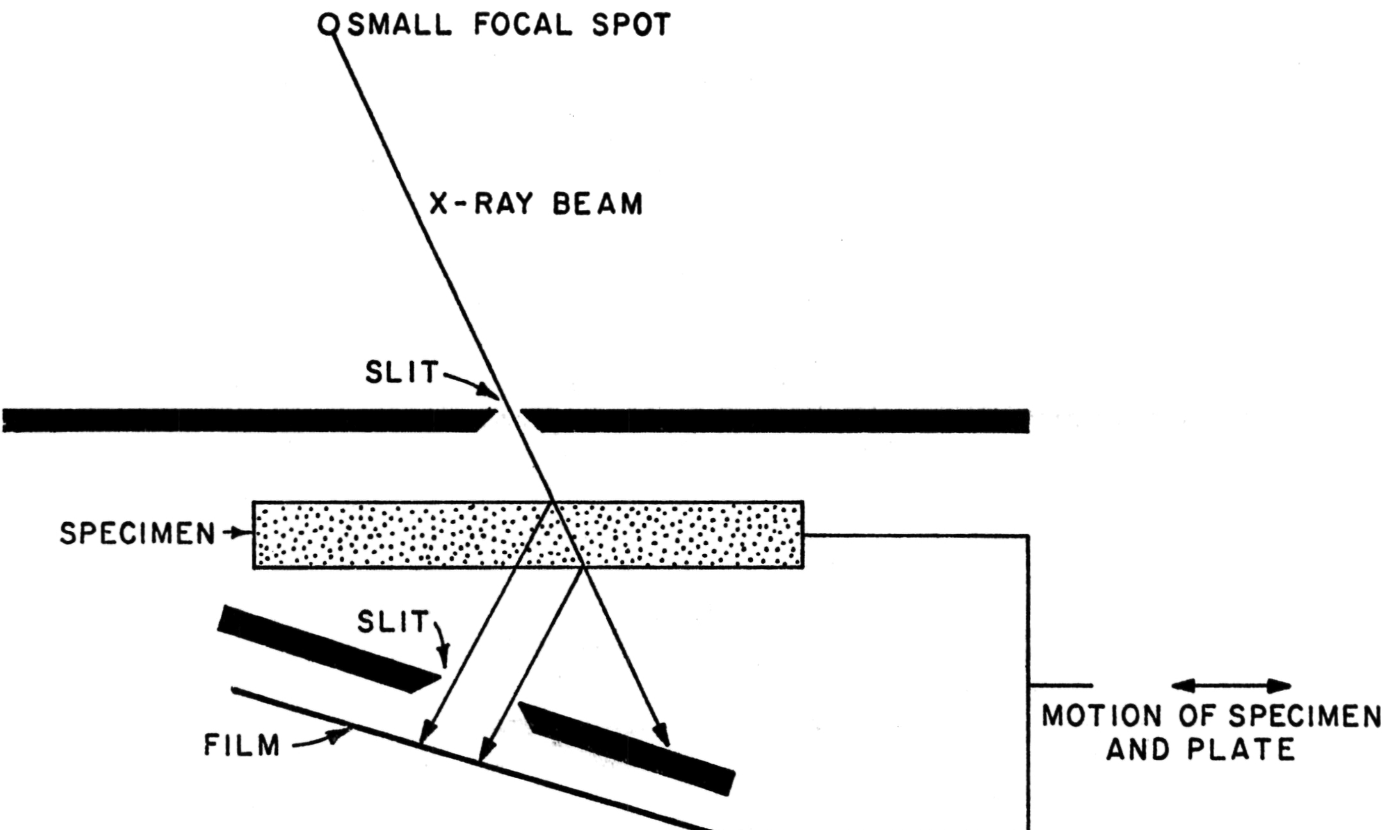

Figure 1. - Arrangement for Lang method. Specimen and film can be translated together.

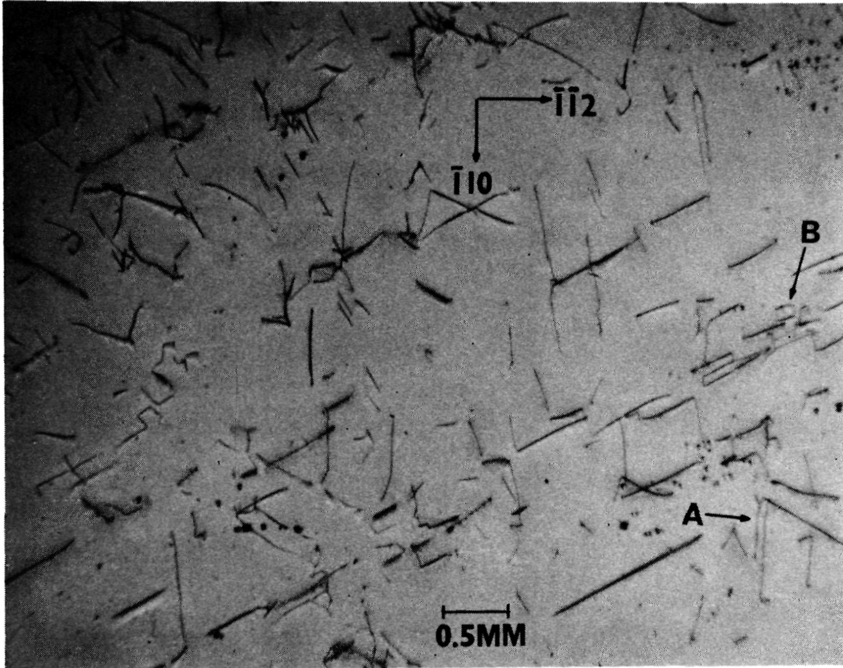

Figure 2. - A $(\bar{2}20)$ X-ray transmission topograph of a silicon wafer in the as-received condition. Magnification 16.9X. (L-65, LP106)

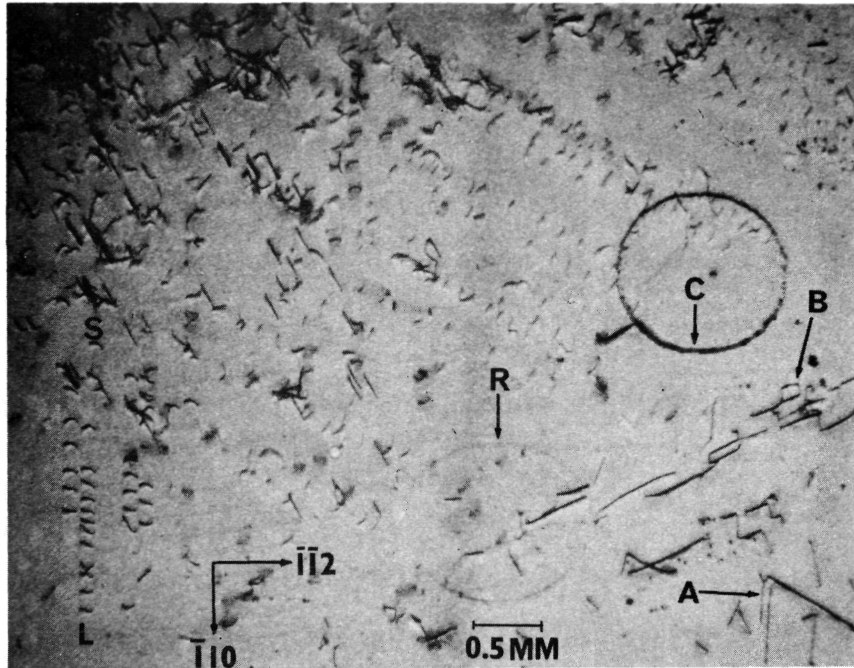

Figure 3. - A ($\bar{2}20$) topograph of the same region after 2 minute diffusion treatment in phosphorous oxychloride at 1100° C. Circular defects at C and R may be similar to electrically "dead" areas seen in commercial cells by scanning electron microscopy. Some dislocations, as at A and B, are visible in both topographs. Many dislocations are introduced by slip during this processing step, as at S-L. Magnification 16.9X. (L-89-LP104)

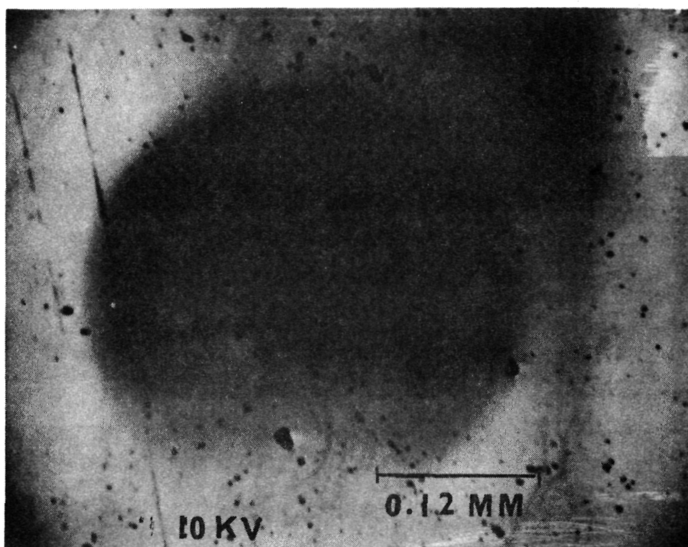

Figure 4. - Electron-voltaic response (short circuit current) from silicon solar cell. Accelerating voltage 10 kilovolts.

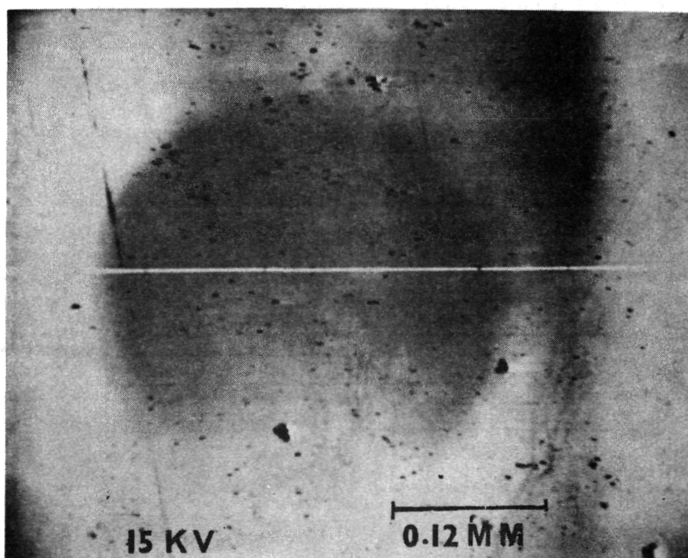

Figure 5. - Electron-voltaic response (short circuit current) from silicon solar cell. Accelerating voltage 15 kilovolts.

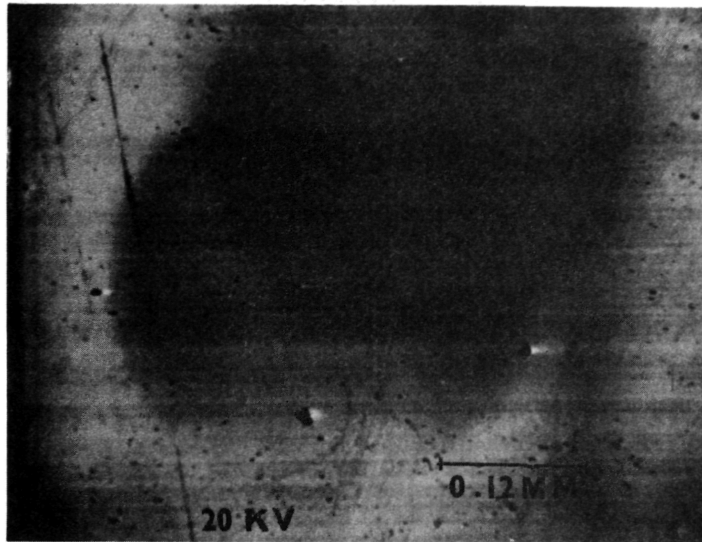

Figure 6. - Electron-voltaic response (short circuit current) from silicon solar cell. Accelerating voltage 20 kilovolts.

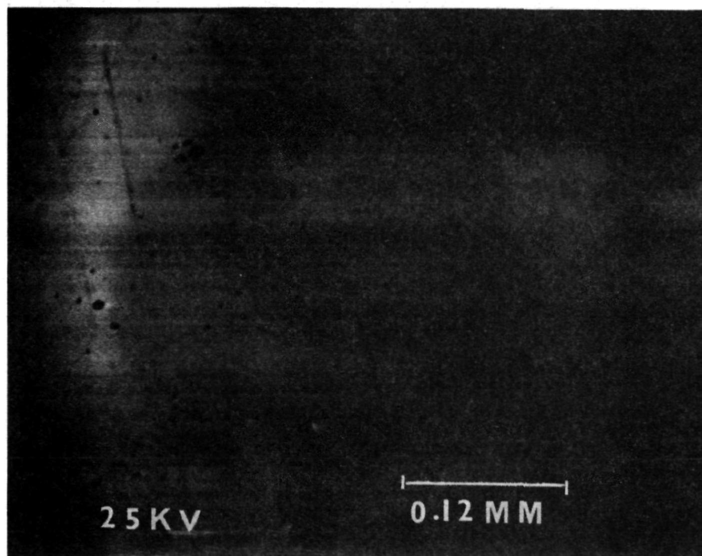

Figure 7. - Electron-voltaic response (short circuit current) from silicon solar cell. Accelerating voltage 25 kilovolts.

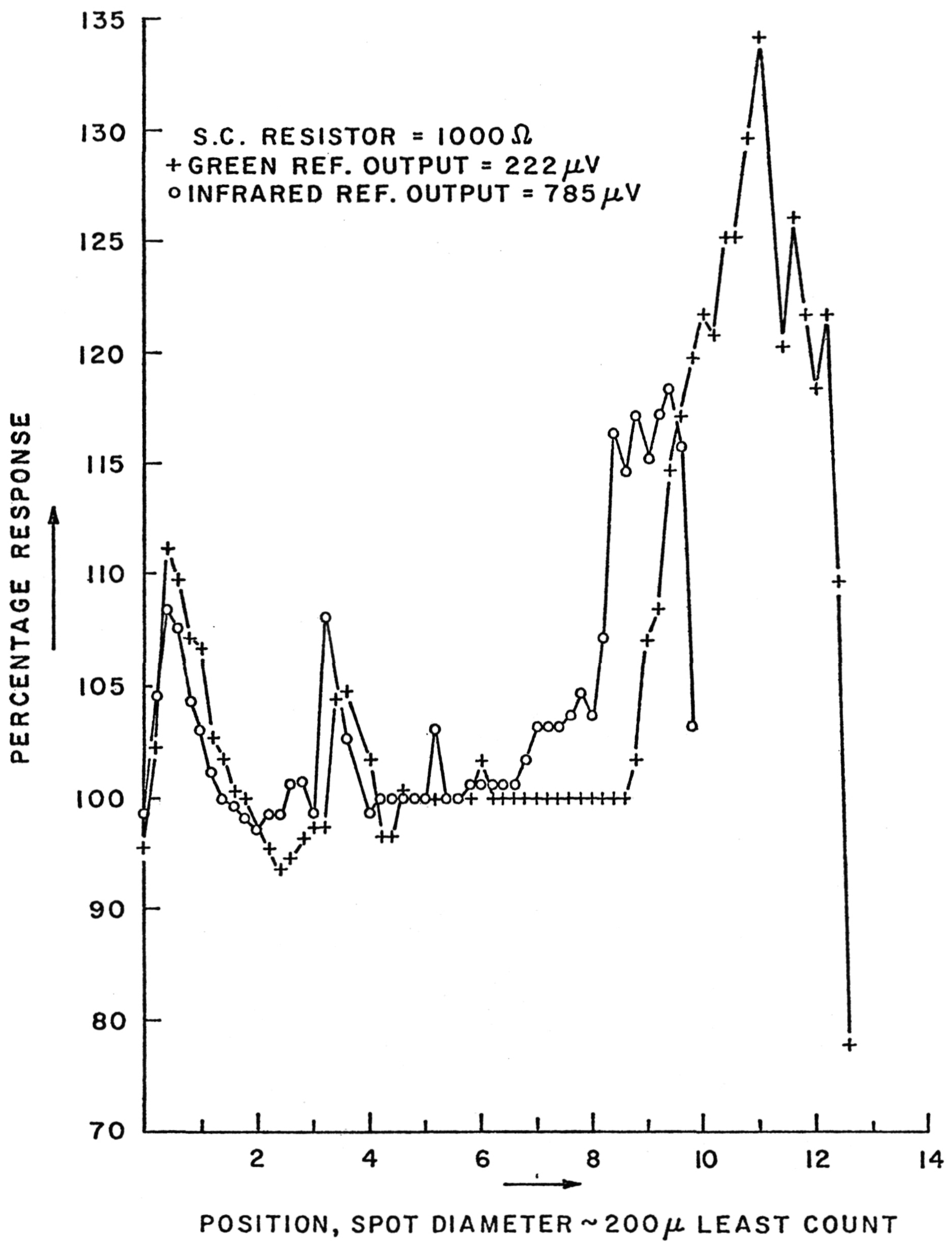

Figure 8. - Photovoltaic response of cell as a function of position on the cell.

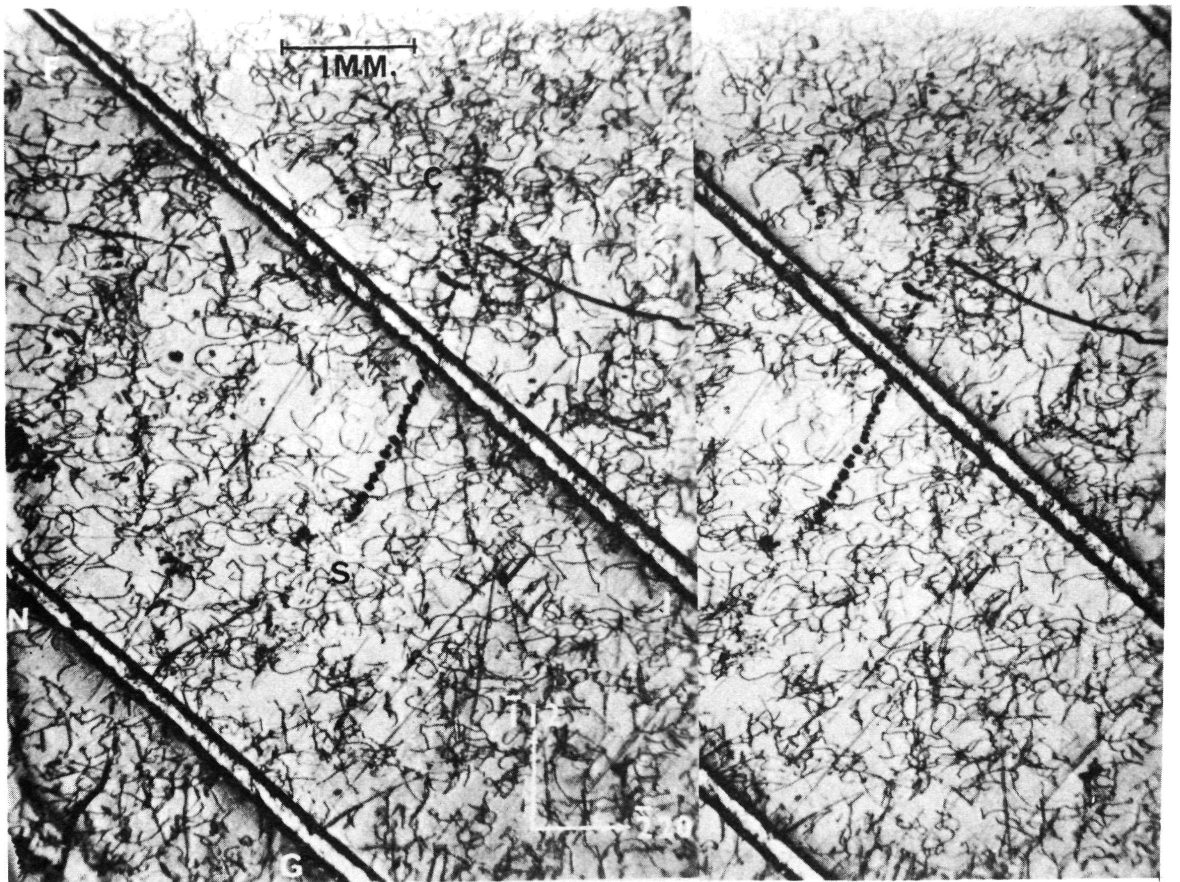

Figure 9. - This is a stereo pair of a finished solar cell recorded with molybdenum radiation. The antireflection coating was present on the cell when these topographs were recorded. The electrical contacts or "fingers" on the front face of the cell run diagonally across the photographs at F, I and N, G. The defect at SC indicates the presence of surface damage in the finished cell. The diffracting planes are ($\overline{2}20$) [LP-189] and (220) [LP-190]. Note that a large number of dislocations present in the cell are not visible in these topographs since their Burgers vectors are contained in the diffracting plane; they are revealed in topographs recorded with a different diffracting plane.

16. EXPERIMENTAL STUDIES OF IMPERFECTION CENTERS IN LOW RESISTIVITY SILICON p-n JUNCTION SOLAR CELLS*

S. S. Li, F. A. Lindholm, and P. J. Chen
University of Florida
Gainesville, Florida 32611
and
C. T. Sah
University of Illinois
Urbana, Illinois 61801

I. Introduction

Defects in silicon p-n junction devices can be induced by irradiation, high-temperature diffusion or impurity-related doping process. If a defect is impurity-related, the probability of its formation will increase with impurity concentration. These defects can act as electron and hole traps and as recombination centers. They, therefore, alter the electrical characteristics of silicon devices.

The charge states of each defect can be determined by comparing its concentration to changes in the steady-state charge in the depletion region. The charge state is important in determining the recombination properties of the defect. These properties affect the operation of various semiconductor devices.

The importance of the electron-hole recombination in the transition region of a p-n junction under forward bias conditions was first analyzed in detail by Sah, Noyce and Shockley(2). This recombination current has been reported by Pfann and Van Roosbroeck(3) in silicon solar cells and has been observed on commercial silicon diodes by Sah(4).

Analyses of recombination and diffusion current components in silicon p-n junction solar cells have been made recently by Wolf(5), Stirn(6) and Hovel(7). Their results indicated that the recombination current component in the junction space charge region may dominate at low current and at low temperatures.

*Research sponsored by NASA Lewis Research Center under Grant No. NSG-3018.

Preceding Page Blank

In this paper analysis of the preliminary experimental results on the I-V characteristics of a 0.1 ohm-cm silicon N^+P junction solar cell fabricated with a MOS guard ring gate is given. Theory of the transient capacitance methods that are employed to determine the carrier emission and capture rates, the energy level and density of defects in the junction space charge region and the substrate of a p-n junction solar cell is described.

II. I-V characteristics of a 0.1 ohm-cm silicon N^+P solar cell

Measurements of current-voltage characteristics of a 0.1 ohm-cm silicon N^+P junction solar cell fabricated in our laboratory have been made between 145°K and 295°K. The results are displayed in Fig. 1. The cross sectional view of the N^+P silicon test diode is shown in Fig. 2. To explain the I-V characteristics shown in Fig. 1, the total junction current may be empirically written as[4]

$$I = I_s \exp(qV/mkT) \qquad (1)$$

where $1 < m < 4$. Eq. (1) is valid for forward junction voltages greater than a few kT/q.

Detail analysis of Eq. (1) has been given by Sah[4]. In general, the total junction current may consist of four components, namely, the bulk diffusion current (i.e., m=1 and I_s proportional to n_i^2; n_i is the intrinsic carrier density), the bulk generation-recombination current in the

transition region (i.e., $1 < m < 2$, and I_s proportional to $n_i^{2/m}$), the surface generation-recombination current (i.e., $1 < m < 2$, and I_s proportional to $n_i^{2/m}$), and the surface channel current (i.e., $2 < m < 4$ and I_s proportional to $n_i^{2/m}$).[4]

Among these four current components, the diffusion current depends most strongly on temperature, while the surface channel current has the smallest temperature dependence. This prediction is consistent with the measured I-V characteristics shown in Fig. 1. The results show that at low current level m=2 for T=295°K and 2 < m < 4 for T=145°K and 196°K, indicating that at low current level the current component due to recombination in the junction space charge region plays dominant role at 295°K and recombination current in the surface channel becomes imminent at 145°K and 196°K. The diffusion current component becomes important only at a higher current level.

Theoretical fit with the experimental data shown in Fig. 1 at the low current level (where recombination current is the dominant component) yields a carrier lifetime of 60 nsec in the junction space charge region for T = 295 °K.

III. Theory of transient capacitance methods

The presence of deep level defects in a semiconductor can be detected by observing the capture and emission rate of charge carriers at the defect site. This can be done by monitoring the reverse bias capacitance of a p-n junction

diode after disturbing the steady state charge condition.

The four processes by which the charge state of a deep level defect is changed, according to the Shockley-Read-Hall model are illustrated in Fig.3.

The net rate of change of the concentration of trapped electrons is obtained by summing the contribution from each of the four processes as follows:

$$\frac{dn_T}{dt} = - \frac{dp_T}{dt} = -e_n^t \, n_T + c_n^t \, np_T + e_p^t \, p_T - c_p^t \, pn_T \qquad (2)$$

This equation is simplified for the case of a depletion region, where $n \sim p = 0$. Thus, Eq. (2) reduces to

$$-\frac{dn_T}{dt} = e_n^t \, n_T - e_p^t \, p_T \qquad (3)$$

Using $N_{TT} = n_T + p_T$ = total concentration of a deep level defect the solution of (3) is given by

$$\Delta n_T(t) = \Delta n_T(o) \; \exp(-e_n^t \, t) \qquad (4)$$

where we assume $e_n^t \gg e_p^t$ if $E_T \geq Eg/2$; Δn_T is the disturbance of the trapped electron density from its steady state value. This disturbance is seen to decay exponentially with a time constant given by the reciprocal of the emission rate, e_n^t. It has been shown that[8]

$$e_n^t \sim \exp(-\Delta E/kT) \qquad (5)$$

where ΔE is the thermal activation energy and is approximately the energy level from a band edge (i.e., E_T).

The presence of deep level defects is determined by observing the presence of the decay implied by Eq. (4). Measurements of this decay constant versus temperature yield values for the thermal activation energy.

The emission of charge carriers from defect sites in a depletion region is observed by monitoring the capacitance of the depletion region. The capacitance of a reverse biased p-n junction in the depletion approximation is given by

$$C^2 = \frac{\varepsilon\rho}{2(V_R+V_B)} \tag{6}$$

for deep acceptor level where

$$\rho = q[N_D - n_T(t)] \tag{7}$$

which illustrates the time and temperature dependence of ρ, comes from the emission of trapped charges at the deep level defects, and C is proportional to $\rho^{1/2}$.

The method of disturbing steady state charge in the depletion region is shown in Fig. 4.

Fig. 4(a) shows the charge state at zero bias condition in which the trap levels are filled with electrons. Fig. 4(b) shows the charge state of the majority carrier traps under reverse bias condition in which the electrons are emitted from trap levels into the conduction band; the time constant is determined by the electron emission rate. Fig. 4(c) shows the charge state of the minority carrier (i.e., holes) traps; the holes were injected into N-region by photo-excitation and capture by the trap levels and re-emitted into the valence band.

In general the defect levels may be switched from a depletion region to a quasi-neutral region and back by momentarily zero biasing a reverse-biased diode. The charge states of the defects are determined by the relative emission rates of electrons and holes. By studying both diode types (i.e., N^+-P and P^+-N diodes), the entire band gap can be scanned for defect energy levels.

The Thermally Stimulated Capacitance (TSCAP) method allows a rapid scan of all the deep level defects which are majority carriers (i.e., electrons in P^+N diodes) traps on the lowly doped side. The diode is cooled to a temperature such that the emission rates are negligible. The diode is zero biased momentarily and then heated at a constant rate. In a characteristic temperature range related to the activation energy, the emission rate becomes large enough for all the trapped electrons to be thermally emitted to the conduction band and swept out of the depletion region. This results in an increase in the charge concentration in the depletion region and a corresponding capacitance increase.

There will be one of these capacitance increase steps for each activation energy in the upper half of the band gap. The magnitude of each step is related to the concentration of defects producing the step[1]

$$\frac{2\Delta C}{C} = \frac{N_{TT}}{N_D} \tag{8}$$

The emission rate versus temperature measurements allows the determination of the activation energy of each defect.

After a momentary zero bias, the capacitance exhibits an exponential transient having a time constant given by the reciprocal emission of the trapped majority carriers (i.e., electrons),

$$\Delta C \sim \exp(-e_n^t\, t) \qquad (9)$$

Measurements of this transient capacitance decay at various temperatures show an exponential temperature dependence[8],

$$e_n^t = A_n (T/300)^m \exp(-\Delta E/kT) \qquad (10)$$

The data is least-square fitted to Eq. (10) to give the thermal activation for m = -1, 0, 1 and 2.

From the aforementioned experimental methods for both n^+p and p^+n junction solar cells, the information concerning defect centers such as N_{TT}, e_n^t, e_p^t, c_n^t, c_p^t and E_T in the entire energy gap can be obtained readily. The electron and hole lifetime as well as diffusion lengths can thus be calculated from these parameters.

These measured recombination parameters are of paramount importance to the understanding of the basic properties of the defect centers and their roles in affecting silicon solar cells performance.

REFERENCES

1. C. T. Sah, L. Forbes, L. L. Rosier and A. F. Tasch, Jr., "Solid State Electronics," vol. 13, pp. 759-788 (1970).

2. C. T. Sah, R. N. Noyce and W. Shockley, Proc. IRE, vol. 52, 1228 (1957).

3. W. G. Pfann and W. van Roosbroeck, J. Appl. Phys., vol. 25, pp. 1422-1434 (1954).

4. C. T. Sah, IRE Trans. Electr. Devices, ED-9, 94 (1962).

5. M. Wolf, Advanced Energy Conversion, vol. 11, 63 (1971).

6. R. J. Stirn, Record of the 9th IEEE Photovoltaic Specialists Conference, p. 72-82 (1973).

7. H. J. Hovel, Record of the 10th IEEE Photovoltaic Specialists Conference, p. 34-39 (1973).

8. C. T. Sah, W. W. Chan, H. S. Fu and J. Walker, Appl. Phys. Letter, vol. 20, 1973 (1972).

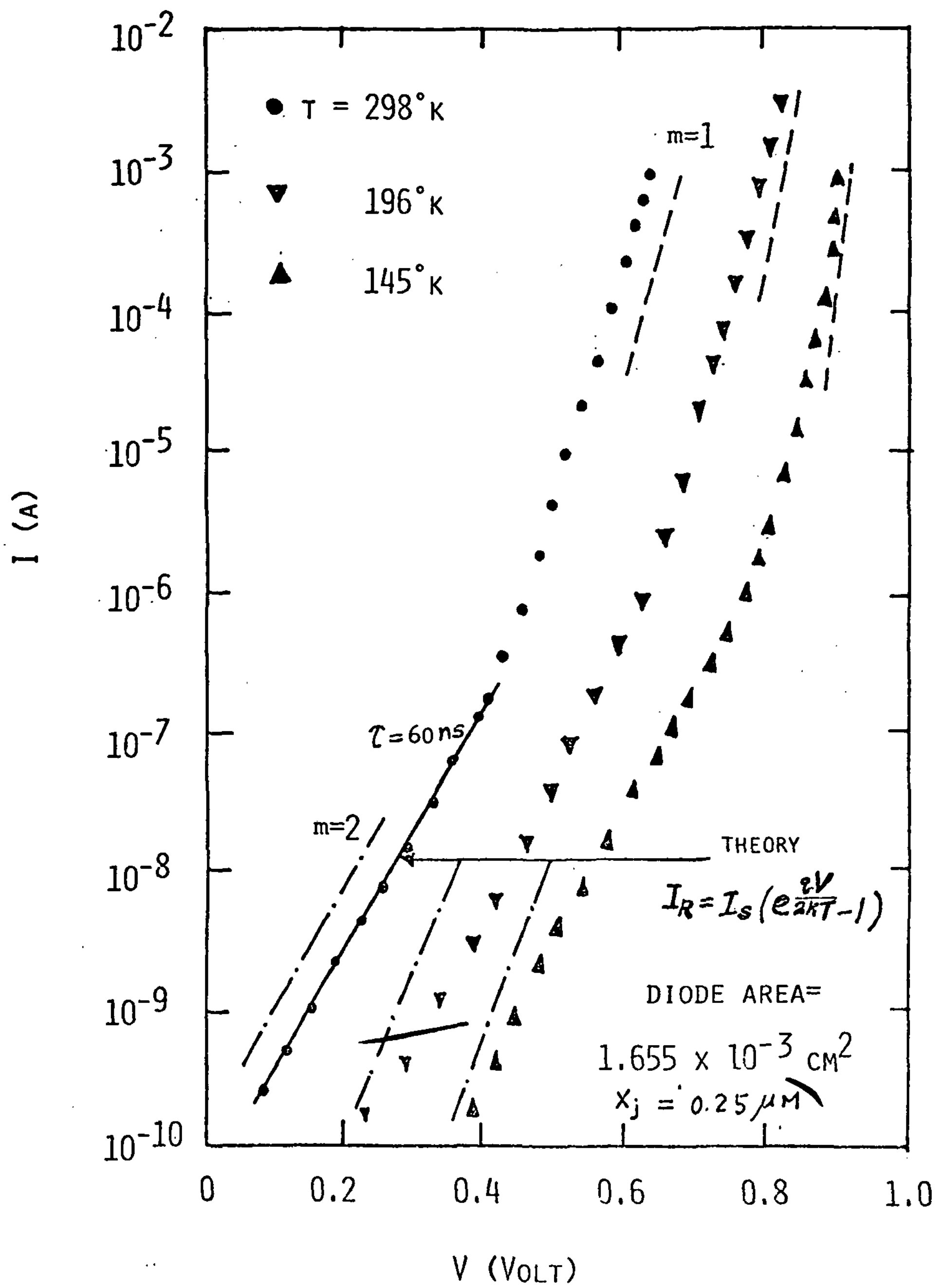

Figure 1. - I - V characteristics for a 0.1 ohm-cm silicon N^+-P junction solar cell.

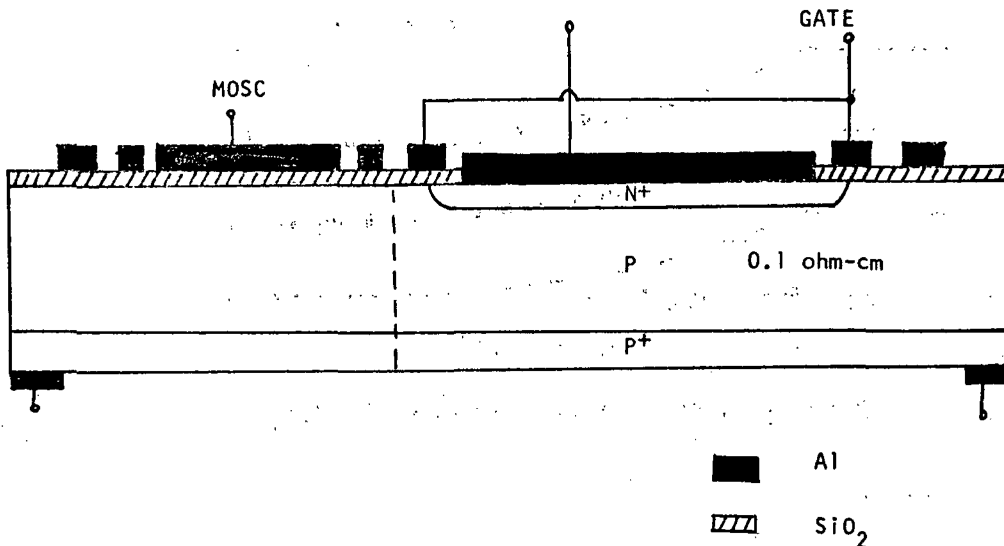

Figure 2. - Cross-sectional view of a silicon N^+P diode with MOS guard ring gate, and a MOS capacitor.

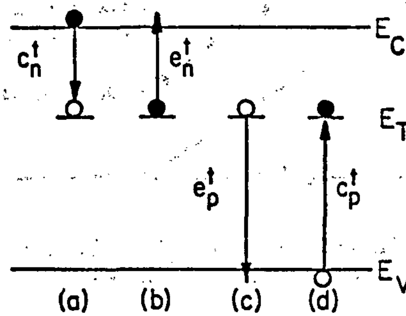

(a) electron capture rate = $c_n^t n p_T$

(b) electron emission rate = $e_n^t n_T$

(c) hole emission rate = $e_n^t p_T$

(d) hole capture rate = $c_n^t p n_T$

$n(p)$ = free electron(hole) concentration

$n_T(p_T)$ = trapped electron(hole) concentration

$e^t_{n(p)}$ = electron(hole) thermal emission coefficient

$c^t_{n(p)}$ = electron(hole) capture coefficient

Figure 3. - Charge state changes at deep level defects. (Shockley-Read-Hall process through a single trap-level.)

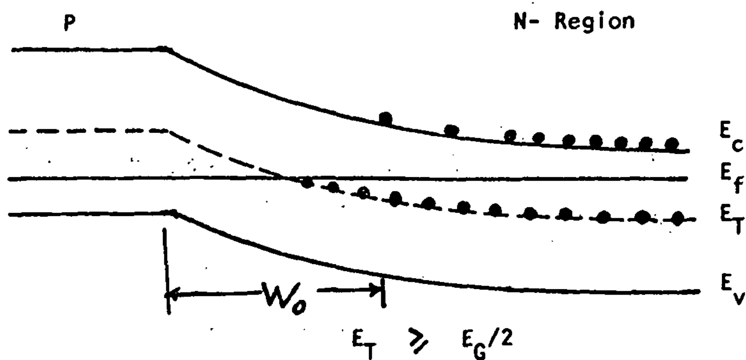

(a) V = 0, majority carrier (electron) traps.

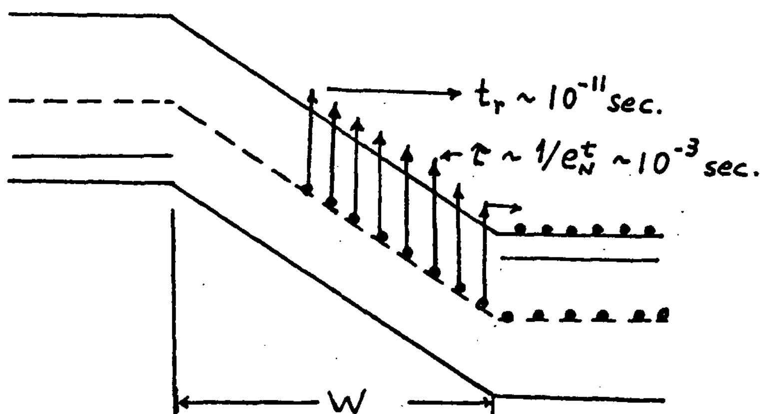

(b) V = $-V_R$, Electron emission from trap centers into conduction band ; $e_N^t >> e_p^t$

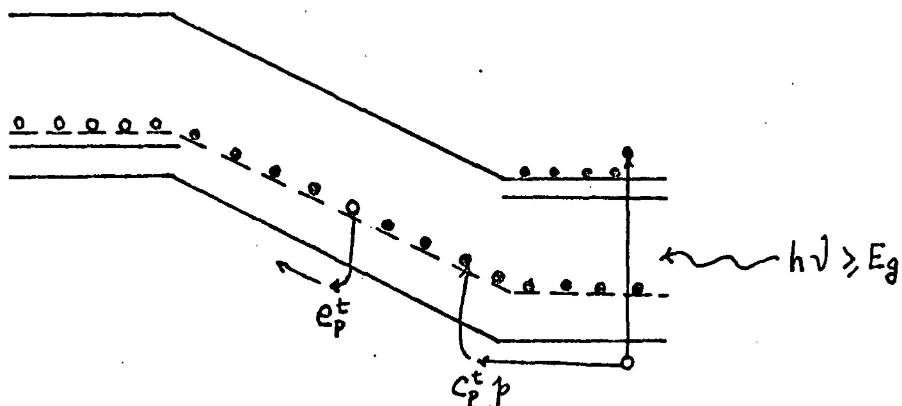

(c) V =$-V_R$, hole emission or hole capture at trap centers

Figure 4. - Methods of disturbing steady-state charge in the space charge region of a N-P junction diode.

DEVICE ANALYSIS

Presentations of the most recent approaches to the mathematical modeling of solar cells

Preceding Page Blank

17. ROLE OF RECOMBINATION CURRENT ON PHOTOVOLTAIC PARAMETERS*

Richard J. Stirn
Jet Propulsion Laboratory
Pasadena, California

For obtaining maximum conversion efficiency in solar cells, the electrical properties of the p/n junction are second in importance only to high minority carrier lifetime. For solar cells with more heavily doped substrates, the junction performance can even become of primary importance mainly because of excessive space-charge recombination current. Most reported measurements of junction characteristics have given widely varying and erroneous values even for standard cells due to series resistance effects and to the presence of localized current-shunting paths.

The pertinent equations for the following discussion are given in Fig. 1, where V_d is the voltage drop across the junction, I_{01} and I_{02} are the reverse saturation currents for diffusion and recombination in the space-charge region, respectively. R_s and R_{sh} are the series and ohmic shunt resistance, respectively. The last equation does not include other possible current mechanisms such as surface channel or surface recombination as it is felt that proper processing can sufficiently control these mechanisms, and since extensive measurements on 2- and 10-ohm-cm cells have indicated negligible effects. A computer program has been developed

* This paper presents the results of one phase of research carried out at the Jet Propulsion Laboratory, California Institute of Technology, under contract no. NAS 7-100, sponsored by the National Aeronautics and Space Administration.

Preceding Page Blank

that accurately solves for the five variables: I_{01}, I_{02}, A_2, R_s, and R_{sh} from the dark forward current-voltage characteristics. Since each one of these variables affects the solar cell parameters of open-circuit and maximum-power voltages (V_{oc} and V_{mp}), fill factor (F.F.), and efficiency (η), another computer program was written which will calculate these parameters and draw the light I-V curves for any combination of the five variables for any temperature or light level. This paper presents some results for room temperature when the space-charge recombination current is varied.

For comparison, a standard Mariner 2-ohm-cm solar cell at earth-orbital conditions is presented in Fig. 2, where I_{02} is the variable. The change in four of the photovoltaic parameters is given in Fig. 3. The average value of I_{02} measured on such cells is indicated as are average values of the V_{mp}, V_{oc}, F.F., and η. The small difference is well within experimental error and may also be accounted for by shunting effects which were not included in calculating the solid curves. The results show that for typical values of I_{02} in standard solar cells, the loss in efficiency is no more than about 10%. The loss in more advanced solar cells having (incidentally) narrower space-charge regions is considerably less.

The situation in more highly doped solar cells is quite different, however, due to the relatively much smaller value of diffusion component. Fig. 4 gives the light I-V curves for a substrate resistivity of 0.1 ohm-cm and an assumed light-generated current of 46 mA/cm^2. The resulting variation in photovoltaic parameters is shown in Fig. 5. Now one can see that the loss in efficiency, for example, can be as much as 100%. Even if the reverse saturation current density due to space-charge recombination in 0.1 ohm-cm material is comparable to that typically measured in conventional 2 to 10 ohm-cm material, the efficiency of the 0.1 ohm-cm cell is reduced from 18% to about 13%.

The choice of 1.0 ohms for the series resistance may be somewhat harsh. The shallower junctions required to get as much as 46 mA/cm^2 have considerably higher sheet resistances. However, photolithographic grid contacts have reduced the total series resistance to values lower than 1 ohm.

Consequently, the numbers for efficiency and fill factor on Fig. 5 probably can be raised somewhat. Figure 6 gives some values for the case of I_{02} = 1×10^{-7} A/cm^2. The values for $I_{02} = 1 \times 10^{-9}$ A/cm^2 are:

R_s(ohms)	η (%)	F.F.
0	19.2	.843
0.5	18.5	.812
1.0	17.8	.782
2.0	16.5	.723

The specific impurities and/or impurity defect complexes responsible for the amount of recombination current are presently unknown. Planned experiments of thermally stimulated capacitances and capacitance transients on high-doped silicon and on low-cost ribbon silicon, where the excess current problem is equally bad, should provide some answers. I believe that processing - both on the silicon blank and in junction fabrication - are crucial steps, no matter what the starting densities of deep-level impurities are. In the case of low-cost silicon, such as ribbon-grown or sheet silicon, the presence of grain boundaries and other lattice defects can cause impurity segregation and enhanced localized excess leakage current. Even with single crystal silicon, the recombination current may well be enhanced by the diffusion process itself. It is well known that the phosphorous "glass" formed from P_2O_5 is an efficient getter of metallic impurities. Consequently, it is quite likely that one may have a situation such as given in Fig. 7, where the original background density N_o has been reduced in the bulk by the gettering, but has been actually increased near the surface. Thus, the space-change region at x_j may have an unexpectedly large concentration of deep level impurities injurious to the junction characteristics. It is for these reasons that various junction formation processes should be explored in conjunction with the low resistivity high efficiency cell program.

In conclusion, the development of highly efficient low resistivity solar cells or moderately efficient very low cost silicon solar cells will require reducing the presently measured values of reverse saturation current density due to space-charge recombination two to three orders of

magnitude. This will best be accomplished by identifying the responsible deep level impurities by transient capacitance measurements, minimizing the source of such impurities during the silicon crystal growth, and by changing cell processes to minimize segregation effects.

$$I = I_l - I_D$$

$$V = I R_s + V_D$$

$$I_D = I_{01}\left[\exp q(V_D + IR_s)/kT - 1\right] + I_{02}\left[\exp q(V_D + IR_s)/2kT - 1\right] + V_D/R_{sh}$$

Figure 1. - Solar cell equations.

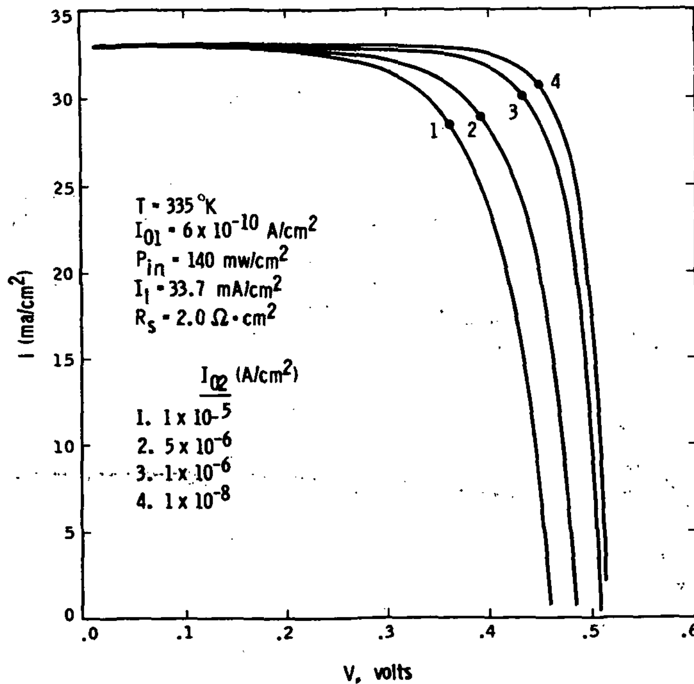

Figure 2. - Light I-V characteristics.

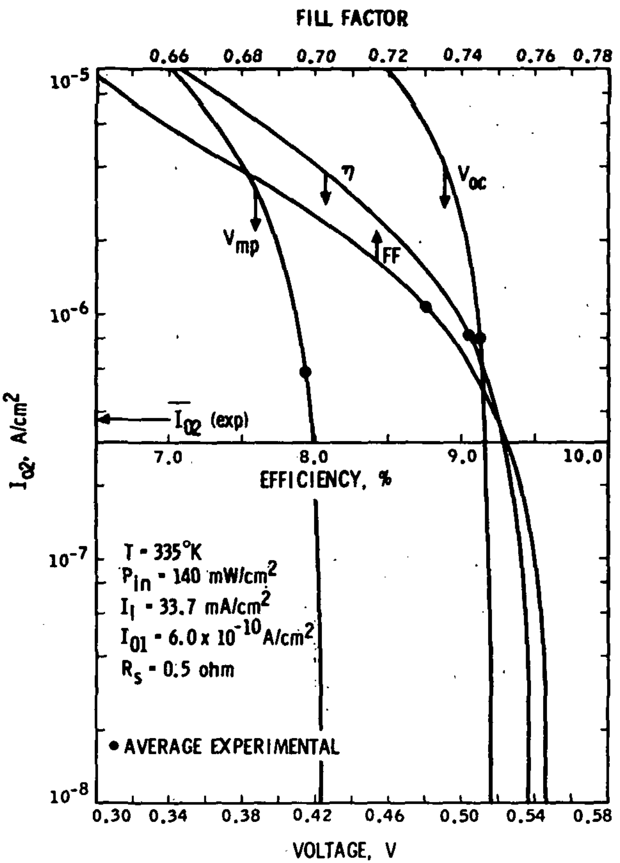

Figure 3. - Changes in photovoltaic parameters for 2-Ω-cm cell.

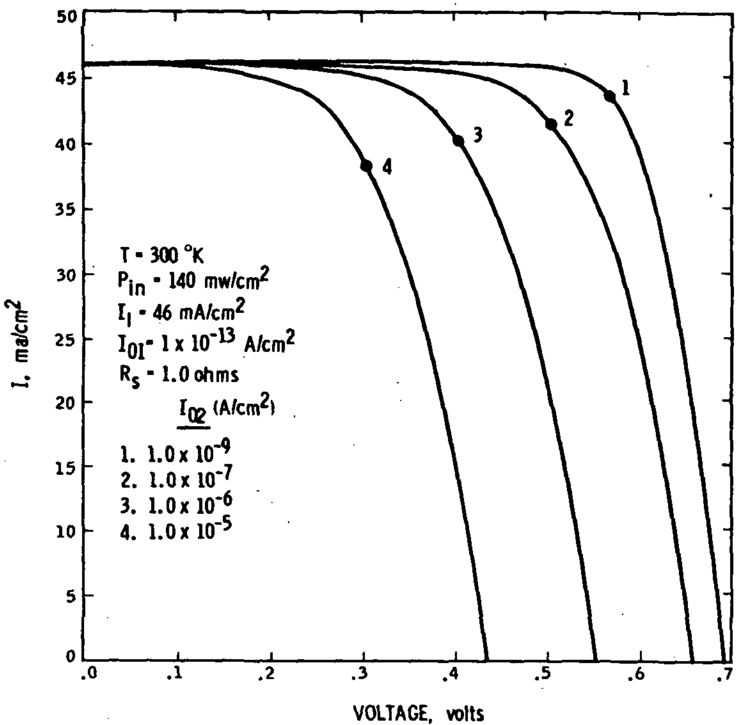

Figure 4. - Effect of recombination current.

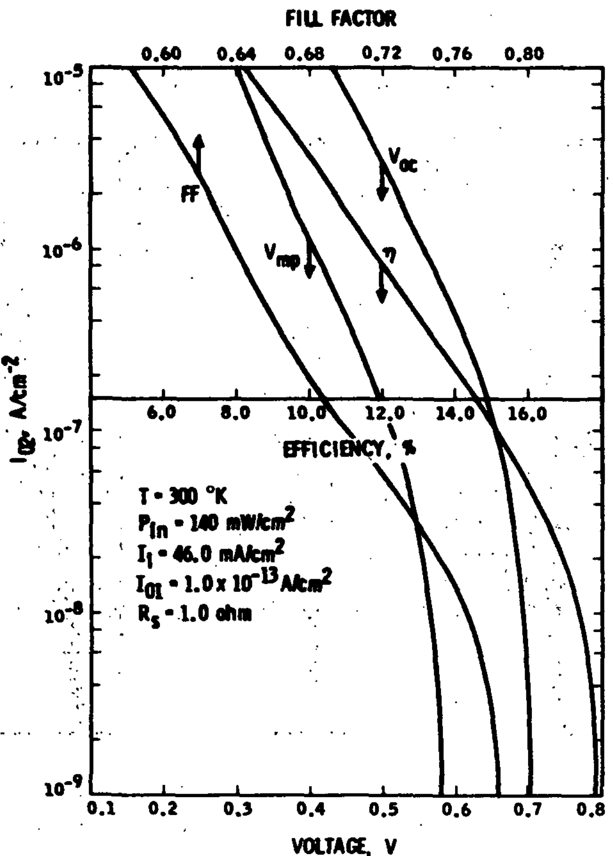

Figure 5. - Changes in photovoltaic parameters for 0.1-Ω-cm cell.

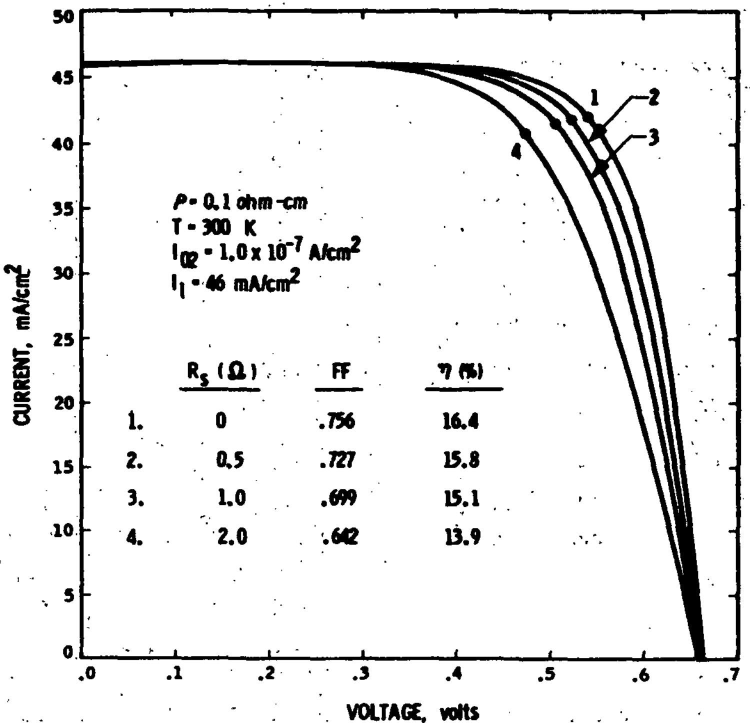

	R_s (Ω)	FF	η (%)
1.	0	.756	16.4
2.	0.5	.727	15.8
3.	1.0	.699	15.1
4.	2.0	.642	13.9

Figure 6. - Effect of series resistance.

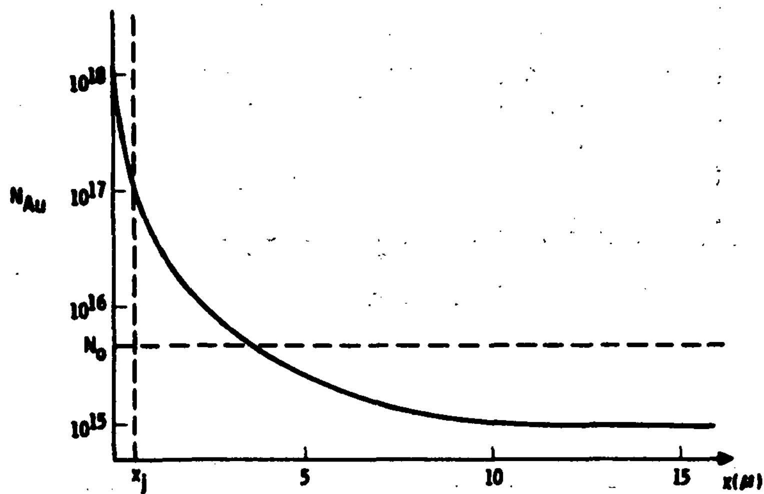

Figure 7. - Gettering of deep impurities by diffusion process and possible distribution at junction.

18. A SEMI-EMPIRICAL ANALYSIS OF SILICON SOLAR CELL PARAMETERS AS A FUNCTION OF SOLAR INTENSITIES*

E. Y. Wang
Wayne State University
Detroit, Michigan 48202

I. Introduction

It has been known for years that the electrical characteristics of silicon solar cells have an important effect on open circuit voltage, V_{oc} and fill factor FF. These parameters have been studied previously for AMO solar intensity based on ideal diffusion limited current-voltage characteristics of the silicon solar cells. For terrestrial application, the solar intensity is less than the AMO condition, or considerably more than the AMO condition if a concentrated optical system is used. In this paper, we have investigated the solar cell parameters as a function of solar intensity based on various models of junction current. The models considered in the calculation are, bulk recombination, [1] space-charge region recombination, [2] surface channel effect, [3] and ohmic shunting paths. [4,5] The cells considered in the studies are of 0.01, 0.1, 1., and 10 ohm-cm resistivity. The short circuit current I_{sc} is assumed to be linearly dependent on solar intensity. In addition, we also present the effect of the series resistance for a typical cell on fill factor at high solar intensities.

*Major portion of this work is performed under NASA Grant NGR 23-006-057 and NGR 23-006-063.

Preceding Page Blank

II. Calculation Results

The total junction current of the silicon solar cell consists of the contribution from the diffusion current due to bulk recombination, generation-recombination current in the transition region, and currents due to surface channel and shunting resistance. The total junction current can then be empirically written as:

$$I_j = I_D(\exp \frac{qV}{kT} - 1) + I_R(\exp \frac{qV}{2kT} - 1) + I_Q(\exp \frac{qV}{4kT} - 1) + \frac{V}{R_{SH}} \quad (1)$$

where I_D, I_R, I_Q are saturation currents due to diffusion, recombination and surface channel respectivily. R_{SH} is the shunting resistance and other symbols have their usual meanings.

(A) Short-circuit Current

Equation (1) gives the current-voltage relationship based on the theory of junction current in silicon solar cells. Under illumination, the I-V characteristics becomes:

$$I = I_L - I_j = I_L - I_D(\exp \frac{qV}{kT} - 1) - I_R\exp(\frac{qV}{2kT} - 1) - I_Q(\exp \frac{qV}{4kT} - 1) - \frac{V}{R_{SH}} \quad (2)$$

where I_L is the source current due to photogenerated excited carriers. By the definition of the short-circuit current, we set V equal to zero and solve for I. The short-circuit current, I_{sc} is simply equal to the source current, I_L. Furthermore, the I_{sc} is independent of any excess junction mechanisms.

(B) Open-circuit Voltage

The open-circuit voltage is obtained by setting the net

junction current equal to zero under illumination. For low illumination intensities, such as terrestrial applications or a Jupiter mission in space, the V_{oc} decreases as we include the other excess junction current mechanisms. Since the dependence of V_{oc} on excess junction currents is through the logrithmic function (except the current component form shunting resistance effect), the V_{oc} is relatively insensitive to the various excess junction mechanisms. Figure 1 is the plot of V_{oc} as a function of solar intensities for various excess current mechanisms. The I_{sc} is assumed to be linearly dependent on solar intensity. The value of I_{sc} is taken as $35mA/cm^2$ at AMO condition. The numerical values of I_D, I_R, R_{SH} and I_Q in equation 12 used in calculations were listed in Table I for various resistivity cells.

As shown in Figure 1, the junction current at AMO condition is dominated by diffusion current, and the excess junction has little effect on V_{oc}. For a diffusion current limited solar cell, V_{oc} is obtained from equation (2) and becomes the well-known expression:

$$V_{oc} = \frac{kT}{q} \log_e\left(\frac{I_{sc}}{I_D} + 1\right) \quad (3)$$

As shown in equation (3), larger V_{oc} requires smaller saturation current. Theoretically, this can be achieved by doping heavily in the base region of the solar cells. Figure 2 illustrates the ideal diffusion-limited solar cells for various base resistivity material. Figure 3 shows the results for generation-recombination limited solar cells.

(C) Fill Factor:

Fill factor is defined as the ratio of the $I_m V_m$ product to the $I_{sc} V_{oc}$ product where I_m, V_m are the current and voltage to give the maximum power output. It also means to extract the maximum area of a current-voltage curve when solar cell is under illumination [6]. The fill factor depends on the series resistance and the current-voltage characteristics of the n-p junction. The saturation current of a typical silicon solar cell junction exhibits at least one or two orders of magnitude larger current than that of diffusion-limited current. This excess junction current leads to decreasing conversion efficiency primarily through the decrease in fill factor. By using equation (2), the current-voltage curves under illumination for various combinations of excess junction current mechanisms can be generated. I_{sc} is taken as $35mA/cm^2$ and a linear dependence of I_{sc} on illuminating intensities is assumed. Fill factor values can be obtained from the generated I-V curves under illumination. Figure 4 gives the results of fill factor values for various excess junction current mechanisms at various solar intensities. The results show that the reduction in conversion efficiency through the decrease in fill factor becomes more acute for low illumination environments. Figure 5 and 6 show the fill factor results for the diffusion-limited and generation-recombination limited solar cells respectively. At high solar intensities, the excess junction current has little effect on the fill factor of solar cells; however, the series resistance, typically 0.3-0.5 ohm, will tend to decrease the fill factor. This effect is illustrated in Figure 7. Figure 8 shows the results on the fill factor if zero series resistance

is assumed. Therefore, for terrestrial applications in a concentrated optical system, the problem of series resistance should be the prime concern of the research. It should be pointed out that base resistivity of the cell might play a important role in determining the series resistance at high solar intensities.

(D) The Effect of the Base Resistivity of Solar Cells on the Relative Conversion Efficiency:

Based on diffusion theory, low base resistivity cells should provide a higher efficiency cell as illustrated in Figure 2 and 5. In practice this is not the case. This is because the low resistivity solar cells are found to exhibit much more excess junction current that those of high resistivity solar cells, hence a decrease in efficiency through the decrease in fill factor is expected. The relative cell conversion efficiency is simply the product of the fill factor and open-circuit voltage. As shown in Figure 9, the concept of the lower resistivity of the base material yielding more efficient solar cells is true only for the diffusion limited current-voltage characteristics. Realistically, cells will probably be generation-recombination current limited. Therefore, there will be an optimum value of the base material resistivity for achieving optimum efficiency at particular solar intensities. Figure 10 shows the results for the G-R limited case for various base resistivity cells. The results suggest that at AMO condition, 0.1 ohm-cm cell gives the optimum efficiency; at 0.1 solar intensity illumination, the 1 ohm-cm cell has the best conversion efficiency; and 0.01 ohm-cm cell gives the best efficiency at 5 sun intensity illuminations. Figure 11 shows the results including

surface channel current and shunting resistance effect. Again, the optimum conversion efficiency at different solar intensities corresponds to different base resistivity cells.

III. Summary

The effect of the excess junction currents and series resistance on silicon solar cell conversion efficiency at various solar intensities for various base resistivity solar cells has been theoretically analyzed in detail. The highlights of the results can be summarized as follows:

(1) Short-circuit current is independent of any excess junction mechanism.

(2) Open-circuit voltage is relatively insensitive to the various junction mechanism, paritcularly at solar intensity higher than AMO conditions.

(3) Fill factor strongly depends on junction current mechanism, particularly at solar intensity lower than AMO conditions.

(4) At high intensity, series resistance, typically 0.2-0.3 ohm, will tend to decrease the fill factor.

(5) The concept of the lower resistivity of the base material yielding more efficient cells is true only for diffusion limited current-voltage characteristics. Realistically, however, at a particular solar intensity there is an optimum value of the base material resistivity for achieving optimum efficiency cell.

References

1. W. Schockley, Bell Syst. Tech. J., 28, 435, (1949)

2. C. T. Sah, R. N. Noyce and W. Schockley, Proc. IEEE, 45, 1228, (1957)

3. C. T. Sah, Proc. IEEE, 49, 1623, (1963)

4. M. Wolf and R. Rauchback, Adv. Eng. Conv., 3, 455, (1963)

5. R. J. Stirn, Conf. Record of 9th IEEE Photovoltaic Specialists Conf., p. 72, (1972)

6. M. P. Prince, J. Appl. Phys., 26, 1, (1955)

TABLE I NUMERICAL VALUES USED IN CALCULATIONS

	10 ohm-cm	1 ohm-cm	.1 ohm-cm	.01 ohm-cm
I_R Amp/cm^2	1×10^{-8}	1.25×10^{-8}	3.34×10^{-8}	1.0×10^{-7}
I_D Amp/cm^2	2.64×10^{-11}	2.1×10^{-12}	1.5×10^{-13}	1.37×10^{-10}
I_Q Amp/cm^2	1×10^{-5}	1×10^{-4}	1×10^{-3}	1×10^{-2}
R_{SH}	100,000 ohm	100,000 ohm	100,000 ohm	100,000 ohm

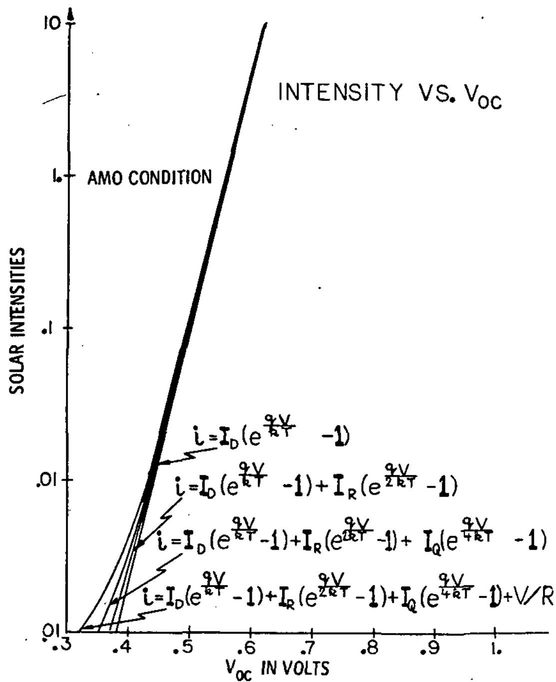

Figure 1. - Dependence of V_{oc} on solar intensities for various excess junction current mechanisms.

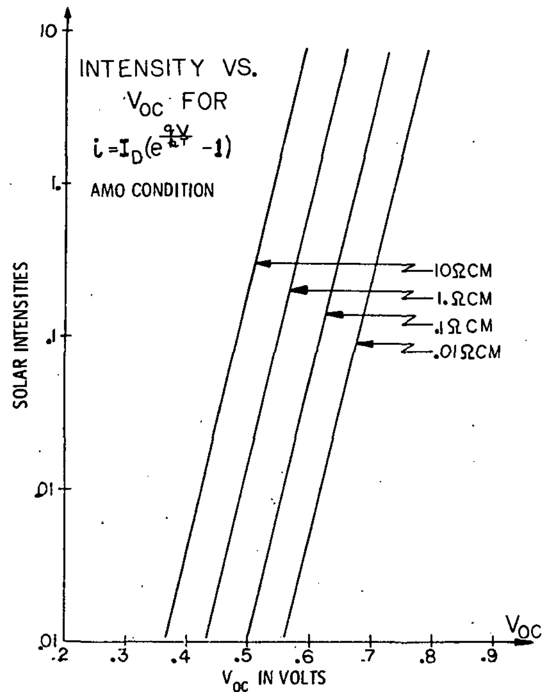

Figure 2. - Dependence of V_{oc} on solar intensities for diffusion limited solar cells with various base resistivities.

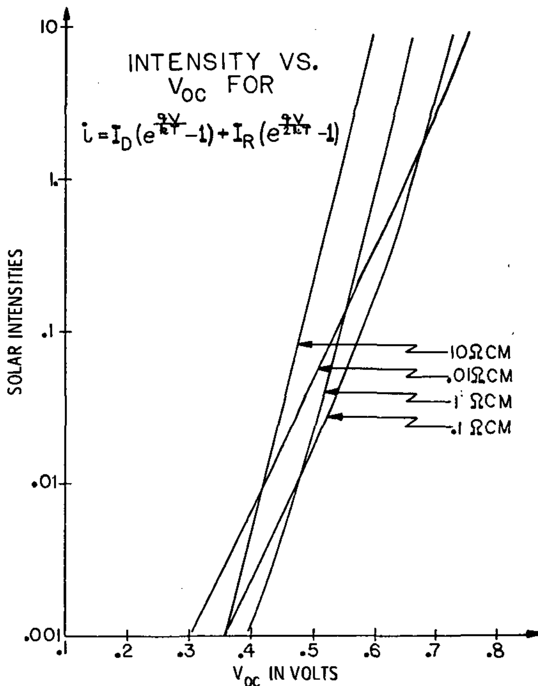

Figure 3. - Dependence of V_{oc} on solar intensities for generation-recombination limited solar cells with various base resistivities.

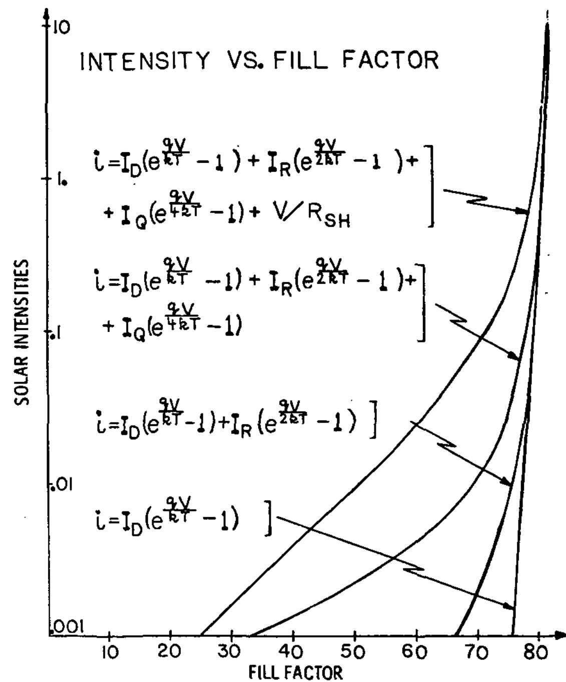

Figure 4. - Dependence of fill factor on solar intensities for various excess junction current mechanisms.

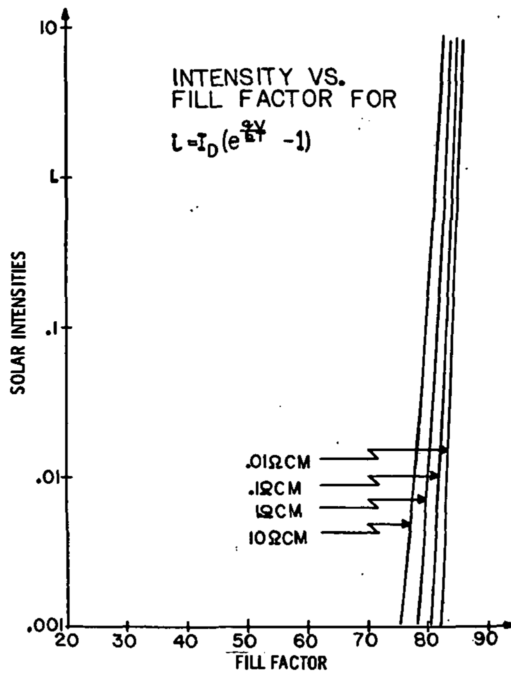

Figure 5. - Dependence of fill factor on solar intensities for diffusion limited solar cells with various base resistivities.

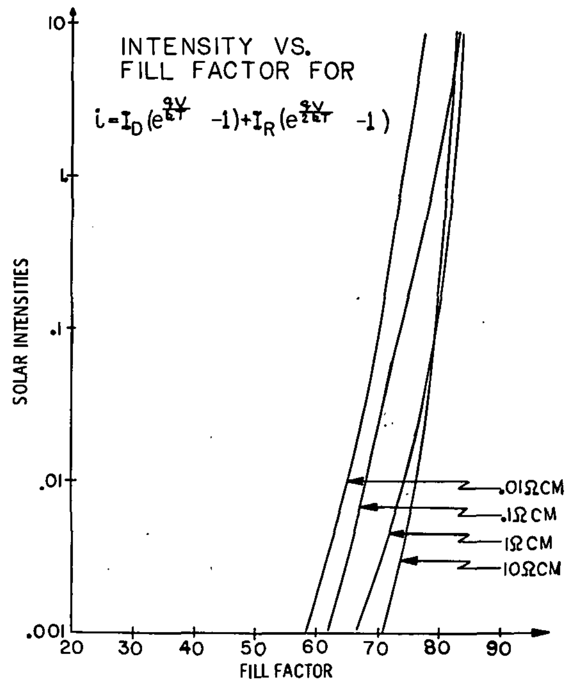

Figure 6. - Dependence of fill factor on solar intensities for generation-recombination limited solar cells of various base resistivities.

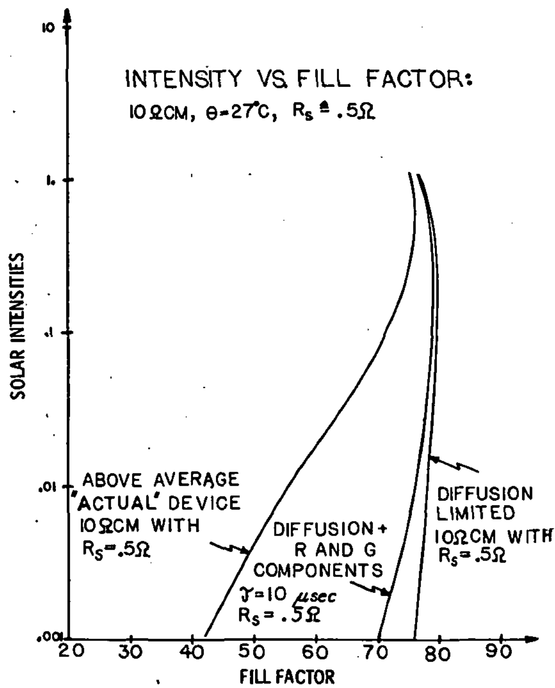

Figure 7. - Dependence of fill factor on solar intensities for solar cells with $R_s = 0.5$ ohm.

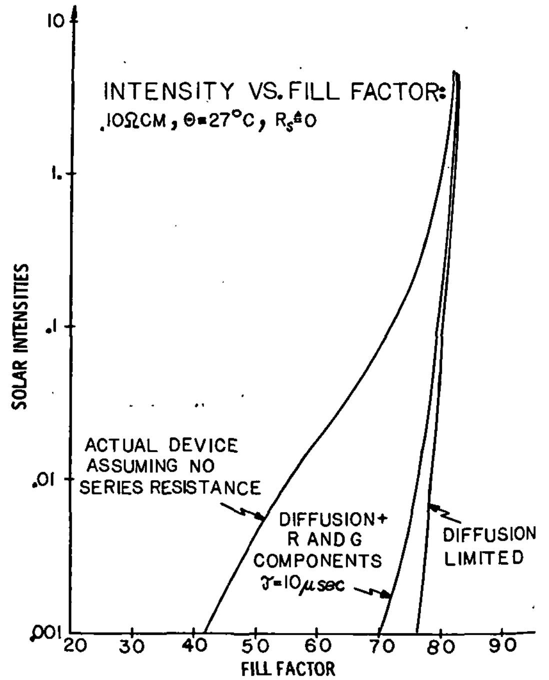

Figure 8. - Dependence of fill factor on solar intensities for solar cells with $R_s = 0$.

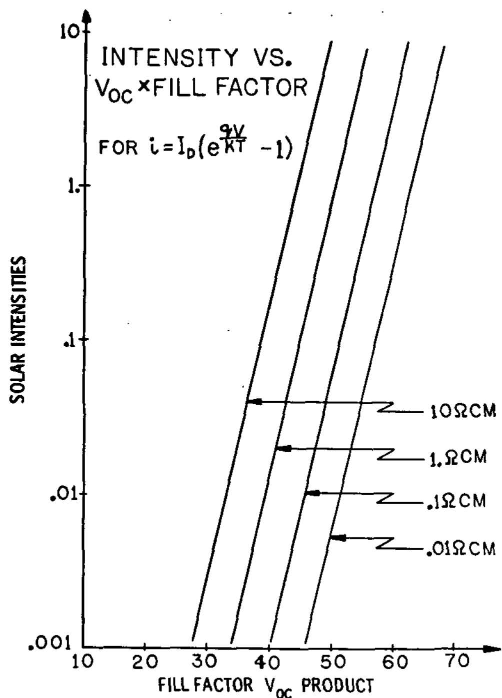

Figure 9. - Dependence of relative conversion efficiency on solar intensities for diffusion limited solar cells of various base resistivities.

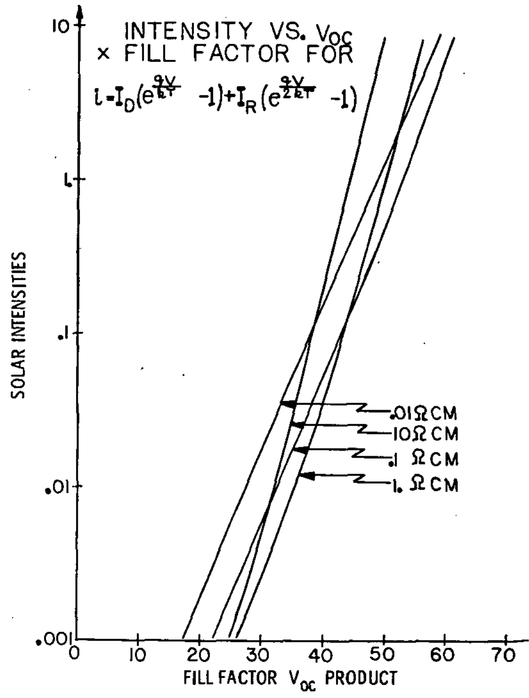

Figure 10. - Dependence of relative conversion efficiency on solar intensities for generation-recombination limited cells of various base resistivities.

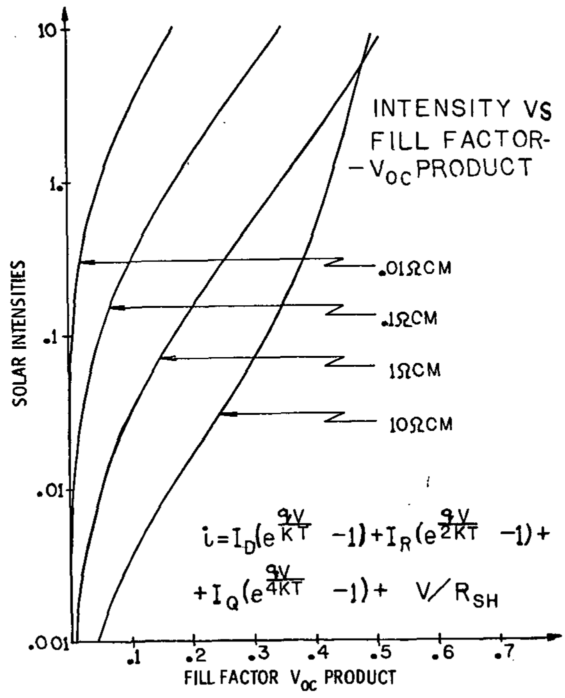

Figure 11. - Dependence of relative conversion efficiency on solar intensities for various junction current mechanisms.

19. SOME COMPUTER STUDIES OF SILICON SOLAR CELL EFFICIENCY*

J. R. Hauser and P. M. Dunbar
North Carolina State University
Raleigh, North Carolina 27607

Introduction

The basic starting point for the analysis of semiconductor devices is the current density and continuity equations:

$$
\begin{aligned}
J_n &= q\mu_n nE + qD_n \frac{\partial n}{\partial x}, \\
J_p &= q\mu_p pE - qD_p \frac{\partial p}{\partial x}, \\
\frac{\partial n}{\partial t} &= -U + G_e + \frac{1}{q}\frac{\partial J_n}{\partial x}, \\
\frac{\partial p}{\partial t} &= -U + G_e - \frac{1}{q}\frac{\partial J_p}{\partial x},
\end{aligned}
\qquad (1)
$$

where U is the net internal thermal generation-recombination rate and G_e is any external generation rate (due to light for example). The generation-recombination rate U is modeled in this work by a single Shockley-Read-Hall recombination level which gives

$$U = \frac{pn - n_i^2}{\tau_{po}(n+n_1) + \tau_{no}(p+p_1)}. \qquad (2)$$

In addition to the above equations, Poisson's equation must be used to relate E to the doping profile as

$$\frac{\partial E}{\partial x} = \frac{q}{\varepsilon}(p - n + N(x)), \qquad (3)$$

where N(x) is the net donor-acceptor impurity density.

The above set of equations must be applied to a device and solved in order to accurately calculate the terminal current-voltage characteristics. In solving the above equations, it is convenient to reduce the equations to a set of three coupled, nonlinear, second order differential equations.

*This work has been supported by a NASA Lewis research grant.

In this process one has several choices for the three variables in which the equations can be expressed. For example the three variables may be electrostatic potential, electron density and hole density or electrostatic potential, electron quasi-Fermi level and hole quasi-Fermi level. In the present work the latter choice of three variables has been made where the quasi-Fermi levels ϕ_n and ϕ_p are related to n and p as

$$n = n_i \exp[q(\psi-\phi_n)/kT],$$

$$p = n_i \exp[q(\phi_p-\psi)/kT]. \qquad (4)$$

The device equations expressed in terms of electrostatic potential and quasi-Fermi levels have been reported elsewhere [1,2] along with a discussion of the numerical techniques used in solving the device equations. Figure 1 shows a block diagram of the computer program which has been developed to solve the equations for ψ, ϕ_n and ϕ_p. The solution technique employed to solve the nonlinear device equations is an iterative technique whereby initial approximations to ψ, ϕ_n and ϕ_p are used to generate more accurate values and the process repeated in a nonlinear equation iterative loop (see Figure 1).

Other features of the computer analysis program which are important to the present study are discussed below. Doping and field dependences of mobility are included in the work. An optical carrier generation subroutine allows the calculation of carrier generation due to AM0, AM1 or monochromatic spectral irradiance. After the calculation of potential and quasi-Fermi levels, the carrier densities and current densities are printed and plotted for any desired device terminal voltage.

Solar Cell Analysis

The computer analysis program briefly discussed in the previous section has been applied to a variety of p-n junction and solar cell structures. The present work concentrates on one series of these calculations which was designed to explore the dependence of solar cell efficiency on resistivity (or doping) of the cell. The basic solar cell structure studied is shown in Figure 2. It consists of a thin diffused n^+ layer into a base p-type layer. The analysis allows for the presence of a back surface field or p^+ back surface layer [3,4].

In order to concentrate on the effects of varying base layer resistivity, as many dimensional and material parameters as possible were held constant in the present studies. A collection of these parameters is shown in the Table I (see Figure 2). Basically the cells studied were 250 μM in total thickness with 0.25 μM n^+ layers and 0.5 μM p^+ layers (when present). The n^+ layer was modeled by a Gaussian impurity profile with a surface concentration of $10^{20}/cm^3$. The lifetime in the n^+ layer for most of the calculations was held at 100 nsec. Some calculations to be reported later were made at a lifetime of 1 nsec. A surface recombination velocity of 10^3 cm/sec was used at the n^+ surface. Calculations with varying surface recombination velocities have shown that this is not a major parameter in determining solar cell efficiency. Varying surface recombination from zero to infinity was found to vary solar cell efficiency by only about 0.2%.

In addition to the parameters shown in Table I, the minority carrier lifetime, or diffusion length in the p-type base layer is a very important parameter in determining solar cell efficiency. The dependence of diffusion

length on doping density has been based in this work on the experimental data shown in Figure 3. The data points show experimentally measured diffusion lengths in n- and p-type material [5]. The solid lines are empirical curves which have been generated to bracket the experimental data. In the present computer calculations the upper solid curve has been used to model the p-type diffusion length. In some first order model calculations to be presented later, calculations using data corresponding to the upper curve are indicated as "high lifetime range" while calculations using data corresponding to the middle curve are indicated as "low lifetime range".

Using the above data, the efficiency of n^+-p and n^+-p-p^+ cells has been calculated at AMO for several p-type doping levels. The results of the efficiency calculations are shown as data points in Figure 4. The circle points are for the n^+-p-p^+ cell while the triangle points are for the n^+-p cell. In order to have a comparison basis for the computer device analysis program, the results of fairly simple first order models of solar cell efficiency are also shown as solid and dotted curves in Figure 4. The assumptions used in the first order calculations are briefly discussed below.

First for the n^+-p-p^+ cell the first order model calculations assume that the cell collects with 100% efficiency all carriers created to a depth of either the total cell thickness or the diffusion length whichever is smaller. Also, in calculating the forward dark current, the minority carrier reflecting properties of the back surface p^+-p junction are incorporated into the analysis. The presence of a single layer SiO

antireflecting coating is also included in the analysis. All solid curves in Figure 4 have been calculated using diffusing length values represented by the upper solid curve in Figure 3. The upper curve in Figure 4 labeled ideal p^+ contact is a first order calculation assuming that the back p^+ layer acts as an ideal minority carrier reflecting contact. The solid curve labeled n^+-p-p^+ cell is a calculation including the non-ideal nature of a back p^+ layer with the parameters of Table I.

First order calculations for the n^+-p cell give the solid curve labeled n^+-p cell in Figure 4. In this calculation, it is assumed that carrier collection occurs with 100% efficiency to a depth equal to either one-half the cell thickness or the diffusion length whichever is the smaller value. The back surface is also model as an ideal ohmic contact. The major difference between the n^+-p cell and the n^+-p-p^+ cell is a larger forward dark current in the n^+-p cell. This results in a lower open circuit voltage for the n^+-p cell and a reduced efficiency.

The first order calculations in Figure 4 also include one other factor which is not included in many first order calculations for solar cell efficiency. This is the inclusion of high injection effects in the model for high resistivity cells. This becomes important in n^+-p-p^+ cell at doping levels below about $10^{15}/cm^3$ and results in the almost constant efficiency regions of the two upper solid curves in Figure 4 below about $10^{15}/cm^3$.

The results of the detailed computer calculations can now be compared with the corresponding first order models. The circle points in Figure 4 are to be compared with the solid curve labeled n^+-p-p^+ cell and the triangle points are to be compared to the solid curve labeled n^+-p cell.

In general the detailed calculations exhibit the same general shape as the first order models but lead to a lower efficiency at all base doping levels. The peak efficiency is slightly above 16% while the first order models predict a peak efficiency of about 18%. The major differences between the complete computer calculations and the first order models has been identified and are discussed later in this paper.

Two calculated points are shown in Figure 4 using a lifetime of 1 nsec in the diffused n^+ layer. In general it was found that the n^+ minority carrier lifetime had little effect on cell efficiency for lifetimes of 100 nsec or larger. Below this value, however, the n^+ lifetime was found to influence efficiency at high doping levels in the p region. At a lifetime of 1 nsec, there is little effect on efficiency for a 10 Ω·cm cell but the efficiency of a .01 Ω·cm cell was reduced about 1% in total efficiency to about 15%. It can also be seen that at low n^+ lifetimes, low resistivity cells have little or no advantage in efficiency over high resistivity cells.

The dotted curve in Figure 4 is a first order calculation of solar cell efficiency for both the n^+-p-p^+ and n^+-p cells when low lifetime values are used corresponding to the center range of diffusion lengths of Figure 3. This curve when compared with the solid curves illustrates the effect of diffusion length on efficiency. Also the increased efficiency of the back surface field cell disappears when the diffusion length becomes significantly less than the cell thickness. These conclusions concerning diffusion length effects have also been verified by the complete computer analysis program.

The major differences in predicted efficiency of the first order models and the complete computer analysis have been identified as an over estimation of the minority carrier collection depth of the first order models. From the detailed computer calculations, it is possible to determine the exact depth to which carriers are being collected in the solar cell. This can be done by looking for the spatial point at which the minority carrier current in the base layer reverses sign. This must then represent the effective depth to which carriers are collected. Data from the computer program on the actual collection depth for n^+-p and n^+-p-p^+ cells are shown in Figure 5. Consider first the n^+-p cell. In the first order calculations the collection depth was assumed to be the smaller or L_n or W/2. The actual collection depth was found to be considerably smaller, being around W/3 when the diffusion length is much larger than the cell thickness and around $L_n/2$ for small diffusion lengths. For the n^+-p-p^+ cell the actual collection depth was also found to be considerably smaller than assumed in the first order model. For example at doping densities between $10^{16}/cm^3$ and $10^{17}/cm^3$ the actual collection depth was less than half the cell thickness even though the diffusion length was considerably longer than the cell thickness.

The reduced minority carrier collection depth has been found to be the major source of the lower efficiency obtained from the exact computer calculations as opposed to the collection depth normally assumed in first order efficiency calculations. When the first order models were corrected for the actual collection depth, there was close agreement between the first order models and the exact computer analysis. The reduced collection depth appears to occur because of the very non-uniform generation of carriers

in the solar cell, resulting in a diffusion of carriers away from the collecting p-n junction. These combined effects of non-uniform carrier generation and diffusion are not easily combined in a first order model to give a realistic collection depth. With the computer analysis program these effects are all included giving more realistic efficiency predictions.

In the present device analysis program a major effort has been made to model the solar cell with as exact a model and input data as possible. However, there is one major area where the present computer calculations do not accurately describe solar cell behavior. This concerns the effects of heavy doping in the n^+ region. There are several modifications of the basic device equations which must be considered for doping densities above about $10^{18}/cm^3$ in silicon [6,7]. Probably the most important effect as far as solar cell operation is concerned is the reduction in energy band gap which occurs at heavy doping. This leads to a decreased "effective doping" in the n^+ region as far as minority carrier injection into this region is concerned. Heavy doping can result in an increase in back injection of minority carriers into the n^+ region as well as an increased importance of surface recombination due to the decreased field acting to aid minority carrier flow away from the surface.

In an initial look at the influence of heavy doping on solar cell performance, the band gap reduction has been modeled by an empirical expression [8] and included in the first order model calculations of cell efficiency. The results are shown in Figure 6. Curve number 1 is the ideal n^+-p-p^+ cell with a lifetime of 100 nsec or longer in the n^+ layer. Curve number 2 corresponds to a lifetime in the n^+ layer which varies with doping according to the high diffusion length data of Figure 3. Curve number 3 includes both the variable lifetime and heavy doping effects.

As the curve illustrates, heavy doping effects can significantly reduce the predicted efficiency of solar cells at all doping levels. In fact it appears that heavy doping effects may eliminate the predicted enhanced efficiency of low resistivity solar cells. From this preliminary investigation it appears to be very important to include heavy doping effects in any complete analysis of solar cells. Presently these effects are being included in the detailed computer analysis program to accurately evaluate the importance of heavy doping in the n^+ region.

Summary and Conclusions

A detailed computer device analysis program is being used to study silicon solar cell efficiency. A series of calculations of solar cell efficiency at several doping levels has indicated lower efficiencies than are predicted by simple first order models of solar cell performance. The maximum calculated efficiencies are about 16% as opposed to about 18% for first order models. The calculations have been made for a single SiO antireflecting layer and slightly higher efficiencies would result from the textured surface cells [9,10]. The major problem with first order models of cell efficiency has been found to be the overestimation of the depth to which minority carriers are collected. A preliminary look at heavy doping effects in the diffused n^+ layer of cells has also indicated that these effects may have important limitations to solar cell efficiency in low resistivity material.

List of References

1. E. D. Graham and J. R. Hauser, Solid State Electronics, 15, 303-310, 1972.

2. E. D. Graham, Ph.D. Thesis, N. C. State University, Raleigh, N.C., 1970.

3. M. P. Godlewski, C. R. Baraona, and H. W. Brandhorst, Jr., "Low High Junction Theory Applied to Solar Cells", Tenth IEEE Photovoltaic Specialists Conference, 1974.

4. H. W. Brandhorst, Jr., C. R. Baraona, and C. K. Swartz, "Performance of Back Surface Field Cells", IEEE Photovoltaic Specialists Conference, 1973.

5. Based upon unpublished data obtained by P. A. Iles, Centralab Inc., work performed under NASA contract NAS 3-17360.

6. M. P. Godlewski and H. Brandhorst, "Effects of High Doping Levels on Silicon Solar Cell Performance", paper presented at this conference.

7. F. A. Lindholm, S. S. Li, and C. T. Sah, "Studies of Some Fundamental Limitations on the Performance of p-n Junction Silicon Solar Cells", Paper presented at this conference.

8. J. R. Hauser, "Minority Carrier Transport in Heavily Diffused Semiconductor Devices", Final report on NSF Grant GK-1615, September 1969.

9. J. Haynos, J. Allison, R. Arndt and A. Meulenberg, "The COMSAT Non-Reflective Silicon Solar Cell: A Second Generation Improved Cell", paper presented at this conference.

10. C. R. Baraona, "V-Grooved Silicon Solar Cells", paper presented at this conference.

TABLE I. - MATERIAL AND DIMENSIONAL PARAMETERS

Parameter	Value
Overall cell thickness	250 μM
n^+ thickness	0.25 μM
p^+ thickness (n^+-p-p^+ cell)	0.50 μM
n^+ surface concentration	$10^{20}/cm^3$
p^+ doping concentration	$10^{18}/cm^3$
p doping concentration	variable
Lifetime in n^+ region	100 nsec
Lifetime in p region	variable
Surface recombination velocity	10^3 cm/sec
SiO antireflecting layer thickness	800 Å

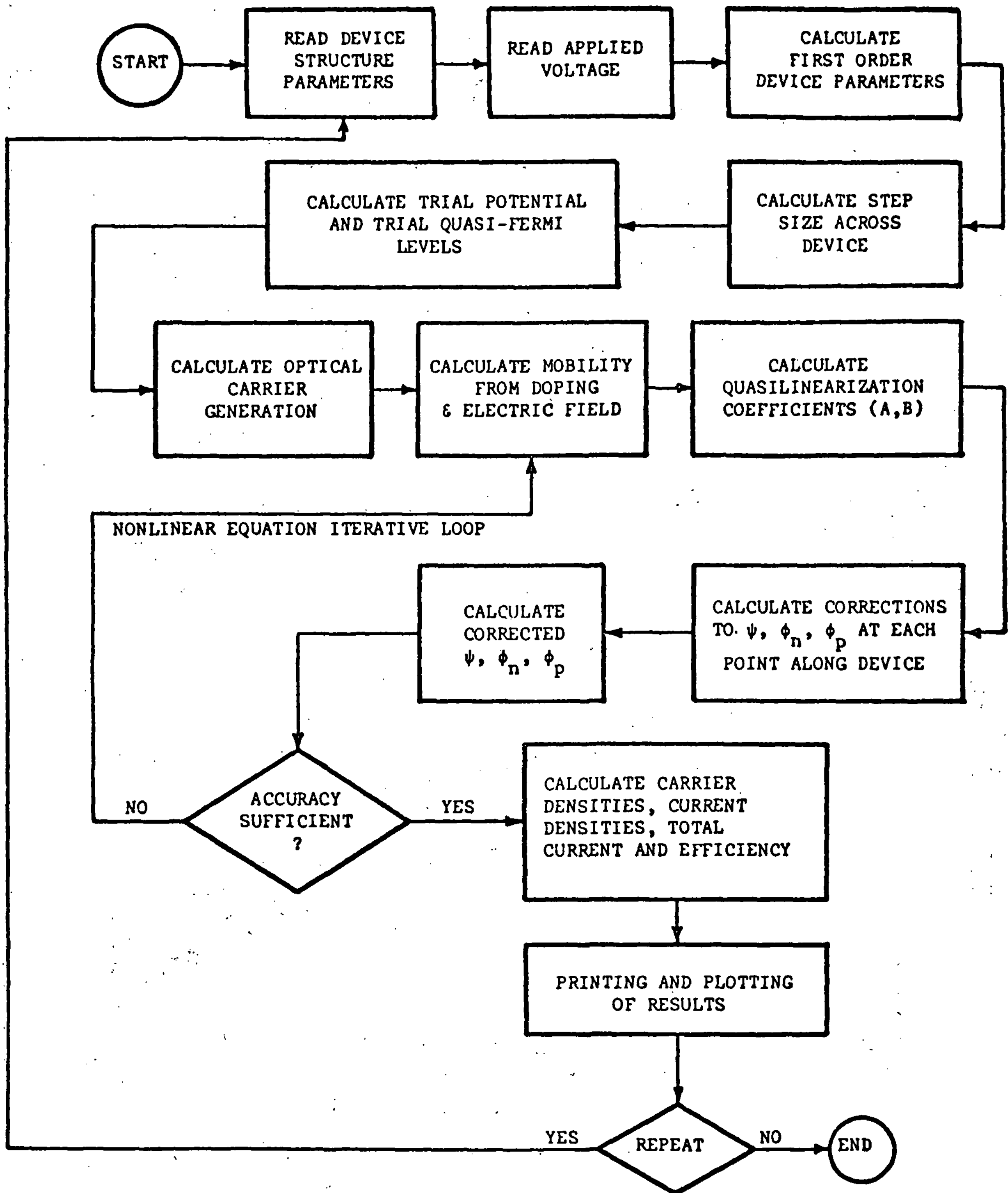

Figure 1. - Outline of computer program for solar cell analysis.

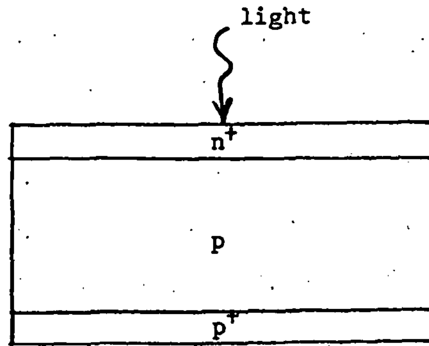

Solar cell structure studied.

Figure 2. - Basic solar cell structure.

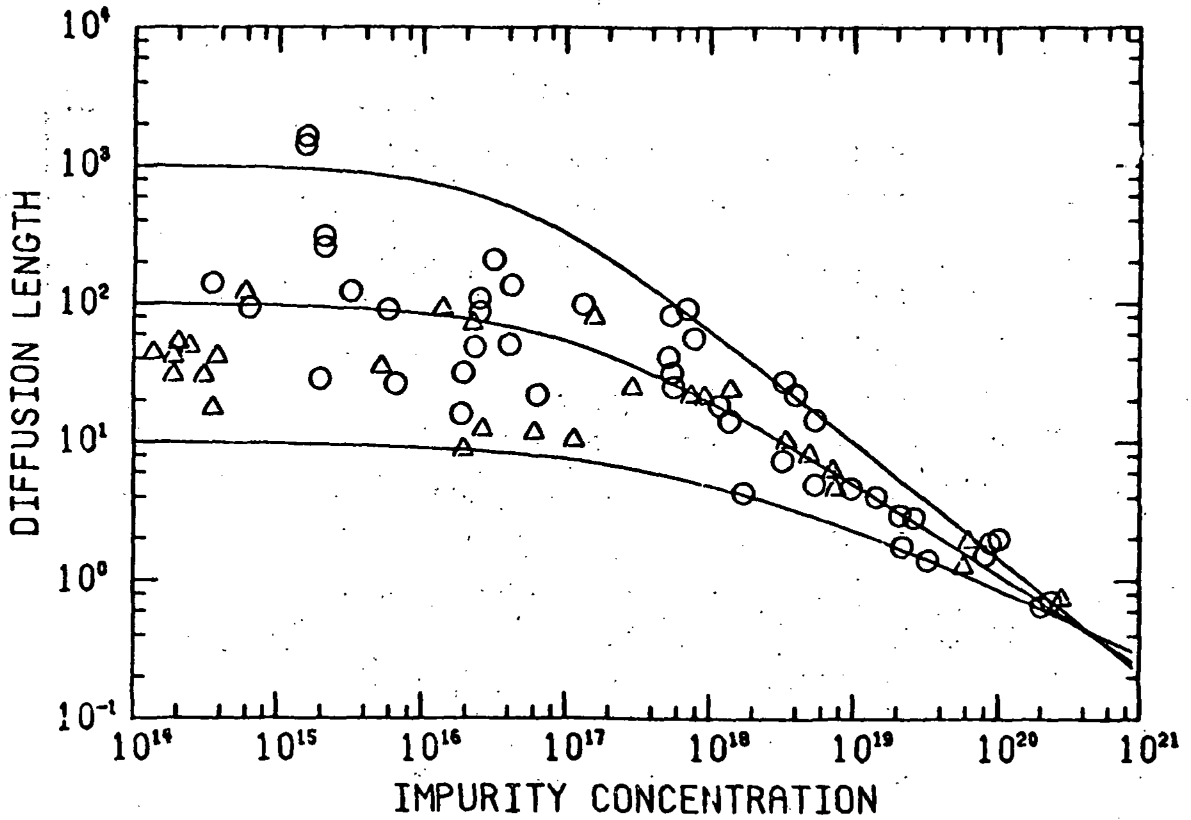

Figure 3. - Variation of diffusion length with impurity concentration.

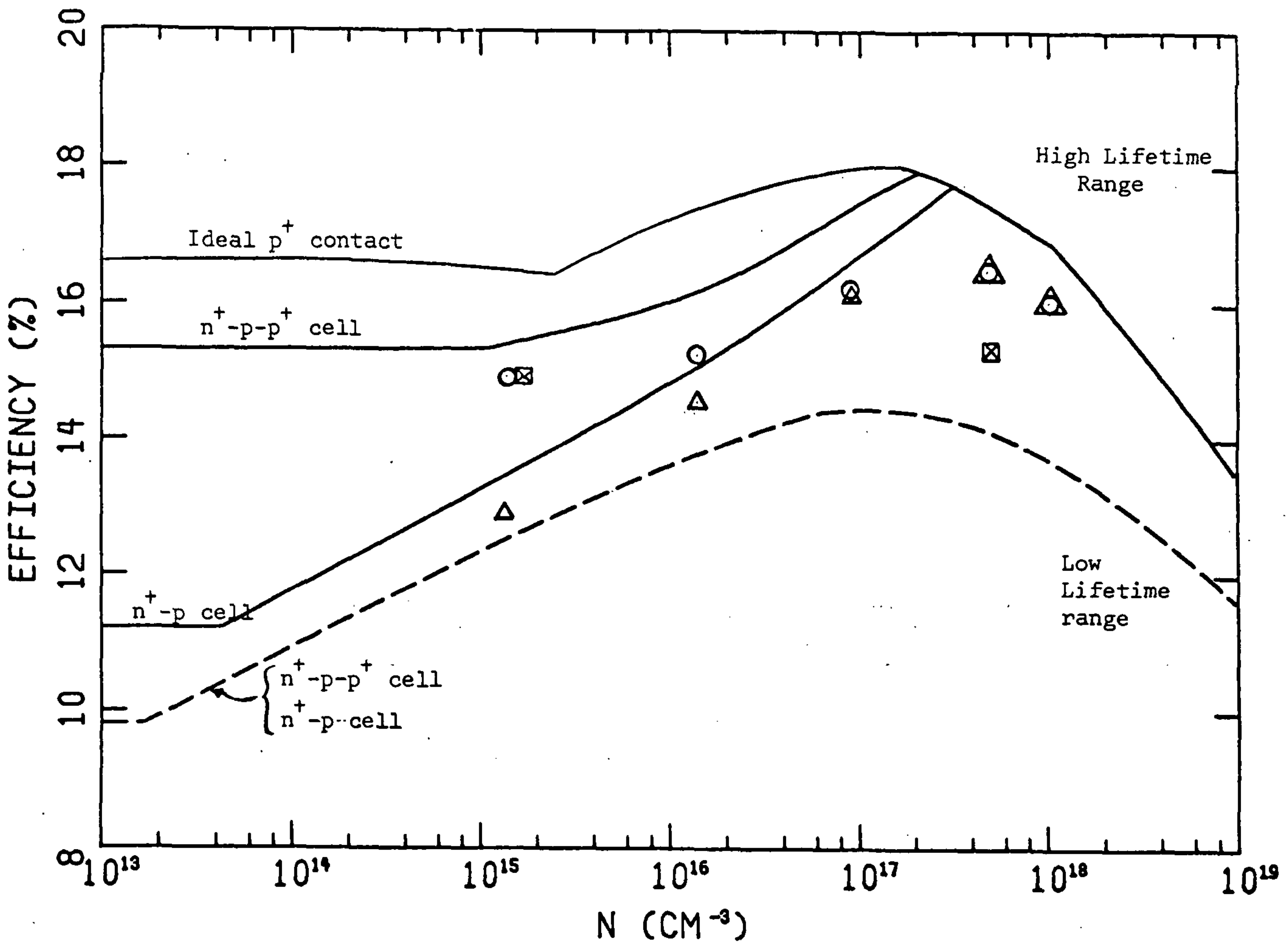

Figure 4. - Comparison of first order models for solar cell efficiency and results of exact computer solutions. Data points are results of exact computer calculations. ⊠ Indicates 1 nsec n^+ lifetime. Other points are for 100 nsec n^+ lifetime.

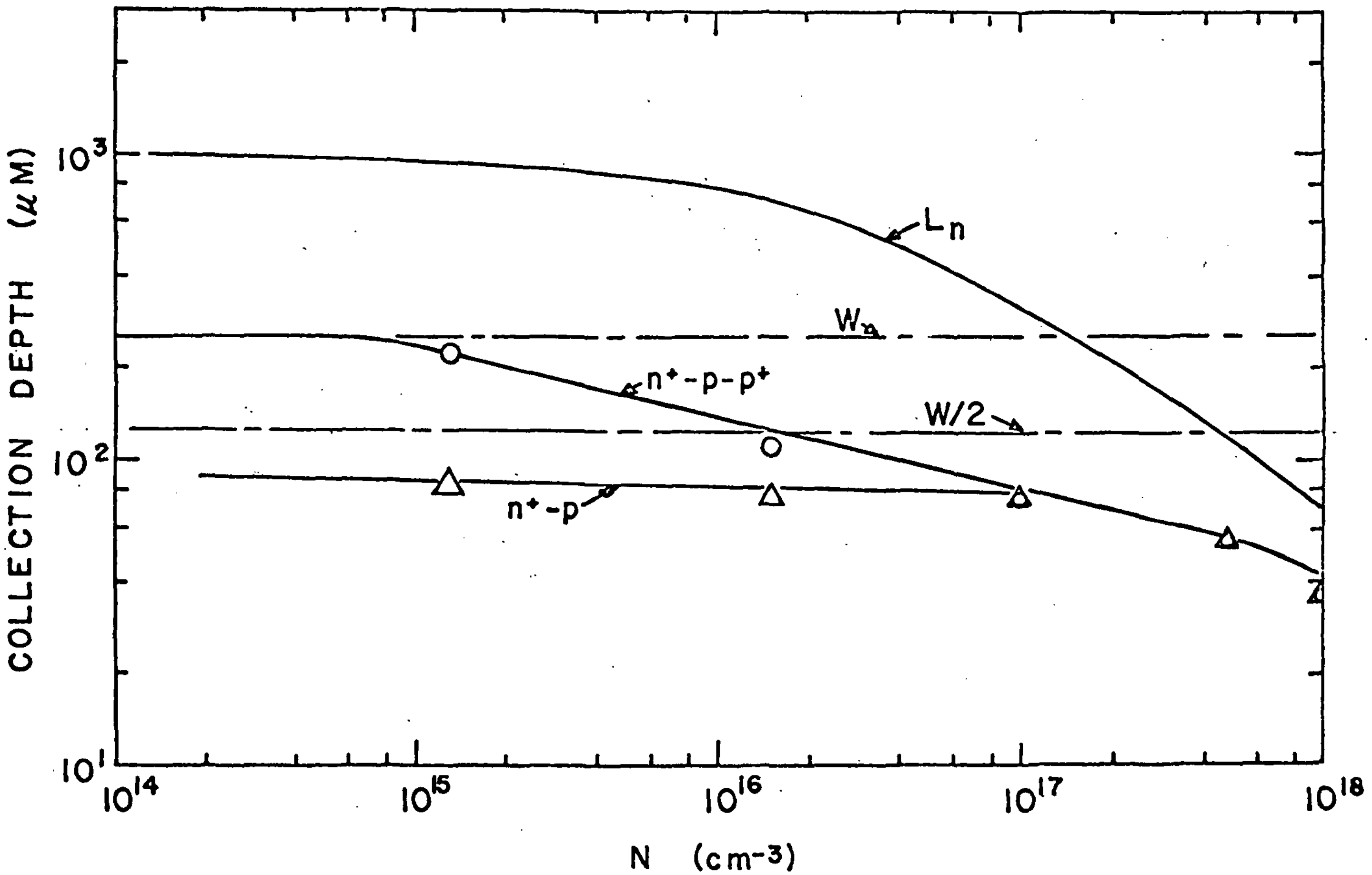

Figure 5. - Actual collection depth as a function of doping as obtained from computer calculations.

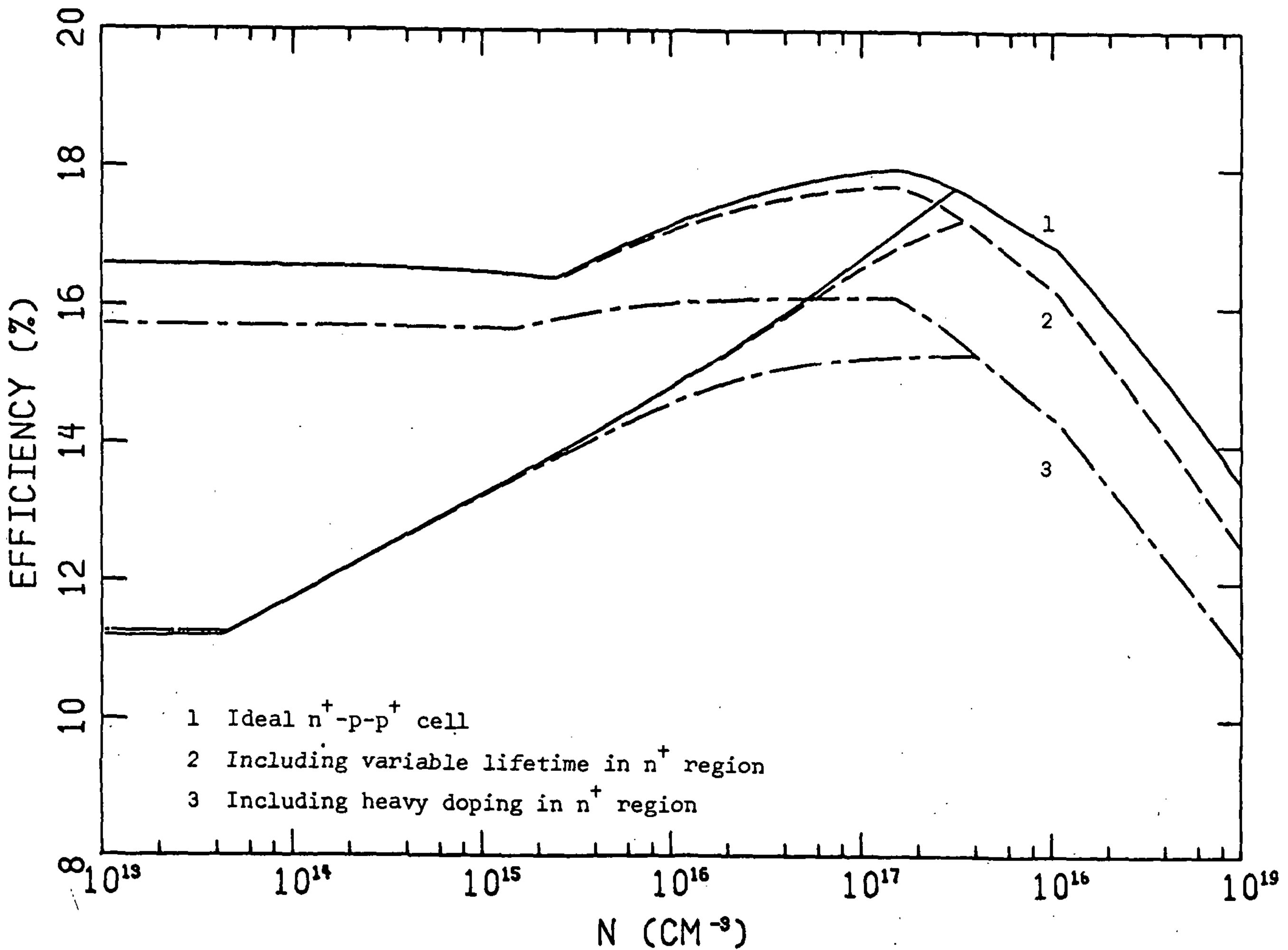

Figure 6. - Illustration of the effects of low n^+ lifetime and heavy doping in n^+ region on solar cell efficiency.

20. COMPARISON OF RECENT SOLAR CELL PERFORMANCE IMPROVEMENTS

Martin Wolf
University of Pennsylvania
Philadelphia, Pennsylvania

In a recent paper,[1] the efficiency improvements achieved in the Comsat "violet" cell were compared to those predicted previously[2] and shown as goals in Table I. Now, after the announcement of the Comsat "non-reflective" cell,[3] this analysis can be updated (Table II), and several important conclusions can be drawn:

1. The entire predicted collection efficiency improvement has been achieved.
2. The entire predicted reflection loss reduction has been achieved.
3. While the "violet" cell brought the anticipated improvement in short-wavelength collection efficiency, it suffered some reduction in long-wavelength collection efficiency. This loss has been erased in the non-reflective cell not by an increase in diffusion length, but by a reduction of the average photon absorption depth measured normal to the - now roughened - surface plane. The same measure helped reduce reflection losses without further work on the antireflection coating. Diffusion length and AR coating improvements may now yield a further, although small collection efficiency increase.

   A suspicion exists that the old p/n solar cells, which were not polished, but underwent a heavily etching BCL_3 diffusion treatment and emerged "black" from this process step, never requiring an AR coating, may have had a surface texture similar to that of the

"non-reflective" cell.

4. Active area coverage by the contact grid structure has been slightly increased from that of the commercial cell. There may be a technology and cost-effectiveness barrier against significant improvement.
5. The voltage factor (relating open circuit voltage to energy gap) in the "non-reflective" cell appears slightly decreased from that of the "violet" cell, but this apparently is due to use of an average value for the former in contrast to a close to best value for the latter. Both show a slight improvement over the 2-3 Ω cm commercial cell. Here, however, a major improvement had been predicted by going to 0.01 Ω cm base material, and this is the area requiring the major future research effort, either to achieve the improvement or to firmly establish the basic limitations against such an accomplishment, as may be posed by bandgap narrowing or formation of recombination centers by unionized donors or acceptors which would be required for resistivity reduction.
6. The curve factor improvement is directly connected with the voltage factor improvement.
7. The additional curve factor, connected with an "A-factor" greater than 1 or with "excess current" has been eliminated in the "violet" cell and practically eliminated in the "non-reflective" cell as an influence on maximum power output under standard operating conditions, as analysis of the current-voltage characteristic reveals. This is important, since it answers the old question, wether "generation-recombination currents" due to deep centers in the depletion region and "surface channel currents" can be adequately reduced. These currents can, however,

still cause a slight distortion of the current voltage characteristic at voltages below the maximum power point, and can influence the maximum power output in operation at low light levels or at low temepratures.

8. Series resistance has been decreased further than expected, at least partially through a trade-off against increased active area coverage by the contact grid system (point 4 above).

Table III further illuminates the above statements through a listing of the physical parameters of both the "violet" and the "non-reflective" cell. The effective optical path length in each region is about 50% greater in the latter cell than in the former. Using Fig. 1 of [4], the photon fraction absorbed in each region can be determined.

Explaining the open circuit voltage in either type cell requires a saturation current of about $4 \cdot 10^{-12}$ A cm^{-2} as a diffusion current, which, in turn, requires a base region diffusion length of about 90 μm, or a minority carrier lifetime τ of 2.5 μs. Using this diffusion length and the graphs of [4], one of which is represented in Fig. 2, the collection efficiency for each region can be obtaind and combined with the fractions absorbed to yield the total collection efficiency. Thus, for the "violet" cell, a total collection efficiency of 0.83 is obtained, against a value of 0.79 derived from the short circuit current. Part of this difference may be explained by a larger reflection loss of the "violet"cell [3] than used in ref. 2). In comparison, the "non-reflective" cell shows a collection efficiency of 0.86 with this value of diffusion length, against an observed value of o.88. The latter would require a base region diffusion length of 120 μm (τ = 4.5 μs), or a less likely increased optical path length.

Although a 2% discrepency could arise from any number of errors, one may want to speculate about a single cause: what

could create a higher saturation current than compatible with diffusion current at a given diffusion length? Generation - recombination current from the depletion region is always a favored candidate. But it was seen, than the curve factor indicates no excess current connected with an $A > 1$ in the exponent of the current-voltage relationship, thus no effect of energetically deep traps in the depletion region. However, ref. 5) indicates that energetically shallow traps can result in excess current with $A = 1$, which thus would have the characteristics of a diffusion current, and which could be isolated only by detailed temperature dependance measurements. This could be another area of future fruitful investigations.

References

1. Wolf, M., "Potential Improvements in Efficiency and Cost of Solar Cells", Proc. 10th IEEE Photovoltaic Spec. Conf., IEEE Cat. No. 73 CH 0801-ED, pp. 5-14, Nov. 1973.

2. Wolf, M., "A New Look at Silicon Solar Cell Performance", Energy Conversion 11, pp. 63-73, 1971.

3. Haynos, J., et al, "The Comsat Non-reflective Silicon Solar Cell: A Second Generation Improved Cell", in Photovoltaic Power Generation", pp. 487-500, Proc. of an Int'l Conf., Hamburg, Sept. 25-27, 1974, DGLR, Köln, Germany.

4. Wolf, M., "Research for the Improvement of Silicon Solar Cell Efficiency", NASA grant NGL-39-010-001, Status Report SR18, July 1971.

5. Sah, C.J., Noyce, R.N., and Shockley, W., "Carrier Generation and Recombination in p-n Junctions and p-n Junction Characteristics", Proc. IRE 45, 1228, (1957).

TABLE I. - PREDICTED PERFORMANCE COMPARED WITH THAT OF VIOLET CELL

Attribute	Symbol	Units for Output Quantities	Commercial Cell (nominally 2-3 Ωcm n/p) Eff'cy Contrib.	Commercial Cell Output Quantity	Goal (nominally 0.01 Ωcm) Eff'cy Contrib.	Goal Output Quantity	Goal Potential Improvement %
Basic Losses	-	mW m^{-2}	0.45	63.0	0.45		
Collection Efficiency	η_{coll}	mA cm^{-2}	0.71	39.6	0.88	49.0	22
Reflection Loss (incl. absorption in coating)	R	mA cm^{-2}	0.905	35.9	0.97	47.5	7.6
Grid Line Coverage	-	mA cm^{-2}	0.96	34.4	0.96	45.5	-
(Applicable Cell Area)	A	mA	(3.8 cm^2)	131	(1 cm^2)	45.5	
(Open Circuit Voltage)	V_{oc}		(0.580 V)		(0.788 V)		
Voltage Factor	(V.F.)	mW	0.522	76.0	0.71	35.8	36.5
Curve Factor	(C.F.)	mW	0.82	62.2	0.86	30.8	5
Add'l Curve Factor	-	mW	0.91	56.7	1.0	30.8	10
Series Resistance	R_s	mW	(0.17Ω) 0.96	53.6	0.97	29.9	1
Conversion Efficiency	η	mW cm^{-2}	0.104		0.22		

TABLE II. - REVISION OF ANALYSIS OF NONREFLECTIVE CELL

Attribute	Symbol	Units for Output Quantities	Comsat "Violet" Cell (nominally 2-3 Ω cm) Eff'cy Contrib.	Comsat "Violet" Cell Output Quantity	Comsat "Violet" Cell Achieved Improvement %	Comsat "NR" - Cell (nominally 2-3 Ωcm n/p) Eff'cy Contrib.	Comsat "NR" - Cell Output Quantity	Comsat "NR" - Cell Achieved Improvement
Basic Losses	-	mW m^{-2}	0.45			0.45		
Collection Efficiency	η_{coll}	mA cm^{-2}	0.79	44.0	11	0.88	49.2	22
Reflection Loss (incl. absorption in coating)	R	mA cm^{-2}	0.951	41.7	6	0.97	47.7	7.6
Grid Line Coverage	-	mA cm^{-2}	0.95	39.6	-1	0.95	45.4	-1
(Applicable Cell Area)	A	mA	(4 cm^2)	158.4	-	(4 cm^2)	181.5	
(Open Circuit Voltage)	V_{oc}		(0.595 V)			(0.591 V)		
Voltage Factor	(V.F.)	mW	0.535	94.2	3	0.531	107.3	2
Curve Factor	(C.F.)	mW	0.825	77.8	0.5	0.822	88.2	0.2
Add'l Curve Factor	-	mW	1.0	77.8	10	0.99	87.1	10
Series Resistance	R_s	mW	(0.05) 0.985	76.5	2.5	(0.05) 0.984	85.7	2.5
Conversion Efficiency	η	mW cm^{-2}	0.14		36	0.153		47

TABLE III. - PHYSICAL PARAMETERS OF VIOLET AND NONREFLECTIVE CELLS

Base Majority Carrier Concentration:	$7 \cdot 10^{15}$
Diffusion Depth	0.1 µm
Depletion Region Width	0.4 µm
Wafer Thickness	300 µm
Minority Carrier Lifetime (Base)	2.5 µs (4.5 µs)

	Diffused Region		Depletion Region		Base Region	
	Violet	NR	Violet	NR	Violet	NR
Path Length (µm)	0.1	0.15	0.1-0.5	0.15-0.75	0.56-300	0.75-450
Portion Absorbed Cumulative	0.12	0.14	0.24	0.30	0.94	0.96
Portion Absorbed in Region	0.12	0.14	0.12	0.16	0.70	0.66
Diffusion Length (µm)	~0.1	~0.1	-	-	90	90 (120)
Collection Efficiency	0.98	0.98	1.0	1.0	0.85	0.85 (0.88)
Portion Collected	0.116	0.137	0.12	0.16	0.595	0.561
Total Collect'n Efficiency			0.83	0.86 (0.88)		

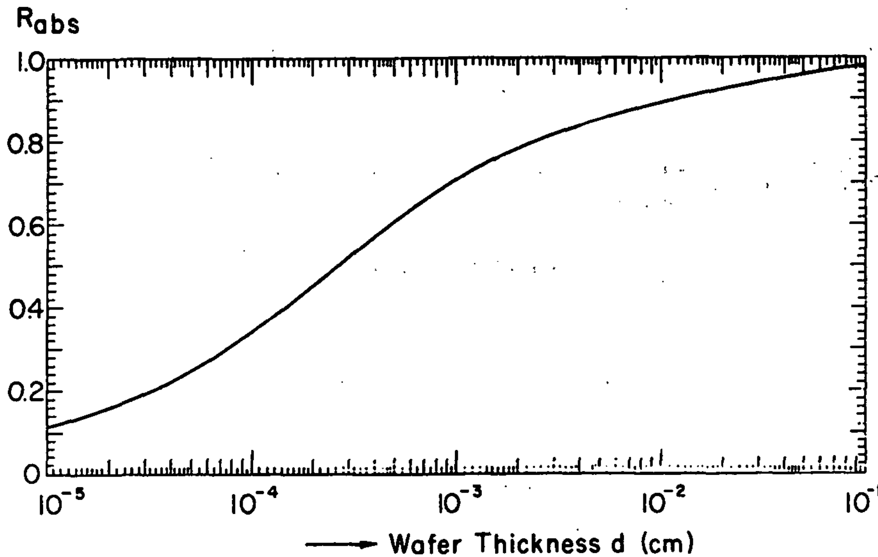

Figure 1. - Ratio R_{abs} of the number of photons absorbed in a single pass through a silicon layer of thickness d to the number entering the layer, as contained in airmass zero sunlight up to 1.125 µm wavelength. T = 300° K.

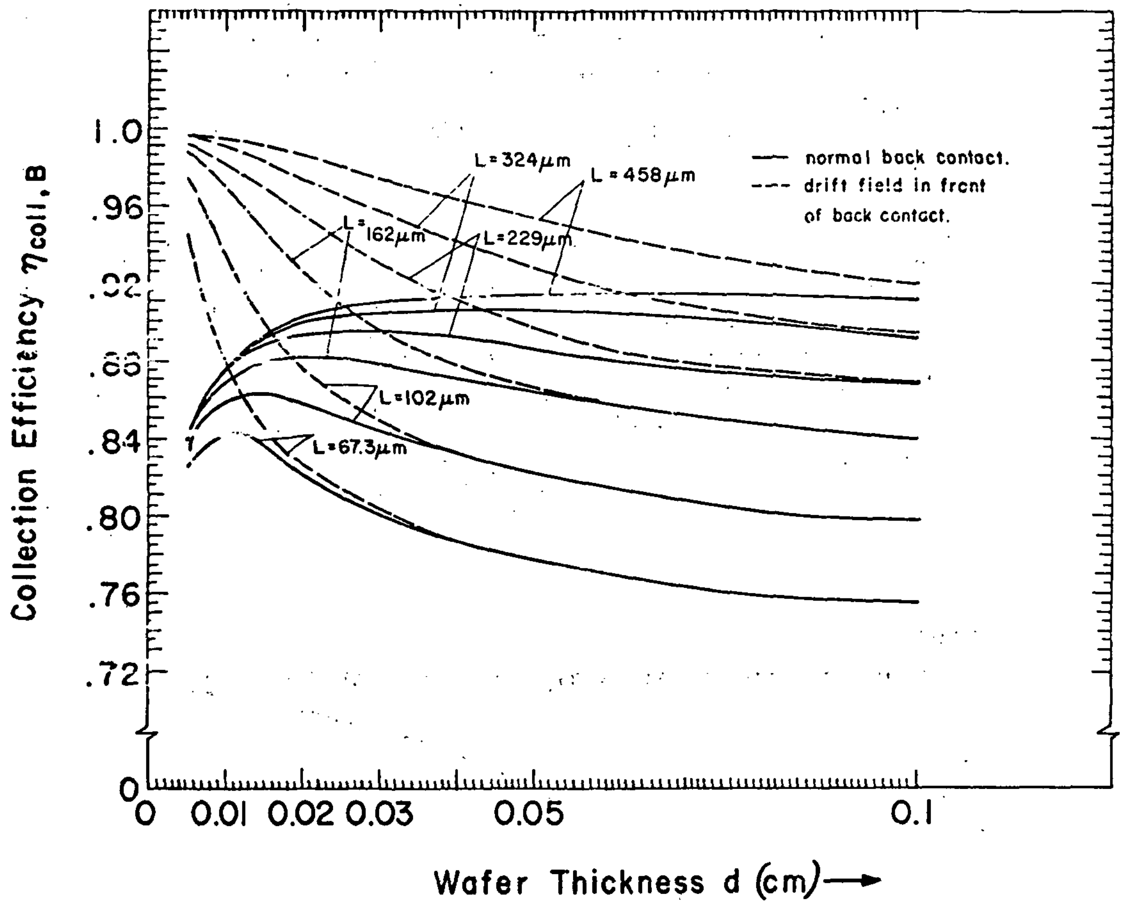

Figure 2. - Collection efficiency $\eta_{coll,B}$ from the base region as function of wafer thickness d, for 3 values of diffusion length in the base region, with and without a drift field in front of the back contact. Airmass zero sunlight, T = 300° K. $x_{T,R}$ = 0.8 µm.

21. STUDIES OF THE BSF CELL

Joseph Mandelkorn, John H. Lamneck, and Larry R. Scudder
NASA Lewis Research Center
Cleveland, Ohio

The Back Surface Field Cell, BSF Cell, is made by fabricating a p^+ region at the back of the conventional cell structure, as shown in Figure 1. Although BSF cells are now in production[1] the mechanism giving use to the increased V_{oc}, open-circuit voltage, of such cells is the subject of continuing investigations. The investigation at Lewis is presently concerned with the characteristics and behavior of p^+, p cells.

The p^+,p cells are fabricated from parent, n^+,p,p^+, BSF cells as shown in Figure 1. Following the removal of the top n^+ region and contacting of the p region exposed, the p^+,p structure formed is illuminated on the p^+ side, and photovoltages are measured.

Much higher photovoltages were obtained from 100Ω-cm cells as shown in Table I. The data indicate that the V_{oc} of p^+,p cells increases with increasing bulk thickness.

Table II shows that, for equally thick p^+,p cells, values of V_{oc} correlate directly with the V_{oc} of the "parent" BSF cell. This result suggests that the increased V_{oc} of n^+,p,p^+, BSF cells, compared to n^+,p cells, is caused by the p^+,p junction generating a photovoltage. The back p^+,p photovoltage then adds to the photovoltage at the front, due to the n^+p junction. It should be noted that high light intensity or high injection level is not required to achieve this effect since BSF cells have higher voltages than conventional cells even at low illumination levels.[2] Another noteworthy advantage of BSF cells shown in Table II is that the V_{oc} of 100Ω-cm cells can equal that of the maximum V_{oc}

Preceding Page Blank

attained for 10Ω-cm BSF cells; i.e., the V_{oc} of BSF cells is independent of bulk resistivity.

Solid state voltage generators have characteristic V_{oc} temperature coefficients. As shown in Table III, the V_{oc} temperature coefficient of n^+,p cells is negative (V_{oc} decreases as temperature increases) whereas that of p^+,p cells is positive. The temperature coefficients of both types of cell increase with increasing resistivity. It appears from the data that, within the n^+,p,p^+ BSF cell, the coefficients of the back, p^+p, junction and front, n^+p, junction combine to give high resistivity BSF cells an advantage, unusually low V_{oc} temperature coefficient. The data on V_{oc} temperature coefficient further substantiate the concept that the p^+p junction functions as a voltage generator within the BSF cell.

In 1953, Brattain published the theory for p^+p and n^+n junction photovoltages.[3] Basically, a photovoltage is possible because of the difference in Fermi level between the p^+ and p regions. Table IV points out the changes in Fermi level difference, ΔF, which occur for cells as bulk resistivity is increased. Theoretically, a decrease in ΔF should result in a decrease in V_{oc}. The n^+,p cell and p^+,p cell behavior shown are in accord with the stated theory. Considering the n^+p cell, as bulk resistivity is increased, ΔF between n^+ and p regions is decreased and, correspondingly, V_{oc} will decrease. As illustrated, the 100Ω-cm n^+,p cell has a lower V_{oc}, 0.48 volts, compared to the 0.55 volt V_{oc} of the 10Ω-cm n^+p cell. However, for p^+,p cells, an increase in bulk resistivity produces an increase in ΔF and, therefore, an increase in V_{oc}. The increased V_{oc} of the 100Ω-cm p^+,p cell apparently adds to the decreased V_{oc} of the 100Ω-cm n^+,p cell to yield a V_{oc} value for 100Ω-cm BSF cells equal to that of lower resistivity cells; equal V_{oc} values of 0.6 volts were obtained for 10 and 100Ω-cm BSF cells as shown. Once again, we find that the V_{oc} behavior of BSF cells

appears tc result from a combination of p^+p cell and n^+p cell V_{oc} behavior.

An additional unique V_{oc} characteristic of BSF cells appears in Table V. BSF cells were made at Lewis from wafers taken from the same region of an ingot using a selected fabrication process to yield maximum V_{oc} values. V_{oc} values of 0.6 volts were obtained for cells independent of bulk thickness up to the maximum thickness investigated, 0.084 cm. It is concluded that the mechanism for generation of the p^+p voltage within the BSF cell apparently makes the generated voltage completely independent of bulk thickness for thicknesses up to at least 0.084 cm. A long history of measurements at Lewis shows minority carrier diffusion lengths preserved in the bulk of thick cells made from the best available silicon are in the range of 250μm (0.010 inch). This eliminates the possibility of p^+,p junction activation arising from generated minority carriers; such activation would result in diminished V_{oc} values as cell thickness increased. It is therefore proposed that the mechanism for the V_{oc} behavior of BSF cells is based upon majority carrier activation of the p^+,p junction. The proposed mechanism is depicted in Figure 2. The difference in hole concentration between the p^+ and p regions of the BSF cell result in diffusion of holes from the p^+ region into the p region. A depletion region is established as well as an equilibrium hole density at the back of the cell bulk. Under illumination, electron-hole pairs are generated within the bulk. Most of the generated excess electrons leave the bulk by being collected, crossing over the n^+p junction. Excess holes cannot cross the n^+p junction because the n^+ region constitutes a barrier for holes. The presence of the unbalanced excess holes disturbs the equilibrium at the p^+,p junction and a balancing flow of holes into the p^+ region occurs. This flow constitutes hole collection at the p^+,p junction and produces the

photovoltage shown. This mechanism of hole collection permits an undiminished photovoltage to be generated at the p^+p junction even when the junction is far-removed from illuminated surface of the cell. Figure 2 simply depicts the mechanism for generation of the p^+,p photovoltage. Since the value of a photovoltage depends upon the forward bias characteristic of the junction generator, the V_{OC} increase affected by the p^+p junction within a BSF cell depends upon the properties of the cell bulk as well as the quality of the back and front junctions. The two junctions interacting through the common bulk region represent a complex feedback circuit.[2]

Analysis of the unique behavior of BSF cells has opened the door to creation of advanced cells made from very high resisitivity material. The previous limitations of high resistivity cells, for example, low values of V_{OC}, can now be eliminated, and full advantage can be taken of the beneficial aspects of using high resistivity bulk material. This is pointed out in Table VI.

It is emphasized that future advances made in silicon solar cells will involve design and fabrication of unique structures advantageously combining developments in other aspects of solar cells with p^+ back region effects. The possibility now exists that the highest efficiency cells will be high resistivity modified structure BSF cells rather than very low resistivity cells.

REFERENCES

1. These Proceedings: "Volume Production of Improved Efficiency Solar Cells," John Scott-Monck.

2. Mandelkorn, J. and Lamneck, J. H.: Proceedings of the IEEE Ninth Photovoltaic Conference, May 1972, pg. 66.

3. Brattain, J. H. and Garett, C. G. B.: Annual New York Academy of Science, 58, 951, 1954.

TABLE I. - V_{oc} OF p^+,p CELLS

Cell	Thickness		V_{oc},mV
	cm	mils	
10 Ω-cm	0.030	12	5-10
100 Ω-cm			
1	.033	13	64
2	.058	23	74
3	.076	30	91

TABLE II. - V_{oc} OF $n^+,p,p^+ \rightarrow p^+,p$

[100 Ω-cm; 0.03 cm (12 mils).]

Cell	As n^+,p,p^+	As p^+,p
	V_{oc}, volts	
100 Ω-cm		
443-3	0.526	0.038
443-2	.540	.038
441-2	.587	.049
457-2	.602	.063
457-3	.605	.064
10 Ω-cm	.6 (max.)	-----

TABLE III. - V_{oc} TEMPERATURE COEFFICIENT

Junction	Resistivity, Ω-cm	
	10	100
	Temperature coefficient, mV/°C	
n^+,p	-2.3	-2.6
p^+,p	+0.14±0.02	+0.65±0.05
n^+,p,p^+	-2.15±0.02	-1.9±0.01

TABLE IV. - RESISTIVITY EFFECTS ON FERMI LEVEL DIFFERENCE, ΔF, and V_{oc}

[$\Delta F_{decreasing} \rightarrow V_{oc,decreasing}$.]

(a) Changes as p resistivity increases

	n^+,p	p^+,p	n^+,p,p^+
ΔF	Decrease	Increase	No change
V_{oc}	Decrease	Increase	No change

(b) Values of V_{oc}

Cell resistivity, Ω-cm	n^+,p	p^+,p	n^+,p,p^+
	V_{oc}, volts		
10	0.55	0.050	0.6
100	.48	.120	.6

TABLE V. - V_{oc} AND THICKNESS OF BSF CELLS

1. Wafers used taken from same region of ingot
2. Controlled fabrication process
3. Thickness τ varied from 0.010 to 0.084 cm (0.004 to 0.033 in.)
4. Maximum V_{oc} of 0.6 volt for all thicknesses
5. Minority carrier diffusion length L measured in thick (0.127 cm; 0.050 in.) cells made from best silicon is approximately 250 μm (0.010 in.)

TABLE VI. - FEATURES OF HIGH RESISTIVITY BSF CELLS

Readily Achievable

1. Highest preserved minority carrier diffusion lengths
2. Increased radiation damage resistance - epitaxial BSF or thin BSF cell
3. Excellent quality extremely shallow junctions - no need for passivation

Achievable

1. High fill factors, 78 percent
2. High V_{oc}, 0.6 volt
3. Low V_{oc} temperature coefficient

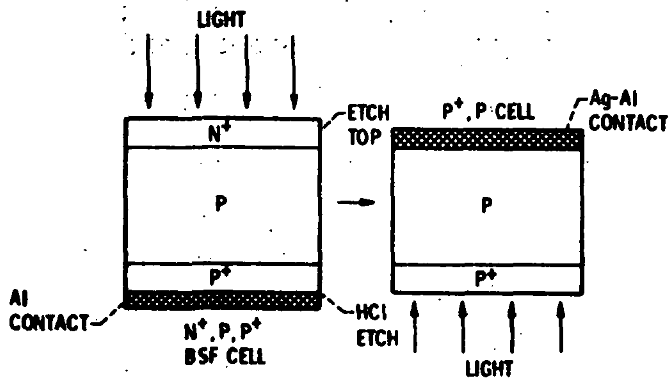

Figure 1. - Fabrication of p^+, p cells.

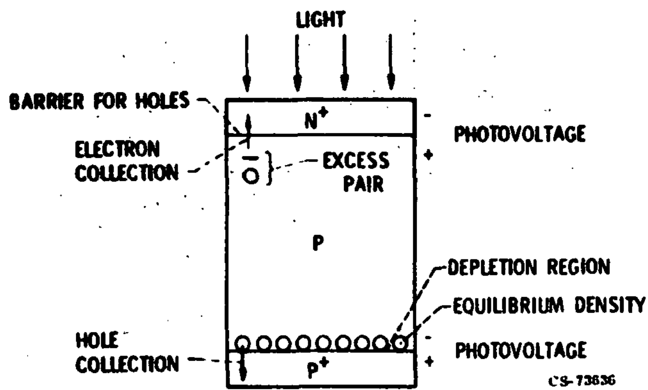

Figure 2. - Mechanism for generation of voltages in n^+, p, p^+ cells.

LIMITS TO PERFORMANCE

Considerations of high doping and recombination phenomena as influences controlling cell performance

Preceding Page Blank

22. LOW RESISTIVITY SILICON SOLAR CELLS - PROMISE AND PROBLEMS

S. Soclof and P. Iles
Centralab Semiconductor
El Monte, California

Most recent increases in solar cell output have been achieved without much increase in Voc.

Even with the highest Isc and CFF values achieved to date, to reach conversion efficiencies of 18% or 20% would require Voc exceeding 700 mV or 750 mV respectively. For several years lower resistivity silicon has been studied in attempts to obtain increased Voc. Simple diffusion diode theory predicts a steady increase in Voc as doping concentration is increased, thereby decreasing the saturation current (Io). In practice, however, solar cells or diodes made using low resistivity silicon did not show large Voc increases; instead, Voc reached a peak around 620 mV for concentrations around 10^{18} cm^{-3}, and fell off rapidly for higher concentrations. If modifications are made to the simpler diode theory (using realistic values for diffusion constant and diffusion lengths, and including effects of bandgap narrowing), the Voc versus concentration resembles the experimental curve more closely. This Voc limitation is one problem in the chance of obtaining high output from low resistivity silicon.

Other problems result from the rapid decrease in measured minority carrier diffusion length (L) at higher doping levels. The decrease in L leads to reduced photocurrents. Multiplying the observed Voc and predicted Isc values gives an estimate of peak conversion efficiency around 15% for doping concentrations around $10^{17} cm^{-3}$ (corresponding to 0.1 ohm-cm).

Experimental results on cells made using a wide range of resistivities showed a more rapid fall-off in conversion efficiency because of the rapid decrease in CFF at high doping levels.

Thus it may be difficult to retain high Isc and CFF values already achieved if low resistivities are used in attempts to obtain higher Voc. If the reduced L-values are the result of deep traps (impurities like Fe or Au), there is experimental possibility of decreasing the effect of these traps; on the other hand, if the cause for lower L-values at high doping levels is a direct consequence of shallow traps caused by the intentional dopants, the prospect for high Isc in low resistivity silicon is bleak.

Preceding Page Blank

The present picture we have is that at high doping levels, Io is increased by several independent mechanisms including:

a) reverse injection from the bulk into the thin, highly doped diffused layer, aided by band gap narrowing in the diffused layer

b) the effect of low lifetimes in the depletion region. At high doping levels, the depletion region is very narrow (less than 1 μm) and about half the region is in the low lifetime diffused layer. Using plausible values for the low and high lifetimes in portions of the depletion region, it was possible to simulate observed I-V characteristics. The increased Io-values can decrease both Voc and CFF as observed.

Looking to the future, the requirements to make high output cells from low resistivity silicon are very demanding, for the following reasons.

i) high L-values are needed at high doping levels, requiring increased control of crystal perfection. Fortunately many of the steps presently used to obtain high Isc (surface texturing, greater active area and improved coatings) are possible for low resistivity silicon

ii) reduced Io-values are needed

iii) good quality shallow PN junctions may be difficult to achieve, because reduced surface concentrations will not overdope the highly doped bulk sufficiently, the high total impurity concentration may increase the incidence of precipitates (with shunting of the junction), and the higher vacancy density may make diffusion control more difficult.

iv) present indications are that the radiation resistance of highly doped silicon is lower.

v) back surface fields will be more difficult to establish

vi) to avoid these problems, hybrid structures (epitaxial etc.) may be needed, with added complexity and cost.

Thus it is seen that before improved cells can be made from low resistivity silicon, much increased understanding is required of highly doped silicon and of PN junctions made therein.

TABLE I. - PV PARAMETERS

Cell type	I_{sc}, max	CFF	V_{oc}, mV	P_m, mW	η, percent
Achieved					
Conventional 10-Ω-cm	144	0.73	550	58	10
Enhanced bulk	160	.76	600	73	13
Conventional 2-Ω-cm	142	.75	590	63	11+
Violet	165	.78	590	76	13.5
Advanced violet	183	.79	590	85	15
Estimated					
18-Percent cell	183	0.79	700	100	18
20-Percent cell	183	.79	775	112	20

TABLE II. - ESTIMATE OF ACHIEVED CELL PERFORMANCE

Cell parameter	Fraction of peak value		
V_{oc}	0.99	0.89	0.77
I_{sc}	.88	.55	.34
CFF	.98	.68	.35
P_{max}	.86	.35	.09

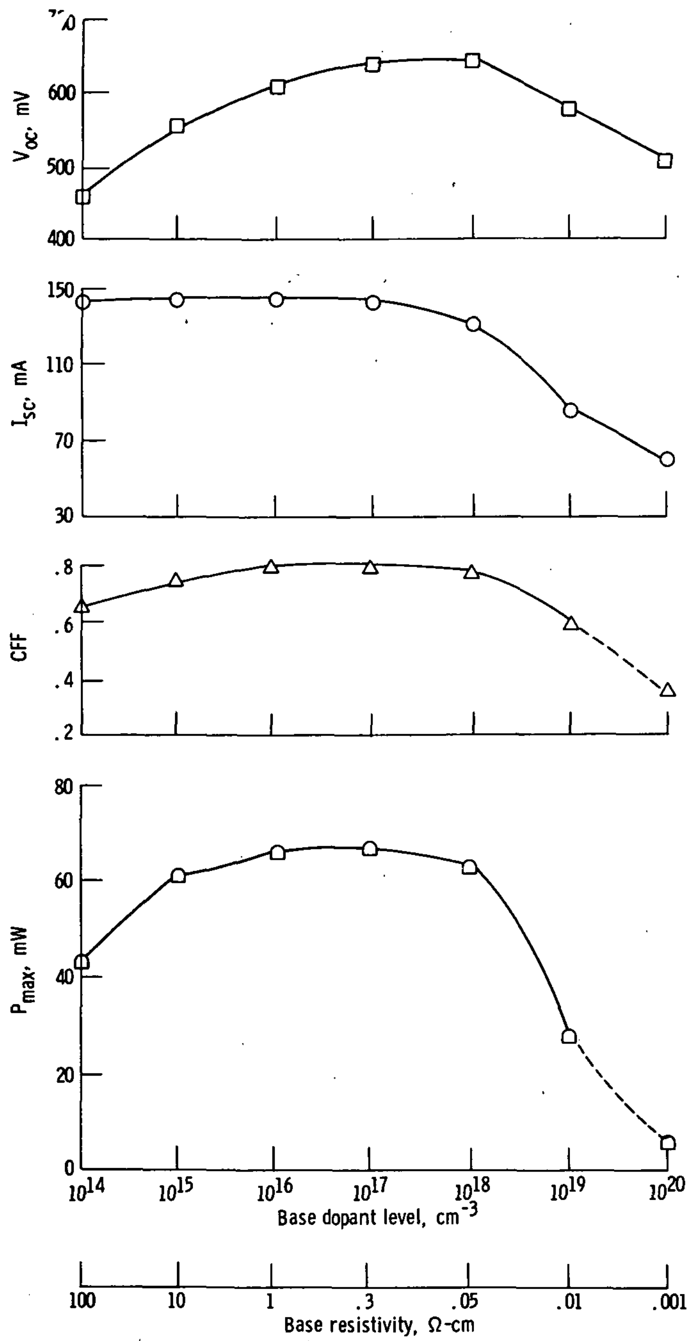

Figure 1. - Cell performance as function of base resistivity.

23. EFFECTS OF HIGH DOPING LEVELS ON SILICON SOLAR CELL PERFORMANCE

Michael P. Godlewski and Henry W. Brandhorst, Jr.
NASA Lewis Research Center
Cleveland, Ohio

INTRODUCTION

There has been considerable interest in raising the efficiency of silicon solar cells to near its limit. Analyses (1, 2) have been made to define what gains can be expected and also what areas of research are most likely to yield the necessary improvements (or to identify the principal obstacles that must be overcome).

It has been suggested that the maximum practical silicon solar cell air mass zero efficiency of 18 percent would occur in 0.1 ohm-cm material. Realization of this efficiency depends heavily on obtaining an open-circuit voltage close to 0.7 volt calculated from simple diffusion theory. The best present-day performance of low resistivity cells, however, falls substantially short of these predictions. Measured efficiency and voltage are typically about 10 percent and 0.61 volt, respectively. It is believed that improvement of the voltage is the key factor leading to high efficiency. However, the difference between the achieved and predicted voltage performance is one area for which a satisfactory explanation is not available.

It has been widely hypothesized that the low observed performance of the 0.1 ohm-cm cell is a result of undesirable carrier recombination processes occurring in the base and depletion regions. However, measurements show that the short-circuit current and the base diffusion length are not primarily responsible for the low cell performance. A study of low resistivity cells by Soclof and Iles (3) not only supports this, but also strongly indicates that other mechanisms which influence junction injection efficiency must be considered. One such mechanism is the narrowing of the silicon bandgap by high dopant concentrations.

The theoretical work of Kane (4) and Morgan (5) demonstrates that donor or acceptor concentrations in excess of 10^{18} atoms/cm^3 alter the conduction band and broaden the impurity band densities of states. This work has been applied to silicon material by several investigators (6-10). Their results suggest that high impurity concentrations can indeed change the bandgap. Additional theoretical and experimental studies are cited in (10).

An important consequence of bandgap narrowing for p-n junction device operation is the increase of the intrinsic carrier concentration, N_i. Van Overstraeten et al. (11) have incorporated in detail the impurity level-dependent N_i in the basic semiconductor device transport equations. Similar equations modified to include bandgap narrowing

have been used to analyze and reconcile the long-standing discrepancy between the predicted and measured current gain in bipolar transistors (6, 12-16).

The alteration of the bandgap and the intrinsic concentration by high impurity concentration effects, which will be referred to as the Heavy Doping Effect (HDE) in this paper, may also have significant effects on silicon solar cells.

The purpose of this paper is to make a preliminary analytical assessment of the significance of the HDE on the open-circuit voltage of silicon solar cells. Voltage calculations based on diffusion theory (such as used in (17)) are modified to include the first order features of the HDE. Comparisons of the open-circuit voltage measured for cells of various base resistivities are made with those calculated using the diffusion model with and without the HDE.

THEORETICAL BACKGROUND

Open-Circuit Voltage

The open-circuit voltage (V_{oc}) is calculated using

$$V_{oc} = \frac{kT}{q} \ln\left(\frac{I_{sc}}{I_o} + 1\right) \tag{1}$$

where the diode saturation current (I_o) with the HDE, given by

$$I_o = n_{id}^2 \frac{kT\ \mu_d(N_{Id})}{N_{Id}\ L_d} G_d\left(\frac{W}{L}, s\right) + n_{ib}^2 \frac{kT\ \mu_b(N_{Ib})}{N_{Ib}\ L_b} G_b\left(\frac{W}{L}, s\right) \tag{2}$$

is the sum of the diffused and base region components ($I_o = I_{od} + I_{ob}$). The subscripts d and b refer to the diffused and base regions, respectively. All calculations are made for an n^+-p device and assume ohmic contacts, uniform n^+ region impurity level, a 0.25 μm junction depth, a 300 μm cell thickness, and an operating temperature of 300 K. For the purpose of this paper, the effect of bandgap narrowing on the short-circuit current (I_{sc}) is neglected. Values of I_{sc} used in the calculations are typical of the various cell resistivities. The mobilities (μ_d, μ_b) and impurity concentrations (N_{Id}, N_{Ib}) corresponding to material resistivities were selected from the literature (18). A diffused region diffusion length (L_d) of about 1.0 μm is assumed. However, the base region L_b values are based on typical experimental data. The geometry factors G_d and G_b are given in detail in (17). However, these factors reduce to the coth W/L form when an infinite surface recombination velocity is assumed.

For those calculations which include the HDE, the values of n_{id} corresponding to a net impurity concentration are selected from the calculated data of (11). These data are shown in figure 1. It is seen that for net impurity levels below $10^{18}/cm^3$, n_{id} has the classical value (n_{ic}) of $1.1\times10^{10}/cm^3$. More importantly, however, n_{id} increases rapidly for levels above 10^{18}. Typical solar cells have diffused region impurity concentrations in excess of $10^{19}/cm^3$; thus the variation of n_i must be taken into account. The implication of figure 1, suggested in (4, 5), is that the conduction and valence band edges are no longer well-defined at high impurity levels. Hence the bandgap is narrowed and n_i increased, compared to a lightly doped, slightly extrinsic crystal.

Calculations which do not include the HDE are referred to as the simple diffusion theory. For this case equations (1) and (2) are also used; however, the intrinsic carrier concentration n_i is independent of impurity level and equal to the classical value (n_{ic}) of $1.1\times10^{10}/cm^3$.

Effective Impurity Profile

An effective impurity concentration is defined by

$$N_{eff}(x) = \frac{N_{Id}(x)}{\left(\frac{n_{id}(N_{Id})}{n_{ic}}\right)^2} \tag{3}$$

$N_{eff}(x)$ is the actual donor concentration at some location x in the material and the ratio $n_{id}(N_{ID})/n_{ic}$ is a heavy doping factor based on the data of figure 1. When equation (3) is used, the diffused region saturation current component I_{od} can be written in the form

$$I_{od} = \frac{n_{ic}^2(kT)(\mu_d)}{N_{eff}} \frac{G_d}{L_d} \tag{4}$$

Note that for $N_{Id} < 10^{18}$

$$N_{eff} = N_{Id}$$

and for $N_{Id} > 10^{18}$

$$N_{eff} < N_{Id}$$

Because I_{od} becomes large when N_{eff} is small, the diffused region properties can dominate the voltages calculated from equation (1).

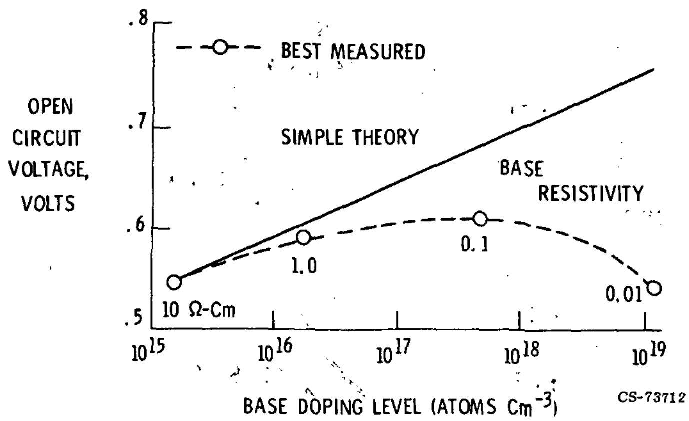

Figure 3. - Experimental and predicted open-circuit voltage dependence on base doping levels.

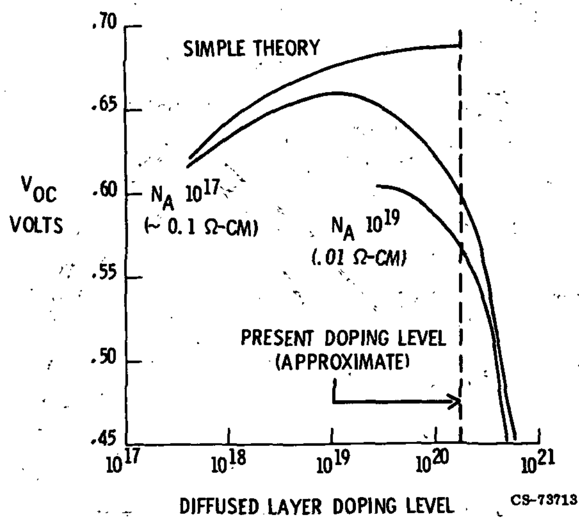

Figure 4. - Influence of diffused layer heavy doping effects on open-circuit voltage.

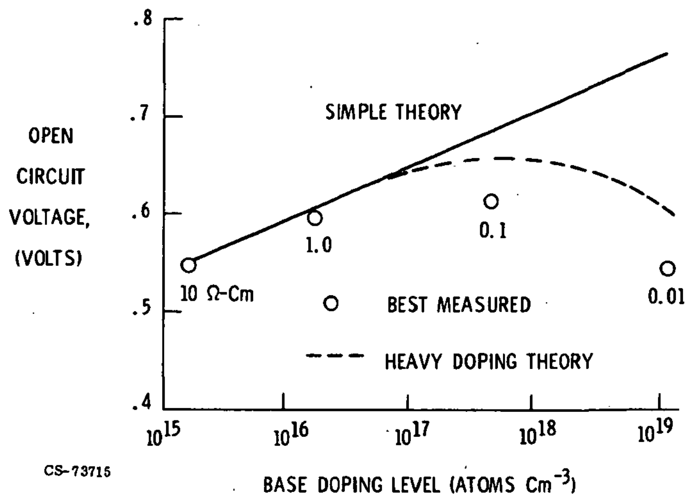

Figure 5. - Experimental and predicted open-circuit voltage dependence on base doping level.

24. STUDIES OF SOME FUNDAMENTAL LIMITATIONS OF THE PERFORMANCE OF pn JUNCTION SILICON SOLAR CELLS*

F. A. Lindholm and S. S. Li
University of Florida
Gainesville, Florida 32611
and
C. T. Sah
University of Illinois
Urbana, Illinois 61801

1. INTRODUCTION

To predict the performance of a device requires accounting for all of the phenomena present that dominate in determining its performance. Past descriptions of pn junction solar cells have failed to take detailed quantitative account of various competing phenomena that accompany high doping in either the diffused layer or the substrate.

The intent of this paper is to describe these phenomena, mainly from a theoretical standpoint, and to indicate which of them may be the dominant contributors to solar cells characteristics. The distortion of band structure produced by high doping receives special attention, particularly its consequences in the junction space-charge region. There, many different kinds of electronic transitions can occur between localized and delocalized (or extended) energy levels. The performance of a pn junction solar cell can depend sensitively on these transitions, which in turn depend critically on the doping profile and the processing used in fabrication.

2. EXAMPLE ILLUSTRATING COMPETING PHENOMENA

Recombination in a junction space-charge region can be characterized by the Sah, Noyce, and Shockley model [1]. In this model, electronic transitions between the conduction and

*Research sponsored by the NASA Lewis Research Center under grant No. NSG-3018.

Preceding Page Blank

valence bands occur via localized states of a single energy level lying deep within the forbidden gap. This, however, is only one of the possible mechanisms for electron-hole recombination. Among the many possible rival mechanisms, one example involves a two-step electronic transition, in which an electron in the conduction band is first captured by a localized deep level and subsequently tunnels to the valence band or to the valence-band tail states; Sah has suggested this as the excess-current mechanism in silicon tunnel diodes [2]. Depending on the temperature and the doping of the junction, this two-step process can wholly dominate the Sah-Noyce-Shockley process, and can impose a fundamental limitation on the performance of the solar cell.

3. SOME PHENOMENA ACCOMPANYING HIGH DOPING

At high doping concentrations, various deviations from the conventional band structure can occur, such as:

a. The band edges need no longer be sharp; rather, states can extend beyond the band extrema describing lowly-doped silicon, forming thereby so-called band tails [3-5];

b. The impurity states can broaden into an impurity band [6,7] with increasing impurity concentration; at very high levels of doping these states can become delocalized;

c. A spatial variation of the energy gap can result from macroscopic lattice strain introduced by a high-concentration diffused impurity profile, the strain arising from the misfit of the impurities in the silicon lattice [8].

For both conduction and recombination-trapping processes, it is important whether the energy states are localized or delocalized. Thus:

d. Borrowing from the concepts used in models describing amorphous semiconductors, we identify a critical energy, the Cohen mobility edge [9], which separates localized from delocalized states; the mobility edge plays a role

in describing charge transport in disordered solids similar to that which the band edge plays in periodic solids.

Then:

e. For delocalized states, conduction can occur by drift and diffusion; if the variation in doping produces spatial dependence of the band gap or of the electron affinity, quasi-electric fields [10] can influence the transport of electrons and holes.

f. For localized states, conduction can occur from <u>hopping</u> between neighboring states [11] due to thermally activated transfer of the trapped charges in the Mott model [12] or by tunneling in the Anderson model [13].

g. Transitions among localized and delocalized states that constitute recombination-generation-trapping processes occur via several energy-momentum conservation mechanisms, including phonon-assisted, photon-assisted, and Auger-impact processes [14].

4. EQUIVALENT CIRCUIT MODEL

This list, which is not exhaustive, of phenomena accompanying high doping indicates the complexity of the physics undergirding the operation of silicon solar cells. Sah [14] has provided a network representation that can be extended to include explicitly all of the additional effects due to high doping.

In this paper we indicate the necessary extensions, including those needed when the collision scattering rate and the generation-recombination-trapping-tunneling rate become comparable [15] and when the band gap or electron affinity become position-dependent. We demonstrate the use of the equivalent circuit model both as an aid in physical insight and as a tool in the numerical computation of the performance of solar cells.

5. HIGH DOPING IN EXISTING DEVICE THEORY

Recently, strides have been made toward including the effects of high doping in the operation of the bipolar transistor [16].

This inclusion has enabled a closer agreement between experiment and prediction than was obtained previously, particularly for the forward-active current gain and the gain-bandwidth product and their dependence on collector current.

The model for high doping now used in bipolar transistor theory is based, essentially, on the Kleppinger-Lindholm extrapolation [17] of the models of Morgan [7] and Bonch-Bruyevich [4]. It excludes much of the physics indicated in Section 3 above.

We give a critical appraisal of this theory of high-doping effects now being used in describing the behavior of silicon bipolar transistors, assessing the appropriateness of its application to silicon solar cells. Temperature dependence receives particular attention in this appraisal.

6. PERSPECTIVE

Silicon solar cells contain regions of high doping; hence the physics underlying their operation is complex. Many different phenomena compete to determine the behavior.

Thus, a major problem in understanding the operation and the efficiency of the solar cell lies in determining which of these phenomena are dominant and which may be neglected. A second problem, relating to design, lies in controlling both the dominance and the magnitude of the phenomena via controlling the device structure and the steps used in fabrication.

This paper deals with these issues from mainly a theoretical standpoint. A companion paper [18] reports experimental results.

REFERENCES

1. C.T. Sah, R.N. Noyce, and W. Shockley, Proc. IRE, 45, 1228 (1957).

2. C.T. Sah, Phys. Rev., 123, 1594 (1961).

3. I.M Lifshitz, J. Exp. Theor. Phys., 2, 117, 137, 156 (1942).

4. V.L. Bonch-Bruyevich and A.G. Mironov, Sov. Phys. Solid State, 3, 2194 (1962).

5. E.O. Kane, Phys. Rev., 131, 1532 (1963).

6. G.W. Castellan and F. Seitz, Phys. Rev., 79, 216 (1950);
C.S. Hung, Phys. Rev., 79, 727 (1950);
C. Ererginsoy, Phys. Rev., 80, 1104 (1950).

7. T.N. Morgan, Phys. Rev., 139, A343 (1965).

8. V. Fistul, Heavily Doped Semiconductors, Plenum Press, N.Y. (1969).

9. M.H. Cohen, H. Fritzsche, and S.R. Ovshinsky, Phys. Rev. Lett., 22, 1065 (1969).

10. H. Kroemer, RCA Review, 333 (1957).

11. E.M.Conwell, Phys. Rev., 103, 51 (1956).

12. N.F. Mott, Can. J. of Physics, 34, 1356 (1956).

13. P.W. Anderson, Phys. Rev., 109, 1492 (1958).

14. C.T. Sah, Physica Status Solidi a, 7, 541 (1971).

15. C.T. Sah and F.A. Lindholm, Solid-State Electronics, 16, 1447 (1973).

16. H.J.J. DeMan, IEEE Trans. on Electron Devices, ED-18, 833 (1971);
R.J. Van Overstraeten, H.J. De Man and R.P. Mertens, IEEE Trans. on Electron Devices, ED-20, 290 (1973);
H.J. De Man, R.P. Mertens and R.J. Van Overstraeten, Electronic Letters, 9 (1973);
R.P. Mertens, H.J. De Man and R.J. Van Overstraeten, IEEE Trans. on Electron Devices, ED-20, 772 (1973);
M.S. Mock, Solid-State Electronics, 16, 1251 (1973);
R.P. Mertens, F.A. Lindholm, R.J. Van Overstraeten, H.J. De Man and D.P. Kennedy, "Influence of high doping on the design of bipolar transistors," Tech. Digest of 1974 Int. Electron Devices Meeting, Washington, D.C. (to appear).

17. D.D. Kleppinger and F.A. Lindholm, Solid-State Electronics, 14, 199-206 (1971);
D.D. Kleppinger and F.A. Lindholm, Solid-State Electronics, 14, 407-416 (1971).

18. S.S. Li, F.A. Lindholm, S.C. Pao, P.J. Chen and C.T. Sah, "Studies of I-V characteristics and defect centers in low resistivity silicon PN junction solar cells," submitted to the 11th IEEE Photovoltaic Specialists Conference (following paper).

SUMMARY OF ROUND TABLE DISCUSSION

An assessment of the near and far term directions of future efficiency improvement efforts and specific recommendations and conclusions

Preceding Page Blank

SUMMARY OF ROUND TABLE DISCUSSION

Daniel T. Bernatowicz
NASA Lewis Research Center
Cleveland, Ohio

About 35 representatives of government, industry, and university groups active in silicon materials research, photovoltaic research, and device development participated. The organizations represented are listed in figure 1.

PRESENT STATE OF THE ART

The recent efficiency improvements were described and are summarized in figure 2. The Helios cell was in production at Spectrolab and could be supplied with a minimum efficiency of 12 to 13 percent (AMO). The Violet cell was reported to be nearing production at Centralab (now OCLI) and had an efficiency between 13.5 and 14 percent (AMO). The COMSAT Non-Reflective (CNR) cell was still made only in the laboratory at COMSAT. Although it had not been thoroughly optimized, an efficiency of 15 percent (AMO) was measured. Although these cells are different, they reflect several similar technological thrusts. All the cells have p^+ backs, Ta_2O_5 antireflection coatings, shallower junctions, and thinner grid fingers. Conspicuous differences are the 20 ohm-cm resistivity in the Helios cell and the etched, low reflection (textured) surface of the CNR cell. Discussions of these recent technology developments made clear the importance of production factors, such as integration of processes, yield, and cost, to the development of a marketable solar cell. Considerable process development, which may involve performance compromise, is involved in integrating new technologies into the commercial production of a solar cell.

IMPROVEMENTS IN THE NEAR FUTURE

Further gains in efficiency are expected in the near future (2 to 3 years). These are expected to be extensions of recent improvements and process development:

p^+ Back (Back Surface Field)
Better antireflection coatings
Textured (non-reflective) surface
Better junctions
Thin structures
Narrow grid fingers

Preceding Page Blank

Adhesive or cover bonding methods that admit more blue light

The improved production cells in this period are expected to have a base resistivity in the range of 40-100 ohm-cm and to have a back surface field.

DIRECTIONS FOR THE LONGER TERM

The longer range efficiency gains centered about research activities rather than process and technology development were discussed. Although the technological improvements were reducing the gap between achieved performance and the theoretical limit, it was agreed that further research was appropriate and necessary.

Several general areas of need, for an effective efficiency improvement program, were identified. These consisted of

- Better modelling of the solar cell, including detailed description of the structure and of the physical processes.
- Better techniques for making and interpreting lifetime and diffusion length measurements. Bulk and surface effects on these parameters should be separated.
- Better knowledge of the solar spectrum in space. Space tests on the Violet cell suggest that the blue end of the spectrum has been underestimated.
- Space tests for new solar cells on a timely basis.

There was an extended discussion on what was a reasonable efficiency goal. The maximum theoretical efficiency of 22 percent was not disputed, but it was agreed that the goal should be the maximum practical efficiency, which would allow for such losses as reflection, shadowing, and series resistance. Some disagreement on these losses and junction losses, and further uncertainty due to the newly recognized band gap narrowing due to heavy doping, led to adoption of a range for the maximum efficiency. It was agreed that the maximum practical efficiency for silicon solar cells lay between 17 and 20 percent (AMO).

Although certain combinations of the technological thrusts listed earlier might yield a new device whose efficiency could approach this goal, it was agreed the main research path should continue to be on low resistivity silicon. The principal range of interest should be near 0.1 ohm-cm. Research on 0.1 ohm-cm silicon should investigate

- Lifetime as a function of dopant concentration, defects, processing procedures, and geometry.
- Band gap narrowing due to heavy doping.
- Dopants other than boron and various dopant profiles.

NASA-Langley, 1976

- Radiation damage and the effects of oxygen and carbon on radiation damage.

There was some concern that the reduction in lifetime, increase in recombination current, and increase in radiation damage as the doping level is increased may be due to the dopant itself rather than other impurities or defects due to processing. There might then be little potential for improvement of these parameters.

Since the meeting was concerned primarily with cells for space use, discussions were held on directions for radiation damage work to raise the end-of-life efficiency. The following devices and structures were identified as those that may be more tolerant to radiation damage and therefore deserve attention:

- Vertical multijunction cell.
- Thin cells and cells with very thin epitaxial layers.
- Cell with high resistivity base and a p^+ back surface field.
- GaAs cell, if the price of gallium can be reduced.

Although no specific deficiencies in radiation damage theory were identified, it was agreed that a larger store of basic information should be acquired. Research in the following areas should be conducted:

- Determination of the generation rate of primary defects by electrons and protons.
- Determination of the cross sections for the capture of primary defects by dopants and impurities.
- Search for getters for primary defects.
- Investigation of photon-induced degradation in silicon, especially float zone material.

MAJOR CONCLUSIONS OF THE ROUND TABLE DISCUSSION

The major conclusions reached in the round table discussion at the High Efficiency Silicon Solar Cell Meeting were as follows:

- The maximum practical efficiency of silicon solar cells is between 17 and 20 percent (AMO) and is still a reasonable goal.
- The long range R&D approach toward this goal should continue to focus on low resistivity (0.1 ohm-cm) silicon.
- Near term R&D should continue to focus on higher resistivity silicon, back surface fields, thinner grid fingers, and surface texturing to produce efficiency improvements.

- More research should be undertaken in radiation damage to raise end-of-life efficiency.
- Development of a production cell involves tradeoffs among fabricability, cost, and performance.

OBJECTIVE

- REVIEW PROGRESS IN RAISING EFFICIENCY
- ASSESS THE REMAINING PROBLEMS
- OUTLINE DIRECTIONS FOR FUTURE WORK

PARTICIPATING ORGANIZATIONS

CENTRALAB	HELIOTEK	MONSANTO	SIMULATION PHYSICS
COMSAT	HUGHES	MOTOROLA	SOLAREX
DOW CORNING	IBM	NORTHROP	TEXAS INSTRUMENTS

UNIVERSITY		GOVERNMENT	
FLORIDA	PENNSYLVANIA	NASA-GSFC	JPL
ILLINOIS	WAYNE STATE	NASA-HQ.	NSF
N. CAROLINA ST.	BROWN	NASA-LaRC	NRL
		NASA-LeRC	USAF-WPAFB

CS-73683

Figure 1. - High efficiency silicon solar cell meeting objective and participating organizations.

DESCRIPTION	EFFICIENCY	STATUS
HELIOS CELL 20 Ω-CM P^+ BACK SHALLOW JUNCTION THIN GRID FINGERS Ta_2O_5	12% TO 13% (AMO)	IN PRODUCTION
VIOLET CELL 2 Ω-CM P^+ BACK VERY SHALLOW JUNCTION VERY FINE GRID FINGERS Ta_2O_5	13.5 TO 14% (AMO)	NEARING PRODUCTION
COMSAT NON-REFLECTIVE CELL ETCHED, LOW REFLECTION SURFACE OTHERWISE LIKE VIOLET CELL	15% (AMO)	LABORATORY, NOT OPTIMIZED

CS-73684

Figure 2. - Summary of present high efficiency solar cells.

E-8425

*U.S. GOVERNMENT PRINTING OFFICE: 1975 - 635-275/47

NATIONAL AERONAUTICS AND SPACE ADMINISTRATION
WASHINGTON, D.C. 20546

OFFICIAL BUSINESS
PENALTY FOR PRIVATE USE $300

SPECIAL FOURTH-CLASS RATE
BOOK

POSTAGE AND FEES PAID
NATIONAL AERONAUTICS AND
SPACE ADMINISTRATION
451

POSTMASTER: If Undeliverable (Section 158 Postal Manual) Do Not Return

"The aeronautical and space activities of the United States shall be conducted so as to contribute . . . to the expansion of human knowledge of phenomena in the atmosphere and space. The Administration shall provide for the widest practicable and appropriate dissemination of information concerning its activities and the results thereof."

—NATIONAL AERONAUTICS AND SPACE ACT OF 1958

NASA SCIENTIFIC AND TECHNICAL PUBLICATIONS

TECHNICAL REPORTS: Scientific and technical information considered important, complete, and a lasting contribution to existing knowledge.

TECHNICAL NOTES: Information less broad in scope but nevertheless of importance as a contribution to existing knowledge.

TECHNICAL MEMORANDUMS: Information receiving limited distribution because of preliminary data, security classification, or other reasons. Also includes conference proceedings with either limited or unlimited distribution.

CONTRACTOR REPORTS: Scientific and technical information generated under a NASA contract or grant and considered an important contribution to existing knowledge.

TECHNICAL TRANSLATIONS: Information published in a foreign language considered to merit NASA distribution in English.

SPECIAL PUBLICATIONS: Information derived from or of value to NASA activities. Publications include final reports of major projects, monographs, data compilations, handbooks, sourcebooks, and special bibliographies.

TECHNOLOGY UTILIZATION PUBLICATIONS: Information on technology used by NASA that may be of particular interest in commercial and other non-aerospace applications. Publications include Tech Briefs, Technology Utilization Reports and Technology Surveys.

Details on the availability of these publications may be obtained from:

SCIENTIFIC AND TECHNICAL INFORMATION OFFICE

NATIONAL AERONAUTICS AND SPACE ADMINISTRATION

Washington, D.C. 20546